Smoke Emission and Transport Modelling

Research Report 102

Martin Cope, Sunhee Lee, Mick Meyer, Fabienne Reisen, Camila Trindade, Andrew Sullivan and Nic Surawski, Alan Wain, David Smith, Beth Ebert, Christopher Weston, Luba Volkova, Kevin Tolhurst, Thomas Duff, Sean Walsh, Nigel Tapper, Sarah Harris, Chris Rudiger, Alex Holmes, Musa Kilinc, Clare Paton-Walsh, Elise-Andree Guerette, Maximilien Desservettaz, Grant Edwards, Katrina Macsween and Dean Howard

May 2019

VICTORIA State Government | Environment, Land, Water and Planning

Acknowledgements

We would like to acknowledge the great support of Liam Fogarty, Elizabeth Ashman and Natalie Tostovrsnik from DELWP for managing the many useful introductions and discussions with personnel from DELWP, the CFA and more broadly within EMV. Thank you also for helping to smooth the many logistical challenges associated with a project of this complexity.

We would also like to acknowledge the NSW Office of Environment and Heritage and the Victorian Environment Protection Authority for the provision of air quality and emissions inventory data sets. The Tasmanian and South Australian EPAs also kindly provided air quality data sets. Thank-you Grant Williamson (University of Tasmania) for processing the Tasmanian air quality data.

Project Team

CSIRO Oceans & Atmosphere:	Martin Cope, Sunhee Lee, Mick Meyer, Fabienne Reisen, Camilla Trindade	Project design and lead, Modelling framework, emission characterisation
CSIRO Land & Water:	Andrew Sullivan and Nic Surawski	Pyrotron experimental burns, fire behaviour
Bureau of Meteorology:	Alan Wain, David Smith and Beth Ebert	Smoke forecast modelling
University of Melbourne:	Christopher Weston, Luba Volkova	Fuel load mapping
	Kevin Tolhurst, Thomas Duff, Sean Walsh	Fire behaviour modelling
Monash University:	Nigel Tapper, Sarah Harris, Chris Rudiger, Alex Holmes, Musa Kilinc	Fire radiative power and heat flux
Wollongong University:	Clare Paton-Walsh, Elise-Andree Guerette, Maximilien Desservettaz	Emission characterisation
Macquarie University:	Grant Edwards, Katrina Macsween and Dean Howard	Mercury

Printed by CSIRO, Aspendale, Victoria.

ISBN 978-1-76077-455-4 (print)

ISBN 978-1-76077-455-4 (pdf)

Contents

List of Acronyms

AAQS	Ambient Air Quality Standard
ACCESS	Australian Community Climate and Earth System Simulator
ADFD	Australian Digital Forecast Database
AGREPS	ACCESS Global and Regional Ensemble Prediction System
BC	Black Carbon
BCO	Burn Coverage Objective
BEF	Burning Efficiency
BLANkET	Base Line Air Network of EPA Tasmania
BoM	Bureau of Meteorology
CC	Carbon Content
CFA	Country Fire Authority
CH_4	Methane
CO	Carbon monoxide
CO_2	Carbon dioxide
CRDS	Cavity Ring-Down Spectrometer
CSIRO	Commonwealth Scientific and Industrial Research Organisation
CTM	Chemical Transport Model
CWD	Coarse Woody Debris
DEFM	Dry Eucalypt Forest Fire Model
DEH	Department of Environment and Heritage Protection
DELWP	Department of Environment, Land, Water and Planning
EC	Elemental Carbon
ECMWF	European Centre for Medium-range Weather Forecasts
EF	Emission Factor
EOFS	End of Fire Spread
EPA	Environment Protection Agency
EPS	Ensemble Prediction System
ER	Emission Ratio
FDI	Fire Danger Index
FEPS	Fire Emission Product Simulator
FFBT	Forest Fire Behaviour Table
FFDI	Forest Fire Danger Index
FFFM	Forest Fire Danger Meter
FL	Fuel Load

FMC	Fuel Moisture Content
FP	Fuel Pyrolysed
FRB	Fuel Reduction Burn
FRE	Fire Radiative Energy
FRP	Fire Radiative Power
FTIR	Fourier Transform Infrared Spectrometer
GEM	Gaseous Elemental Mercury
GFAS	Global Fire Assimilation System
GFDI	Grass Fire Danger Index
GFED	Global Fire Emissions Database
GHG	Greenhouse Gas
HB	Heap Burn
HCN	Hydrogen cyanide
Hg	Mercury
HPAEC-PAD Detection	High-Performance Anion-Exchange Chromatography with Pulsed Amperometric
IBRA	Interim Biogeographic Regionalisation for Australia
JAXA	Japan Aerospace Exploration Agency
K	Potassium
MACC	Monitoring Atmospheric Composition and Climate
MALT	Multiple Atmospheric Layer Transmission
MCE	Modified Combustion Efficiency
MFB	Mean fractional bias
MFE	Mean fractional error
MODIS	Moderate Resolution Imaging Spectroradiometer
MU	Macquarie University
N_2O	Nitrous oxide
NEPM	National Environment Protection Measure
NOAA	National Oceanic and Atmospheric Administration
NPI	National Pollutant Inventory
nssK	Non-Sea Salt Potassium
NSW	New South Wales
NT	Northern Territory
OC	Organic Carbon
OEH	Office of Environment and Heritage
OP-FTIR	Open Path- Fourier Transform Infrared Spectrometer
PHg	Mercury content of the particulates

PM	Particulate Matter
PSF	Point Spread Function
QLD	Queensland
SA	South Australia
SB	Slash Burn
SCC	State Control Centre
SIFT-MS	Selective Ion Flow Tube Mass Spectrometry
TAS	Tasmania
TSP	Total Suspended Particles
UNEP	United Nations Environment Program
UoW	University of Wollongong
UTC	Coordinated Universal Time
VFMP	Victorian Forest Monitoring Program
VIC	Victoria
VOCs	Volatile Organic Compounds
WA	Western Australia
WHO	World Health Organisation

Introduction

This report documents the outcomes of the Schedule 9+10 Smoke Emissions Modelling and Smoke Transport Modelling projects (henceforth called 'the project'). The project commenced in November 2012 with the aim of "Improving the Department of Environment, Land, Water and Planning (DELWP's) capacity to model the spread and accumulation or dissipation of smoke for planned and unplanned fire events through improved smoke trajectory and accumulation or dissipation modelling".

At the commencement of the project it was recognised that the information needed to improve quantitative concentration predictions would include the following.

- a better understanding of fuel/fire behaviour/emissions;
- state-of-the-art meteorological modelling (to improve uncertainty in model forecast fields);
- state-of-the-art high-resolution modelling of smoke plume transport (and chemical transformation) processes;
- validation of model components by field and remote sensing monitoring.

The project was designed to provide DELWP with the following deliverables.

- A definition of state-of-the art smoke modelling science, modelling and technology and good practice;
- an appropriate smoke modelling, monitoring and improvement framework;
- training and development of DELWP personnel in smoke management science - including prediction and monitoring; and
- new knowledge of smoke modelling through PhD and post doctoral research

A key driver of the project is the imperative to undertake prescribed burning for bushfire risk mitigation in a manner which also minimises population risk from smoke exposure. Bushfires in southern Australian forests can have catastrophic effects on the land, property and people. A Royal Commission into the 2009 Black Saturday fires (which took the lives of 173 people and devastated over 450,000 ha of land), concluded that one of the contributing factors was the heavy fuel load present in the areas burnt, and consequently recommended that the annual rate of prescribed burning for fuel reduction should increase to 5% of total State managed forest area.

Fuel reduction burns are designed to be of low intensity and to be well contained within a designated burn zone. As such, the program of prescribed burning is generally limited to light winds, minimal convection, low ambient temperatures, and moderate humidity. However, such conditions are also characterised by low levels of atmospheric ventilation and the potential for a build-up of air pollution. This can be further exacerbated if the burning season extends into the early winter when the smoke emissions add to those of domestic wood heaters and other near-surface sources of air pollution. When considering wood combustion, the principal pollutant of concern for population health (with a well-established risk for mortality) is fine (less than 2.5 μm) particles ($PM_{2.5}$). There is also an attendant risk of smoke damage to some agricultural sectors (e.g. vineyards where smoke taint can be of particular concern).

Due to recent significant incidents, there is a heightened awareness within Victoria's community about the risk of fire and smoke, and thus an increased pressure on fire and land management agencies to achieve planned burning while minimising the impact of smoke on communities.

- In February 2014, the Hazelwood mine fire burned over 45 days and caused a significant air pollution event affecting some 45,000 residents in nearby towns *(EPA Victoria 2015a; EPA Victoria 2015b)*. This event prompted the development of a State–wide smoke management framework to manage public health impacts from large scale extended smoke events. It also highlighted the importance of understanding health impacts and predicting the movement of smoke from prescribed burning and bushfires and predicting smoke levels at the local, state and regional levels.

- In October 2015 the Lancefield–Cobaw fuel reduction burn breached containment lines and developed into a fire that burned over 3,000 hectares and destroyed dwellings, sheds and fences. A subsequent inquiry into prescribed burning practices led to 22 recommendations aimed at improving the management of prescribed burning in Victoria *(Carter et al. 2015)*. The State Government also abandoned the annual 5% target for fuel reduction burns in favour of a new risk–based strategy.
- The 2015 Separation Creek/Wye River bushfire resulted in a subsequent enquiry into the use of back burning to reduce the risk of bushfire progagation and intensification.

Because prescribing burning generally occurs under conditions that may also lead to air pollution accumulation, there is an imperative for access to tools which can identify/forecast conditions in which the build-up of existing particle pollution is low, and in which smoke plumes from prescribed burning will have a low probability of impacting populated areas. For situations in which the latter is not possible, fire managers need the capability to provide advance warning to populations potentially affected by high smoke levels. This will enable at-risk individuals to take steps to minimise their exposure to the smoke.

Numerical weather and smoke forecast modelling are now being widely adopted by land management agencies around the world to help manage prescribed burning.

- The BlueSky smoke modelling framework developed by the U.S. Forest Service *(Larkin et al. 2009)* combines models and data encompassing weather, fires and fuels, emissions, and terrain into a unified framework to predict smoke concentrations and trajectories. The framework has been implemented by several agencies in the US and Canada (http://firesmoke.ca; http://www.bcairquality.ca/bluesky/west/index.html) to create smoke forecasts for land and fire managers, and for use as a tool for public health protection *(Yao et al. 2013; Yuchi et al. 2016)*. Other smoke modelling systems have been developed from BlueSky such as a regional system in the Pacific Northwest of the US *(O'Neill et al. 2008)*, and the Southern Smoke Simulation System *(Liu et al. 2010)*.

- The National Oceanic and Atmospheric Administration (NOAA) have developed a similar daily operational Smoke Forecasting System to provide guidance to air quality forecasters and the public about fine particles emitted from large wildfires and agricultural burning *(Rolph et al. 2009)*.

In Australia, the routine operation of smoke transport and smoke emissions forecasting models has primarily been restricted to the Bureau of Meteorology where a unit-emissions tracer model formed the basis of The Australian Smoke Management Forecast System *(Wain and Mills (2006)*). Although useful to the smoke management community, this system was not designed to include other sources of fine particles, nor particle production due to atmospheric chemistry. The inclusion of these processes is essential for developing a 'whole-of-airshed' assessment of smoke impacts within the context of existing sources of air pollution. Given this, it then follows that a more comprehensive modelling framework optimised for Victoria is a critical step if land management agencies are to be well equipped to assess the potential impacts of prescribed burning events on our rural and urban communities.

This document describes the development of a prototype forecast modelling framework which is based on state-of-the-art observational data sets, models and protocols which has been optimised for Victoria. The framework leverages research programs operated by the university and government research teams contributing to the project and broader research within the national and international research communities and builds on operational systems previously developed by CSIRO and the Bureau of Meteorology for meteorological and air pollution forecasting.

The remainder of the main body of this report comprises the following.

- The system design and the knowledge gaps which had to be addressed by the project.
- A synthesis of the different project components which targeted the knowledge gaps.
- A synthesis of case studies in which the forecasting framework was tested.
- Considerations for making the framework operational.
- Considerations for on–going research.

Detailed descriptions of key project components are given in the Appendices.

Part I Modelling system design and knowledge gaps

In February 2013, a workshop was undertaken with DELWP to gain an understanding of the operational procedures for undertaking prescribed burning, and hence to identify where contemporary science and modelling systems could be used to aid this process. Figure 1 summarises key decision points and time frames in the prescribed burning management process, together with the modelling tools which can be deployed to guide the process. It can be seen that tools can be deployed which are able to inform the planning process for a period extending from sub–daily to 10 days. Figure 1 suggests that the management process and supporting tools can be represented by three tiers of information and technology.

1. Tier 1 generates forecasts of general- and fire weather parameters (i.e. forest fire danger index (FFDI), grass fire danger index (GFDI)) - median and uncertainty, out to 10 days. The purpose of this tier is two–fold 1/ for advising on periods suitable for prescribed burning, 2/ for periods of potential bushfire hazard.

2. Tier 2 generates regional air pollution forecasts out to three days. These forecasts incorporate all inventoried sources of air pollution (with a focus on particulate matter) at an outer scale of the Australian continent; downscaling to 3 km grid spacing across Victoria and Tasmania. The purpose of these forecasts is to inform district managers of the current and forecast airshed loading of air pollution- including the persistence of smoke from earlier fuel reduction burns and bush fires. The Tier 2 product provides critical information on the capacity of an airshed to assimilate additional air pollution associated with fuel reduction burning.

3. Tier 3 generates high resolution fuel reduction smoke forecasts out to 24 hours. Designed to be run using a next day inventory of proposed burns provided by the district planners, this product combines regional pollutant loading and forecast smoke emissions and smoke transport to provide advice on the likely individual and combined airshed loading of smoke from the inventory of fuel reduction burns.

The framework of the prototype smoke forecasting system developed in this project is shown in Figure 2 and is based upon the BlueSky framework (http://www.airfire.org/bluesky) with several modules replaced by localised products. Specifically:

- The fire information reporting system uses DELWP active fire area data within Victoria, similar land agency data in other states, or either the European Centre for Medium-range Weather Forecasts (ECMWF) products or daily satellite–based observations of fire hotspots for regions outside of Victoria without real-time local fire reporting.

- Fuel loading for Victoria uses a fuel inventory developed specifically for this project which has been calibrated for fine fuels and coarse woody debris (CWD) using in situ empirical data sets. Information on the distribution of CWD for Victorian vegetation was identified as a knowledge gap at the start of the project and so resourcing was deployed within the project to address this issue. Fuel loading for the rest of Australia uses the approach described in *Meyer et al. (2008)*.

- Fire behaviour uses PHOENIX FireFlux, which includes PHOENIX RapidFire for bushfires and a new burn simulator for fuel reduction burns. The ability to generate robust fire behaviour diagnostics using data from a planned burn proposal was identified as a knowledge gap and addressed within the project. The use of remote sensing to relate observed fire intensity to smoke emissions and plume rise was also investigated within the project.

- Emissions of aerosols and gases from the combustion of fine and CWD fuel layers are modelled using a purpose-built module. Emissions specific to Victorian fuels was identified as knowedge gap which was addressed in the project by undertaking

laboratory and field experiments which measured emission factors.

- Meteorological modelling uses output from Bureau of Meteorology (BoM's) Australian Community Climate and Earth System Simulator (ACCESS) Global and Regional Ensemble Prediction System (AGREPS), ACCESS-R and ACCESS-C forecast runs.
- Transport-dispersion modelling uses the CSIRO chemical transport model (CTM) that has been coupled to ACCESS.
- Fuel reduction smoke modelling. The existing HYSPLIT module in the BlueSky framework was replaced by the CTM running smoke tracer forecasts at 1 km resolution.

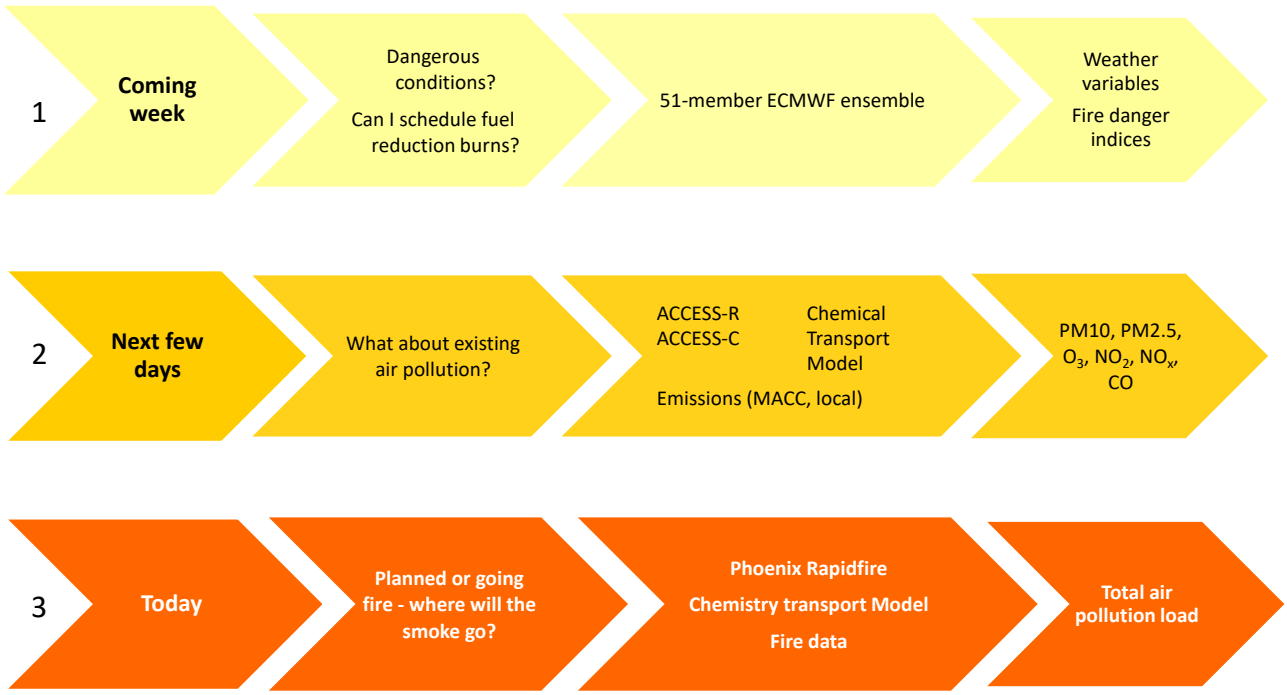

Figure 1 The three-tier, cascading time scale forecasting system developed for the project.

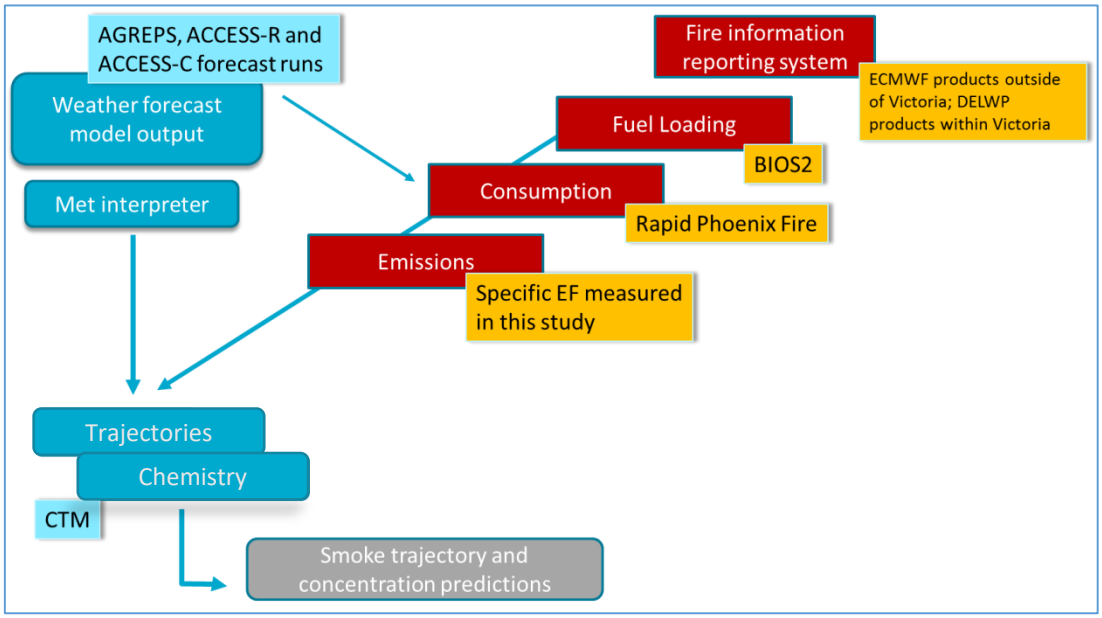

Figure 2. The numerical modelling framework used for generating smoke forecasts.

Part II Addressing the knowledge gaps

The smoke forecasting model builds on a number of components as shown in Figure 2. This section covers the knowledge gaps pertinent to both the forecasting system and to the application and future development of the forecasting/planning system (some of which were identified in the last section). The main findings for each component are highlighted here with more detailed information on each section provided in the appendices. At project inception, the data gaps pertinent to the forecasting system included:

- Fuel load maps, with a particular focus on coarse woody debris which is relevant to low-level and persistent emissions of smoke from smouldering.
- The links between fire behaviour and coarse fuel load (6-50mm in diameter).
- Observational data on the characteristics of gaseous and particle emissions from prescribed burns in sclerophyll forests of south-eastern Australia and from residual smouldering of coarse woody debris.
- Predictive fire consumption models for prescribed burns.

Data gaps pertinent to the application and future development of the forecasting system include:

- Mercury emissions from fires and prescribed burns and impacts on firefighters and downwind communities (Appendix E)
- The use of fire radiative power as a predictive tool for smoke emission characterisation, and the heat flux of fires.

Fuel load maps

Fuel maps are essential for fire and smoke prediction since fuel type and fuel amount affect combustion and emission during wildfires and prescribed burns.

In south-eastern Australia fuel characterization and classification approaches have focused on providing inputs for predicting fire spread (McArthur Meter and PHOENIX fire spread model) and have focused only on fine fuels components *(McArthur 1967)*. Fire spread is driven by flaming combustion and is a key determinant of the progression of a surface fire. Typical fire spread models however are not designed to estimate fire effects associated with post-frontal combustion so that heavy fuels (i.e. CWD), are not well simulated/described in fire spread models. Post-frontal combustion of heavy fuel has potential for high impact on smouldering emissions.

In this study we used two new empirical fuel load data sets *(Volkova and Weston 2015)* (V&W), and State Government forest monitoring data (DEPI Victorian Forest Monitoring Program (VFMP)) (Figure 3) to develop fuel maps. To derive comprehensive maps of fine and CWD fuels we tested two approaches for estimating fuel loads.

The first approach assumes that fuel accumulation is an attribute of vegetation class (see the fuel load component of the PHOENIX Rapidfire model *(Tolhurst et al. 2008)*) (Figure 4).

The second approach applies a process-based carbon cycle model used mostly for continental and global scale carbon budget studies (the biogeochemical model, BIOS2 *(Haverd et al. 2013)*).

While neither of the approaches were accurate over a full range of fuel loads, we concluded that BIOS2 biases can be corrected with a single linear correction (Figure 5).

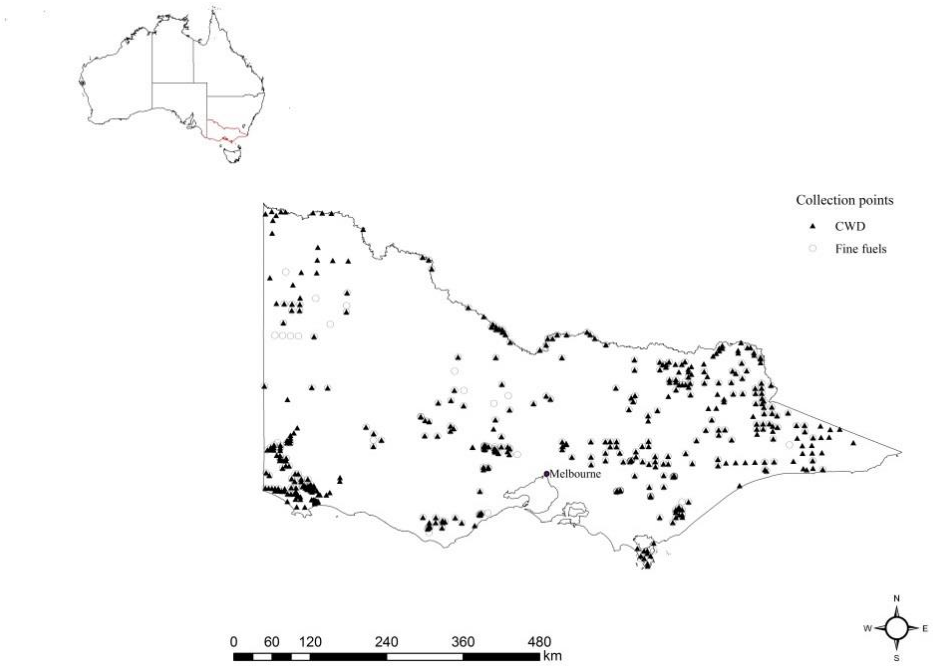

Figure 3 Map of the VFMP and V&W collection points used in the analysis and IBRA (Interim Biogeographic Regionalisation for Australia) boundaries

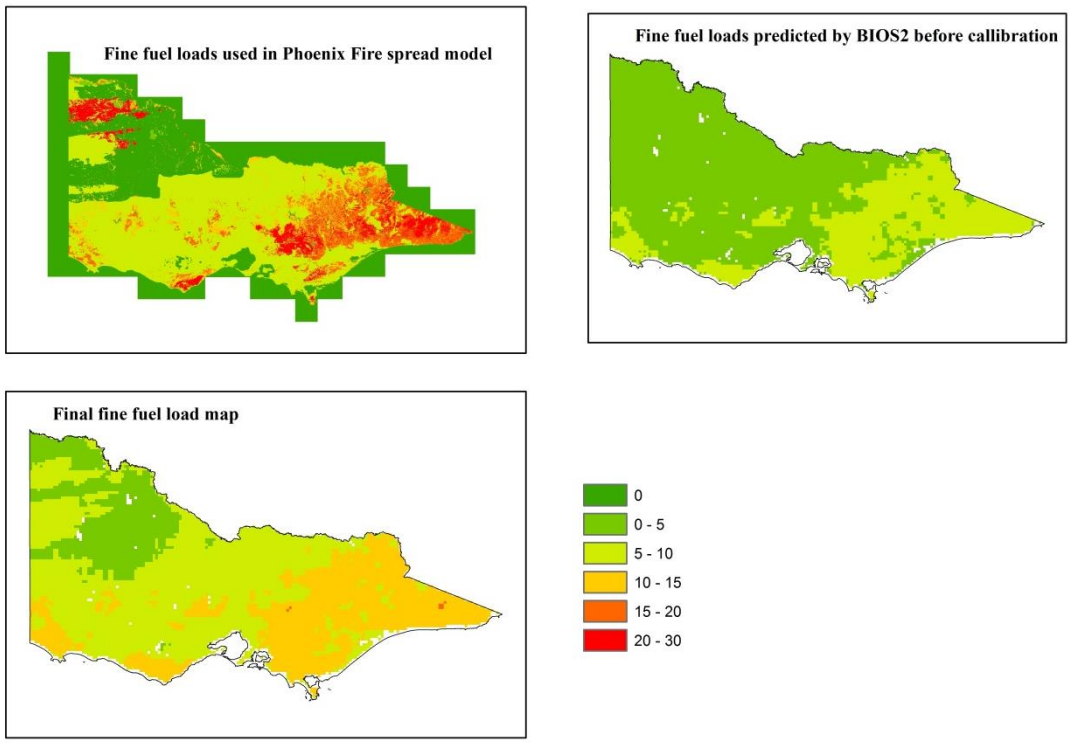

Figure 4 Map of fine fuel loads for Victoria before and after correction. Fine fuels include duff, and litter and twigs with diameter ≤6 mm. Fuel loads are expressed in t ha^{-1}

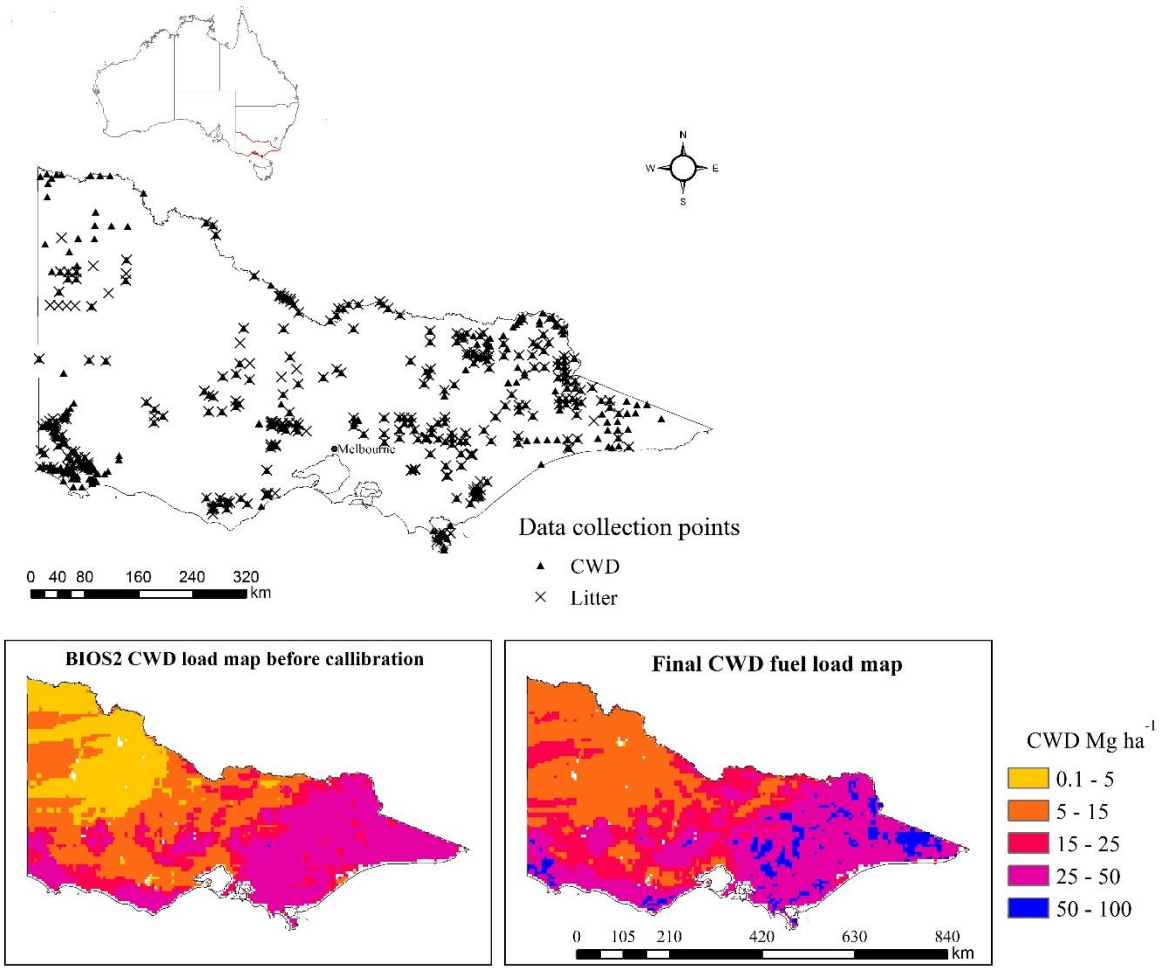

Figure 5 Map of data collection points (top); map of CWD fuel loads for Victoria before and after correction. CWD fuels include twigs and logs with diameter >6 mm.

Fire behaviour: How coarse fuel loads affect fire behaviour

Current Australian forest fire behaviour prediction systems such as the McArthur Forest Fire Danger Meter (FFFM,*(McArthur 1967)*), the Western Australian Forest Fire Behaviour Tables (FFBT,*(Sneeuwjagt and Peet 1998)*) and the Dry Eucalypt Forest Fire Model (DEFFM, *(Gould et al. 2007a; Gould et al. 2007b; Cheney et al. 2012)*) consider only the contributions to fire behaviour from the fine (<6 mm diameter) fuels. Combustion of these fine fuels and their influence on the behaviour and spread of a bushfire has been the focus of much of past research into bushfire behaviour. Combustion of CWD (e.g. fallen branches, boughs and toppled stems) has not received much attention in this regard.

However, the combustion of CWD fuel components does play a significant role in other aspects of bushfire behaviour, particularly behind the fire front, including the radiant heat flux and firefighter safety *(Sullivan et al. 2002)*, the fire intensity, severity and burning depth *(Cruz et al. 2012)*.

This component of the project undertook controlled burning experiments involving fallen branch material in the range 6 – 50 mm in diameter to quantity the effect of CWD on fire behaviour (in particular rate of spread) for fires burning under a fixed set of wind and fuel moisture conditions. Fuel conditions for the experimental burns were fine fuel litter only (Control) and fine fuel litter to which 2t/ha, 6t/ha and 12t/ha of CWD respectively was added (three treatments).

The experimental results have shown that there was little difference in combustion efficiencies either across treatments or fire spread mode as measured

after the experiment. However, there were clear differences observed in the way in which fuels were consumed. Residual burning after the passage of the flame zone was highest in the heading fires and highest in the CWD, many of which continued flaming long after the fine fuels had ceased combustion. The backing fires had very little residual combustion in the CWD as a result of the slower rates of spread.

We found that, under the same burning conditions, the presence of CWD had a direct impact on the rate of forward spread of fires (Figure 6) but not on the rate of backing spread of fires. In heading fires the rate of spread in the presence of CWD was approximately half that of heading fires in the absence of CWD, regardless of the amount of CWD Figure 7. For backing fires, no significant effect of CWD was detectable (Figure 8). This suggests that the mechanisms that influence the speed of a fire burning into the wind through fine fuels occurs over the same time scale as the ignition of the CWD and that the relative time scales of these processes between heading fires and backing fires is markedly different.

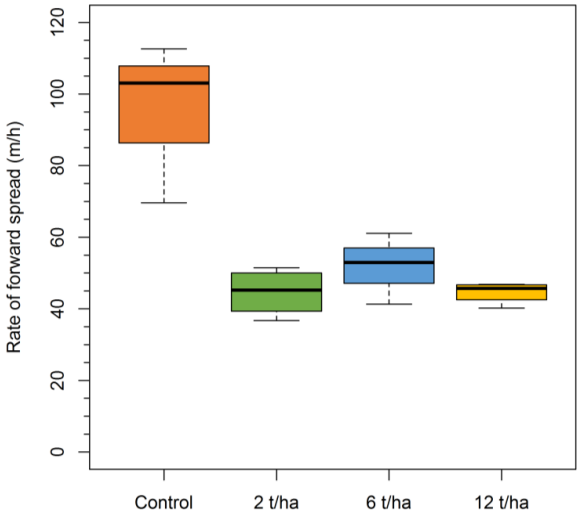

Figure 6: Box plot of the distributions of mean cumulative rates of spread for the control (fine fuel only) and three treatments (2t/ha, 6t/ha and 12t/ha of CWD). The control is clearly statistically different from all the treatments.

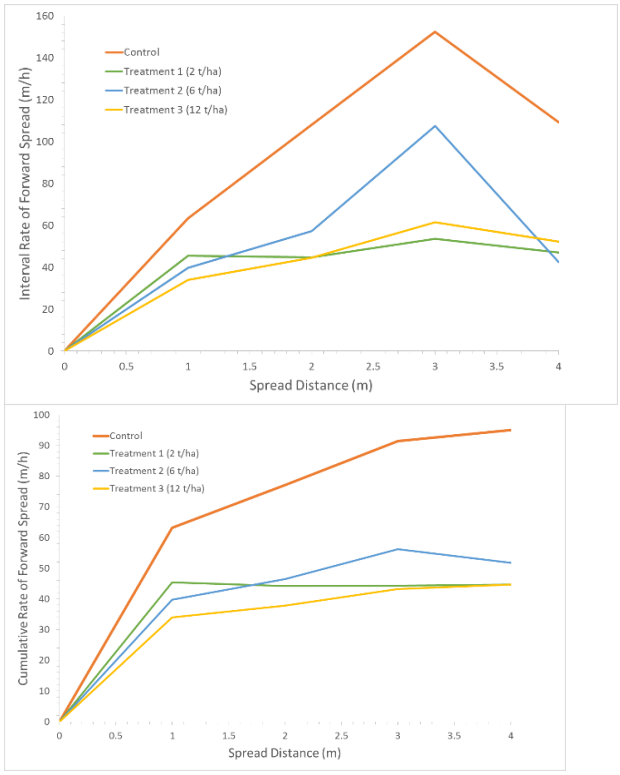

Figure 7: **Summary graphs of the heading fire experiments rates of spread. Top) The interval rate of heading spread. Bottom) The cumulative rate of heading spread.**

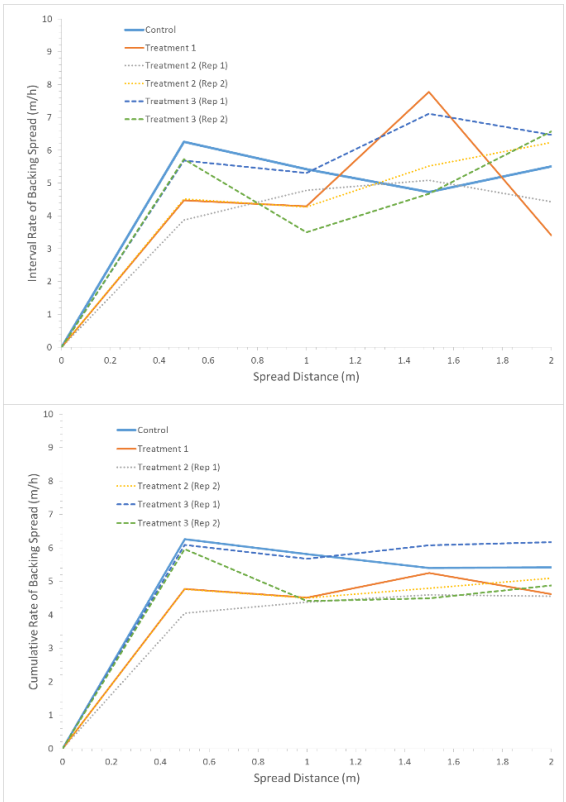

Figure 8: Summary graphs of the backing fire experiments rates of spread. Top) The interval rate of backing spread. Bottom) The cumulative rate of backing spread.

Emission factors

Emission factors (EFs) are a critical input into dispersion models to analyse or forecast smoke dispersion and estimate impacts on air quality and populations. EFs specify the mass of a gas or aerosol species emitted per unit mass of fuel burned.

EFs are usually derived from emission ratios (ERs) of combustion products (see Appendix D). They can be determined either through controlled measurements in the laboratory, smoke plume measurements using aircrafts or ground level sampling in the field. In this study both laboratory and ground-level field measurements are used to derive EFs for key pollutants. The study aimed at finding explanatory variables (such as combustion efficiency) that can be easily measured or estimated and can explain much of the observed variation in EF. These explanatory relationships can then be used to extrapolate measured EFs to a wider range of fuel and burning conditions. The derived particle EFs and chemical characteristics along with the explanatory relationships will help to better forecast and manage air quality impacts from prescribed burns on nearby communities.

Laboratory measurements

Controlled burning experiments involving fallen branch material in the range 6 – 50 mm in diameter were done to quantity the greenhouse gases (GHG), particulate matter (PM), reactive volatile organic compounds (VOCs) and mercury emissions released by CWD under a fixed set of wind and fuel moisture conditions using the CSIRO pyrotron.

Table 1 lists the EFs of carbon dioxide (CO_2), carbon monoxide (CO), methane (CH_4), $PM_{2.5}$ mass, a number of PM chemical components and selected VOCs for the different fuel treatments. Table 1 also lists the modified combustion efficiency (MCE), which is used to characterize the relative amount of flaming and smouldering combustion (see Appendix D).

Fine fuel (6mm) vs coarse fuel (6-50mm)

As can be seen in Table 1, the coarse fuel fraction had no effect on the MCE or on the $PM_{2.5}$ and VOC EFs. In terms of chemical composition of $PM_{2.5}$, the ratio of levoglucosan to non sea-salt potassium (nssK) (both wood smoke tracers) increased with increased coarse fuel fraction, suggesting that levoglucosan is dominantly emitted from coarse fuel while nssK is emitted from fine fuel (e.g. leaves), consistent with a previous research study *(Schmidl et al. 2008)*.

Evolution of the smoke plume

Three distinct phases could be identified for each burn:

- flaming propagation which covers the period between ignition and time when fire reached the end of the fuel bed
- flaming stationary which covers the period between the end of forward spread and the extinction of fine fuels
- smouldering combustion

The results for the three combustion phases are shown in Table 2 and indicate that the EFs for $PM_{2.5}$ and VOC species show a strong dependence on MCE. The highest EFs were observed for the smouldering phase, while the lowest EFs were observed for the flaming propagating phase, which consumed on average about 50% of the fuel in the Pyrotron fires (Table 2).

Emissions in the field

Until this study there were no reliable EFs of $PM_{2.5}$ from fires or burns in sclerophyll forests of south-eastern Australia and also very little on emissions from residual smouldering combustion of CWD. In order to attempt to fill this gap, measurements of $PM_{2.5}$ and trace gases were carried out at prescribed burns in Victoria focusing on both the flaming and smouldering combustion.

The team attended four prescribed burns in Victoria in 2015. Emissions in the field were determined by two sampling approaches: via direct sampling close to the emission source (i.e. within 1 m) and via open path infrared spectroscopy adjacent to or within the fire boundary.

Table 1: Emission factors (g kg^{-1} fuel) of CO, CO_2, CH_4, $PM_{2.5}$ and selected VOCs by fuel load.

	0 t/ha CWD Control	2 t/ha CWD	6 t/ha CWD	12 t/ha CWD	Average heading	Average backing	Method
MCE	0.94	0.94	0.93	0.94	0.94 ± 0.1	0.94	
CO_2	1714 1734	1725 1725	1707 1715	1716 1707	1716 ± 22 1719 ± 24	1714 1697	CRDS OP-FTIR
CO	72.8 65.7	65.9 64.8	76.2 65.8	70.5 63.6	71 ± 13 64.9 ± 13.0	71.9 79.0	CRDS OP-FTIR
CH_4	1.89 1.9	1.89 1.5	2.44 1.7	2.35 2.2	2.17 ± 0.55 1.8 ± 0.4	2.21	CRDS OP-FTIR
$PM_{2.5}$	6.57	6.07	5.15	5.00	5.57 ± 1.21	7.0	
Levoglucosan	0.75	0.84	0.73	0.89	0.82 ± 0.19	0.92	
nssK	0.015	0.010	0.009	0.007	0.010 ± 0.003	0.014	
Levo/nssK	54.6	82.4	85.3	127.2		81.3	
Na^+	0.011	0.010	0.015	0.005	0.010 ± 0.005	0.014	
Cl^-	0.068	0.075	0.051	0.030	0.054 ± 0.023	0.118	
Ca^{2+}	0.021	0.081	0.066	0.014	0.049 ± 0.070	0.013	
Mg^{2+}	0.005	0.011	0.015	0.002	0.008 ± 0.013	0.002	
NH_4^+	0.018	0.026	0.016	0.015	0.019 ± 0.008	0.039	
NO_3^-	0.008	0.010	0.008	0.007	0.009 ± 0.003	0.014	
SO_4^{2-}	0.031	0.033	0.030	0.020	0.028 ± 0.006	0.028	
Organic carbon (OC)	4.7	3.5	2.8	3.2	3.6 ± 0.8	4.1	
Elemental arbon (EC)	0.88	0.64	0.56	0.62	0.67 ± 0.14	1.00	

Black Carbon (BC)	1.38	1.07	0.83	0.87	1.04 ± 0.25	1.4	
Acetaldehyde	0.30	0.32	0.30	0.31	0.31 ± 0.08	0.37	SIFT
Acetic acid	2.07	1.82	1.44	1.2	1.58 ± 0.67	1.4	OP-FTIR
Acetone	0.25	0.24	0.22	0.22	0.22 ± 0.06	0.29	SIFT
Acetonitrile	0.039	0.057	0.057	0.059	0.055 ± 0.020	0.068	SIFT
Acetylene	0.091	0.12	0.11	0.096	0.10 ± 0.03	0.20	SIFT
Ammonia	0.97	0.66	0.76	0.74	0.76 ± 0.16	0.8	OP-FTIR
Benzene	0.16	0.21	0.19	0.21	0.19 ± 0.05	0.22	SIFT
Butadiene	0.054	0.058	0.034	0.030	0.043 ± 0.023	0.030	SIFT
Butanone	0.069	0.082	0.075	0.084	0.078 ± 0.029	0.099	SIFT
Ethane	0.20	0.17	0.18	0.20	0.19 ± 0.03	0.22	FTIR
Ethene	0.73	0.76	0.78	0.74	0.76 ± 0.16	0.78	OP-FTIR
	0.60	0.57	0.59	0.63	0.60 ± 0.16	0.92	FTIR
Eucalyptol	0.026	0.032	0.017	0.017	0.023 ± 0.012	0.037	SIFT
Formaldehyde	0.83	1.00	0.96	0.86	0.92 ± 0.22	0.97	OP-FTIR
Formic acid	0.23	0.19	0.19	0.18	0.19 ± 0.05	0.23	OP-FTIR
Hydrogen cyanide (HCN)	0.035	0.11	0.084	0.070	0.080 ± 0.055	0.075	SIFT
Isoprene	0.14	0.094	0.10	0.090	0.10 ± 0.03	0.20	SIFT
Methanol	0.63	0.86	0.52	0.44	0.61 ± 0.45	0.73	OP-FTIR
	0.55	0.59	0.61	0.59	0.59 ± 0.19	0.67	SIFT
Monoterpenes	0.078	0.11	0.028	0.042	0.064 ± 0.052	0.10	SIFT
Pyrrole	0.032	0.026	0.020	0.016	0.023 ± 0.015	0.031	SIFT
Trimethylbenzene	0.062	0.067	0.059	0.057	0.061 ± 0.028	0.09	SIFT
Toluene	0.43	0.42	0.39	0.39	0.41 ± 0.13	0.49	SIFT
Xylenes	0.21	0.072	0.077	0.080	0.10 ± 0.11	0.39	SIFT

Table 2: Emission factors (g kg^{-1}) and MCE for different fire phases

	Flaming propagation	Flaming stationary	Smouldering
MCE	0.98 ± 0.01	0.93 ± 0.03	0.82 ± 0.04
CO_2	1790 ± 20	1690 ± 50	1470 ± 90
CO	20 ± 10	80 ± 30	190 ± 40
CH_4	0.5 ± 0.3	2.6 ± 0.7	7.3 ± 1.7
N_2O	0.06 ± 0.02	0.07 ± 0.03	0.06 ± 0.02
$PM_{2.5}$	3.3 ± 1.6	6.4 ± 2.6	15.0 ± 9.2
Acetic acid	0.4 ± 0.4	3.0 ± 2.0	5.0 ± 1.0
Ammonia	0.2 ± 0.1	0.8 ± 0.2	2.2 ± 0.4
Ethene	0.2 ± 0.1	1.1 ± 0.5	1.5 ± 0.4
Formaldehyde	0.3 ± 0.2	1.3 ± 0.7	2.1 ± 0.8
Formic acid	0.06 ± 0.04	0.3 ± 0.1	0.6 ± 0.2
Methanol	0.3 ± 0.4	0.8 ± 0.6	1.9 ± 0.9

Table 3: Emission factors (g kg^{-1} fuel) and MCE from ground measurements of flaming combustion

	Greendale (13/04/2015) N = 9	Castlemaine (23/4/2015) N = 15	Bambra (30/09/2015) N = 8	Campbells Creek (1/10/2015) N = 15	Average all
MCE	0.94 ± 0.01	0.95 ± 0.01	0.93 ± 0.01	0.95 ± 0.01	0.94 ± 0.02
CO_2	1715 ± 21	1743 ± 19	1691 ± 27	1735 ± 27	1726 ± 29
CO	71.6 ± 12.0	54.4 ± 11.1	85.6 ± 16.2	58.8 ± 15.9	64.7 ± 17.5
CH_4	2.3 ± 0.7	1.9 ± 0.4	2.7 ± 0.7	2.2 ± 0.7	2.2 ± 0.7
$PM_{2.5}$	15.4 ± 5.2	14.6 ± 7.9	24.9 ± 8.1	18.2 ± 6.0	17.5 ± 7.5
Levoglucosan					1.54 ± 0.97
nssK					0.046 ± 0.028
Na^+					0.014 ± 0.010
Cl^-					0.169 ±0.088
Ca^{2+}					0.017 ± 0.013
Mg^{2+}					0.003 ± 0.003
NH_4^+					0.057 ± 0.018
NO_3^-					0.016 ± 0.004
SO_4^{2-}					0.082 ± 0.028

Table 4: Emission factors (g kg^{-1} fuel) and MCE from ground measurements of smouldering combustion

	Greendale (13/04/2015) N = 6	Castlemaine (23/4/2015) N = 4	Bambra (30/09/2015) N = 8	Campbells Creek (1/10/2015) N = 6	Average all
MCE	0.84 ± 0.04	0.81 ± 0.02	0.83 ± 0.04	0.85 ± 0.02	0.83 ± 0.04
CO_2	1504 ± 91	1456 ± 36	1486 ± 91	1549 ± 45	1499 ± 77
CO	192.6 ± 53.9	212.6 ± 27.3	197.2 ± 49.3	161.8 ± 24.9	190.9 ± 43.6
CH_4	9.4 ± 4.0	15.9 ± 3.9	13.2 ± 6.6	11.1 ± 3.8	12.4 ± 5.3
$PM_{2.5}$	51.5 ± 37.2	73.0 ± 40.0	55.2 ± 40.1	26.2 ± 12.0	51.0 ± 36.2
Levoglucosan					7.58 ± 3.11
nssK					0.022 ± 0.027
Na^+					0.039 ± 0.043
Cl^-					0.219 ± 0.167
Ca^{2+}					0.024 ± 0.014
Mg^{2+}					0.010 ± 0.012
NH_4^+					0.11 ± 0.06
NO_3^-					0.012 ± 0.007
SO_4^{2-}					0.066 ± 0.029

Emission factors from near source sampling

Near source sampling of CO, CO_2, CH_4, N_2O and fine particles ($PM_{2.5}$) was done for both flaming and smouldering combustion and results are shown in Table 3 and Table 4. EFs for CO, CH_4 and $PM_{2.5}$ were significantly higher during the smouldering combustion.

Figure 9 shows the relationship of MCE vs EF(CH_4) (left) and vs EF($PM_{2.5}$) on the right. For both compounds we can see a significant increase in the EF with decreasing MCE and also a larger scatter in EF values as MCE decreases. EFs of $PM_{2.5}$ for flaming combustion range from 3 to 34 g kg^{-1}, while the range for smouldering combustion is from 10-133 g kg^{-1}.

For the smouldering combustion we observe two distinct trends in EF($PM_{2.5}$). The significant difference in particle emissions during smouldering combustion is due to the combustion processes as described in *Bertschi et al. (2003)*. This is further detailed in Appendix D.

Figure 10 shows the $PM_{2.5}$ EFs by combustion phase with values in the boxplot representing the median EF($PM_{2.5}$) and recommended EF($PM_{2.5}$) for Australian temperate forest fires. As can be seen in Figure 10, there are significant differences in EFs between the flaming and smouldering combustion. The largest variability is observed for smouldering combustion.

While emissions during the rapid and intense flaming combustion are lofted by convection, particles emitted during the slow and prolonged smouldering combustion remain closer to the ground and can therefore significantly impact on the air quality of nearby communities.

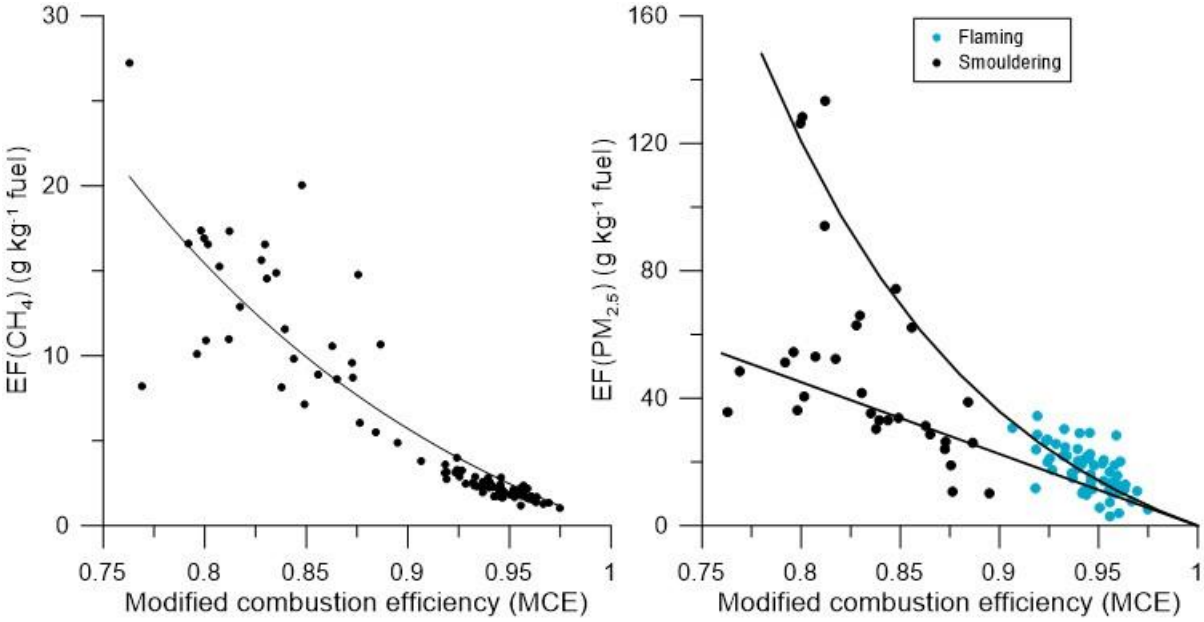

Figure 9: Emission factors (g kg^{-1}) as a function of MCE for CH_4 (left) and $PM_{2.5}$ (right)

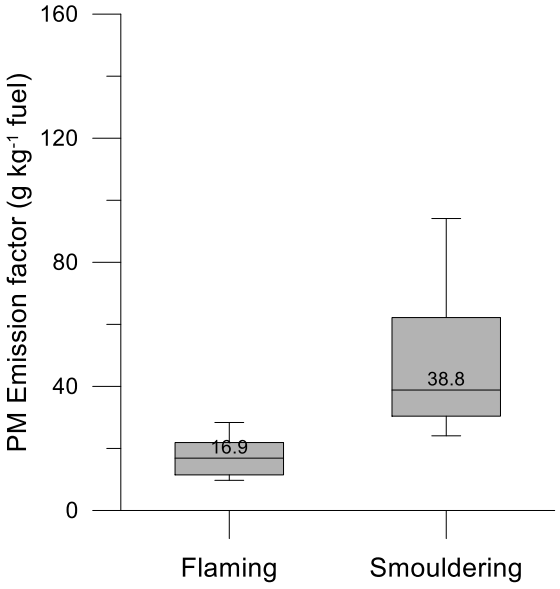

Figure 10: Distribution of $PM_{2.5}$ EFs by combustion phase. Boxplots show median, 25-75%iles (box) and 10-90%iles (whiskers)

Surface smoke plume

Open Path Fourier Transform Infrared Spectrometer (OP-FTIR) measurements were conducted at two autumn burns in Victoria, Greendale and Castlemaine in 2015 and at five prescribed burns in NSW in 2012 and 2013. The results for trace gases are shown in Table 5. These EFs fall within the range of EFs measured by similar techniques at hazard reduction burns in NSW *(Paton-Walsh et al. 2014)*.

Table 5: Emission factors (g kg^{-1}) of VOCs

	Greendale (13/04/2015) N = 9	Castlemaine (23/4/2015) N = 15	Average VIC all	Average NSW all	Extratropical forest (Akagi et al., 2011)
MCE	0.93	0.91	0.92 ± 0.01	0.89 ± 0.02	0.93
CO_2	1670	1650	1660 ± 14	1620 ± 32	1509
CO	84	101	93 ± 12	118 ± 16	122
CH_4	3.1	3.3	3.2 ± 0.1	3.6 ± 1.1	5.7
Acetic acid	6	6.5	6.3 ± 0.4	3.9 ± 1.3	4.08
Ammonia	1.5	1.7	1.6 ± 01	1.6 ± 0.7	2.46
Ethene	1.1	1.2	1.2 ± 0.1	1.3 ± 0.2	
Formaldehyde	1.3	1.5	1.4 ± 0.1	1.8 ± 0.4	1.92
Formic acid	0.57	0.53	0.55 ± 0.03	0.4 ± 0.2	0.54
Methanol	1.5	1.7	1.6 ± 0.1	2.4 ± 1.1	2.70

Plume emission factors from peat/organic soils

In 2016 large bushfires started in January across Tasmania and continued burning into February. Two distinct smoke plumes were observed at the Cape Grim Baseline Air Pollution Station, located near the north-west tip of Tasmania. During both plume events which occurred on 25th January and 12th February, measured pollutant concentrations were significantly elevated above background concentrations. Satellite images of the smoke plumes are shown in Figure 11.

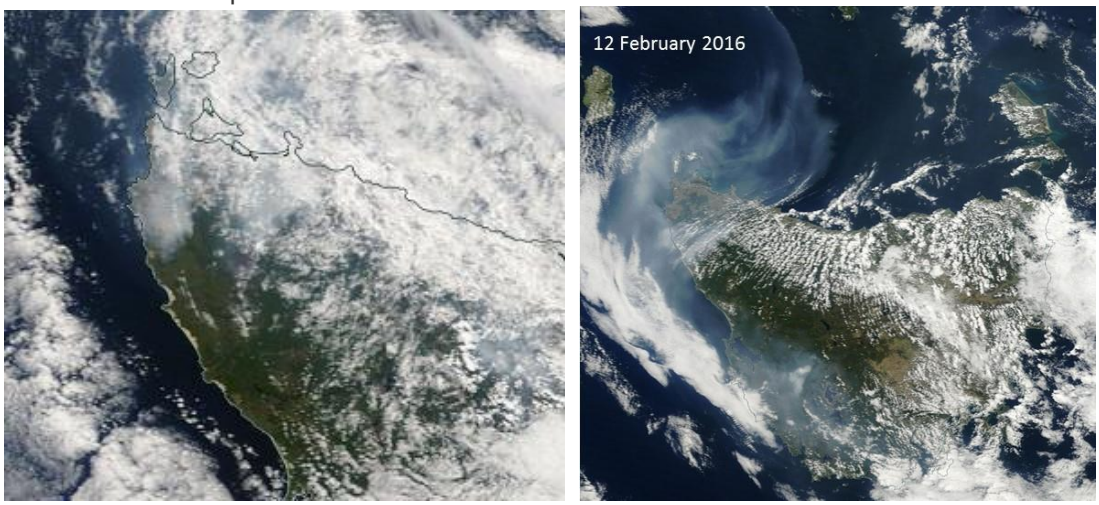

Figure 11: Satellite images of smoke plumes on 25th January 2016 (left) and 12th February 2016 (right)

Figure 12 shows the time series of CO, CO_2, CH_4 and black carbon (BC) concentrations measured between 22 January and 16 February 2016. Emission ratios (ER) were calculated using measured ambient concentrations during the two smoke plume events and from these we derived emission factors for CO_2, CO, CH_4 and BC (Table 6). The observed MCEs were lower than those measured at fire and/or prescribed burns in forested areas and may result from burning in peat which burns less efficiently relasing more reduced compounds such as CO, NH_4 and particles. Comparing the EFs during the smoke plume events against averaged literature data suggest that the plume was a mixture of emissions from organic peatlands and forests.

Table 6: Emission factors (g kg^{-1} fuel) and MCE from ambient measurements during smoke plume events at Cape Grim, TAS during 2016.

	Plume event (25-27 January)	Plume event (11-13 February)	Peatlands (Akagi et al., 2011)	Extratropical forest (Akagi et al., 2011)
MCE	0.86	0.87	0.90	0.93
CO_2	1567	1591	1563	1509
CO	157.9	145.6	182	122
CH_4	6.5	5.0	11.8	5.7
BC	0.31	0.25	0.2	0.56

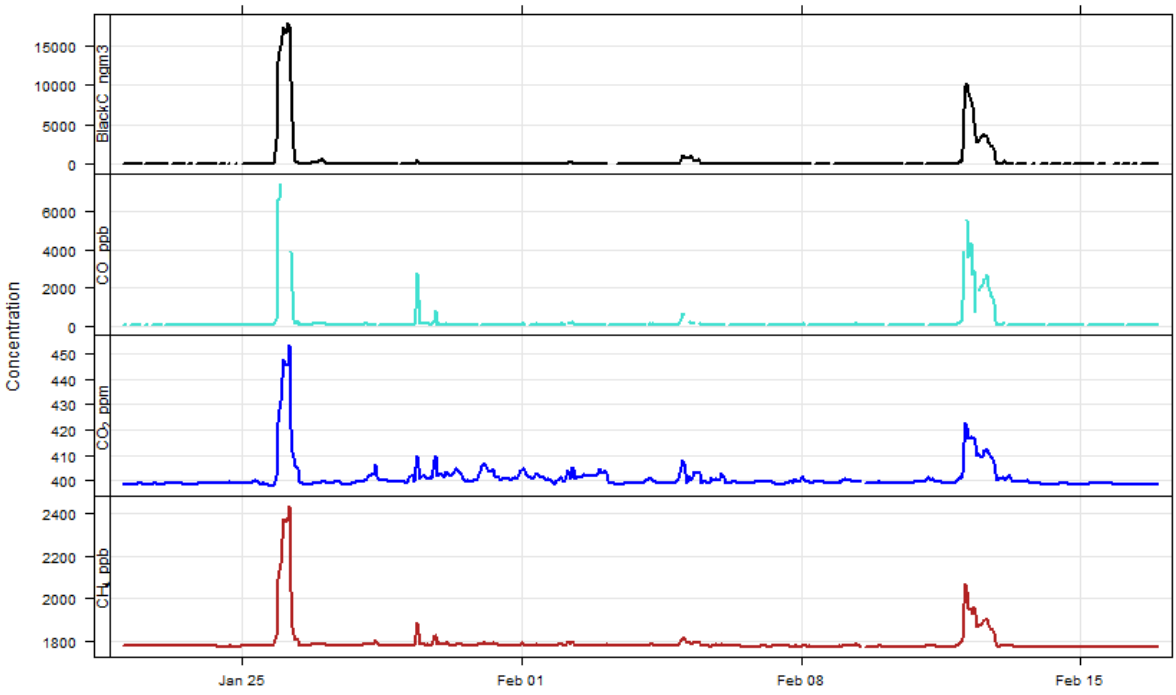

Figure 12: Time series of Black carbon, CO, CO_2 and CH_4 measured at Cape Grim between 22 January and 16 February 2016

Emission of mercury compounds and impacts on people

Mercury (Hg) is a globally transported neuro toxin that poses significant health risks for human populations. Hg stored in vegetation, leaf litter and soil can be mobilised into the atmosphere during a fire, predominantly in the form of gaseous elemental mercury (Hg^0) and potentially impact on populations. The frequency of both prescribed and wildfires results in Australia being one of the largest contributor to Hg emissions from biomass burning, contributing 3% of total Hg global emissions *(Friedli et al. 2009)*. Little focus has been given to understanding Hg emissions and dispersion from Australian bushfires and no published work has been undertaken to measure real time Hg concentrations from fires, prescribed or otherwise.

This section of the report presents the findings from laboratory experiments on Hg from fires and on the modelling of the transport and fate of Hg from prescribed burns including firefighter exposure and risk.

Emission ratios and emission factors from CSIRO Pyrotron experiment

Hg emissions from each of the individual burns show an initial spike in emissions, followed by a sharp decrease (Figure 13). Hg concentrations return to approximate background concentrations (<2 ng m^{-3}) soon after the fine fuels have been extinguished. The elevated Hg concentrations measured in the initial stages of the burn suggest that the majority of Hg is released during combustion of the fine fuels, with coarse fuels contributing little to the overall emissions.

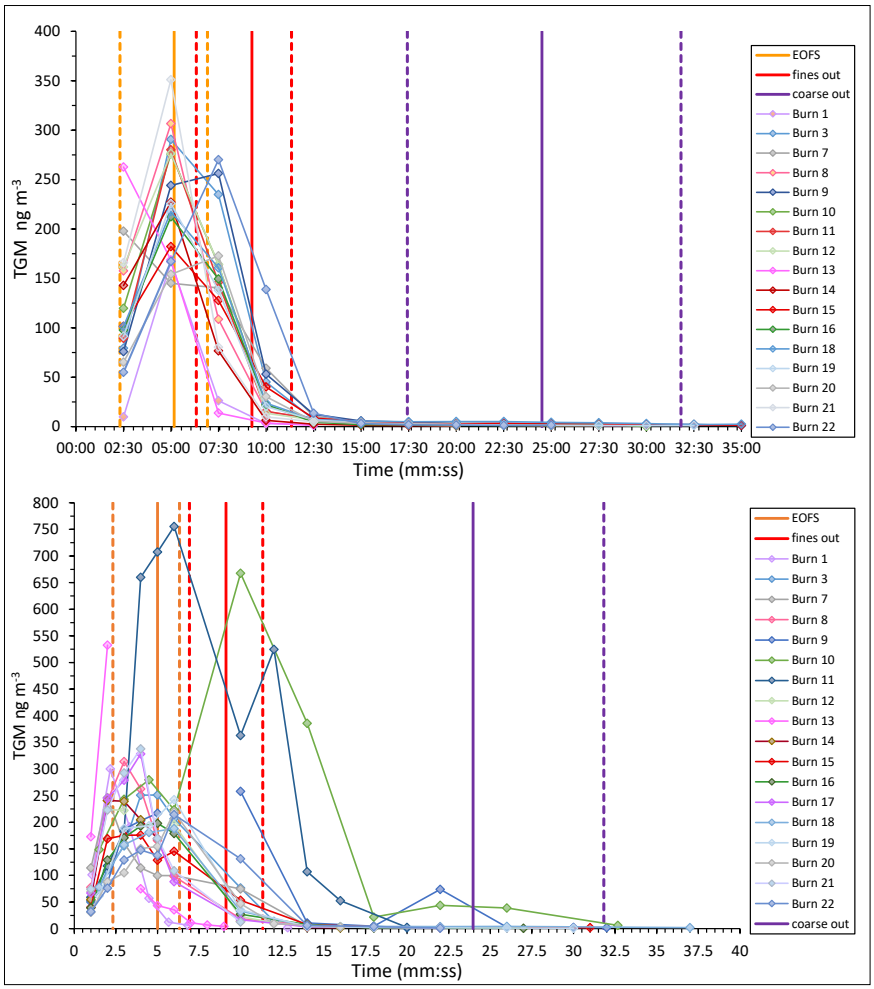

Figure 13: Continuous burn data against time (top), Hg concentrations measured using the bag method (bottom).

In order to determine EFs for Hg, relationships between carbon and Hg was looked at. Hg is strongly adsorbed to available carbon within an ecosystem and will therefore behave similarly to carbon when volatilised during a fire *(Kolka et al. 2014)*. Correlations between Hg and CO_2 were significantly better than those observed between Hg and CO for all fuel loads. This is most likely a reflection of Hg being primarily released from leaf litter during flaming combustion, rather than during smouldering combustion *(Friedli et al. 2003a)*. As a result, CO_2 was used as a reference gas for the calculation of EF.

EFs were calculated for each fuel load using the CO_2 ERs and equations described in appendix D and are shown in Table 7. The EFs are in agreement with current published EFs for temperate forests *(Friedli et al. 2003a; Packham et al. 2009)*.

Hg EF plotted against MCE shows a positive correlation (Figure 14), which further indicates that Hg emissions predominantly occur during flaming combustion and decrease as the fire transitions to the smouldering phase.

Table 7: Hg emission factors.

	Continuous tekran data (µg kg^{-1})	Bag samples (µg kg^{-1})
0 t/ha CWD (Control)	92.7	80.0
2 t/ha CWD	72.7	86.2
6 t/ha CWD	54.1	79.7
12 t/ha CWD	43.9	64.0
Average heading	58.1	76.7
Average backing		62.7

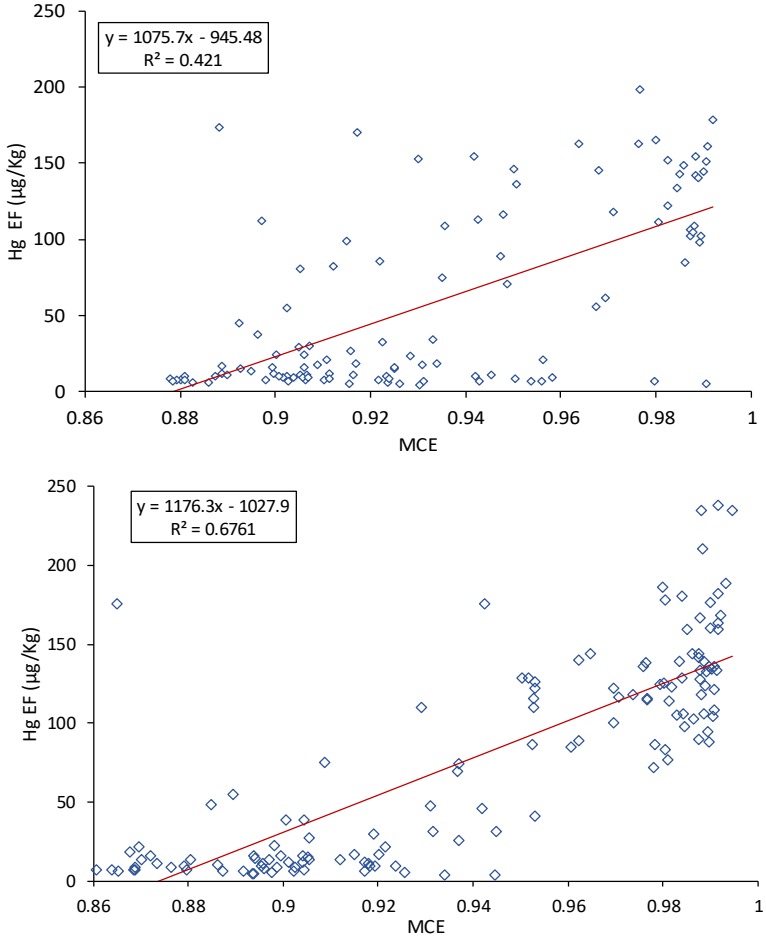

Figure 14: MCE plotted against Hg emission factors for CO_2 + CO. Top shows continuous Hg EF measurements, Bottom shows bag measurements Hg EF.

The EFs calculated here only consider Hg emitted from leaf litter and do not include emissions of Hg from soil and live vegetation. Soils have been found to contribute up to 20% Hg emitted during a fire and therefore need to be taken into consideration when calculating EF for prescribed and wild fires *(Webster et al. 2016)*. As Hg measurements were not done at prescribed burns due to logistical reasons, the influence of soil emissions on the EF for Australian forests could not be quantified.

The experimental burns have shown that EF for Hg decrease with increasing coarse material, indicating that fine fuels contain the majority of Hg released during fires. During prescribed burns, the fine fuel is predominantly burned, and the fire severity is generally insufficient to volatilise Hg from the soil (only a small portion will be emitted). Therefore, the EFs calculated here are likely to be good indicators of Hg emissions from prescribed burns.

Firefighters exposure to mercury during prescribed burns

Firefighters attending prescribed or wildfires are potentially at risk of exposure to Hg released into the smoke plume. Elemental mercury vapour (Hg^0) is the dominant species emitted within the smoke plume and can pose severe health risk if inhaled in high enough levels.

In an attempt to quantify the potential risk to firefighters while attending a fire, personal CO monitors were attached to firefighters attending prescribed burns across Australia. These monitors were used as proxies to calculate potential Hg exposure as detailed in Appendix E. Despite the better correlation observed between CO_2 and Hg, personal CO_2 monitors were not available to be deployed during prescribed burns. Therefore, exposure calculations relied on the data collected with the personal CO monitors.

Overall hourly average concentrations were low with an overall average of 8 ng m^{-3}, well below the World Health Organisations (WHO) standard of 1000 ng m^{-3}. Peak one-minute average Hg concentrations were at times significantly higher than the calculated hourly averages, reaching a maximum of 683.4 ng m^{-3}. While the peak values are still below both the Work Safe Australia standards (25,000 ng m^{-3}) and WHO exposure standards, they have the potential to pose significant health risks since 80% of the Hg inhaled is absorbed into the lungs where it is then transported around the body.

The cumulative impacts of Hg exposure levels need also be taken into consideration. In fact, while exposure to Hg do not put firefighters at immediate danger of Hg poisoning, the concentrations are still adding to the other toxins they are exposed to, reducing their overall health.

No comprehensive studies have been undertaken to date that looks at identifying exposure of firefighters to Hg while attending fires. The preliminary study undertaken as part of this report suggests that firefighters could potentially be at risk of Hg exposure both from spikes in Hg concentrations during a fire and the possible cumulative effects over the course of a fire season.

Population exposure to mercury emitted during fires

Mercury has a long atmospheric life time (3 to 12 months) that allows it to travel great distances before being deposited back into an ecosystem. To investigate potential population exposure, the Tasmanian January 2016 bushfires were chosen as a case study.

Hg emissions were modelled using the CSIRO CTM and an Hg EF of 58.1 µg kg^{-1} (Table 7, all fires continuous data). Model parameters were adjusted to incorporate the mechanisms and chemistry specific to Hg in the atmosphere *(Nelson et al. 2012)*. Average Hg emissions over the entire modelled period are displayed in Figure 15. The Hg emitted during the fire was quickly dispersed into the atmosphere and concentrations significantly decreased with distance from the fire. As the Hg emissions for this fire event were established using EF calculated from the pyrotron experiment, only emissions from leaf litter were considered. The severity and duration of the Tasmanian fires would have produced higher emissions than shown here as there would also have been contributions from the soil.

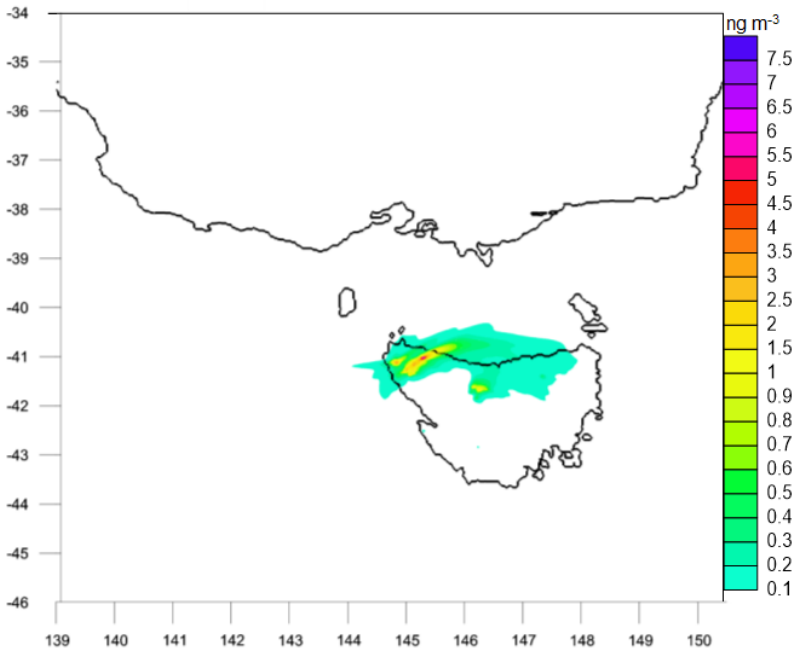

Figure 15 Hg concentrations from the January 2016 Tasmanian fire event. Concentrations are presented for four days during the event modelled using the CTM

The Lancefield, Victoria Bushfire was a moderate intensity fire which initially started as a prescribed burn that broke containment lines. The Lancefield fire was located approximately 60km north of Melbourne's CBD and as can be seen in Figure 16 the smoke plume covered most of this heavily populated region. Maximum concentration was measured at 0.00096 ng m^{-3}, significantly lower than the Tasmanian fire concentrations and the WHO Hg thresholds.

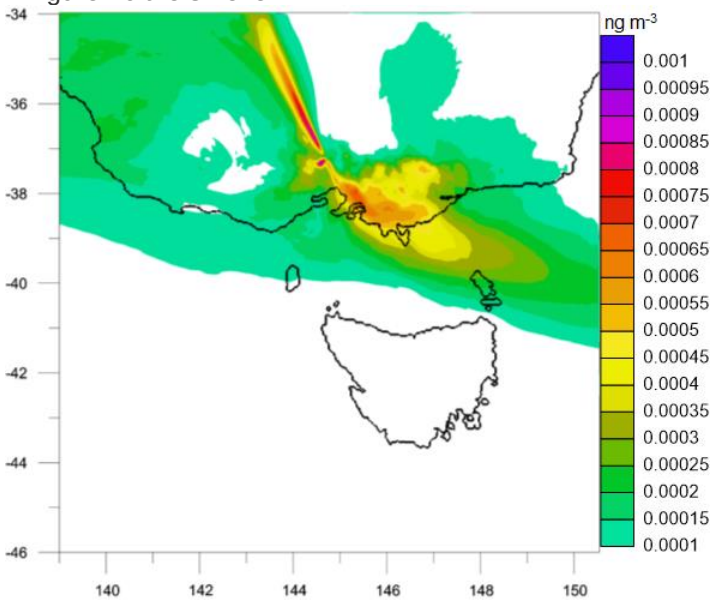

Figure 16 Lancefield October 2015 bushfire. Figure shows the average emissions across the duration of the fire.

Fire Radiative Power (FRP), Fire Radiative Energy (FRE) and Their Potential Role in Smoke Transport Modelling.

Fire Radiative Power (FRP) is defined as a measure of the rate of radiant heat output from a fire *(Roberts and Wooster 2008)*. It has been demonstrated by *Wooster et al. (2005)*, in small-scale experimental fires, that the FRP is related to the rate at which fuel is being consumed. *Freeborn et al. (2008)* have also shown how FRP is related to smoke emissions released. *Roberts and Wooster (2008)* explain that this is the direct result of the combustion process, whereby carbon-based fuel is oxidised to CO_2 (and other compounds) with the release of a certain heat yield. Therefore, measuring FRP and then integrating it over the whole fire provides an estimate of the total Fire Radiative Energy (FRE), which for bushfires should be approximately proportional to the total mass of fuel biomass consumed. It therefore follows that FRP/FRE provide a possible path towards more directly operationalizing smoke transport models, rather than more indirectly via assumed fuel loads and combustion factors. See as an example the relationship (Figure 17) between FRE and measured biomass combusted, established during a field experiment in savannah Africa.

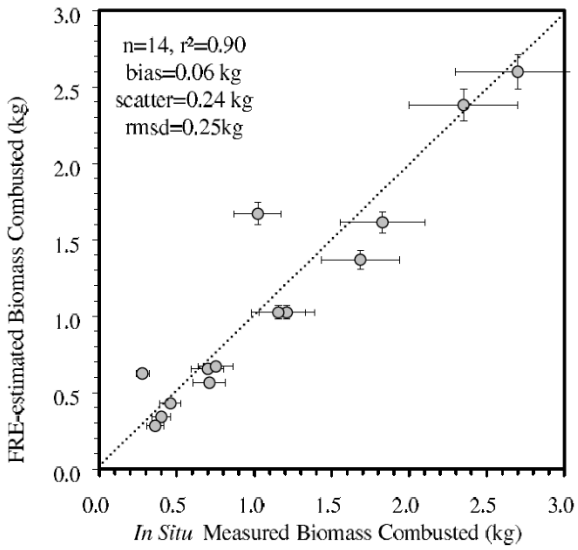

Figure 17. The relationship between biomass consumed and FRE in savanna Africa *(Roberts et al. 2005)*

Within the funding arrangements for our larger smoke transport-modelling project, Monash University was sub-contracted to

1. Undertake a comprehensive review of the current techniques and applications of FRP for determining fire intensity and fuel consumption rates, for possible application to Australian temperate forest fuels; and

2. Undertake a preliminary field experiment to evaluate the potential for using FRP/FRE to estimate emissions for a first time in the SE Australian context.

The review is attached to this report as Appendix F. This literature review highlights the pressing need to evaluate techniques for the direct measurement of fire intensity and heat output for Victorian vegetation for a range of possible purposes including plume rise and emissions calculations. The field experiment was planned, as far as possible, to address the key recommendations of the review. The key objectives of the field experiment were to

a. Determine the heat loss processes from one (or more) SE Australian biomass (forest) fire(s) and in particular the partitioning between radiation (that can be remotely sensed from satellites/aircraft), sensible, latent and soil heat. *This is a more complete specification of total fire energy than has been possible in similar previous work.*

b. Compare/validate measurements of FRP/FRE between satellite, aircraft and surface observations, where possible.

c. Compare/validate overall heat release rates with other estimates (e.g. PHOENIX Fire Model) for improved plume rise calculations.

d. Initiate preliminary evaluation of the relationship between FRE and biomass combustion for SE Australian fuels. *FTIR observations would be integral for this.*

Discussions between the project team and DELWP identified that a planned burn scheduled for the Pumphouse area of Wombat State Forest in October 2015 would provide the best opportunity for a full range of relevant measurements to take place. Accordingly a 30 metre eddy covariance tower collecting a full set of relevant radiation and heat flux data

(mostly at 10 Hz) was established at latitude 37° 29' 21.858"S, longitude 144° 12' 58.092"E in the last week of September 2015 (see Figure 18).

Figure 18. The 30 metre eddy covariance tower erected on a concrete pad in Wombat State Forest, September 2015.

The Monash University research aircraft, instrumented for visible, thermal and multi-spectral measurements was placed on standby so that ideally flux tower data, aircraft and satellite observations could be co-ordinated with the planned burn and associated surface observations. Unfortunately, for weather and operations-related reasons, the burn did not take place during spring 2015. The tower was decommissioned for the following summer and then re-commissioned for autumn 2016 and subsequently again for spring 2016. The burn has still not taken place (December 2016), so the tower has been decommissioned once again until autumn 2017. The system will require complete reconditioning before the autumn 2017 planned burning season in order to assure quality data acquisition. Provided appropriate measurements can be made, Monash University will provide a short supplementary report addressing objectives a-d (above) by mid 2017.

Part III Modelling system components-

As mentioned previously, the modelling system is comprised of three tiers (Figure 1).

1. Tier 1 generates forecasts of general and fire weather parameters (i.e. FFDI, GFDI), median and uncertainty, out to 10 days for advising on periods suitable for prescribed burning and avoiding periods of potential bushfire hazard.

2. Tier 2 generates regional air pollution forecasts out to 3 days for airshed capacity management.

3. Tier 3 generates high resolution fuel reduction smoke forecasts out to 24 hours for advising on the likely individual impact and combined airshed loading of smoke from a proposed program of fuel reduction burning.

Within this framework, the BOM's ACCESS operational weather forecasts will drive the system, providing ensemble forecasts out to 10 days at the global scale (~40–60 km grid spacing); single 72 hour forecasts at the Australian scale (~15 km); and 24 hour forecasts at the city scale (~3 km). Figure 19 shows BOM's current suite of operational weather forecasts. Note that the Tier 1 smoke-weather forecasts are generated using BOM's (currently pre-operational) ACCESS global ensemble prediction system (ACCESS-GE). The Tier 2 regional pollution forecasts are driven by the ACCESS-R and ACCESS-C products; and the Tier 3 fuel reduction forecasts are driven by the ACCESS-C outputs.

Tier 1. Ensemble fire weather forecasts out to 10 days

An ensemble prediction system (EPS) consists of a large number, or ensemble, of possible weather scenarios to simulate the actual forecast uncertainty from which probabilities of high impact weather can be estimated. When averaged together or treated as a distribution, this will lead to more accurate forecasts and quantitative estimates of uncertainty and potential worst-case scenarios.

Figure 20 illustrates how an ensemble is generated using multiple sets of initial conditions (each with equal likelihood within the uncertainty of the analysis) to then generate forecasts. A large spread in the forecast conditions indicates strong sensitivity to the uncertainties in the initial conditions and thus large uncertainty in the forecast. A small spread indicates a more predictable weather pattern resulting in only a small sensitivity to uncertainties in the initial conditions and a higher degree of confidence in the forecast products.

ACCESS-GE provides advanced warning of high impact weather and its uncertainty from a few hours out to 10 days, covering the entire country. This type of forecast for chance of rain, floods, wind, thunderstorms, tropical cyclones, bushfires, and other high impact weather events enables more informed risk analysis and decision making for government agencies, the public, and weather-sensitive industries such as agriculture, tourism, energy, health, and off-shore industries. In particular, emergency event managers receive specific advice on the likelihood and severity of impending weather events that may endanger the population and critical infrastructure, enabling them to more effectively mobilise resources well in advance of an event, and take action based on the most recent detailed predictions.

The ACCESS global ensemble has been running daily for several years (since 2009). Currently ACCESS-GE is running pre-operationally at (nominally) 60 km grid spacing, generating a suite of 24 global 10-day forecasts.

Figure 21 shows how the ACCESS-GE output can be processed to generate spatial plots which (for example) indicate the probability that the threshold of a particular metric (i.e. 10 m wind speed) will be exceeded.

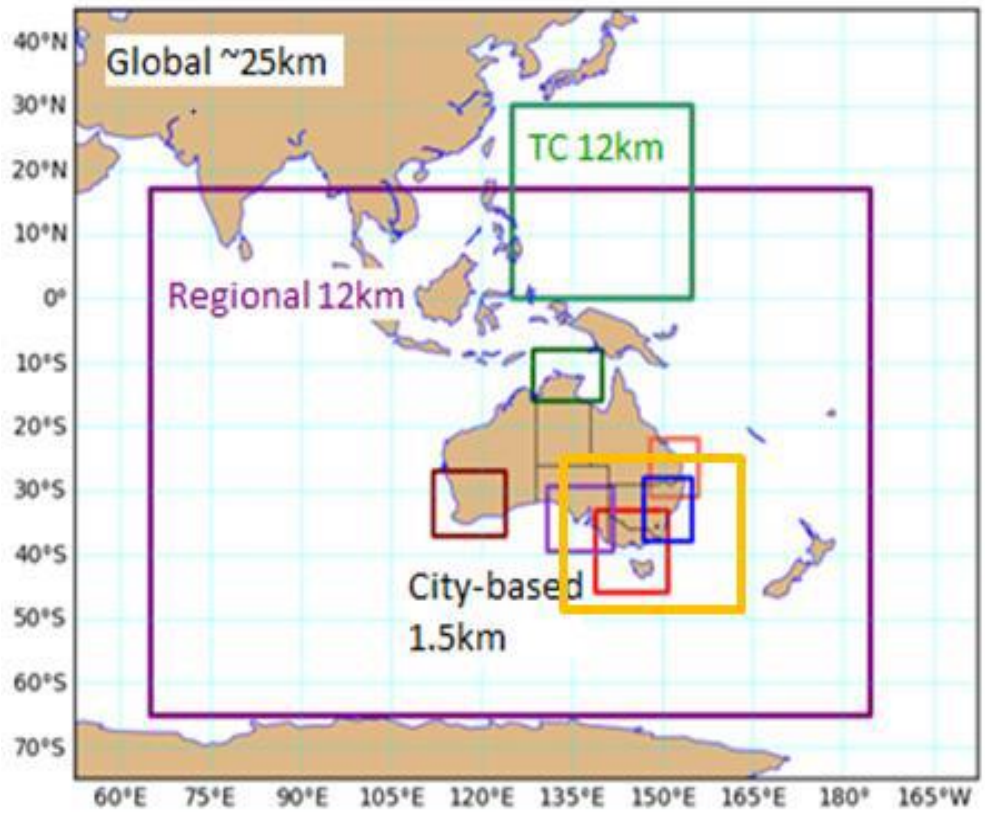

ACCESS weather model domains

Figure 19: Modelling domains for the Australian Community Climate and Earth System Simulator (ACCESS) numerical weather prediction system.

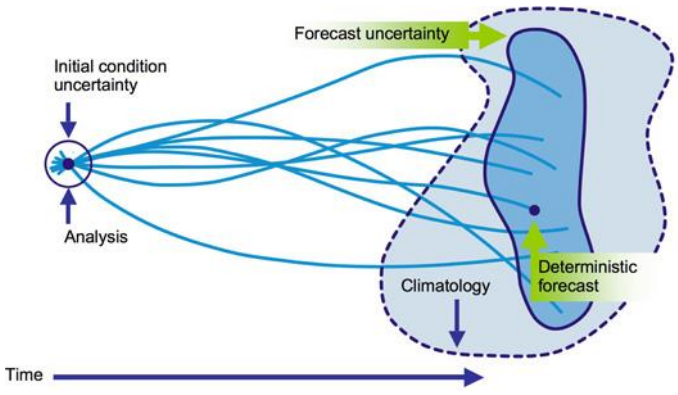

Figure 20 Schematic diagram showing how the forecast uncertainty increases over time.

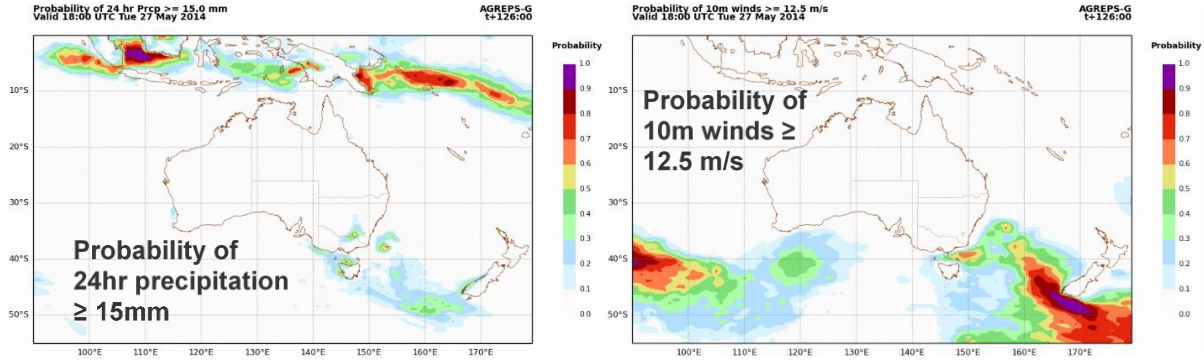

Figure 21: Example of ACCESS-GE spatial probability products for 24h precipitation and 10m wind speed.

A very useful representation of an ensemble forecast for a particular variable of interest is as an "EPSgram", which is a time series over the full range of the forecast of expected (mean and median) values of the variable and its associated uncertainty. Figure 22 shows a set of EPSgrams for a site in Sydney. The uncertainty is plotted using standard box and whiskers format with the 25th to 75th percentile (box) and full range (whiskers) of the distribution of the variable shown every six hours throughout the forecast. For example, the uncertainty of the forecast 10 m wind speed in Figure 22 is seen to be relatively small for the first four days of the forecast. After that the uncertainty grows more rapidly, and by the 9th and 10th days the uncertainty dominates the forecast.

ACCESS-GE forecasts of meteorological variables can be used to compute values of FFDI and GFDI. Forecast daily values of drought factor, fuel load and curing required by FFDI and GFDI are supplied from the Australian Digital Forecast Database (ADFD). This enables Tier 1 generation of EPSgrams of FFDI and GFDI and spatial probability charts of FFDI and GFDI exceeding critical thresholds. Ensemble plots of wind direction have been added, providing a very useful guide for wind direction and its uncertainty. Examples of these products are shown in Figure 23.

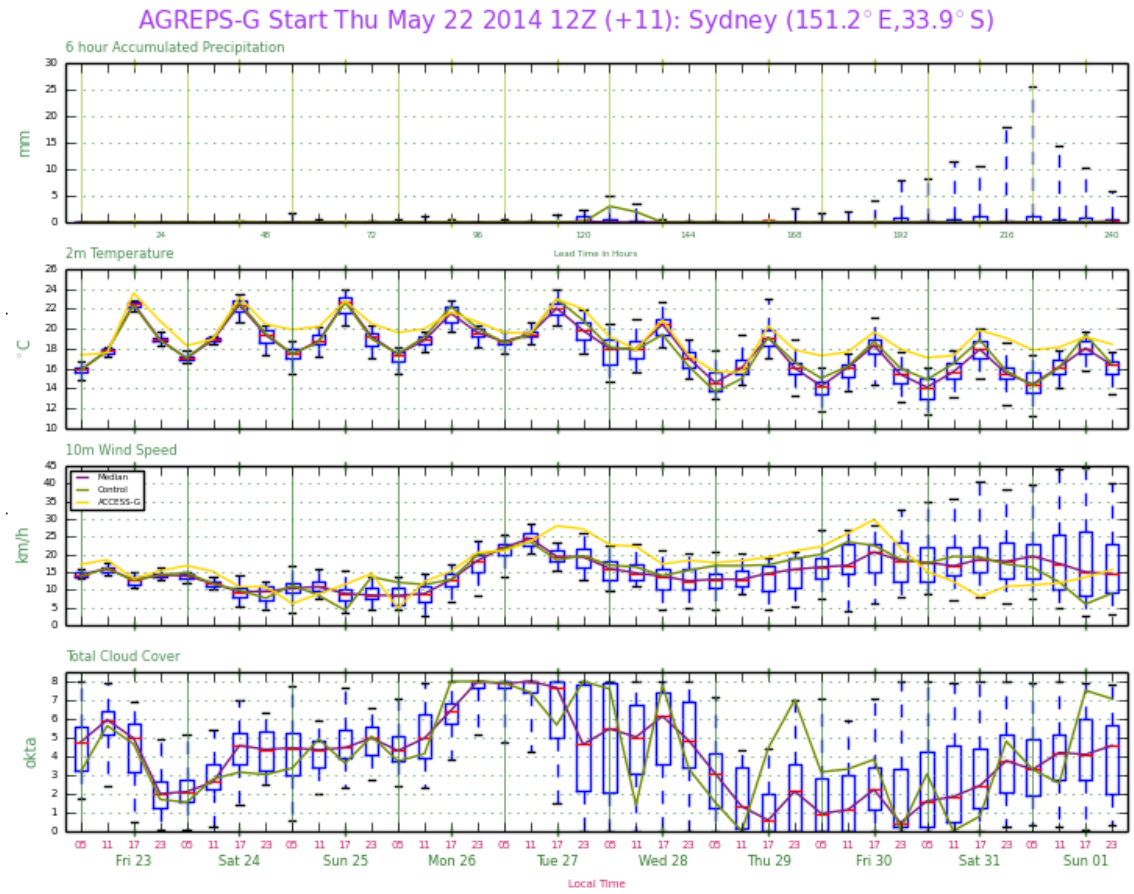

Figure 22: Example of Ensemble Prediction System meteograms (EPSgrams) for precipitation, temperature, wind speed and cloud cover. The forecast is for 10 days. Median and statistical variability is displayed.

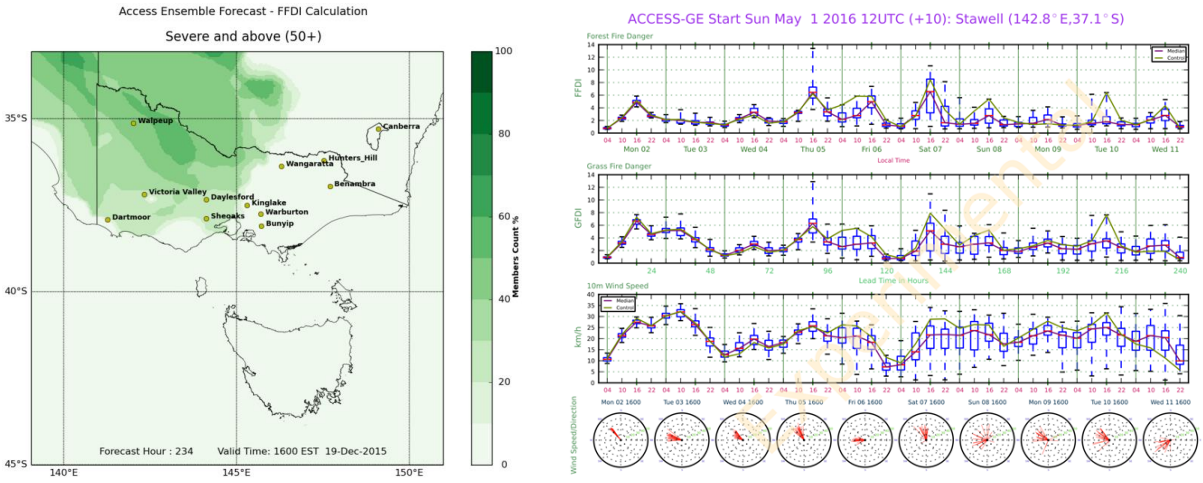

Figure 23 Ensemble 9-day probability forecast for FFDI exceeding 50 on 19 December 2015 (left) and EPSgrams of FFDI, GFDI, wind speed, and wind direction at Stawell for a 10-day period starting on 1 May 2016 (right).

The Regional Air Quality Prediction System for Tier 2 and 3 applications

The regional air quality prediction system is purposed with generating 24–72 hour forecasts of fine particles and fine particle precursors for the Australian region. Its purpose is primarily three-fold- 1/ to generate the background fine particle loading within a region which may be subject to prescribed burning; 2/ to forecast over-the-horizon events (i.e. inter-regional transport of aerosol pollution) which are likely to impact in the Victorian region within the forecast period; 3/ to run Tier 3 tracer forecasts at high resolution for prescribed burns.

Figure 24 shows a schematic diagram of the regional air quality forecasting system consists of the following components.

- Meteorological forecasts- here ACCESS-R and ACCESS-C, ACCESS-C2 as provided by the Bureau of Meteorology.

- Anthropogenic and natural emissions of particles and particle precursors. Included in the module are the Victorian and NSW air pollutant emission inventories *((Delaney and Marshall 2011)*, https://www.epa.nsw.gov.au/your-environment/air/air-emissions-inventory/air-emissions-inventory-2008); sea salt emissions, dust emissions and the biogenic emissions of volatile gases for the subsequent generation of secondary organic aerosol.

  In the case of fires, emissions for the greater Australian region are generated from Sentinal hotspots or a real-time ECMWF product. For Victoria, emissions are generated from DELWP active fire data, and the Phoenix FireFlux modelling system.

- Chemical transport and particle process modelling. In this module, aersol and gaseous emissions are transported and optionally react with other compounds. Particles can optionally nucleate, coagulate, grow and age. Losses of both particles and gases occur through wet and dry deposition.

The forecast pollutant concentrations are post processed and linked to various output platforms for interpretation, and for model verification.

Figure 24 also demonstrates how the model is able to be run at multiple scales. For the Tier 2 regional scale forecasting, the Austalian region is simlated at about 27 km grid spacing; the south-eastern states at about 9 km grid spacing; and Victoria at about 3 km grid spacing. Tier 3 modelling uses a 1 – 3 km resolution grid depending on the application.

Figure 25 demonstates the importance of considering the emission and transport of pollution from all regions of the Australian continent when generating forecasts of local airshed loading for prescribed burning. This is particulary relevant for $PM_{2.5}$ because fine particles have a negligible gravitational settling velocity, and few significant destruction pathways other than wet deposition. Thus, it is not uncommon for long periods of dry summer conditions to be associated with a build up of fine particle haze.

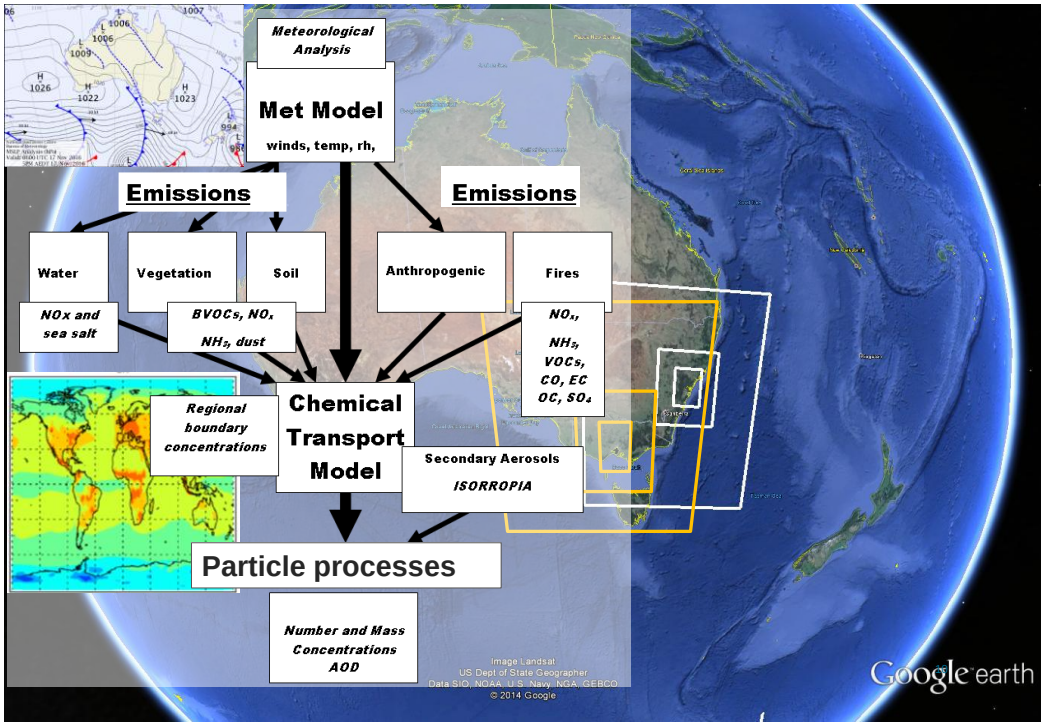

Figure 24. Schematic diagram showing the structure of the regional air pollution forecasting system. Also shown are a series of nested domains run by the model (outer domain covers the area of the Google earth map. Note- ISORROPIA refers to a methodlogy for modelling seconday inorganic aerosols, AOD- aerosol optical depth; BVOC biogenic volatile organic carbon; OC- organic carbon; EC- elemental carbon.

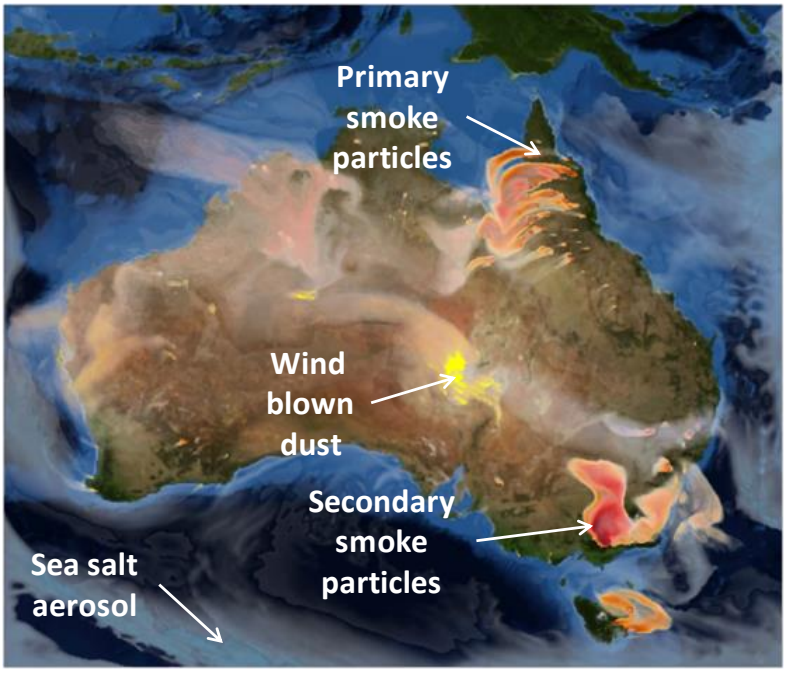

Figure 25. Regional modelling simulation of sources of fine particles ($PM_{2.5}$) across Australia. The slide is taken from a simulation of December 2006 and included emissions from the Victorian Alpine Fires. The plot demonstrates the importance of inter-regional transport of fine particles and also the potential for particles to be generated from multiple source types.

Fire behaviour modelling

This section summarises the work undertaken by the University of Melbourne to predict information about smoke and heat emissions from bushfires and planned burns. For both bushfires and planned burns, it is important to predict the rate of heat release and the rate of smoke emissions. Heat release affects the rate at which the plume rises vertically, which has a significant effect on smoke concentrations downwind of the fire *(Lee and Cope 2014)*. Current practice for forecasting smoke in Victoria includes a combination of manual methods *(Walsh 2014)* and automated tools *(Wain and Mills 2006)*. However, these systems do not include quantitative calculations of the smoke emission rate, which depends on the rate of progress of the fire and the rate at which fuel is consumed.

This problem is addressed by using fire behaviour modelling (PHOENIX FireFlux) to estimate the rate of fuel consumption, and consequently the rates of smoke and heat release. This approach can be applied to fires that have ignited but not finished burning, as well as fires that have not yet been ignited. It can also be adapted to support the prediction of different scenarios, for example by using a range of different weather forecasts to drive the fire prediction model. A simplified outline of the system is shown in Figure 26.

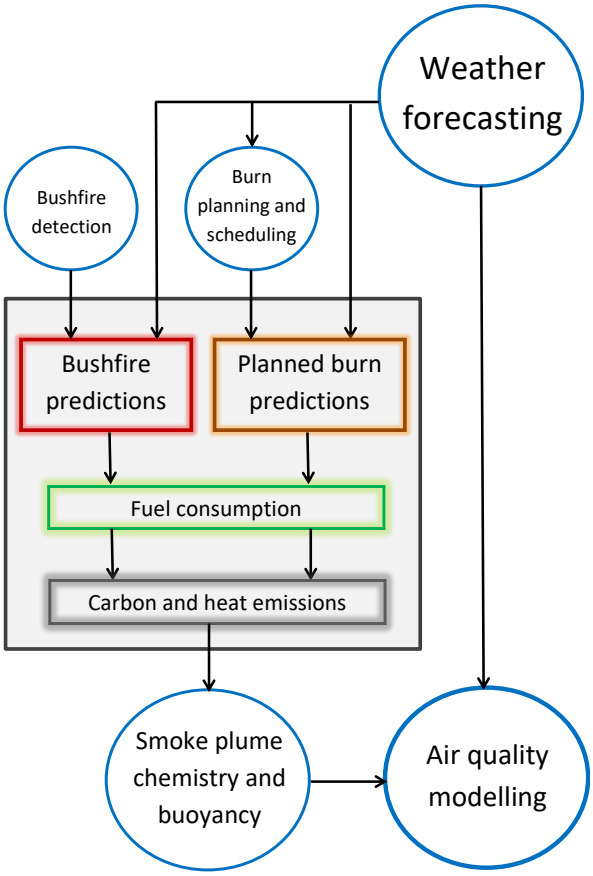

Figure 26. Simplified diagram of the smoke forecasting system. The box indicates the scope of the work described in this section.

Integration of fire prediction and smoke modelling

For modelling bushfires, this project has used an established Australian fire propagation system, PHOENIX RapidFire *(Tolhurst et al. 2008)*, which was incorporated into the FireFlux system. To track the rate at which fuel is consumed in a fire, the model was extended to record details of the incremental area burnt after each time step of the model. Within that area, the consumed fuel is counted, assigned a time and location and a sequence of data on fuel consumption throughout the duration of the simulated fire is generated.

For planned burns, there are no established models that can perform an equivalent prediction. PHOENIX was designed and calibrated for high intensity, fast-moving bushfires, and has not been evaluated for low intensity planned fires. Also, fire propagation modelling is not yet suitable for predicting smoke emissions from future burn, mainly because detailed ignition decisions are made on the day of the burn in response to local weather conditions. For this reason, a specialised simulator for planned burns was developed *(Walsh et al. 2015)*. The objective is to compute the carbon and heat emissions rates from bushfires and planned burns.

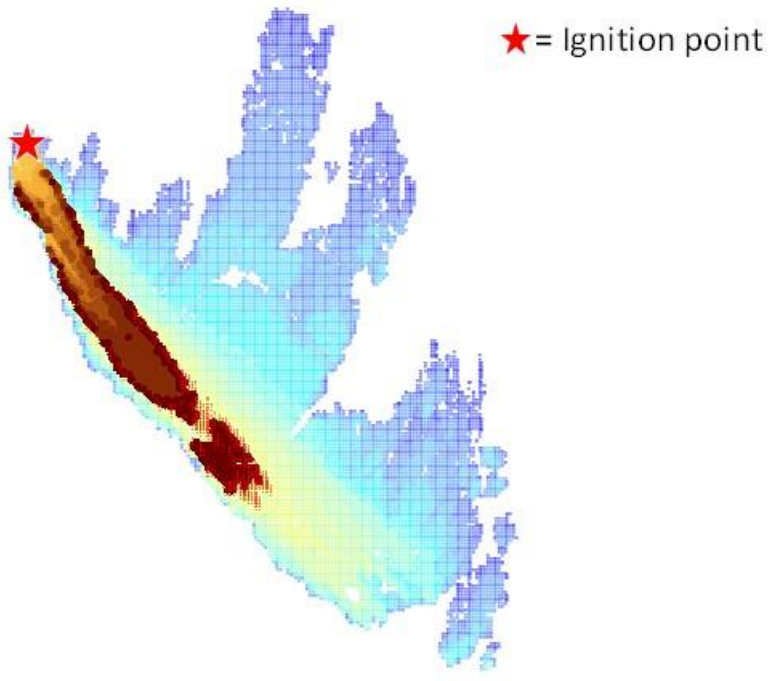

Figure 27. PHOENIX simulation of the Kilmore East Fire on 7th Feb 2009 *(Walsh et al. 2015)*. Fire activity to 4:05 pm is shown in brown, and fire activity from 4:05 to 4:14 pm (one time step) shown in red.

Model development

Bushfire emissions model

The PHOENIX bushfire simulator was used as the basis for building a model of carbon and heat emissions from active fires. Some extensions and modifications were made to the software to compute a time sequence of fire emissions. At the end of each model time step, all the area burnt during that time step is identified (Figure 28), and the total amount of fuel consumed in this area is calculated. The amount of fuel consumed is then converted into carbon and heat emissions data and assigned a location and time.

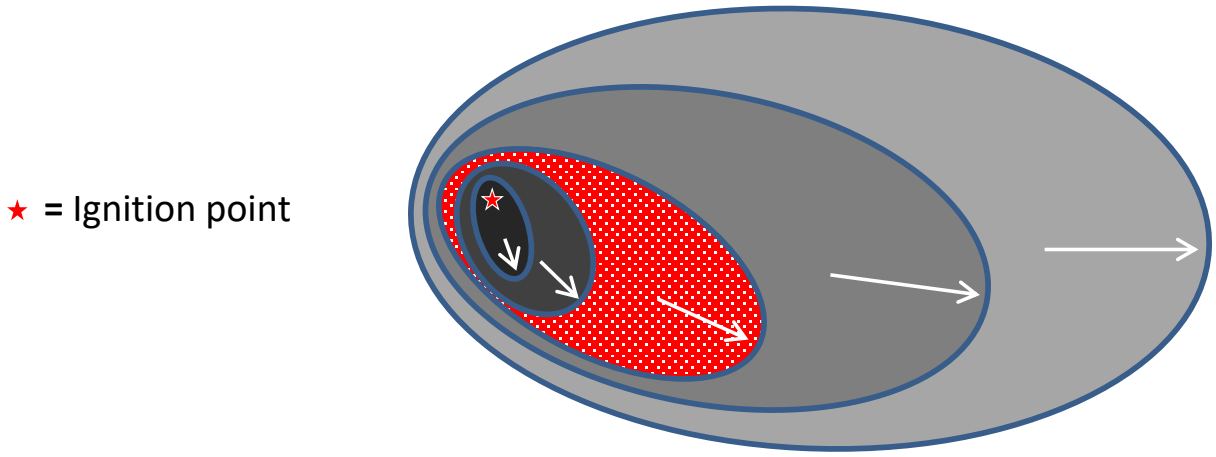

Figure 28 Time steps in a PHOENIX fire simulation. The highlighted area (in red) represents the area burnt during one time step.

The total amount of fuel consumed at a point in the landscape is a dynamic calculation, dependent not only on the fuel load (a function vegetation type and time since last fire), but also on weather forecasts (curing and drought factor) and fire behaviour (as flame height determines which vertical forest strata are consumed).

The amount of carbon released to the atmosphere is calculated by multiplying the fuel consumed in each forest stratum by a carbon mass fraction, while the amount of heat released is determined by the amount of fuel consumed multiplied by a Heat Yield value (H).

Planned burn emissions model

Very few models have been developed for simulating planned burns in a manner that would allow the calculation of fuel consumption and smoke emission rates during the burn. In Australia, the National Pollutant Inventory provides a simple technique which uses an average forest fuel load, the expected burn area and emission factors to estimate total emissions for specific pollutants *(EA 1999)*, but not the rate of emissions during the burn.

Given the lack of suitable models, a custom planned burn simulator was developed for this project. Some key components of the PHOENIX RapidFire software (including fuel, topography, and weather) were used as the starting point for this development. A burn simulation is able to generate estimates of total fuel consumption and hourly rates of carbon and heat release, as well as maps of the predicted burnt area. Carbon and heat emissions are calculated from fuel consumption in the same way as for bushfires.

The burn simulator was tested against a case study (Henderson Creek, Otway Ranges, Victoria, burnt in March 2012) for which detailed ground-based and satellite observations have been made *(Loschiavo 2012)*. The simulator was found to perform well in determining the spatial pattern of burnt area (see Appendix G).

Table 8 shows the total carbon and heat emissions predicted for the Henderson Creek burn. For comparison, results are also derived using the default fuel loading for forests in Victoria (7.22 t/ha) in the National Pollutant Inventory (NPI) Emissions Estimation Manual *(EA 1999)*. For the NPI-based calculation, a 50% burn coverage was assumed, and commonly used values were chosen for carbon fraction (0.5) and heat yield (18,700 kJ/kg).

Table 8. Comparison of predictions with a simple NPI-based method

	PHOENIX FireFlux	NPI Emissions Estimation Manual
Total carbon emissions (t)	924	618
Total heat emissions (TJ)	33.9	23.1

In this case, the prescribed burn simulator gives higher results than the NPI method because the total available surface fuel load within the simulated burnt area (after accounting for the drought factor) was estimated at 11.3 t/ha, reflecting the long period of time since fire at this site, which had previously burnt in 1983.

Prediction uncertainty and model limitations

The emissions models presented in this study rely on an adequate representation of vegetation fuels, and on assumptions about which vegetation elements are consumed by fire and converted to carbon and heat. These limitations must be kept in mind when using the PHOENIX FireFlux system for predictions of carbon and heat emissions from fires.

Modelling the future development of a bushfire contains inherent uncertainties. This is partly due to uncertainties in the input data (such as weather forecasts and fuel loads), but also due to the highly non-linear nature of fire propagation, which can make simulations sensitive to initial conditions *(Dunn 2007)*. The model of emissions presented here considers only flaming phase fuel consumption, and only includes fine fuel *(Tolhurst and Cheney 1999)*.

The burn simulator is best suited to medium to large sized burns, where the ignition process is likely to follow a broad strategy

such as edge burning for fire management followed by ignition of the interior of the targeted area. For small burns which are intensively managed because they are close to residential areas or other sensitive land uses, the model is unlikely to be able to predict the pattern of burnt area because the effects of intensive human intervention is not included in the model.

A fundamental assumption of the burn simulator is that the Burn Coverage Objective (BCO) (specified in advance of the burn) will accurately reflect the proportion of area burnt within the boundary. The uncertainty associated with the coverage objective can be represented by running an ensemble of simulations with different BCO values.

The bushfire and prescribed burn emission models presented here are to be considered preliminary and approximate in nature, with significant future work required to determine model accuracy against experimental data. The accuracy and range of applicability of the models presented in this project may be enhanced through further development.

Key outcomes and findings

Achievments of this project component:

1. An established bushfire simulator was modified to generate information on carbon and heat emissions during the progress of a simulated forest fire or grass fire.

2. A new model was developed that uses fuel moisture calculations, forecast weather and end-user constraints to simulate the progress of a planned burn, allowing calculation of carbon and heat emission rates.

A number of knowledge gaps have been identified, including:

- The need for more comprehensive experimental data on overall smoke emission rates from Australian bushfires and planned burns, to support model verification.

- Further investigation is required into the potential variation in the net heat yield from burning forest fuels due to variations associated with fuel moisture content, differences between flaming and smouldering phases, and the dynamic effects of downward heat loss to soil and unburnt surface materials.

- The absence of records of the fine details of ignition strategies, including ignition patterns and timing for a realistic distribution of burn profiles is a limiting factor in the development of burn simulation models.

Smoke Emissions modelling

Fire emissions are estimated using the approach developed by *Seiler and Crutzen (1980)* in which the emission of a trace species i (E_i) is determined by the mass of fuel pyrolyzed (FP) and the emission factor for each trace species (EF_i).

$$E_i = FP \times EF_i \qquad (1)$$

The mass of fuel pyrolyzed is the product of the area exposed to fire (A), the fuel load (FL) and the burning efficiency (BEF) of the fuel type. For example, the BEF for fine fuels which pyrolyse through flaming will be higher than the BEF for the CWD in which pyrolysis occurs through smouldering.

The area exposed to fire is the area of the fire scar (A') corrected for the patchiness of the fire (P, *Meyer et al., 2012a*), i.e.

$$A = A' \times P \qquad (2)$$

The EFs (see main report/Appendix D) can be defined either relative to fuel mass pyrolyzed *(Andreae and Merlet 2001)* or relative to the fuel elemental content *(Hurst et al. 1994)*. Using the latter definition, the EFs of the carbon species, CH_4, CO and VOCs, are expressed relative to fuel carbon, which is determined from fuel mass by the fuel carbon content (CC_i). Combining these equations:

$$E_i = EF_i \times A' \times P \times FL \times BEF \times CC \qquad (3)$$

To a first approximation, the parameters EF_i, FL, CC are either functions of fire class, fuel size class (i.e. fine or coarse) or land use and therefore spatially variable but temporally stable (e.g.*(Russell-Smith et al. 2009; Meyer et al. 2012a)*). However, A', P and, to some degree, BEF are likely to be time dependent. Patchiness and BEF are partially dependent on fire intensity *(Russell-Smith et al. 2009)*, which in turn, is proportional to the rate of change in area. Hence all three time–

dependent parameters are likely to be determined by the fire growth rate and hence emission rate also will be directly proportional to the fire growth rate.

Given this background, we define the following system of equations to model smoke constituent emission rates from the pyrolysis of fine fuels and CWD.

$$dE_h^{ff}/_{dt} = EF_i \times P \times FL_{ff} \times BEF_{ff} \times CC \times \left(dA'/_{dt}\right) \quad (4a)$$

$$dE_h^{cwd}/_{dt} = EF_i \times P \times FL_{cwd} \times BEF_{cwd} \times CC \times \left(dA'/_{dt}\right) \times (1 - ho) + \ dE_{h-1}^{cwd}/_{dt} \times \ ho \quad (4b)$$

Here E_h^{ff} is the emission for species i (indice omitted for clarity) at hour *h* resulting from the pyrolysis of fine fuels within the flaming area of the fire scar. The fuel load FL_{ff} and burning efficiency is for the fine fuel content of the combustible fuel mass and EF_i is the emission factor resulting from the combination of gaseous and smouldering pyrolysis.

Equation (4b) describes the rate of emission of smoke species due to the smouldering pyrolysis of CWD as it is ignited in the flaming phase of the fire, and from CWD continuing to smoulder from earlier hours. Note that 4b has a similar form to 4a except that here the term dA'/dt is now taken as the rate of ignition of the CWD, and $(1 - ho)$ is the proportion of the CWD burning in the current hour and *ho* (the holdover) is the proportion of CWD left to burn in the following hours (see below).

The holdover is given by a simplified version of the decay or holdover equation used in the Fire Emission Product Simulator (FEPS; *(Anderson et al. 2004)*).

$$ho \ = \ 1/e^{1/RDR} \quad (5)$$

where the CWD resident time constant is given by *Anderson et al. (2004)*

$$RDR = k_{RDR}/(1 - e^{-1}) \quad (6)$$

and k_{RDR} is the RDR coefficient (k_{RDR} = 12).

The total smoke constituent emissions from both flaming and smouldering pyrolysis is given by the sum of equations 4a and 4b.

Note that the equation system given by (4) is effectively one-way coupled. That is, the rate of growth of the flaming proportion of the fire impacts on the rate of combustion of the CWD. However, the combustion of the CWD does not influence the rate of combustion of the fine fuels. This result is consistent with the Pyrotron results which demonstrated that constituent emission rates did not vary strongly with differences in the loading of fine woody debris at least.

Note that the emissions from both gaseous and smouldering pyrolysis are included in the fine fuel emissions to better align with the measurements undertaken during the Pyrotron and field campaigns in which the derived emission ratios were taken from observations of combined fine fuel flaming and smouldering. Additionally, it can be seen from eqn 4a that the carry-over of fine fuel emissions is not modelled. This simplification is used because the emission input time step of the chemical transport model is 1-hour and thus the assumption is made that the fine fuels are consumed within this time.

Figure 29 shows an example of the smoke emission model output for the Cobaw/Lancefield fire. In this example the burn has been modelled for a 10–day period. Fire behaviour modelling (based on both observed fire scars and PHOENIX simulations) demonstrate how the fire extent grew over the period of the episode (Figure 29- bottom right). The rate of change of the area burnt forms the term $dA'/_{dt}$ in equation 4. The fuel loads across the region of the fire (the terms FL_{ff} and FL_{cwd} in eqn 4) were taken from the database built for this study (Figure 29- bottom left) and were approximately 10 tonnes dry mass per hectare (fine) and 40 tonnes dry mass per hectare (CWD). EFs for CO were taken from the data collated in this study (average 65 g kg^{-1} fine fuel; 191 g kg^{-1} coarse fuel) and reflect the effect of the different MCE's associated with flaming and smouldering pyrolysis. We have simulated two burning efficiencies for the CWD (BEF_{cwd} in eqn 4b), 0.55 (being representative of bushfires) and 0.20 (being representative of planned burns) *(Department of the Environment 2014)*, and show the results from an earlier model in which flaming and smouldering combustion were not treated separately.

Figure 29 shows that the effect of including smouldering combustion from CWD can result in significant increases in the modelled CO emission rates, and a substantial increase in the time of smoke emissions following reductions in flaming combustion. The ratio of flaming to total emissions is shown for $BEF_{cwd} = 0.2$ and demonstrates that the emissions of CO from smouldering generally contributes more than 50% of the total emissions. The results show (as expected) a linear sensitivity to burning efficiency, with the $BEF_{cwd} = 0.55$ more than doubling the emissions from smouldering combustion. Speciated emissions from the smoke emissions module are written out in CTM point source format and are then available for input into the smoke modelling system.

In summary, a smoke emissions methodology (and associated software) has been generated which is coupled to PHOENIX and the Planned burn simulator (and is also coupled to other fire scar outputs based on ground survey and/or hot spot data). The software couples to the new fuel load data sets for fine and coarse fuels developed for the current project. For ambient fires outside of Victoria the software uses a fine and coarse fuel data set generated from VAST *(Barrett 2002)*. The software contains a small library of emissions for various fuel types. The library includes the data collected by the Pyrotron and field study experiments, and from a limited analysis of smoke constituent data collected at Cape Grim during the 2016 Tasmania landscape fires. An algorithm for modelling the smouldering emissions from CWD has been based on work done for FEPS, however has been simplified to be more representative of the data detail currently available in Australia.

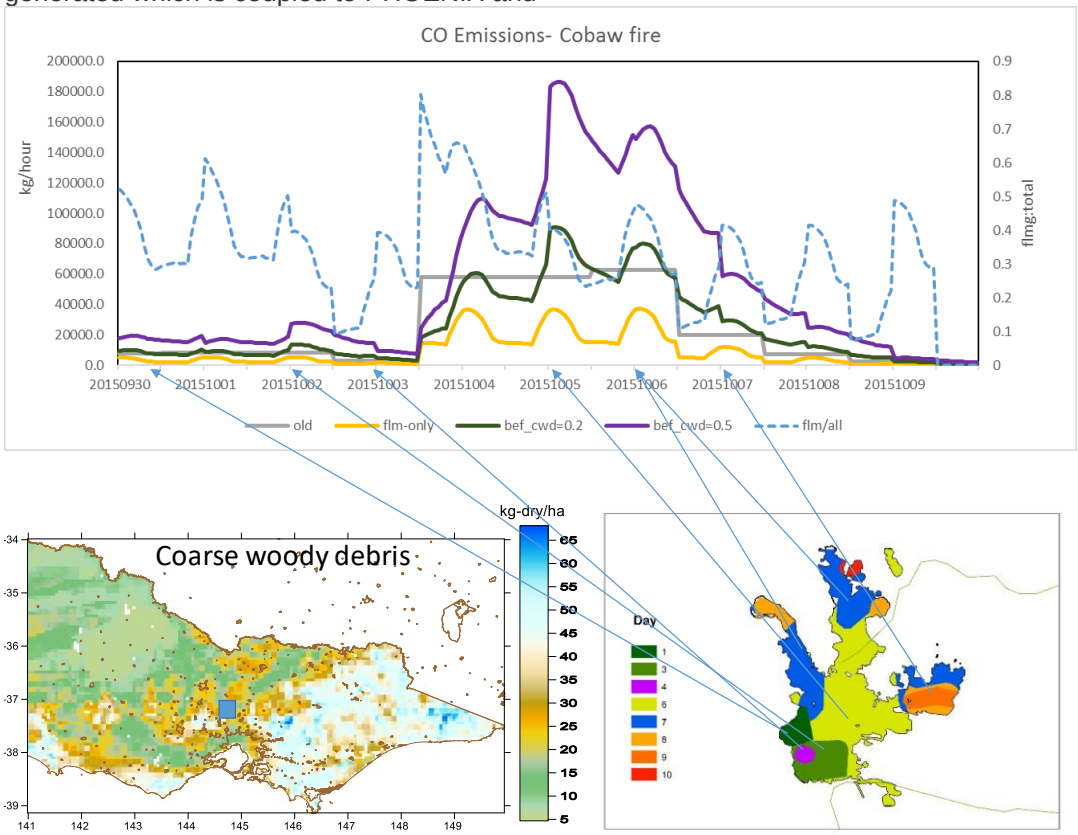

Figure 29 top- Time series plot of modelled CO emissions from the Cobaw fire, old- using VAST with combined flaming/smouldering emissions algorithm, flm-only- emissions from fine fuel pyrolysis only; bef_cwd=0.2 flaming + cwd smouldering with a burn efficiency of 0.2; bef_cwd=0.5- cwd burning efficiency of 0.5. Also shown is the ratio of CO emissions (flaming:total) for the bef_cwd=0.2 example. Bottom left- distribution of CWD; right- fire progression.

Part IV Case studies

In this section, three examples of the smoke forecasting system are summarised, with a focus on the Tier 2 and Tier 3 forecasting capabiliies.

2015 Lancefield-Cobaw fire (Tier 2 modelling)

On 30th September 2015, a 266 ha planned burn was ignited by DELWP in the Macedon Ranges approximately 10km west north west of the town of Lancefield. Three days later the burn breached its containment lines and burned for an additional 10 days covering 3,000 ha of farmland and state forest. The fire unfortunately caused damage to infrastructure and the local economy and triggered a State Government enquiry into the management of the fire.

The daily extent of the area burned by the fire was well characterised. Additionally, the smoke plume was observed by satellite and by the Bureau of Meteorology weather radar. The fire was observed to pass close to Melbourne (and the EPA Victoria monitoring network) and thus provided a useful candidate for testing our prototype smoke forecasting system. In this section, we present results from the Tier 2 modelling of the Lancefield–Cobaw fire.

Emissions

During the Lancefield–Cobaw fire DELWP and the CFA characterised the area burnt by the fire- generally on a daily basis. This information was then used to model the fire propogation rates- 1/ diagnostically using the daily change in area burnt; 2/ prognostically using PHOENIX to simulate the fire propogation over the next 12–24 hours. The area burnt, together with the fine and CWD fuel layers, were used to model the smoke emissions as discussed in the Smoke Emissions section above.

Figure 30 shows the daily and total emissions of carbon monoxide released by the fire and (for comparison) from the sum of all surface based anthropogenic combustion sources for Victoria (includes motor vehicle and commercial-domestic sources, however omits the large elevated industrial sources such as power stations).

Figure 30-top shows a typical diurnal variation of anthropogenic CO emissions resulting from motor vehicle usage, commercial and domestic sources, and ground–level industrial combustion sources. The morning and evening traffic peaks are evident in the plot.

The smoke emissions from the flaming component of the fire also have a significant diurnal component, which results from the drying of fuel, the reduction in moisture in the atmosphere, the deepening of the atmospheric boundary layer, and the increase in winds during the day.

The emissions of smoke from the smouldering of CWD show a weaker diurnal variation. In our smoke emissions model, CWD is ignited as the flame front propagates across the landscape- as thus follows the behaviour of smoke emissions from the ignition of fine fuels in the fire front. However, due to the lower burning efficiency of the CWD, smoke emissions continue for 2–3 days from each ignited area, thus leading to a smoothed diurnal variation in smoke emissions.

Additionally, because 1/ the mass of CWD can exceed that of the fine fuels by a factor of 3–4; 2/ the lower MCE associated with the burning of CWD leads to PM emission rates exceeding those from fine fuels by a factor of 2–3, the total emissions of fine particles from the smouldering of CWD can exceed the emissions from the flaming/smouldering of the fine fuels (Figure 30-bottom). Note that this result will also be influenced by the patchiness of the CWD ignition and day/night variations in the near-surface wind speed and relative humidity, with increased patchiness and reduced wind speed overnight leading to low CWD emissions.

Figure 30 also suggests that the carbon monoxide emissions from the the Lancefield–Cobaw fire totalled about one–quarter of the surface–based anthropogenic emissions of carbon monoxide in Victoria.

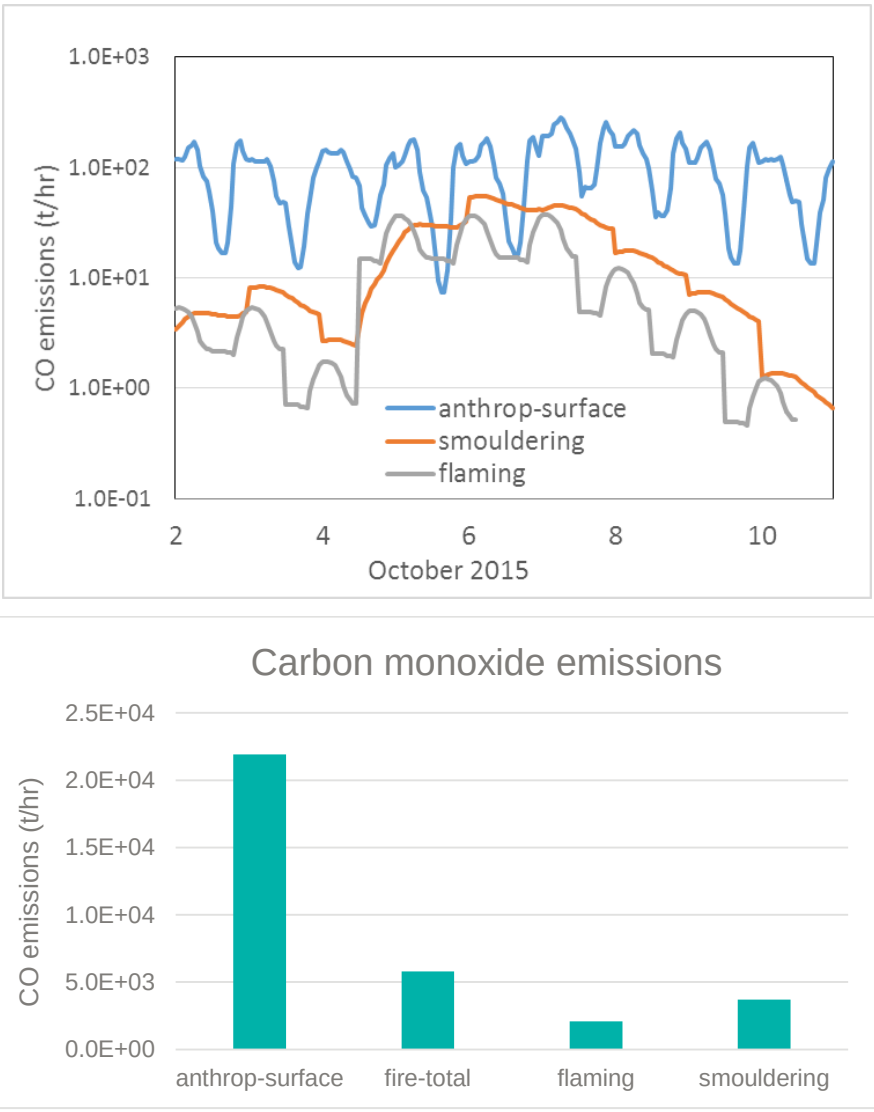

Figure 30. Modelled emissions of carbon monoxide from the Lancefield-Cobaw fire, and from the State-wide EPA Victoria air emissions inventory. The smoke emissions have been broken down into the flaming and smouldering components.

Plume transport

Figure 31 demonstrates how satellite data can be used to verify the presence of smoke emissions and smoke plume transport. In this example, observations from the Himawari satellite have been processed to generate a true colour field, with a pixel size of approximately 1 km and an update time of 10 minutes. The Lancefield–Cobaw smoke plume was clearly visible on the 7th October (note that the times below are in UTC thus add 10 hours for the equivalent local standard time).

The plots in Figure 31 are screen dumps from one of the experimental display systems used to view output from the smoke forecasting model. The left-hand column shows the modelled Lancefield–Cobaw plume (using elemental carbon as a surrogate for the plume smoke in this example) and the right-hand column shows the modelled elemental carbon emissions. The Himawari visible layer is also shown in each plot.

A band of cumulus clouds in the lower half of the domain is evident for hours 23 and 02 and the Lancefield–Cobaw smoke plume is being advected to the north in a south–easterly air flow. When using this information to qualitatively verify the smoke forecast, the key points to note are 1/ the presence of a fire has been correctly captured; 2/ the general good agreement between the observed and modelled transport direction.

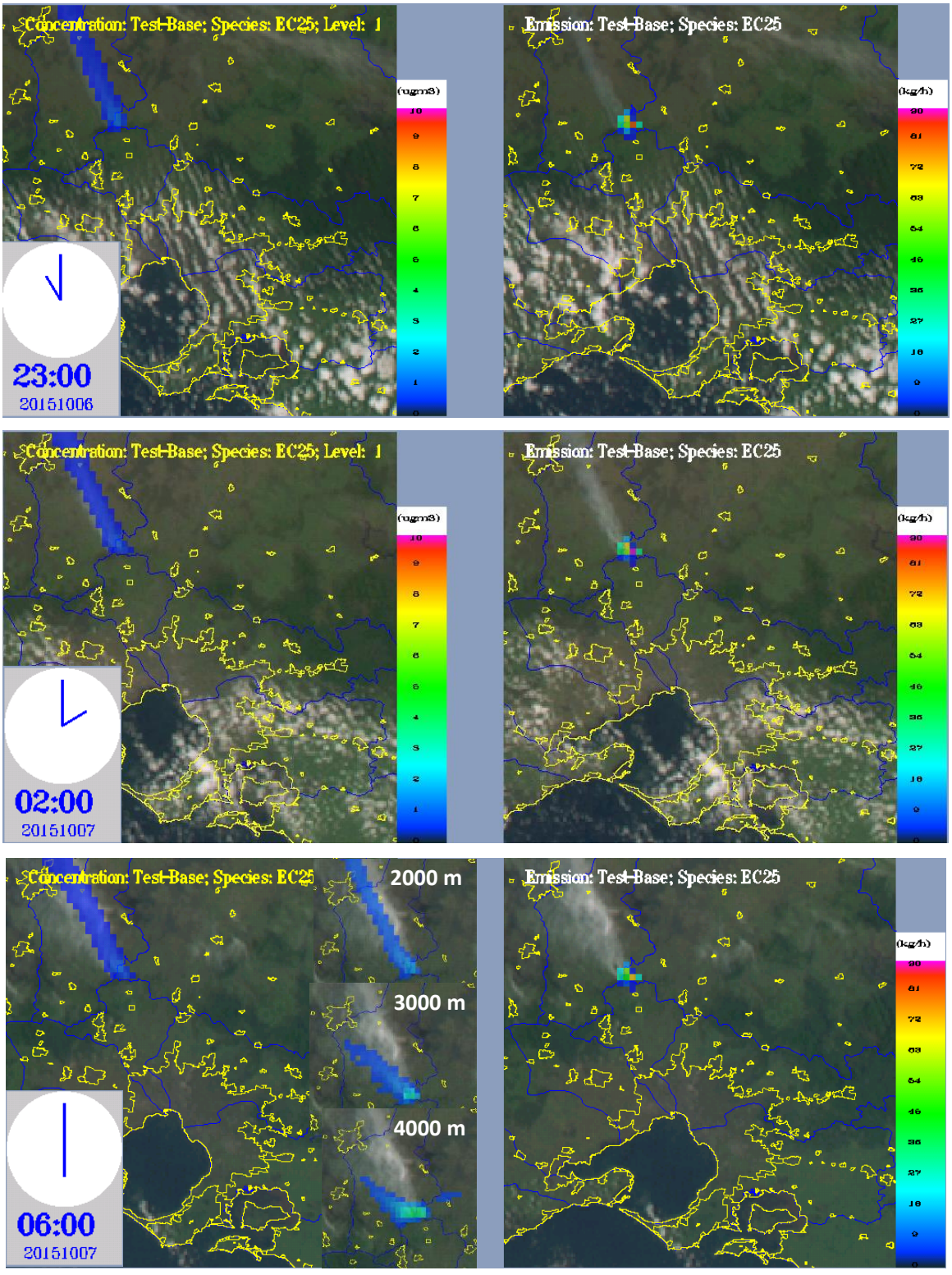

Figure 31 Comparison of forecasts and observed (Himawari satellite) smoke plume positions- 7th October 2015. The modelled model plume is shown in the left column. The observed smoke plume is shown in the right column. Also shown are the modelled Lancefield-Cobaw emissions (right). Note that the times are in UTC.

One final point to note is that the satellite images of the smoke are cumulative across the entire atmospheric column. On the other hand, the simulated smoke plume for hours 23 and 02 is representive of the near surface elemental carbon concentration (although it doesn't have to be only this level). While this works well for smoke plumes constrained close to the surface, or across deeper layers provided there is little horizontal wind share, it is important to consider the entire vertical extent of the smoke plume when the plume is buoyant and wind shear is present.

This is illustrated for hour 6 (16 LST) where it can be seen that the width of the Lancefield–Cobaw plume has increased relative to the earlier hours. The smoke plume simulation for this time suggests that the plume extends up to nearly 4000 m and that wind shear in the top half of the air column causes the plume to spread to the west.

Verification

The verification of forecast model performance can be undertaken at many levels. Two of the most important classes are as follows.

1/ Operational verification in which the performance of the entire forecasting system is tested through comparison of observed and modelled concentrations of ubiquitious ambient pollutants such and $PM_{2.5}$, PM_{10}, ozone, nitrogen dioxide and carbon monoxide.

2/ Diagnostic verification in which routinely available air quality and meteorological data together with more detailed data (i.e. such as the chemical components of $PM_{2.5}$) gathered during field studies can be used to verifiy the ability of individual modules within the forecasting system to simulate important processes. For example, how well does the forecasting system simulate the chemical ageing of bushfire smoke?

In this report the focus is primarily on the operational performance of the smoke forecasting system, although some diagnostic verification is also presented in the sections to follow. Figure 32 shows time series plots of observed and modelled (with and without smoke) 1–hr $PM_{2.5}$ for monitoring stations in the EPA Victoria network that measured $PM_{2.5}$ during the Lancefield–Cobaw fire. Time-space matching of modelled 1–hr $PM_{2.5}$ concentrations with observations is one of the most challenging tests of a forecasting system. However, it is useful because short term concentrations (here hourly average) can often yield useful insights into the processes leading to the observed $PM_{2.5}$ time series.

The time series plots for Footscray (FTS) and Alphington (Alp) monitoring station in Melbourne show that the forecasting system has been able to reproduce the day-to-day variation in $PM_{2.5}$ with quite good skill. Closer examination of these plots also suggests that the Lancefield–Cobaw smoke plume impacted the Alphington site on the 6th October, however the magnitude of the impact was small.

Time series plots are also shown in Figure 32 for Morwell East and Morwell South in the Latrobe Valley. These plots suggest that the forecasting system missed a $PM_{2.5}$ event on the 5th October but captured the remainder of the observed $PM_{2.5}$ time series. It is possible that the 5th October event was due to another fire, and that this source was not correctly represented in the forecasting system. For this case study, the CAMS– Global Fire Assimilation System (GFAS) (European Climate and Weather Forecasting Centre) global fire analysis was used to represent all Australian fires other than the Launcefield–Cobaw fire and, as with any satellite-based system, it is possible to miss fires when cloud cover are present, or the fires are small. This emphasises the need to provide the system with accurate information on the location and rate of growth of fires wherever possible.

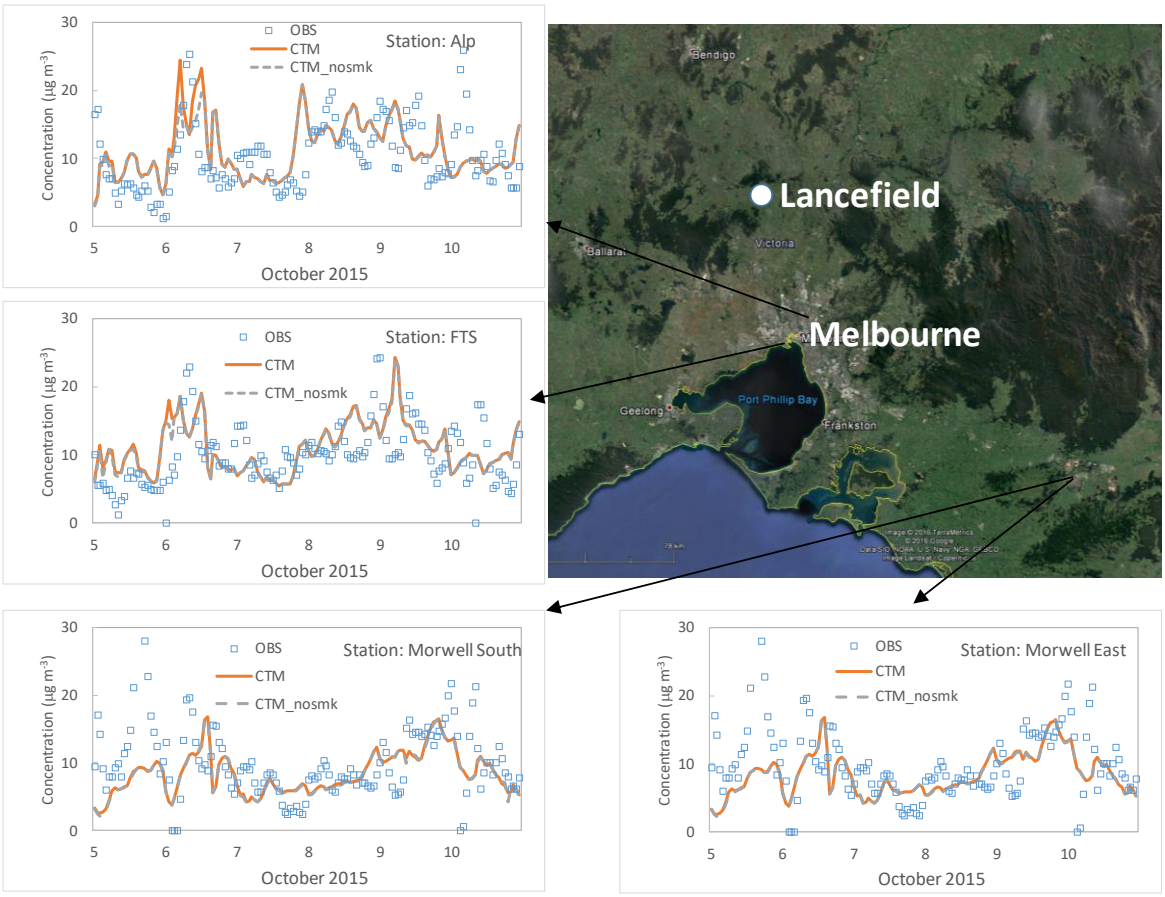

Figure 32. Time series plots of observed (blue squares) and modelled (orange line- with smoke; dashed-grey- without smoke) 1-h $PM_{2.5}$ EPA Victoria monitoring stations.

Figure 33 provides a useful summary of the forecast system performance for daily average $PM_{2.5}$. Daily (24–hr) average is useful to consider in the current context because the Federal government has established a National Environment Protection Measure (NEPM) Ambient Air Quality Standard (AAQS) of 25 µg m^{-3} for 24–h $PM_{2.5}$ and thus this can be used as an indication of compliance/non–compliance. The left-hand plot shows the observed and forecast 24–hr $PM_{2.5}$ plotted on a log-log plot with the parallel lines showing the region within a factor-of-two agreement, the NEPM AAQS for $PM_{2.5}$ and regions for which the forecast has successfully detected a $PM_{2.5}$ event (DT); missed a $PM_{2.5}$ event (MI); falsely forecast a $PM_{2.5}$ event (FA).

The left-hand plot in Figure 33 indicates generally good performance for the daily $PM_{2.5}$ forecasts, and also shows that all daily concentrations fell below the AAQS.

The other plots in Figure 33 ('bugle plots') show the mean fractional bias (MFB) and the mean fractional error (MFE), two commonly used statistics of model performance.

$$MFB = 100\% \times \frac{2}{N} \sum \frac{(M_i - O_i)}{(M_i + O_i)}$$

$$MFE = 100\% \times \frac{2}{N} \sum \frac{|M_i - O_i|}{(M_i + O_i)}$$

Here M_i and O_i are the i^{th} model–observation concentration pair (here coupled in time and space), and N is the number concentration pairs *(Simon et al. 2012)*.

Bugle plots are so named because they include criteria zones for model performance, which for low concentrations, expand to take into account the confounding effect of small differences between modelled and observed concentrations- thus the bugle shape. The bugle plots in Figure 33 suggest good performance by the forecasting system for the Lancefield–Cobaw fire simulations.

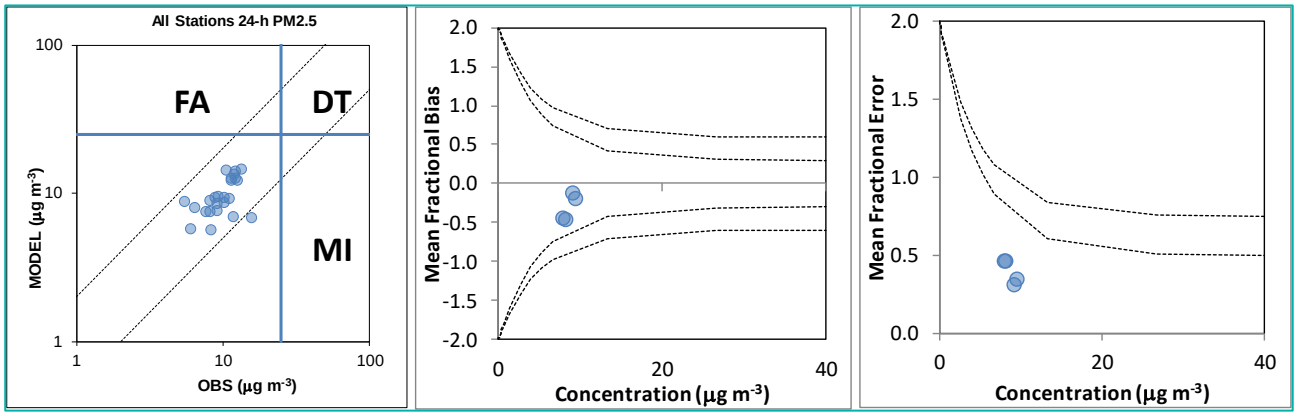

Figure 33. Left- scatter plot of observed and modelled 24–h $PM_{2.5}$. The blue line is the NEPM AAQS for $PM_{2.5}$. MI- missed event region; DT- detected region, FA- false alarm region. The parallel lines are ± factor of two. Centre- bugle plot showing the mean fractional bias of the simulation. The dotted lines correspond to a good performance goal (inner lines) and an acceptable criteria of model performance. Right- mean fractional error.

Analysis

In the Emissions section above, the magnitude of the Lancefield–Cobaw fire was quantified through comparison with the surface–level emissions of carbon monoxide from all anthropogenic sources in Victoria. Similarly, in the case of the downwind smoke impacts, there are various methods of quantifying the magnitude of a smoke plume impact.

1. The hourly, daily or episode peak concentrations;

2. the area in which peak smoke concentrations exceed a given standard;

3. the frequency with which smoke concentrations exceed a given standard;

4. the cumulative health impacts derived using relative risk factors and population exposure estimates.

The analysis of smoke impacts presented in this report is restricted to the consideration of the area in which the NEPM AAQS for $PM_{2.5}$ is exceeded, and the frequency with which the AAQS is exceeded-summed across the length of the smoke event simulation. Figure 34 illustrates this approach for the Lancefield–Cobaw fire forecast which suggests that there is a small region close to the fire in which the AAQS for $PM_{2.5}$ is exceeded, and that the standard was exceeded on 7 days. Note too that the plots in Figure 34 are for a small part of the Vic–Tas 3 x 3 km^2 resolution forecasting domain. The effective resolution of this domain can be seen from the blown-up section in the right-hand plot of Figure 34.

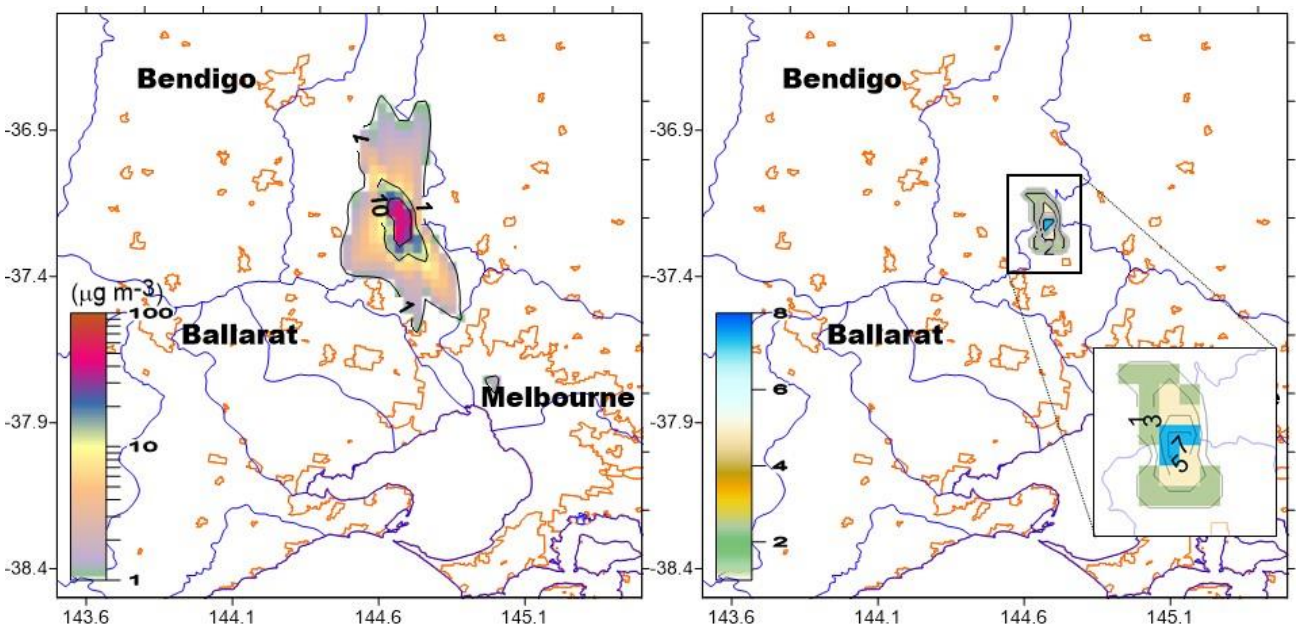

Figure 34. Left- contour plots of the peak 24–h $PM_{2.5}$ concentrations for the modelled period. Concentrations inside the innermost contour are greater than 25 µg m^{-3}. Right- number of days for which the NEPM AAQS (24-h $PM_{2.5}$) is exceeded.

2016 Tasmanian fires

On 13th January 2016, a dry lightning storm ignited multiple fires across north-west Tasmania, including within the Tasmanian Wilderness World Heritage Area (Figure 35). A total of 229 vegetation fires were recorded from 13th January to 15th March burning a total area of 124,742 ha, including 1.27% of the Tasmanian Wilderness World Heritage Area. Loss of life was avoided and damage to material assets and injury to persons was experienced only at low levels.

Records from the Tasmanian Base Line Air Network of EPA Tasmania (BLANkET) air monitoring network that commenced mid 2009 have shown that the smoke from the 2016 Tasmanian fires resulted in the most prolonged and widespread elevations of $PM_{2.5}$ concentrations. The highest 24h-averaged $PM_{2.5}$ concentration of ~ 500 µg/m^3 was recorded at Wynyard station, on the northwest coast, with 10-minute peak concentrations of nearly 2000 µg/m^3. Many air monitoring stations recorded extended intervals of instantaneous $PM_{2.5}$ over 100 µg/m^3. The smoke continued into February, but at lower concentrations with 24-averaged peaks of ~100 µg/m^3 at Wynyard and 30 to 50 µg/m^3 elsewhere in the north *(Innis et al. 2016)*.

Smoke from the Tasmanian fires in the northwest typically moved eastward over the northwest coastal areas into Bass Strait, occasionally returning near the Tamar mouth on a northwesterly flow, impacting on Launceston and Northeast Tasmania.

Experimental forecasts from the DELWP smoke forecasting system were available, and in fact has recently been updated to include information on active fires in Tasmania. This information was sufficient to provide State Control Centre (SCC) personnel with advance warning regarding smoke transport from Tasmania to the Australian mainland.

Figure 36 shows one of the forecast products which the SCC used to fill out the picture of smoke exposure (as defined by calls to 000 from concerned members of the population) and the source of the smoke in Tasmania.

The remainder of this section provides a more detailed analysis of Tier 2 forecast performance for the period 10-31st January 2016. This analysis is based on simulations undertaken since the fires and smoke exposure occurred and wraps in improvements made to the smoke forecasting system since the Tasmanian smoke forecasting was undertaken.

.

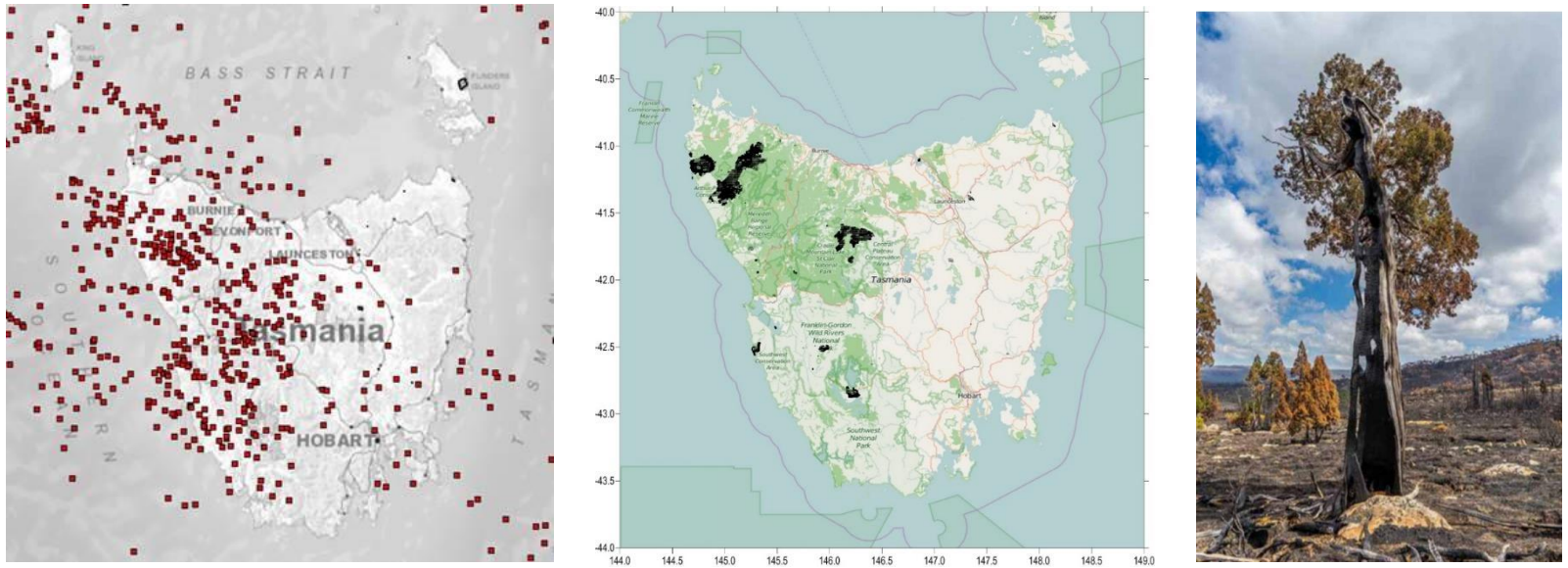

Figure 35 Left- Lightning strikes observed in the Tasmanian region 13th January 2016. Middle- area burnt by the fires. Right- burnt alpine heathland with pencil pine (*Arthrotaxis*).

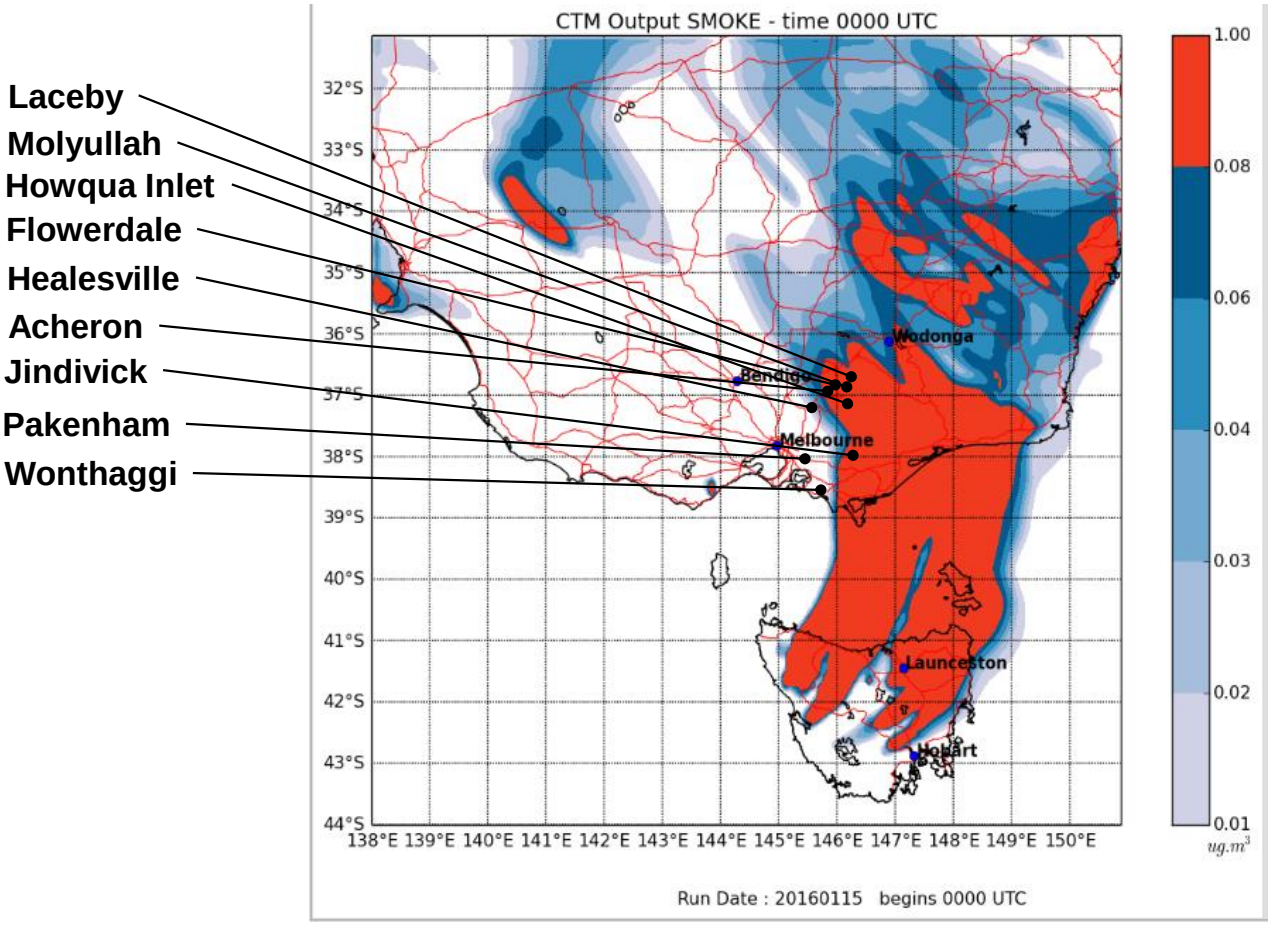

Figure 36 Smoke forecasting product (in this example we have used a levoglucosan tracer in units of μg m^{-3}) for hour 00 UTC (11 am LST) February 15th with the location of 000 calls also shown.

Emissions

Figure 35 shows the area burnt during the period 10-31 January 2016. Between 13th January and 15th March, a total of 229 vegetation fires were recorded which burned a total area of 124,742ha in largely remote, rugged and inaccessible areas *(AFAC 2016)*.

Figure 37 shows the estimated emissions of carbon monoxide from the Tasmanian fires, and also those from ground-based anthropogenic sources in Victoria for comparison. Figure 37 also shows the typical diurnal pattern of CO emissions from anthropogenic sources as they response to bi-daily peaks in vehicle usage and overnight minimums in vehicles and other combustion sources. The fire emissions vary according to the daily area burnt, the flaming area of the fire and the residual smouldering component.

Total CO emissions for the period 10-31 January 2016 are estimated to be 4.5×10^4 tonnes (anthropogenic) and 9.3×10^5 tonnes (fires), thus the CO emissions from the fires are more than an order of magnitude larger than the ground-level CO emissions for the whole of Victoria.

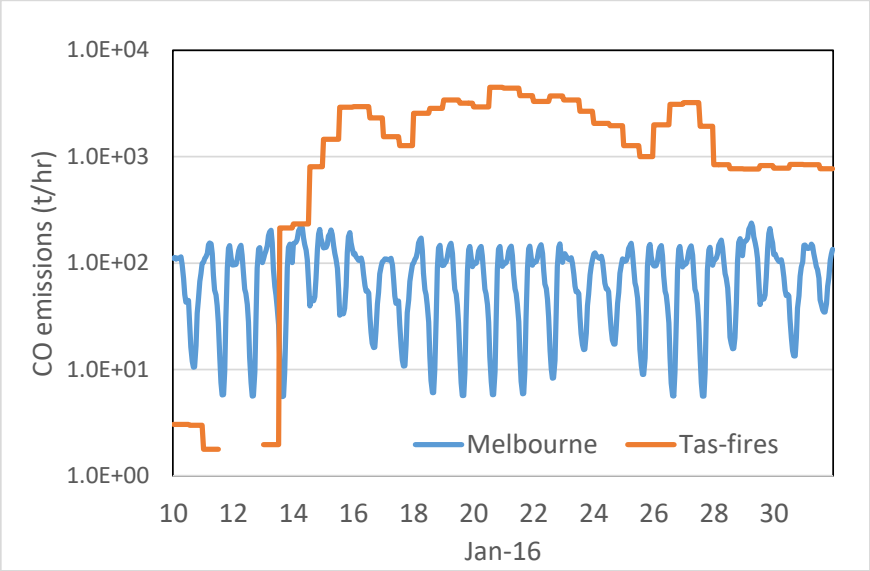

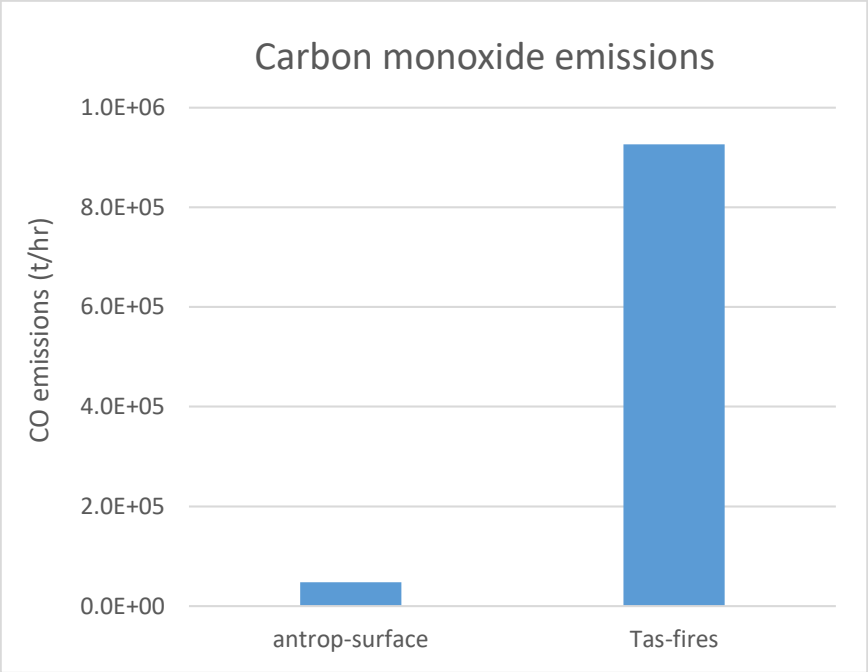

Figure 37 Melbourne CO emissions- 45,000 tonnes. Tasmanian fires 926,000 tonnes. For the period 10-31 Jan 2016 inclusive.

Plume transport

Figure 38 shows plots of Himawari visible imagery with plots of smoke transport (here using the model smoke tracer levoglucosan) shown for the same time snapshot. We have selected some snapshot times to highlight different aspects of the plume transport.

The plots for hour 22 UTC on 22 Jan 2016 (9 LST 23rd Jan 2016) have been selected to highlight the smoke emissions and transport from individual fires on Tasmania and demonstrate the skill of the meteorological forecast in correctly predicting the local wind direction across the fire region.

The plot for 24 hours later (22 UTC on 23rd Jan) is again able to demonstrate that the meteorological forecast has done extremely well in forecasting complex flow patterns to the north of Tasmania.

The plots for 22 UTC on 24th Jan (9 LST 25th Jan) show how the smoke plume is both observed and forecast to be advected across Bass Strait before (eventually) impacting Victoria.

Figure 39 shows the observed and modelled $PM_{2.5}$ concentrations for two times during the Tasmanian fires. Note that the $PM_{2.5}$ includes all sources of fine particles (smoke, sea salt, dust, anthropogenic primary emissions, anthropogenic and biogenic secondary particles). Note that the 0.09x0.09deg cell domain is shown in this example as we will examine the impact of smoke from the fires on NSW and Queensland in addition to Victoria.

The plot of $PM_{2.5}$ for hour 16 UTC on 15th January 2016 (hour 3 LST 16th January) shows how the forecast model has been able to simulate both the influence of smoke emissions from the fires on regions in the north-west of Tasmania, and the transport of the smoke plume across Bass Strait to impact Melbourne.

The forecast $PM_{2.5}$ for 12 UTC 24th January (23 LST 25th January) shows how the smoke is transported up the eastern coast of Australia within a front, impacting both NSW and Queensland. As shown in the plot, and discussed in more detail below, this impact is supported by $PM_{2.5}$ observations in the NSW Office of Environment and Heritage (OEH) and QLD Department of Environment and Heritage Protection (DEH) air quality networks and emphasises the importance of the Tier 2 forecast modelling for capturing significant $PM_{2.5}$ events from 'over the horizon' smoke emission events.

Verification of the $PM_{2.5}$- near field

Figure 40 shows the time series plots of observed and modelled 1-h $PM_{2.5}$ for selected monitoring stations in the EPA Tasmania smoke monitoring network.

The time series plot for Smithton was included because this is the site at which the model was most challenged to forecast rapid changes (i.e. 1-h) in $PM_{2.5}$. It can be seen that there is relatively poor correspondence between the timing of the observed and modelled $PM_{2.5}$ peaks, and we conjucture that this may be a result of errors in prescribing the (near field) plume rise of the smoke at this location. When investigating the smoke forecasts for this site in detail, we saw examples in which the smoke was forecast to remain above ground-level while the observations showed definitive smoke impacts. Similarly, we saw examples when smoke impacts were forecast but not observed, presumably because the smoke plume remained aloft on these occasions.

Figure 40 shows that forecasting system performed much better at sites other than Smithton with most of the frequency of smoke impacts being correctly forecast. Generally, the magnitude is also forecast within a factor of two.

Figure 41 shows the observed and modelled $PM_{2.5}$ time series for monitoring stations in Victoria (Latrobe Valley and Melbourne) and in Sydney. Figure 41 show model forecasts for scenarios in which the Tasmanian smoke is included and excluded.

The time series plots for Traralgon and Footscray show that Tasmanian smoke events are forecast for 15th January and 25th January (UTC). The observed $PM_{2.5}$ time series provides strong evidence for the 25th January impact and less definitive evidence for the 15th January impact, with the latter leading to relatively small increases in $PM_{2.5}$ concentration. This is interesting as it was the 15th January event which led to a flurry of Triple 0 calls in response to the presence of smoke odour and reduced visibility. Perhaps the potential lack of response from the public for the 25th January event may have reflected the forewarning provided by SCC following the initial smoke impacts.

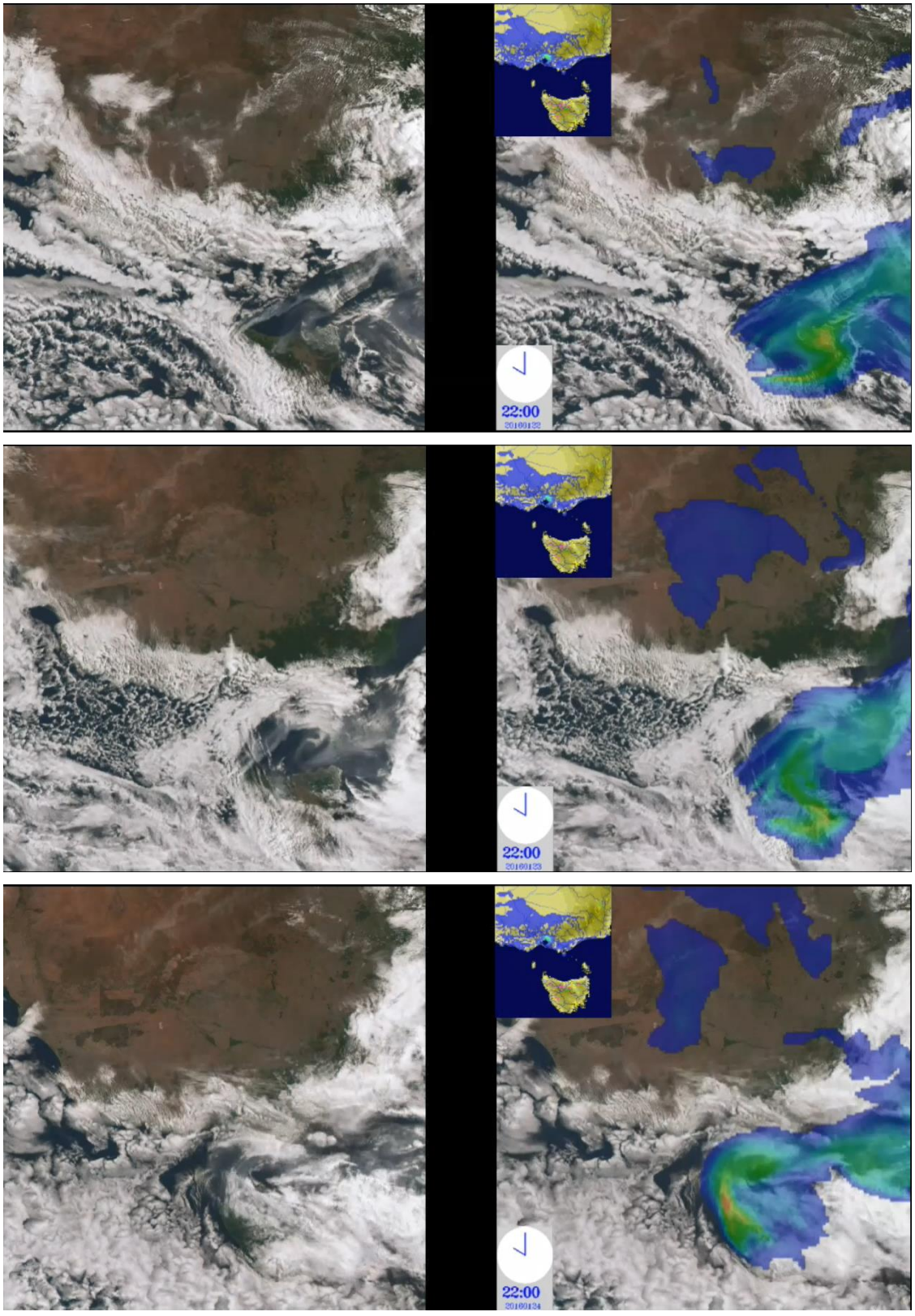

Figure 38 Plots of Himawari visible imagery with plots of smoke transport (a levoglucosan tracer). Note that the times are in UTC. The smoke areas in southern NSW are also a result of the Tasmanian fires.

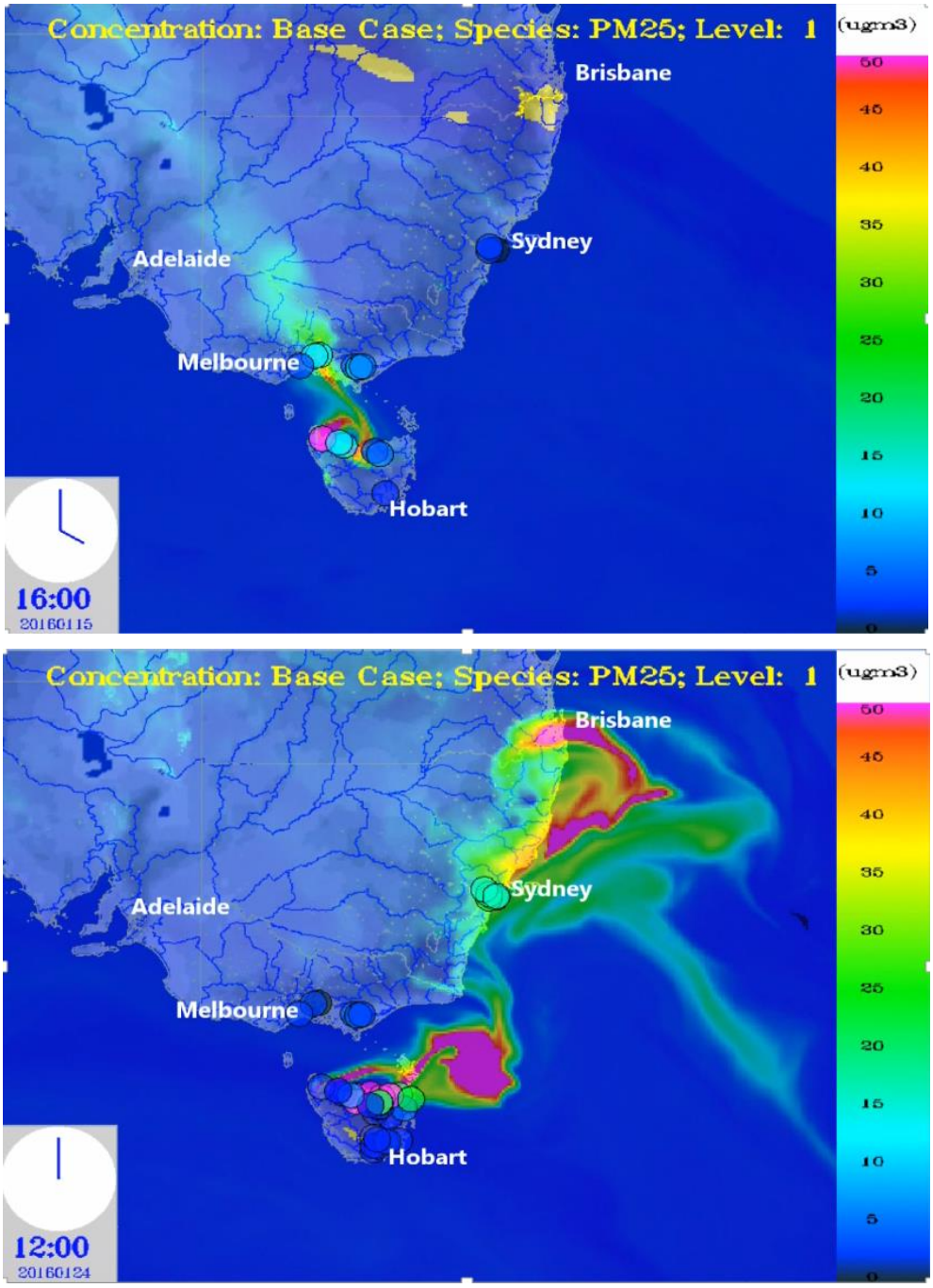

Figure 39 Observed and modelled $PM_{2.5}$ concentrations (µg m^{-3}). Note that the times are in UTC.

.

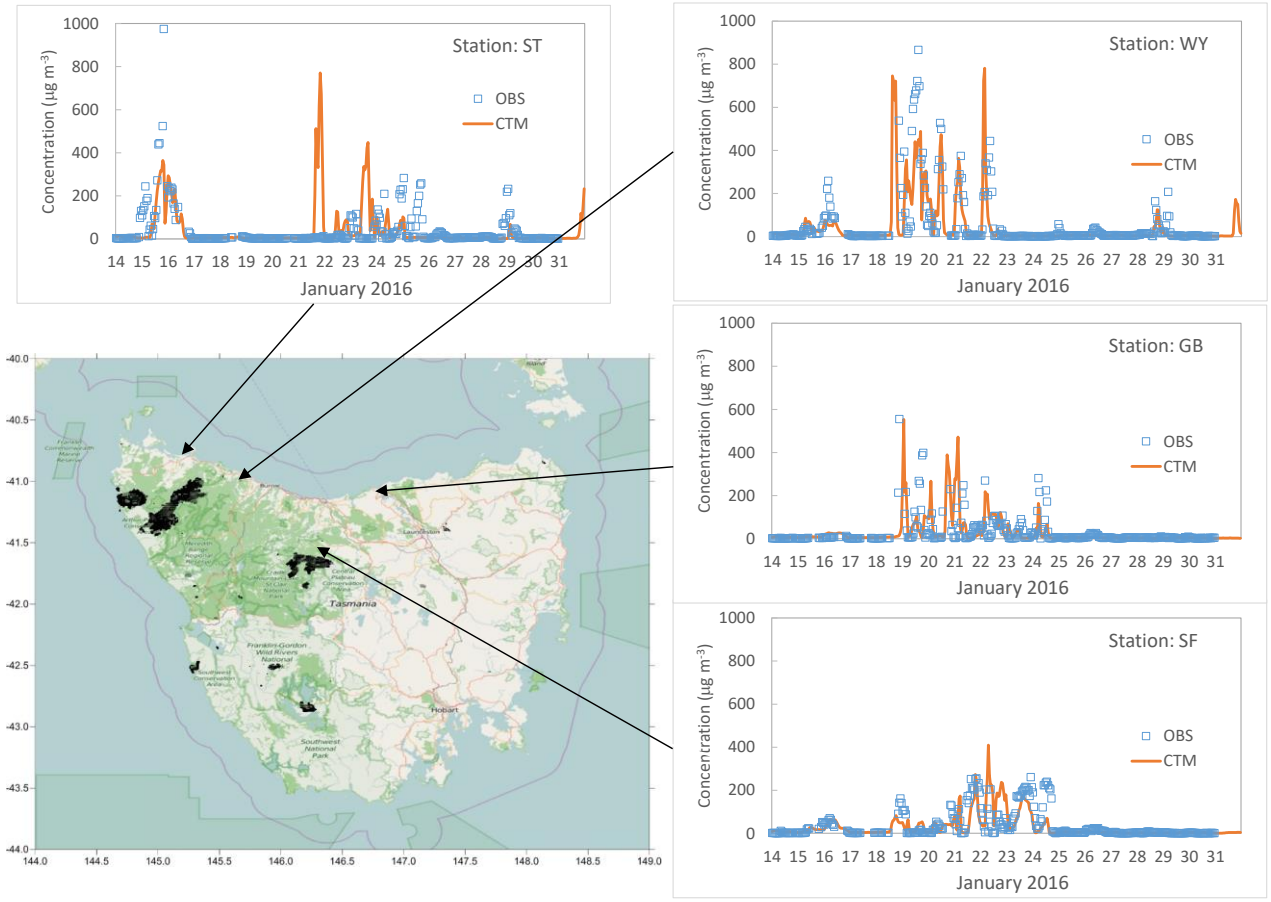

Figure 40 Time series plots of observed and modelled 1-h $PM_{2.5}$ for selected monitoring stations in the EPA Tasmania smoke monitoring network.

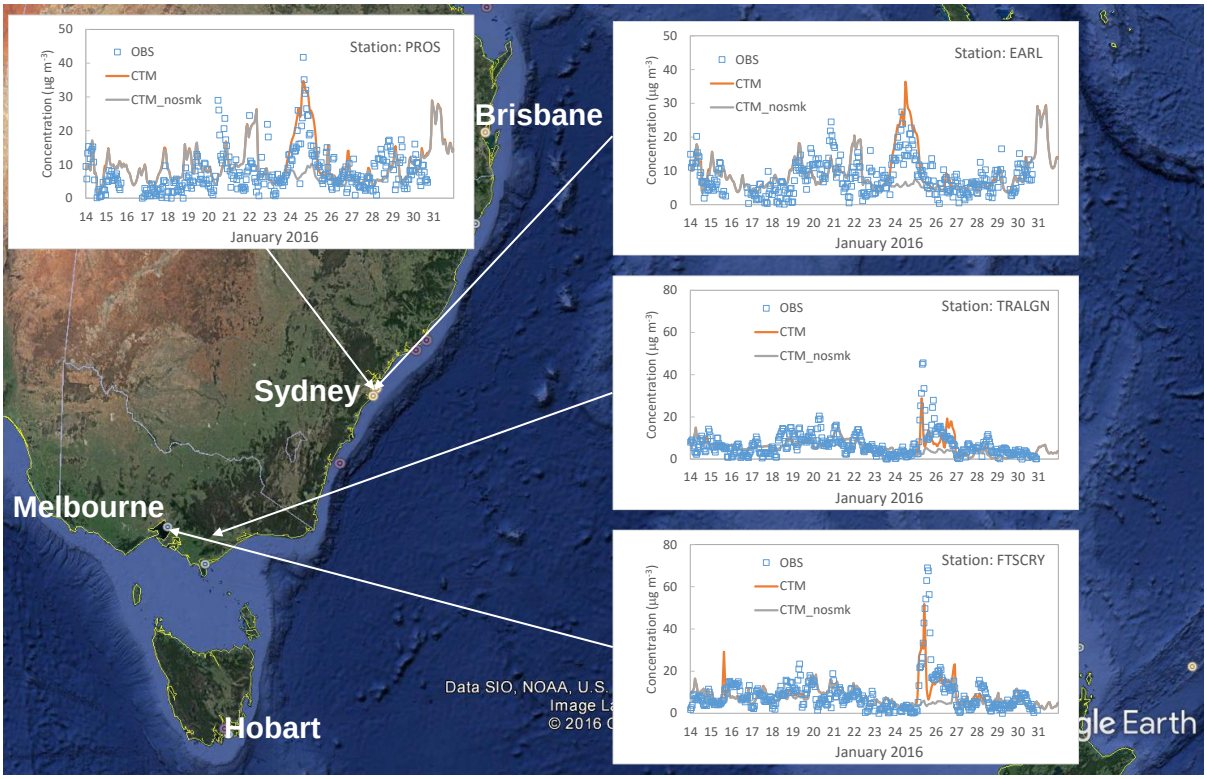

Figure 41 Observed and modelled $PM_{2.5}$ time series for monitoring stations in Victoria and in Sydney

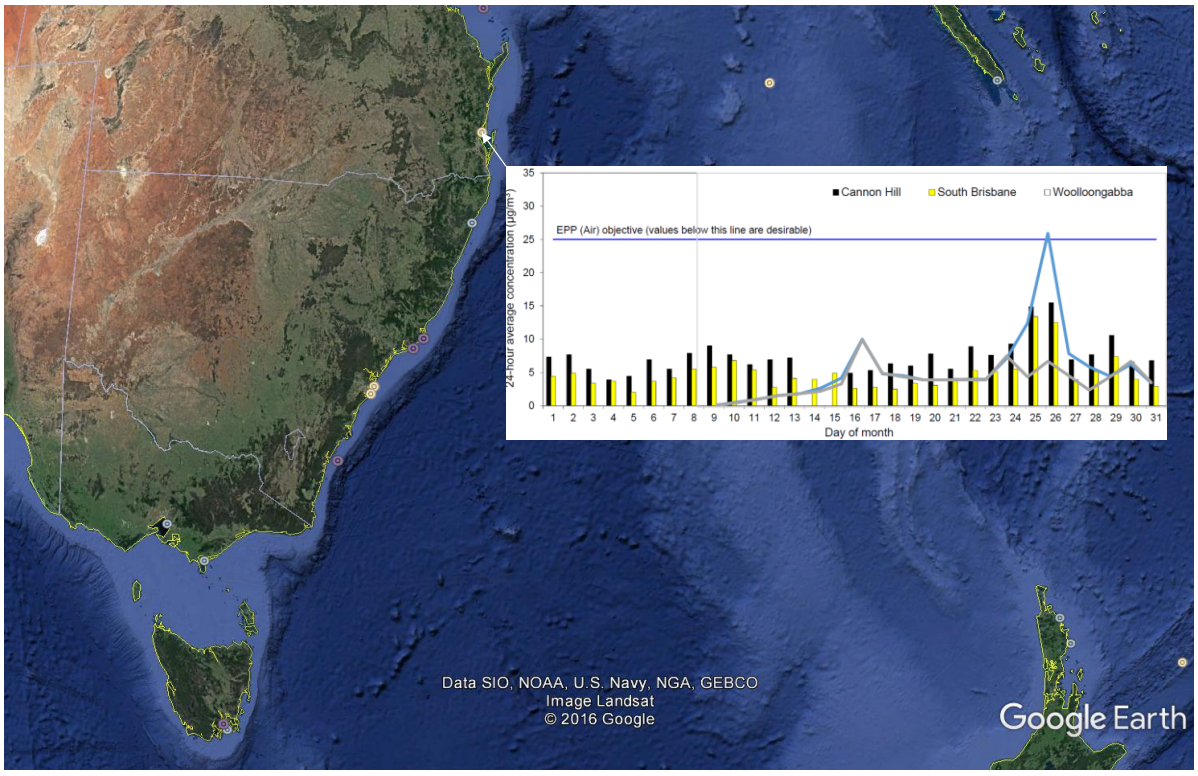

Figure 42 Observed and forecasted 24-h $PM_{2.5}$ for sites in the Brisbane region

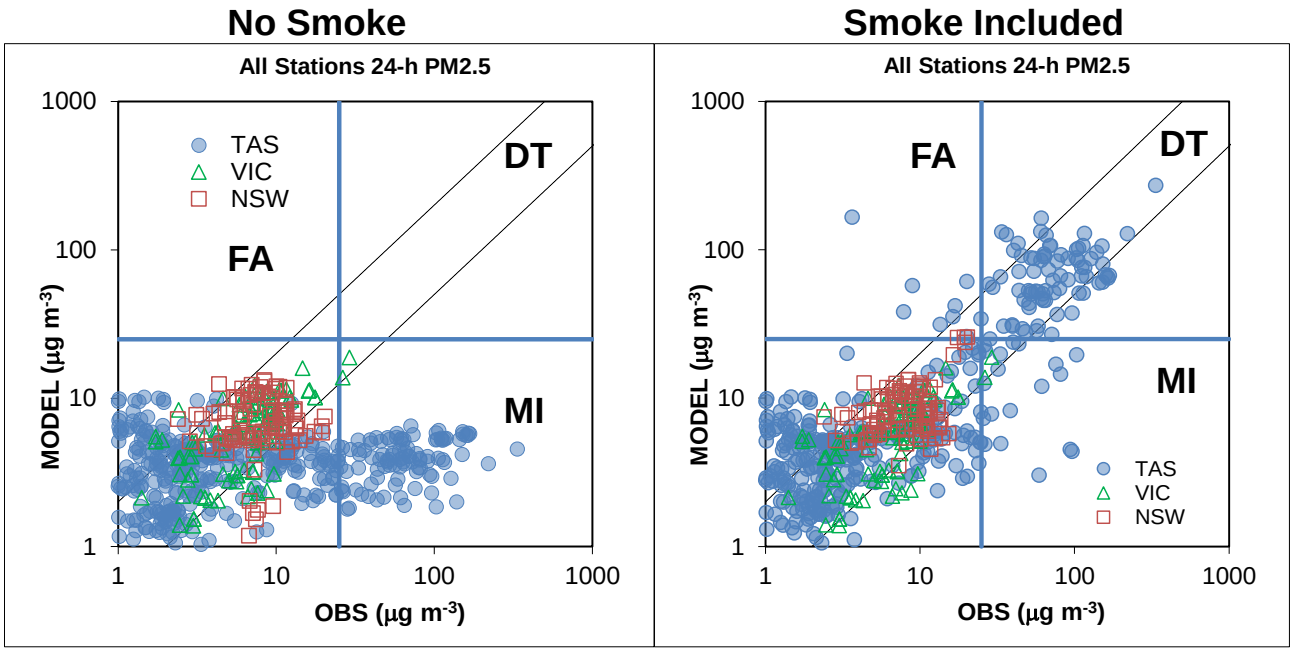

Figure 43 Scatter plots of observed and modelled 24-h PM2.5 for the simulated period.

The time series plots for Earlwood and Prospect in Sydney suggest that smoke from the Tasmanian fires impacted Sydney in the period 24-25th (UTC) January 2016. Note that the forecasting system has done extraordinary well in reproducing both the timing and magnitude of the $PM_{2.5}$ peaks over the forecast period, particulary given that the grid spacing is 0.09x0.09 deg. Note that the Tier 2 forecasting system included the NSW GMR 1x1 km spaced air emissions inventory (reference) thus leading to improved model performance for periods when smoke was not the most significant contributor to the observed $PM_{2.5}$ in Sydney.

Figure 42 shows the observed and forecasted 24-h $PM_{2.5}$ for sites in the Brisbane region. Again, it can be seen that the forecasting system has correctly forecast the timing of the smoke impact. However, the magnitude has been over predicted, an outcome resulting from an over prediction of secondary aerosol formation and/or an under prediction of wet deposition losses during the transport phase of the smoke from Tasmania to Queensland

Figure 43 shows scatter plots of observed and modelled 24-h $PM_{2.5}$ for the simulated period. Plots are shown of the model performance without and with smoke emission model scenarios. Plots are shown on log-log scales so that we can easily view the model performance for concentations in the range 1 – 1000 µg/m^3. Note that we are also interested in low level $PM_{2.5}$ concentrations because current knowledge of $PM_{2.5}$ health effects suggest that there is no lower concentration threshold of population health impact. Figure 43 (together with Figure 44) indicates that the smoke emissions had a large impact on $PM_{2.5}$ concentrations in Tasmania, and relatively small impacts in Victoria and NSW (as expected). The model is generally able to simulate the full dynamic range of the observed concentrations with good skill. However, there is some bias to over prediction of low-level concentrations observed in Tasmania. Analysis indicates that these occurred for modelled $PM_{2.5}$ concentrations which were dominated by other source types such as sea salt.

With respect to the categorical foreasting capability note that the detection rate of AAQS exceedances was 81%, 19% of the observed exceedances were missed, and there was 12% false alarm rate.

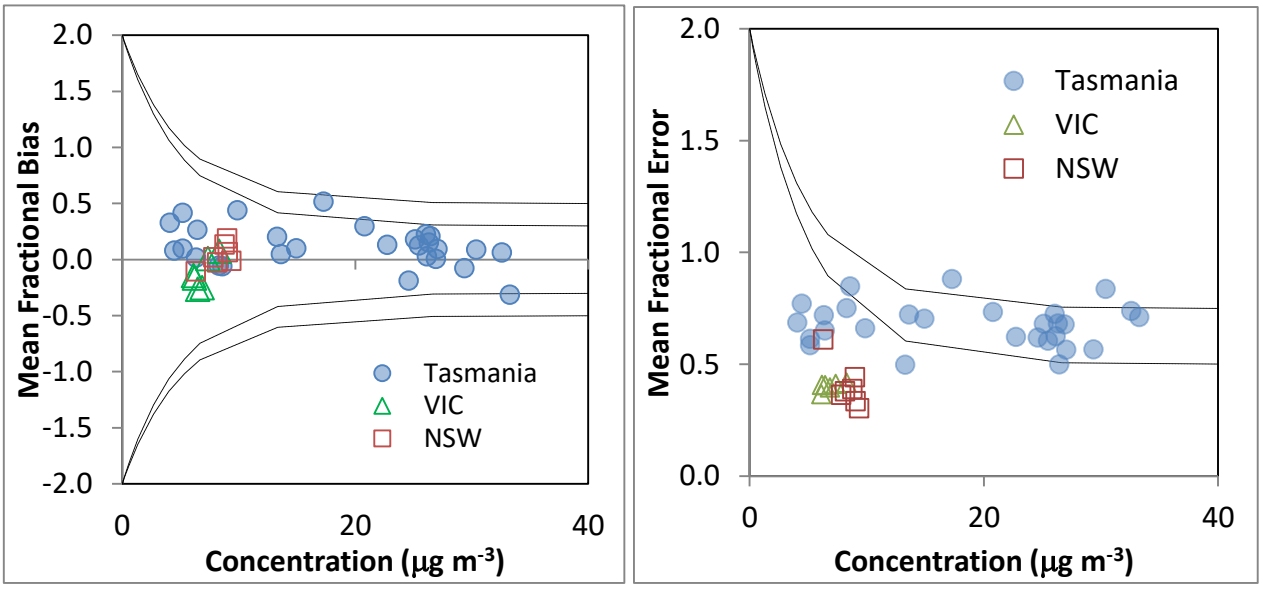

Figure 44. Bugle plots showing the mean fractional bias and mean fractional error for 24–h average PM2.5

Figure 44 shows the mean fractional bias and mean fractional error for 24-h $PM_{2.5}$ for the simulation period. It can be seen that these statistics have been calculated for monitoring stations in Tasmania, Victoria and NSW. The plots include guidance lines which show acceptable (outer lines; bias- asymptoting to ± 50%; error asymptoting to 70%) and aspirational (inner lines; bias- asymptoting to ± 30%, error asymptoting to 50%) goals for model performance *(Dennis et al. 2010; Simon et al. 2012)*. In the case of the bias it can be seen that the forecast results fall within the aspirational goals for all but one monitoring site in Tasmania. In the case of error, the peak 24-h concentrations generally fall between the acceptable and aspirational goals for the Tasmanian sites, and well within the aspirational goals for the Victorian and NSW sites. This is a good outcome for a forecasting system.

Analysis

Figure 45 summarises the $PM_{2.5}$ impacts for the entire simulation period, showing the modelled peak 24-h $PM_{2.5}$ concentrations, and the spatial envelope for exceedances of the 24-h NEPM AAQS. While exceedances of the standard were primary limited to Tasmania and maritime regions downwind the smoke sources, it can be seen that peak 24-h $PM_{2.5}$ concentrations within this envelope were both observed and modelled to exceed the AAQS by more than an order of magnitude.

Note that the regions of AAQS exceedances in northern Victoria are due to wind blown dust.

The AAQS exceedance frequency plot indicates that regions close to the fires in the north-west of Tasmania had greater than 15 days on which the AAQS was exceeded.

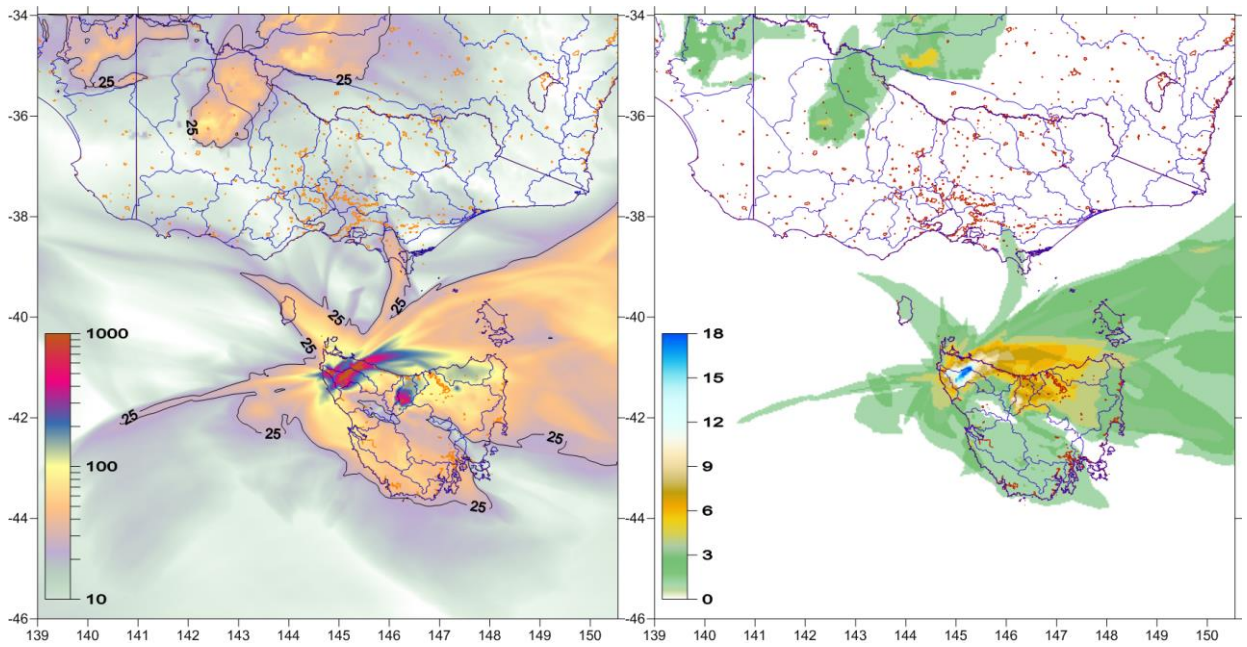

Figure 45. Left- contour plots of the peak 24–h $PM_{2.5}$ concentrations for the simulated period. Right- number of days for which the NEPM AAQS (24-h $PM_{2.5}$) is exceeded.

2016 Hindleton - Granya Gap Rd (Tier 3 modelling)

In this final example, the smoke forecasting system was operated in a Tier 3 mode to investigate the smoke transport from a 97 hectare fuel reduction burn which was carried out by DELWP at Hindleton-Granya Gap Rd (36.1469 S 147.3368 E) on 26 March 2016.

The Tier 3 modelling consisted of the following.

1. Generating a (standard) forecast of the background $PM_{2.5}$ concentrations (covering Vic-Tas, thus including the region of the planned burn).

2. Using information about the planned burn objectives provided by DELWP to model the anticipated fire behaviour characteristics using the Planned Burn simulator.

3. Inputing the simulated area burnt into the smoke emisions module to estimate the hourly emissions of smoke from the burn.

4. Inputing the smoke emissions into a high resolution (1 km grid spacing) tracer version of the chemical transport model and forecasting the smoke plume transport for 24–72 hours.

5. Combining the forecast background $PM_{2.5}$ concentrations with the $PM_{2.5}$ tracer concentrations from the planned burn to establish the likely absolute and relative concentrations of $PM_{2.5}$ within the region affected by smoke from the planned burn.

Planned Burn Simulator

Part III (Fire behaviour modelling) and Appendix G provide detailed information on the use of the Planned Burn Simulator. Routine use of the simulator will require the provision of a Shapefile which details the area to be burned by DELWP. However as none were available for this particular case study at the time of the simulation, a shapefile representing a 0.01 degree square, centred on the burn co-ordinates provided by DELWP, was created. This gave an area of 99.85 ha compared to the 97 ha documented in the burn data. Bureau of Meteorology Graphical Forecasting Editor grids were obtained from archive for the relevant days and provided the meteorological drivers for the simulator.

Burn simulations were run beginning at 10 LST and two burn models were run a) lump all fuel together and burn with a fixed time profile; b) burn from dry to wet until the burn coverage objective is reached. Results from the simulator are summarised in Table 9 and indicate that the burn models yielded similar total amounts of fuel burnt and emitted carbon.

Figure 46 shows the area burnt by the simulator (noting that a fire break shown in Google Earth was not captured by the simplified representation of the burn used in this case study).

Emissions

Figure 47 shows the modelled emissions of carbon monoxide for the burn duration, and for a period after the burn when smouldering of the CWD is predicted to continue. Also shown are the diurnal and total emissions from ground-based anthropogenic sources in Victoria, which demonstrates that the Hindleton-Granya Gap Rd is a small fire compared to both Victorian anthropogenic sources and the fires in the Lancefield-Cobaw and Tasmanian fires case studies discussed above. Figure 47 also suggests that the emissions from the smouldering CWD are larger than those from the flaming component of the fire when integrated across the entire period that smoke is emitted from the region.

Analysis

The purpose of the Tier Three modelling is to provide a 24–hour outlook for planned burn proposals. Thus, on the day prior to a proposed burn, the forecasting system ingests data for one or many planned burns proposed for the following day.

This information is provided on the morning of the day prior, and the forecasting system is run in time to provide information suitable for assessing the potential smoke exposure on the day of the burn. Typically, the final decision will be made in the afternoon of the day prior.

There are many ways in which the forecast data can be provided to DELWP to aid in decision making. In fact, the final form of the data will follow from on-going workshoping of the forecasting system products with DELWP personnel.

Figure 48 shows a prototype set of information for the Hindleton-Granya Gap Rd planned burn simulation. The spatial plot at the bottom of the figure shows 1/ the 24–hr $PM_{2.5}$ concentrations ($\mu g\ m^{-3}$) from background sources of particles (the unfilled red contours); 2/ the surface-level plume footprint of the planned burn (all concentrations greater than 0.1 $\mu g\ m^{-3}$ are shown in this example). Peak concentrations of the smoke $PM_{2.5}$ reach about 5 $\mu g\ m^{-3}$ for the planned burn as modelled and the combined (smoke + background) 24–h $PM_{2.5}$ concentration within the region is about 9 $\mu g\ m^{-3}$. Recall that the NEPM AAQS for $PM_{2.5}$ is 25 $\mu g\ m^{-3}$ thus the modelled peak smoke concentrations is about 36% of this standard.

The diurnal variation of hourly (LST) background and smoke $PM_{2.5}$ concentrations are shown in the time series plot (top). The plot suggests that 1–hr $PM_{2.5}$ concentrations peak in the late afternoon, with smoke PM contributing more than 60% of the fine particle burden at this time.

Table 9 Emissions predicted by the Planned Burn simulator for the Hindleton–Granya Gap Rd fire.

Burn Type	Fuel consumed (tonnes)	Carbon emitted (tonnes)	Heat Released (GJ)
Model A	1317	628	23029
Model B	1305	623	22821

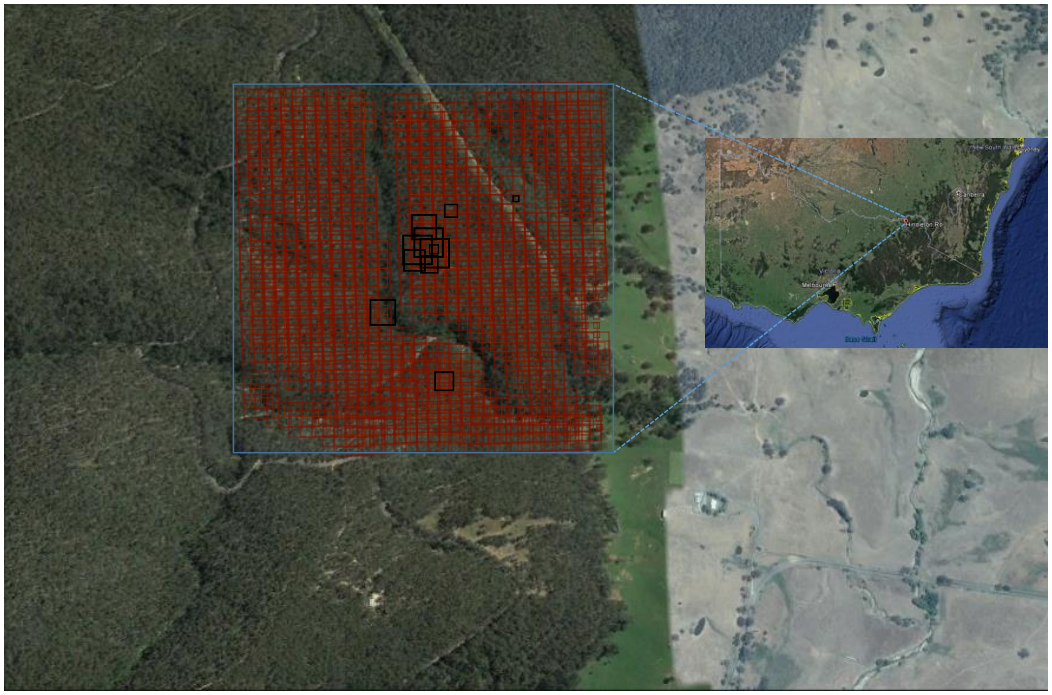

Figure 46. Planned burn simulator output showing 1/ area burnt (sized weighted by fuel load) and 2/ burnt area weighted centroids for each hour of the planned burn- used to input into the chemical transport model. The size of the burnt area is ~100 ha.

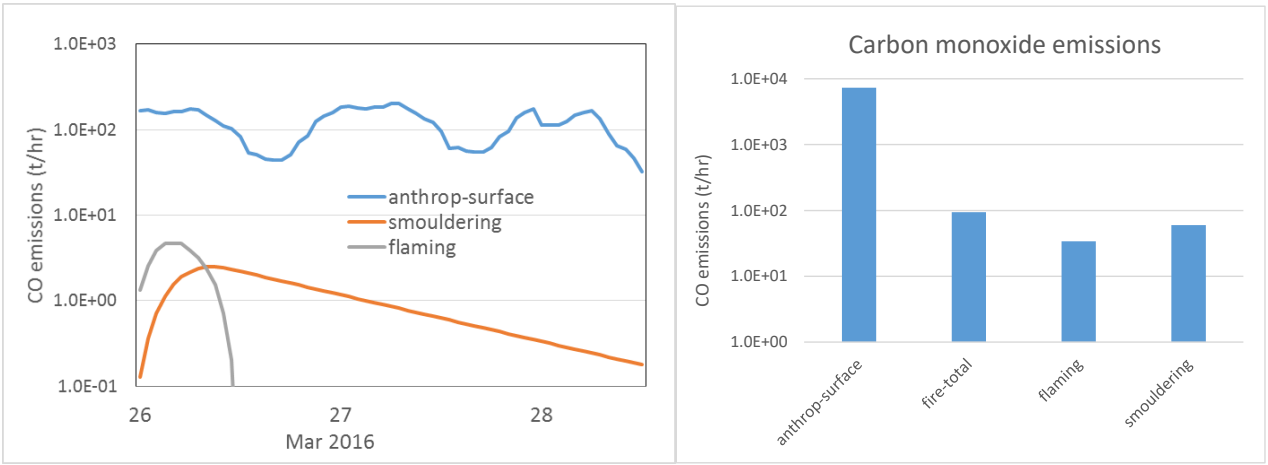

Figure 47. Modelled emissions of carbon monoxide from the Hindleton–Granya Gap Rd. fire, and from the State-wide EPA Victoria air emissions inventory. The smoke emissions have been broken down into the flaming and smouldering components.

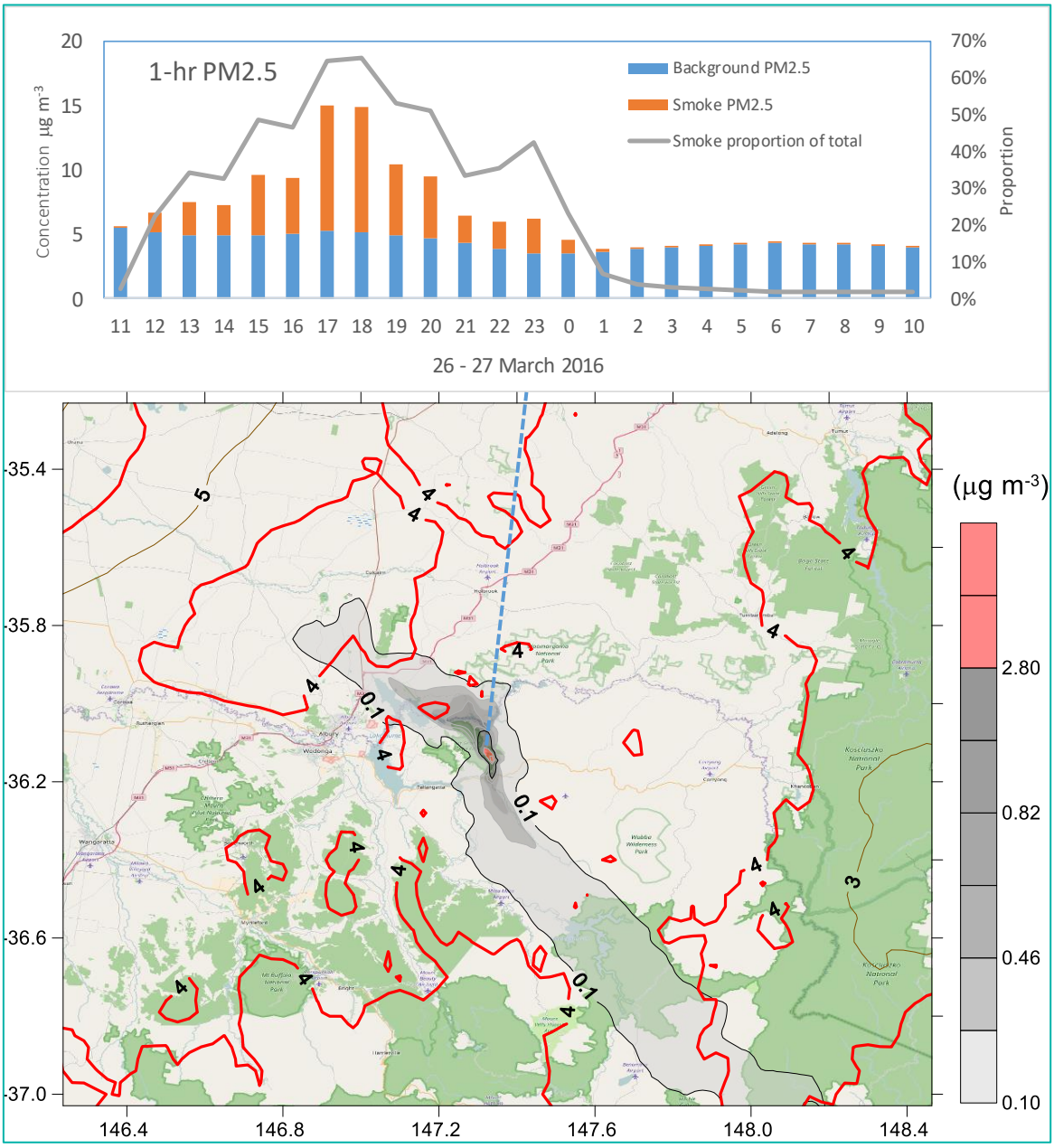

Figure 48. Prototype of an output format for a planned burn simulation. Top- time series of hourly (LST) background and smoke $PM_{2.5}$. Bottom- a spatial plot of 1/background PM (the unfilled red contours); 2/ the planned burn $PM_{2.5}$ footprint. Note that all concentrations are in µg m^{-3} and are 24–hr averages.

Part V Prototype to operational system

The prototype smoke forecasting system was demonstrated in the SCC in January 2016. A project is now underway to operationalise the system in the Bureau of Meteorology. This will involve designing and building the operational architecture and porting the modelling code to run on the Bureau's new supercomputing infrastructure.

Smoke interface services during fire and planned burning seasons are provided by the BOM SCC Meteorologist, consistent with the MOU between BOM and Victorian Emergency Management Agencies regarding BOM SCC meteorologist services. To develop the improved services the project will include routine researcher-stakeholder discussions to evaluate forecasts, output products, and verification results.

In consultation with DELWP users the smoke model web interface will be further developed to improve visualisation, user experience, and trigger communication and other actions.

The online training module for smoke forecasting will be improved and provided to BOM SCC meteorologists and DELWP staff in Head Office and regional centres. This will aid the SSC meteorologist to provide interpretation of the smoke model outputs and describe levels of uncertainty and areas subject to critical change and elevated smoke risk. This quantitative information will help fire behaviour analysts and regional staff to make better decisions.

Subject to successful completion of the operationalisation project, an agreement will be negotiated between BOM and DELWP for provision of ongoing smoke forecasting services.

The products for the three Tiers are shown in Table 10.

Part VI Future

Further improvements to the smoke forecasting system will involve building into the system, methods technologies and data which can be used to calibrate and validate the predictions of smoke spread, dissipation and constituents. This includes calibration for making long-term improvements to models, as well as intelligence to provide improved real-time predictions of the distribution and density of smoke and its impacts on communities, industry and infrastructure (e.g. transport).

Multiple forms of intelligence are required to be collected and integrated dynamically to provide the best assessment of the nature and extent of smoke, and its impact of communities, industry and infrastructure. Three key sources are identified to capture this intelligence and calibrate and validate smoke modelling predictions at suitable spatial and temporal scales.

Social media intelligence

Social media platforms are used by a large number of people and those numbers are growing every year with more and more users venturing into the social media networks, especially via the more widely available Smartphone technology. Social media intelligence has a range of benefits for calibration and validation of smoke modelling predictions, including:

- Geo-locating social media data
- The ability to determine the nature and degree of a particular situation through social media imagery, video and text
- Using social media data mining to identify trending subjects and locations for early and enhanced smoke situational awareness through vulnerability community networks.

Remote sensing intelligence

Remote sensing sources for validation and calibration of smoke predictions include satellite imagery and field-based sensors. High temporal resolution satellite sensors, such as NASA's Moderate Resolution Imaging Spectroradiometer (MODIS) and Japanese Meteorological Agency's Himawari geostationary satellite capture imagery on a daily and sub-hourly scale showing smoke plumes and other atmospheric properties. Bureau radar-based products can provide polar fields of signal reflectance that can identify the structure of smoke plumes when present.

Field Sensor Networks

Field sensor networks of fixed and portable monitoring instruments can be used to directly measure smoke particles or indirectly through visibility reduction measurements. Field-based instruments may form intelligence networks, which collect data across large areas and feed data in real-time to a central location for smoke model prediction validation and calibration.

Additionally, small Unmanned Aerial Vehicles (UAVs) or drones equipped with light-weight sensors can be used to track smoke plumes and complement stationary field sensor networks to improve the accuracy of data assimilation. Unlike stationary monitoring, UAVs can investigate the vertical and temporal variability of air pollutants in smoke plumes and provide data sampling over large areas or areas that are not easily accessible.

Improvements to the smoke forecasting system also include a better characterisation of particle emissions at low MCE where we observed a large scatter in EFs mainly due to combustion conditions. Experimental burns that focus on logs and heavy fuels can provide a better understanding on the combustion conditions (e.g. smouldering vs glowing combustion) and help us to better define particle EFs at low MCE. Since smouldering combustion contributes significantly to CO and PM emissions, refining EFs according to burning conditons can provide great improvements in forecasting population impacts from smoke of prescribed burns or bushfires.

Table 10. Products to be considered in the operational version of the Smoke Forecasting System.

Product	Domain	Input	Variables	Temporal resolution	Spatial resolution
Tier 1: Probabilities of FFDI exceeding critical fire danger thresholds	Victoria & Tasmania	ACCESS-GE	FFDI	6-hourly to 10 days	60km grid
Tier 1: EPSgrams of fire weather and fire danger	Victoria	ACCESS-GE	FFDI, GFDI, 2m temperature, relative humidity, 10m wind speed, 10m wind direction, 6h accumulated precipitation, total cloud cover	6-hourly to 10 days	32 locations in Victoria
Tier 2: Ventilation parameters	Victoria & Tasmania	ACCESS-R	Ventilation index, transport winds, model ABL height	6-hourly to 3 days	11km grid
Tier 2: Peak daily pollution	Victoria & Tasmania	ACCESS-C, CTM, planned burns & going fires, EPA emissions	$PM_{2.5}$, PM_{10}, NO_2, SO_2, O_3, CO, smoke	24h	3km grid
Tier 2: Gridded hourly pollution	Australia, SE Australia, Victoria & Tasmania	ACCESS-R, ACCESS-C, CTM, planned burns & going fires, EPA emissions	$PM_{2.5}$, PM_{10}, NO_2, SO_2, O_3, CO, smoke	Hourly to 24 hours for smaller domain, 72 hours for the two larger domains	27 km, 9km, 3km, respectively
Tier 2: Site hourly pollution	Victoria	ACCESS-C, CTM, planned burns & going fires, EPA emissions	$PM_{2.5}$, NO_2, SO_2, O_3, CO, smoke	Hourly to 24 hours	Selectable locations in Victoria
Tier 2: Verification of hourly pollution	Victoria	EPA monitoring data	$PM_{2.5}$, NO_2, SO_2, O_3, CO	Hourly for 1-week blocks	21 monitoring sites in Victoria
Tier 3: Gridded hourly pollution	Australia, SE Australia, Victoria & Tasmania,	ACCESS-C, CTM, proposed burns & going fires	$PM_{2.5}$, O_3, smoke	Hourly to 24 hours for smaller domain, 72 hours for the two larger domains	27 km, 9km, 3km, respectively
Tier 3: Site hourly pollution	Victoria	ACCESS-C, CTM, proposed burns & going fires	$PM_{2.5}$, O_3, smoke	Hourly to 72 hours	Selectable locations in Victoria

Appendix A: Experimental

Pyrotron experiments

Laboratory experiments were undertaken using the CSIRO Pyrotron, a large combustion wind tunnel, in order to control or isolate as many of the variables involved in the combustion and spread of fire in CWD. Using the Pyrotron enabled the natural ignition and combustion of CWD via spread of fire through a continuous surface fuel, rather than burning pieces of CWD in isolation as has been done in many previous studies (e.g. *(Burrows 2001)*).

Experimental design

In order to address the objectives of this study, the design of this experiment focused on two variables, the amount of CWD and the fire spread mode—fires spreading with the wind (heading fires) and fires spread against the wind (backing fires).

As the fire spread mode is considered mutually exclusive (an experiment can either be heading or backing), the only variable for each series of experiments was that of CWD load. All other burning conditions (wind speed, surface fuel moisture content and surface fuel load) were either non-varying (wind speed and surface fuel load) or variation was limited as much as practical (e.g. surface fuel moisture content). The values of these experimental factors were chosen to represent typical prescribed burning conditions for a dry eucalypt forest in central Victoria *(Tolhurst and Cheney 1999)*. Table 11 summarises the variables, factors and the range of values used in the study.

Table 11: Summary of variables and factors in the Pyrotron experiments and the ranges or conditions selected for study

Variable	Range/condition
Fine fuel moisture content	10-12% ODW (representative of prescribed burning conditions). Fuel moisture content (FMC) was the result of selection of appropriate ambient weather conditions to achieve the desired range.
Fine fuel load	10 t/ha
Branch fuel load	Three treatments: 2, 6 and 12 t/ha and 0 t/ha (control)
Branch diameter	>6-50 mm, distribution of sizes in two classes (>6 – 25 mm,>25—50 mm) to achieve desired treatment.
Branch location and orientation	Branches distributed randomly in location and orientation within 1 m sections of working section
Air speed	1.0 m/s (equivalent to 11 km/h in open if assuming tall dry eucalypt forest, 3:1 conversion factor)
Ignition	1.5 m continuous immediate line on upwind edge (for heading fires) or downwind edge (for backing fires), facilitated by 90% ethanol

Apparatus

The controlled burning experiments were conducted in the CSIRO Pyrotron, a 2×2×25-m-long combustion wind tunnel located in Yarralumla, ACT (Figure 49, *(Sullivan et al. 2013)*). Lined with large observation windows and the ability to incorporate a large array of sensing instrumentation, this apparatus enables the safe and repeatable study of the combustion, spread and behaviour of fires burning in bushfire surface fuels such as that found on a forest floor. Factors such as wind, fuel characteristics and condition (e.g. fuel moisture content) can be selected to enable factorial investigation of independent variables upon fire behaviour characteristics such as rate of spread, flame dimensions, and intensity.

The working section is 4.8 m long by 2 m wide and can accommodate fuel beds up to 4.8 m long by 1.5 m wide. To ensure that combustion and plume development in the fire are not inhibited by the presence of the fixed room (at a height of 2 m), fuel beds should not include fuel elements taller than 70 cm. Fuels burnt in the Pyrotron have included dry eucalypt forest litter, rainforest litter, standing grass, shrubs and pine plantation litter. Analysis of the coefficient of variation of the error in the rate of

spread of fires burning in dry eucalypt litter (the remaining variance when effects of air speed and fuel condition have been accounted for) was 3.1% *(Mulvaney et al. 2016)*, demonstrating the investigative power of the apparatus.

Wind is provided by a large 1.37-m diameter centrifugal fan that can deliver air speeds in the working section up to 5.5 m/s. Straighteners and pressure diffusing screens remove nearly all turbulence from the air flow, resulting in a turbulence intensity of <0.6% *(Sullivan et al. 2013)*.

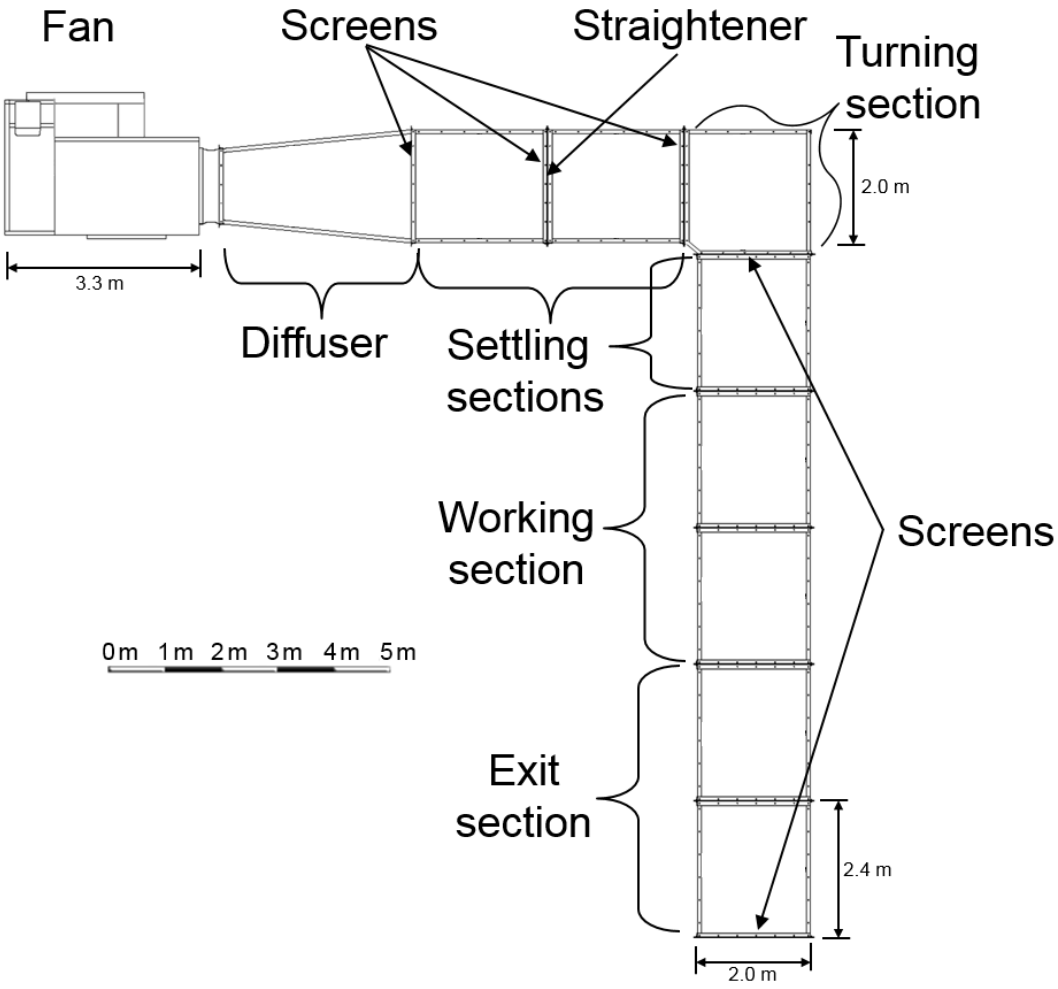

Figure 49: Plan view schematic of the layout of the CSIRO Pyrotron. The working section enables fires burning in a fuel bed of 1.5 m wide by 4.8 m in length to be studied safely and repeatably

Fuels

Fuels, both surface litter and branch material, were sourced from a long unburnt dry eucalypt forest at the Pumphouse site in the Wombat State Forest near Daylesford, Victoria (37°28'57.2"S 144°13'24.1"E). This forest is classified as Shrubby Foothill Forest (ECV 45) with a dominant overstorey of *Eucalyptus obliqua* and *E. dives*.

Surface fuels were first assessed using the Overall Fuel Hazard Guide *(Hines et al. 2010)* to determine *in situ* fuel load (average 8.13 t/ha) and depth (average 14 mm) (Figure 50) and then raked into large nylon wool bale bags (Figure 50). Fallen branch material was collected by hand and placed into a large nylon wool bale bag. Enough surface and branch material were collected to ensure sufficient replications of fire experiments could be undertaken. Bags of fuel were then transported via truck to Canberra for testing in the Pyrotron.

Figure 50: Left) Surface fuels at the fuel source location were assessed to determine in situ fuel hazard level, fuel load and depth). Right) Surface fuels were then raked into large nylon wool bale bags for transport to the Pyrotron. Branch material was similarly collected and put into a wool bale bag for transport

Surface litter was sieved and sorted to remove all non-fuel elements such as duff, dirt and rocks, to remove fuel elements that were partially decomposed and verging on duff, and fuel elements larger than 6 mm diameter. Surface fuels were then distributed into cardboard boxes at the predetermined dry fuel amount for a 0.75 m^2 section of the fuel bed that gave a total dry fuel load equivalent to 10 t/ha (see *Experimental design*).

Branch material was sorted by size class (>6 – 25 mm and 25 – 50 mm) into bins containing the appropriate amount of dry CWD in each class for each 1.5 m^2 section of the fuel bed as required by each particular experimental fire.

Fuel bed preparation

Prior to each experimental fire, boxes of surface fuels were removed from the walk-in oven and distributed evenly across the Pyrotron fuel bed. Fuel bed composition (amount of bark, twig and leaf material) was determined by isolating, drying and weighing each component from a representative (approximately 100 g) sample of the sorted but not boxed fuel. Fuel bed depth was measured at four random locations within the fuel bed.

For the heading fires, the fuel bed was 4.0 m long. For the backing fires, because the rate of spread is so much slower, was 2.0 m long.

In the case of a treatment experiment, branch material was then distributed randomly in each 1.5 m^2 (1.5 m wide by 1 m long, split into 4 by 1 squares) section of the fuel bed. The location of the target square and the orientation (parallel, perpendicular or 45° to the air flow) of the branch selected randomly from the box for that section was determined by a random number sequence generated previously. Some target squares had more than one branch, others had none. Pre-fire diameter of each piece of CWD, measured using Vernier callipers at three points and averaged, was recorded manually. CWD were extracted from the unused collection for determination of gravimetric fuel moisture content via oven drying at 105°C for 24 h *(Matthews 2010)*.

The C/N content of the leaf, bark and twig fraction of litter was measured three times (samples taken on different days i.e. 9 C/N samples in total). The C/N content of CWD was sampled from three different pieces of remaining branch material on the final day of experiments. There were 3 C/N samples for >6-25 mm CWD and 3 samples for 25-50 mm CWD.

Figure 51 illustrates examples of the fuel bed prior to experimentation for the control and the three treatments. In each case, the underlying surface fuels were as consistent as possible in terms of load and depth, thus not a variable. The only differentiating factor between the four cases is the amount of CWD.

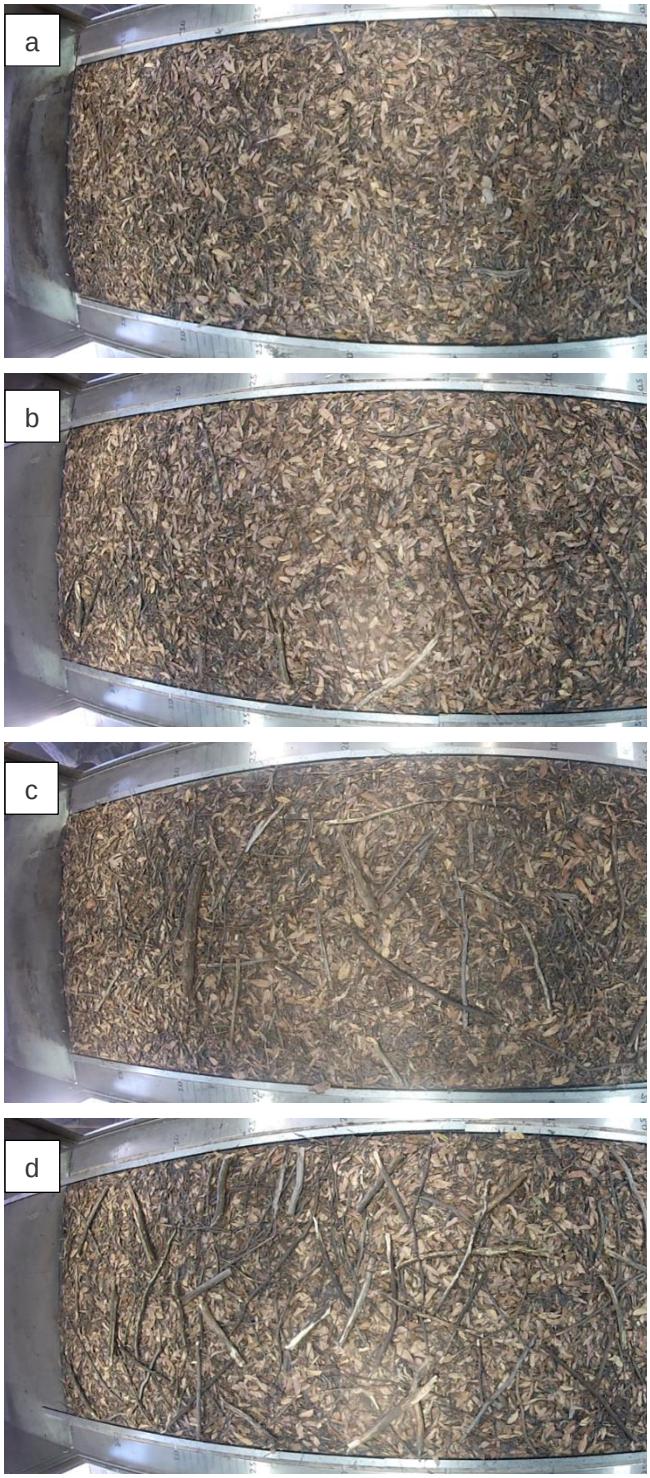

Figure 51: Photograph of heading fire fuel bed with control and three different CWD treatments. a) Control, no CWD. b) 2 t/ha CWD. c) 6 t/ha CWD. d) 12 t/ha CWD. In all cases, CWD was distributed randomly across the fuel bed.

Environmental conditions

Barometric pressure, air temperature and relative humidity in the Pyrotron laboratory were measured continuously at 1 Hz using Vaisala devices. Air speed in the tunnel was measured during each experiment at a location immediately upwind of the working section at 2 Hz using a 2D sonic anemometer. These instruments were connected to a LabView data acquisition system and controlled via a purpose-built LabView control software. The average air speed was calculated for the period of each experiment, defined by the commencement of ignition and cessation of burning of fuel in the fuel bed.

Experimental procedure

Once the fuel bed had been prepared, instrumentation for emissions monitoring was initialised. Just prior to ignition, three grab samples of fuel were taken and placed in steel tins for determination of gravimetric fuel moisture content via oven drying for 24 h at 105°C *(Matthews 2010)*. Data acquisition and video recording commenced at 30 s to ignition. At 3 seconds to ignition ('pre-ignition'), the fan was initialised (i.e. was started spinning to overcome inertia). At ignition, the fan was spun up to the predetermined speed (i.e., 1.0 m/s) and the fuel bed ignited.

Ignition of the fuel bed occurred via a 1.5-m-long, 18-mm-wide channel filled with ethanol Figure 52. The channel was placed on the upwind edge of the 4.0 m fuel bed for the heading fires and on the downwind edge of the 2.0 m fuel bed for the backing fires. The ethanol was ignited with a butane lighter.

Figure 52: Ignition of the surface fuel occurred via a butane lighter and ethanol in a channel placed on the upwind edge of the fuel bed for heading fires and on the downwind edge of the fuel bed for backing fires.

Fire behaviour

Each fire was allowed to burn freely across the fuel bed. Lines of between 5 and 11 thermocouples across the fuel bed and 500 mm apart and connected to the LabView data acquisition system recorded the temperature of gases 1-3 cm above the fuel bed at 10 Hz. From these data arrival time of the 250°C isotherm (assumed to represent the flame front) was recorded.

A video recording of each fire was made using a high-definition digital video camera located in the Pyrotron ceiling looking vertically down to the fuel bed. From the video flaming time and burn-out time for each piece of CWD was estimated.

Flame height was estimated ocularly and recorded in an observation sheet. Arrival time at each of the thermocouple lines was also measured manually using a stopwatch and recorded in the observation sheet.

From the interval arrival times, interval rate of spread, cumulative rate of spread and average rate of spread for the entire experiment were determined.

Post fire observations

When all visible flaming combustion ceased, the experiment was completed and continuous measurement of quantities was stopped. Very shortly after experiment completion, three samples of combustion residue were taken from the fuel bed for C/N chemical and component analysis. Only one sample was taken following backing fire experiments. Post-fire diameters of remaining CWD residue were measured with Vernier callipers.

To determine combustion factor, the final one metre segment (1.5 m^2) of fuel from heading and backing experiments was collected and then split the sample into CWD and litter components and weighed.

Results of environmental conditions

Figure 53 shows a box plot of the component composition of the fuel beds. Twigs dominated every fuel bed (mean 53.4%, std. dev. 4.8%), closely followed by leaves (mean 39.6%, std. dev. 4.4%). Bark was least represented in all fuel beds (mean 7.0%, std. dev. 0.8%). The tight ranges as illustrated in Figure 53 confirm that very little variation in fuel bed composition occurred.

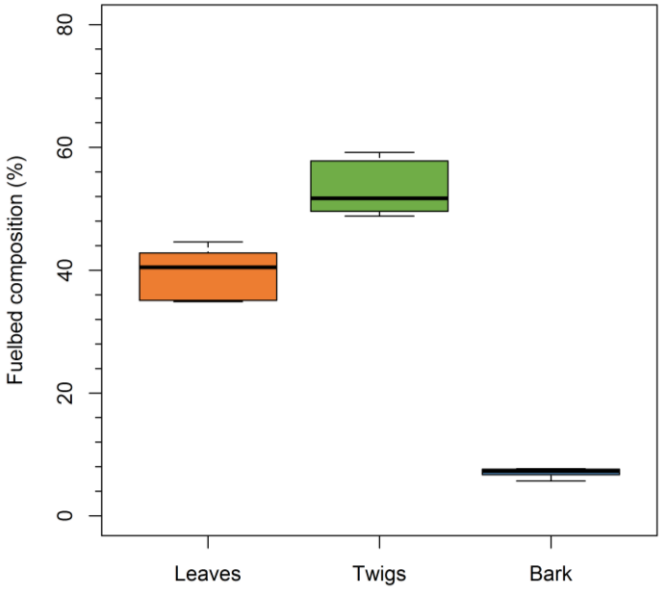

Figure 53: Boxplot of the range of component composition of the fuel bed based on five replicates. Most fuel beds were dominated with twigs while very little bark was present.

A summary of the ranges of values for the experimental conditions across the experimental series is given in Table 12. Fine fuel moisture exhibited a coefficient of variation (i.e. mean divided by the standard deviation) of 7.6% with a range of 4% over the burning period of two weeks. Branch moisture content exhibited a slightly larger coefficient of variation but the range was still relatively small at 5.1%. As is to be expected, wind speed for a single experiment had the lowest coefficient of variation of 2% with a range of 0.14 m/s.

Table 12: Summary of experimental conditions across the experimental series.

Variable	Range	Mean	Std. dev	Coefficient of variation (%)
Fine fuel moisture content	9.8 – 13.8%	11.80%	0.90%	7.60%
Branch moisture content	8.5 – 13.6%	10.80%	1.40%	13.00%
Wind speed[1]	0.94 – 1.08 m/s	0.98 m/s	0.02 m/s	2.00%

Variation in fuel moisture content across the period of the experimental series is given in Figure 54. Fine fuel moisture content exhibited little variation across the period as a result of consistent autumnal weather conditions during the experiments. The moisture content of CWD exhibited a slight increase in moisture early in the period, but due to the slower response of this fuel, the moisture stayed relatively constant for the remainder of the testing.

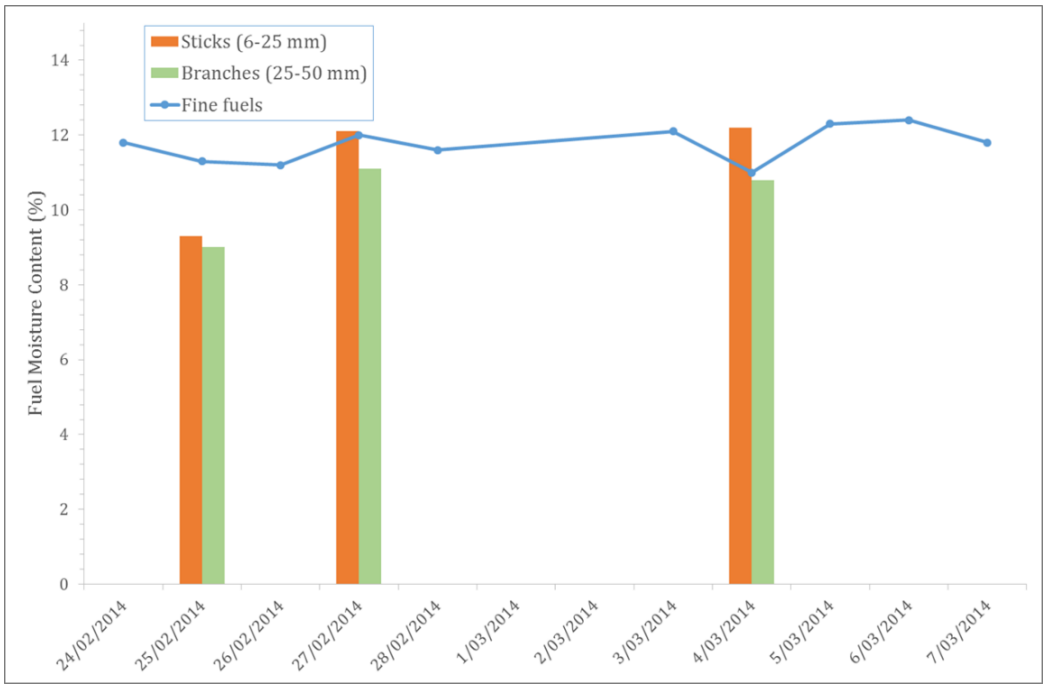

Figure 54: Variation in moisture content of fine fuels and CWD across the period of the experimental series. The moisture content of both fine fuel and CWD (branches and sticks) were not controlled but allowed to vary with ambient conditions.

Table 13 provides a summary of the number of replicates successfully completed for each treatment and the range of FMC and rate of spread measured. Some replicates had to be deleted from the dataset due to incompleteness (such as fuel measurements or rate of spread observations missing or corrupted). Priority during experimentation was given to the heading fire experiments (Figure 55) over the backing fires due to the greater influence on fire emissions expected from these types of fires. One replicate was completed for the control and Treatment 1 in the back fire, two replicates in Treatment 2 and 3. All treatments in the heading fires had at least 3 replicates.

[1] Typical values are provided for one experiment.

Table 13: Summary of experimental conditions across the experimental series.

Fire spread type	Experimental treatment	Replicates	FMC range (%)	ROS range (m/h)
Heading	Control (0 t/ha CWD)	3	11.6 - 12.5	69.6 - 112.6
	2 t/ha CWD	4	11.2 - 12.4	36.7 - 51.5
	6 t/ha CWD	3	11.1 - 12.0	41.3 - 61.1
	12 t/ha CWD	4	10.2 - 12.6	40.2 - 46.8
Backing	Control (0 t/ha CWD	1	10.0	5.4
	2 t/ha CWD	1	11.9	4.6
	6 t/ha CWD	2	11.9	4.55 - 5.1
	12 t/ha CWD	2	11.9 - 12.6	4.88 - 6.2

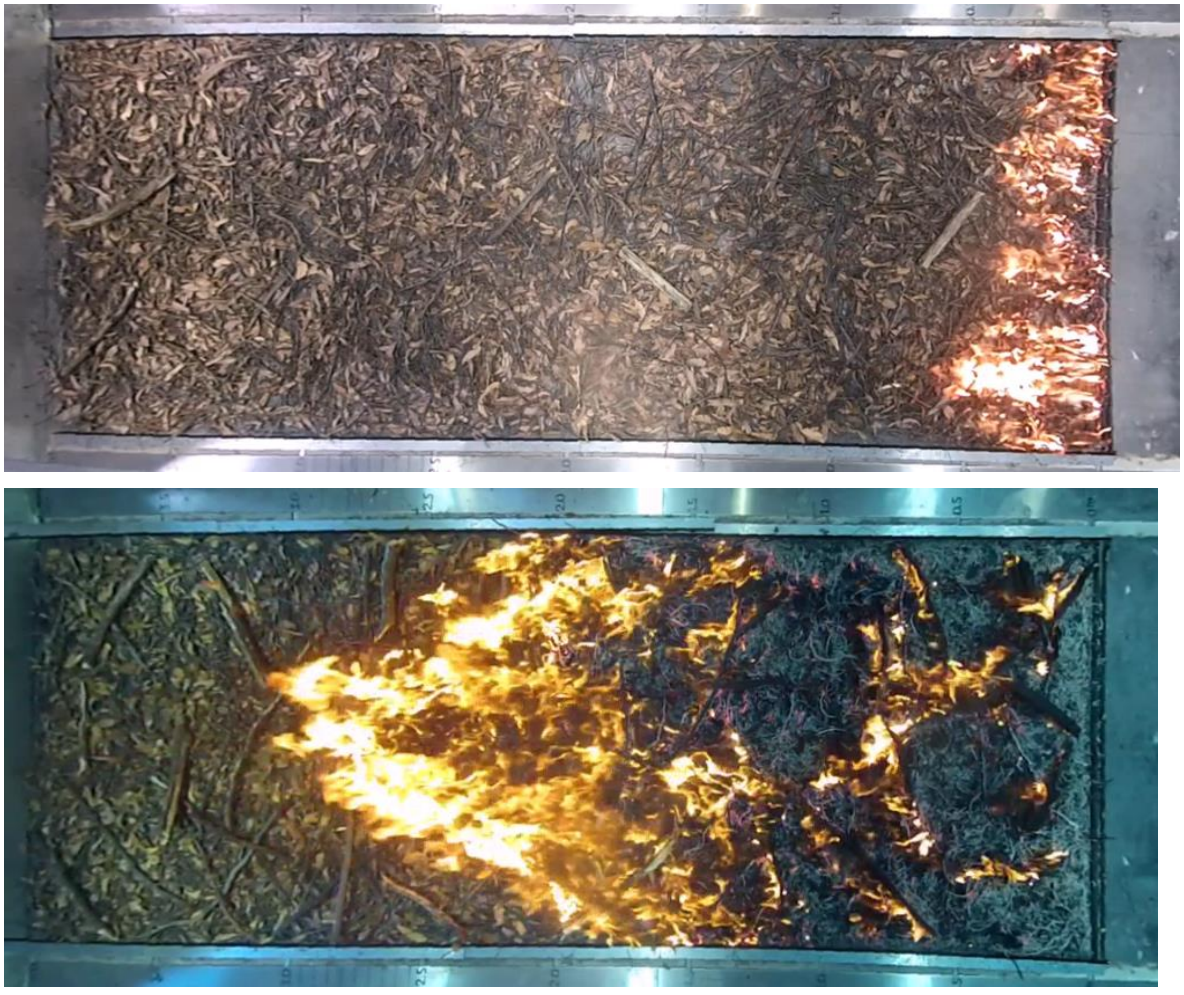

Figure 55: Examples of heading experiment fires. Top) Experiment in 2 t/ha CWD (Treatment 1) 60 seconds after ignition. Bottom) Experiment in 12 t/ha CWD (Treatment 3) 213 seconds after ignition. Residual burning of branches is apparent.

Results of elemental analysis of fuel

Figure 56 shows the summary of the elemental analysis of the fuel as assessed before burning for individual fuel elements such as leaves, bark, branches, etc. Carbon represented between 48.7% and 53.4% of the fuel bed, with small sticks (<25 mm) containing the least carbon and leaves containing the most carbon. The overall average carbon was 49.8% of the fuel bed. Nitrogen represented on a small fraction of the unburnt fuel, with between 0.09% and 0.41% present. Large sticks (25 – 50 mm) had the least nitrogen and leaves had the most. Analysis of elemental composition post experiment was initial separated into residue classes (ash, char, partially charred material, etc.), however for reporting purposes, these are combined into an overall average value for each treatment (Figure 57).

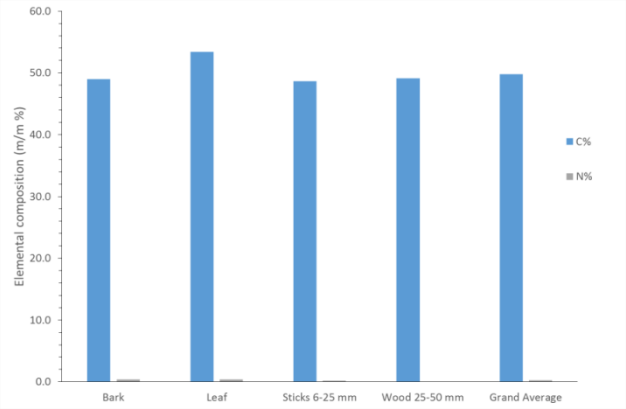

Figure 56: Elemental analysis of the fuel for carbon (C) and nitrogen (N), expressed as gravimetric (weight per weight) percentage.

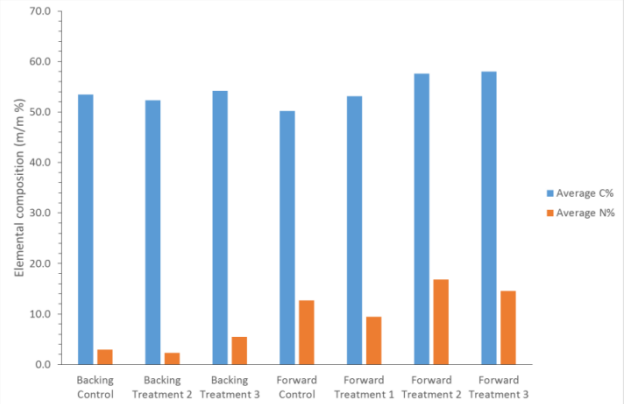

Figure 57: Summary of average post-fire elemental analysis of the combustion residue for carbon (C) and nitrogen (N), expressed as gravimetric (weight for weight) percentage for each fire spread mode (backing, heading) and treatment.

After combustion, there was very little difference in carbon content but there was for the nitrogen content. However, the relative amount of carbon in the residue was much higher than in the fuel prior to combustion. This was also true of nitrogen. These increases are primarily due to consumption of other elemental components such as oxygen and hydrogen.

The average carbon content of backing fires was 53.3%, whereas it was 54.4% for heading fires, however the amount of variation in heading fires was much greater. The average nitrogen content of backing fires was 3.6% whereas for heading fires it was 11.4.

Measurement system and sample analysis

A number of sampling lines were set up downwind of the working section at the end of the wind tunnel approximately 1m above the Pyrotron floor.

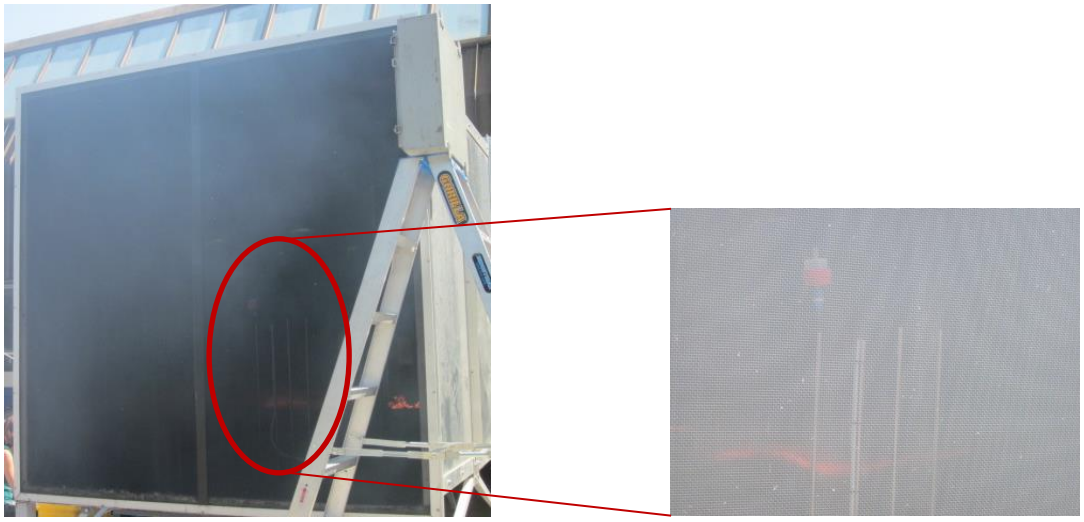

Figure 58: Sampling lines at the exit section of the wind tunnel

Air was drawn from these sample lines into the following instrumentation/filters:

- Two Cavity ring-down spectrometers (CRDS, *Los Gatos Research Inc., CA*) for the continuous measurements at 1 second interval of CO_2 and CH_4 (Greenhouse Gas Analyser GGA-24r-EP, *Los Gatos Research Inc., CA*) and of CO and N_2O (N_2O/CO Analyser 907-0015, Los Gatos Research Inc., CA). The instruments work by directing a pulsed laser beam into a highly reflective cavity containing the gaseous sample. Each pulse of laser is absorbed and/or scattered by trace gases following the Beer-Lambert Law, causing a temporal decay (or ring-down) of the pulse, which is modelled as an exponential decay process *(Okeefe and Deacon 1988)* in order to retrieve the concentrations. A dilution with zero air is necessary to avoid difficulties with the N_2O retrieval due to interference with CO spectral lines when CO concentration goes beyond 10 ppm *(Surawski et al. 2015)*. One of several dilutions ratios (ranging from 4 to 15) were used on the inlet sample line serving both instruments for each fire.

- DustTrak II aerosol monitor (Model 8530, *TSI Inc., USA*), a light-scattering particle monitor that provides continuous measurements of $PM_{2.5}$ every 10 seconds at a flow rate of 1.7 L/min. Calibration of the $PM_{2.5}$ concentrations was done against gravimetric measurements on pre-weighed Teflon filters

- Pre-weighed Teflon filters for gravimetric measurements of PM and chemical composition of PM

- Baked quartz filters for measurements of the organic and elemental carbon composition of PM

- Tekran 2537B Mercury Vapour Analyser providing Hg measurements every 2.5 minutes at a flow rate of 1L/min. The intakes had Teflon filters attached to the end to capture particulate Hg.

- 10L Tedlar Bags were used to collect grab samples over a 1-4 minute period. The samples were analysed for Hg using a Tekran analyser and for trace gases using a Fourier transform spectrometer coupled to a White cell, and for a suite of VOCs via Selective Ion Flow Tube Mass Spectrometry (SIFT-MS).

Emissions were also monitored in real time using an Open Path Fourier Transform Infrared Spectrometer (OP-FTIR). It consists of an FTIR spectrometer (Bomem MB-100 Series FTIR spectrometer, with a resolution of 1 cm-1) operated in open-path mode using an external beamsplitter and mirrors to direct the modulated infrared beam into a 12 inches (305mm) telescope (Meade LX300). The infrared beam was reflected back to the telescope by an array of gold-plated corner cube mirrors, and directed to a liquid nitrogen cooled Mercury Cadmium Telluride detector. It was positioned with its line of sight across the open end of the wind tunnel, downwind of the working and exit sections. A

retro-reflector array was installed atop a 2.4m stepladder, whilst the spectrometer was coupled to a telescope and mounted on a tripod. The total path-length was about 10 m. The open-path FTIR system used in this project is described in detail in *Paton-Walsh et al. (2014)*. A spectrum was recorded approximately every 20 s (by co-adding 3 scans per spectrum at 1.0 cm−1 resolution) for several minutes before ignition and then throughout the fire. The spectra may be subsequently analysed, thereby provided continuous (every ~20s) measurements of CO_2, CO, and CH_4 both before and during the fires. Mixing ratios for ammonia (NH_3), ethene (C_2H_4), formaldehyde (HCHO), methanol (CH_3OH), formic acid (HCOOH) and acetic acid (CH_3COOH) were also be retrieved using this system.

Mole fractions were retrieved from all the acquired FTIR spectra using the Multiple Atmospheric Layer Transmission (MALT) model *(Griffith 1996)* and the spectral windows described in *Paton-Walsh et al. (2014)*. MALT uses a non-linear least square analysis to minimise the difference (mean-squared residual) between a measured gas-phase infrared spectrum and a 'synthetic' spectrum. This 'synthetic' spectrum is initially calculated by MALT using absorption line parameters (mostly from the 2008 HITRAN database *(Rothman et al. 2009)* and an estimation, for each trace gas species, of the amount present in the sample. From these, MALT calculates 'true' absorption coefficients for each molecule at the desired temperature and pressure, and simulates the measured spectrum by scaling and adding the absorption coefficients, converting to transmission, and convolving the transmission spectrum with the appropriate instrument line-shape. The instrument line-shape is determined from instrument parameters that can be 'fixed' or 'fitted' during the retrieval process. If an instrument parameter is "fitted" then the initial assigned value is adjusted (along with the trace gas mixing ratios) during the iterative recalculations of the 'synthetic' spectrum. Once the best fit is achieved, MALT returns mole fractions in the grab samples for each trace gas species (CO_2, CO and CH_4), as well as values for each fitted parameter.

Field experiments

Emissions measurements were undertaken at two prescribed burns in autumn 2015 as well as two prescribed burns in spring 2015.

Prescribed burns

The two autumn burns were conducted on 13 April 2015 at Greendale (293 ha) (Figure 59) and on 23 April 2015 at Castlemaine (Figure 60). These burns were attended by staff from CSIRO, University of Wollongong and University of Melbourne.

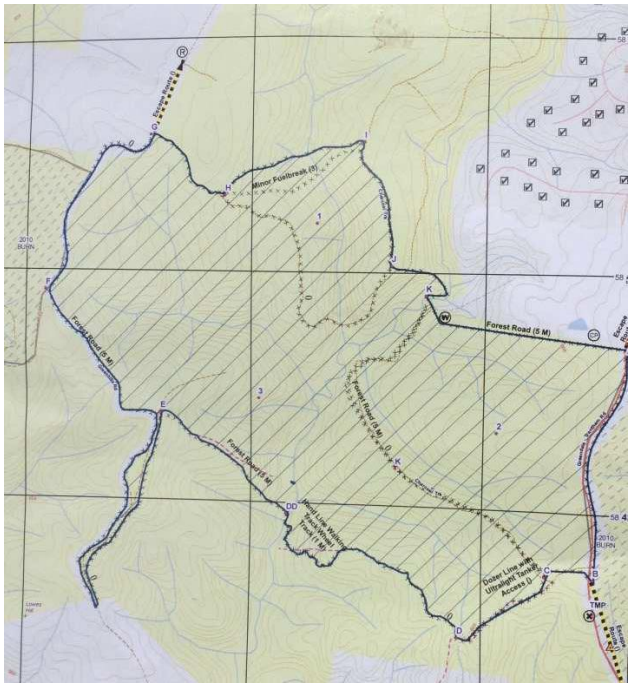

Figure 59 Map of Greendale prescribed burn

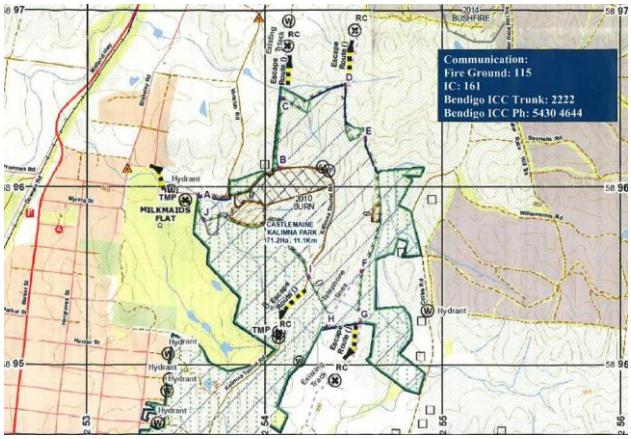

Figure 60 Map of Castlemaine prescribed burn

The two spring burns were conducted on 30 September 2015 (56 ha Bambra-Deans Marsh) (Figure 61) and on 1 October 2015 at Campbells Creek (80 ha). These burns were attended by staff from CSIRO.

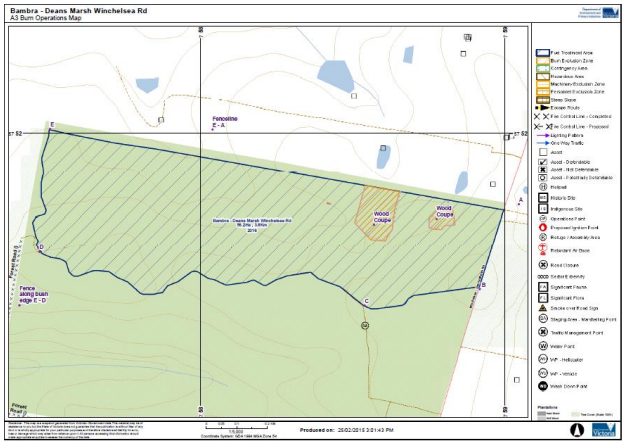

Figure 61 Map of Bambra-Deans Marsh prescribed burn

Backpack sampler

Smoke was collected using a portable backpack smoke collector suitable for sampling close to the emission sources of prescribed fires (Figure 62). The unit comprises a 2.5 m × 12 mm diameter stainless steel sampling probe, in-line Teflon filters and an air pump that delivers the filtered smoke sample to a 10 L Tedlar bag mounted on a backpack. During sampling the tip of the probe was positioned approximately 500 mm above the flame within the entrainment zone. In this region, combustion has ceased due to cooling and dilution by entrained air, but the smoke concentration remains high. The air sampling rate was set at approximately 1 LPM and therefore each sample bag contains smoke sample collected over approximately 10 min. The backpacks are equipped with three additional gas lines; two for continuous measurement of $PM_{2.5}$, CO_2 and CO, and a third for collection of total suspended particulate matter (TSP) on filters. Concentrations of CO_2 and CO were measured continuously with a Q-Trak (model 7565, TSI Inc., USA) and particulates were measured continuously with a DustTrak (model 8530, TSI Inc., USA).

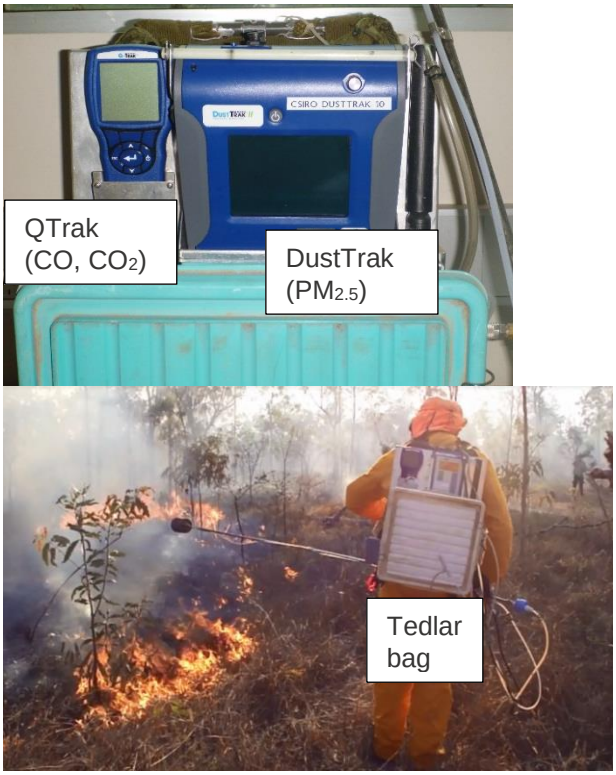

Figure 62: Backpack sampler system used at prescribed burns

Smoke was collected from flaming combustion, from targeted sampling of smouldering-phase combustion behind the fire front and from burning of heavy fuels and logs.

At each burn, two clean air samples were collected into Tedlar bags to provide background concentrations of CO, CO_2, CH_4 and N_2O.

Sample analysis

All samples collected within the Tedlar bags were taken back to the CSIRO laboratory at Aspendale and analysed for CO, CO_2, CH_4 and N_2O within 12 hours of collection using cavity ring-down spectrometer (*Los Gatos Research Inc., CA*).

The pre-weighed 47mm Fluoropore membrane filters (1 µm pore size, Merck Millipore) were analysed for gravimetric mass using a Mettler UMT2 ultra-microbalance with a specialty filter pan in a temperature and humidity controlled environment. Filters collected for gravimetric mass concentrations were also used for analysis of anhydrosugars including levoglucosan and water-soluble ions.

Levoglucosan and water soluble ions were extracted from the filters by adding 100 µl of methanol, to wet

the hydrophobic filter, and 5 cm^3 of de-ionised water produced from a Millipore Milli-Q Advantage 10 system. To prevent loss of levoglucosan and soluble ions from bacterial action, 50 µl of chloroform was added. Levoglucosan was determined by high-performance anion-exchange chromatography with pulsed amperometric detection (HPAEC-PAD). The development of the HPAEC-PAD technique is based on a previous study to measure levoglucosan in $PM_{2.5}$ from biomass combustion *(Engling et al. 2006)*. Anion and cation concentrations were determined by suppressed ion chromatography (IC) with a Dionex ICS-3000 reagent free ion chromatograph.

Open-path FTIR

The open-path FTIR was set up so that smoke from the fire fills the path between the spectrometer and the retro-reflectors (Figure 63). Typically, the system is set up and starts recording before the fire is ignited, and is left to run until mole fractions return to ambient values. This means the instrument captures emissions from all stages of the fire.

Figure 63: The open-path FTIR instrument set up at a prescribed burn

Appendix B: Fuel loads

Introduction

Fuel maps are essential for fire and smoke prediction since fuel type and fuel amount affect combustion and emission during wildfires and prescribed burns.

In south-eastern Australia fuel characterization and classification approaches have focused on providing inputs for predicting fire spread (McArthur Meter and PHOENIX fire spread model) and have focused only on fine fuels components *(McArthur 1967)*. Fire spread is driven by flaming combustion and is a key determinant of the progression of a surface fire. However, typical fire spread models are not designed to estimate fire effects associated with post-frontal combustion so that heavy fuels (i.e. CWD), are not well simulated/described in fire spread models. Post-frontal combustion of heavy fuel has potential for high impact on smouldering emissions,

In this study we used two new empirical fuel load data sets, *Volkova and Weston (2015)* (V&W), and State Government forest monitoring data (DEPI VFMP) (Figure 64), the biogeochemical model, BIOS2 *(Haverd et al. 2013)* and the PHOENIX Rapidfire model *(Tolhurst et al. 2008)* to derive comprehensive maps of fine and CWD fuels for the State of Victoria, Australia.

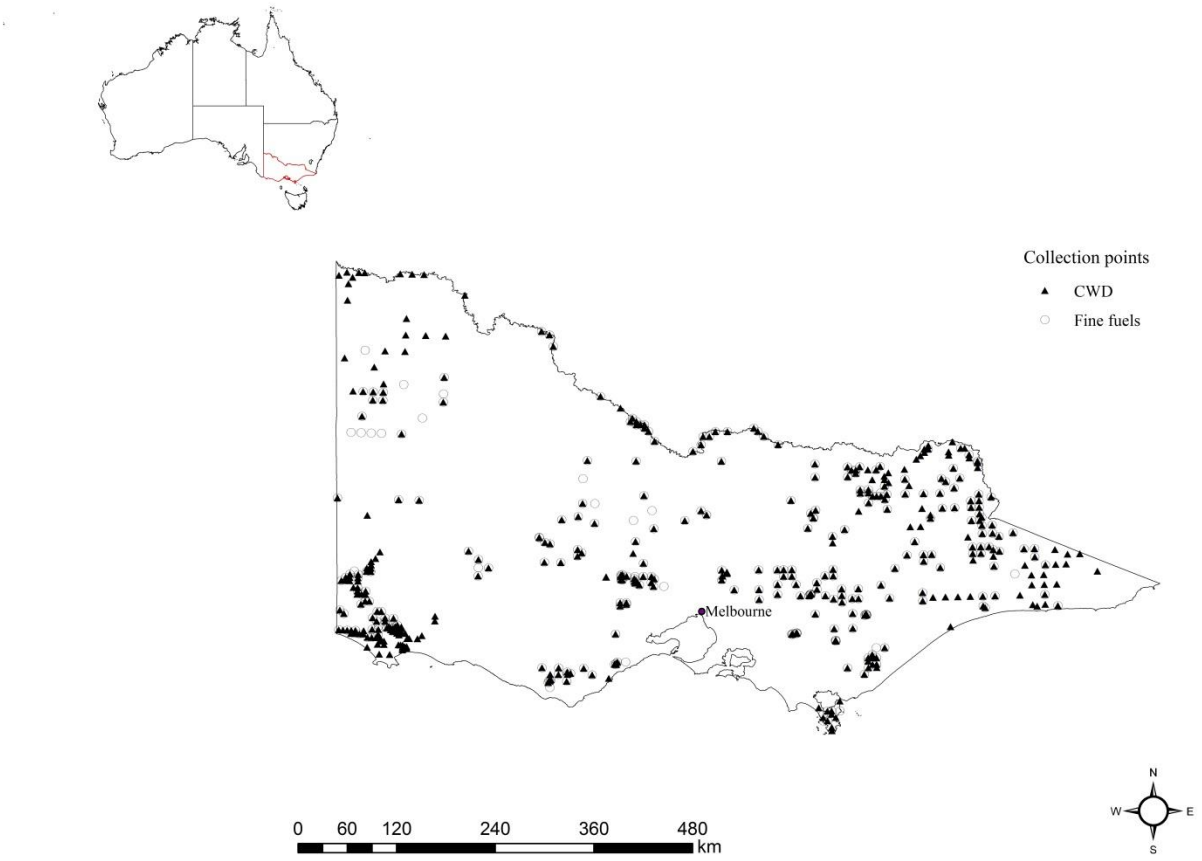

Figure 64: Map of the VFMP and V&W collection points used in the analysis and IBRA boundaries

Materials and Methods

Fuel load data sets

Volkova and Weston (V&W) dataset

This dataset included duff layer (partly decomposed leaf organic material <2 mm); litter (dead plant material such as fruits, leaves, bark, and small branches with diameter <2.5 cm) CWD (woody materials on the forest floor with diameter ≥2.5 cm).

Litter was separated into classes: fine litter and small branches <=6 mm in diameter, and small branches with a diameter 6-25 mm. The sampling procedure and biomass estimation is described in detail in *Volkova and Weston (2013)*. Additional fuel dataset, collected by the same authors in SW Victoria as part of the Smoke Transportation and Emission Modelling Project was also included in this study.

The VFMP dataset

The VFMP dataset included litter, i.e. duff and leaves, bark and twigs less than 10 mm in diameter (SOP 17, *(DSE 2011)*) and CWD, i.e. branches and logs, substantially detached from the parent tree and in contact with the ground, with diameter >= 10 cm in two cross-sectional directions (SOP 16, *(DSE 2012)*). Each CWD piece was assigned a decay class and included sound, moderate and rotten and very rotten (*(DSE 2012)*, SOP 16).

Litter loads were calculated as the total weight of litter (g/m^2) collected from four 0.5m by 0.5m soil sampling quadrats at each sample plot, converted to tonnes per hectare. The volume of CWD was estimated assuming a cylindrical shape for CWD pieces then multiplied by wood density for measured decay class (451 kg/m^3 for sound; 340 kg/m^3 for moderate, 226 kg/m^3 for rotten and 100 kg/m^3 for very rotten (from *(Aponte et al. 2014)*).

Adjustments of field datasets to uniform CWD classes

The VFMP dataset required adjustment for small branches of 6-25mm diameter not measured as part of fine fuel pool and for 25-100 mm diameter branches and logs not measured in CWD pool (Table 14). To account for those two categories the V&W dataset was analysed for ratios of total litter to 6-25 mm branches and of 25-100 mm logs to total CWD loads (Table 14). An average scaling factor was used to adjust the VFMP data for each pool.

Table 14 Description of initial and final fuel classes used to develop fuel maps

Fuel map	Datasets	Volkova and Weston (V&W)	VFMP	Comments
FINE	Duff	Well decomposed leaf organic material collected down to the mineral soil surface and sieved to <2 mm or <6 mm fraction	Well decomposed leaf organic material collected down to the mineral soil surface and sieved to <2 mm	Difference in factions between <6 and <2 mm in V&W data was disregarded as <6 mm was used only in 10 data points (out of 42)
	Fine litter	Litter material including twigs with a diameter up to 6 mm	Litter material including twigs with a diameter up to 10mm	Difference (6 mm vs. 10 mm) in twig sizes was disregarded
CWD	Fine twigs	6-25 mm	Not measured	VFMP data was scaled up by 11% to account for 6-25 mm pool (see Results section)
	CWD	25 mm+	100 mm+	VFMP data was scaled up by 12% or 33% forest type depending to account for 25-100 mm logs (see Results section)

Models used in fuel map development

The biogeochemical model, BIOS2 *(Haverd et al. 2013)* simulates the dynamics of the canopy, live and dead woody pools and the live and dead grass pools. Fuel types are ranked by NDVI index and in general “fine grassy” represent grass leaves, “fine woody” is fine tree litter and CWD is the rest of tree biomass without separation by diameter classes.

The PHOENIX Rapidfire model *(Tolhurst et al. 2008)*, widely adopted across south-eastern Australia for prediction of wildfire spread, uses an aggregation of Ecological Vegetation Classes (EVC groups) to apply fine fuel loads in models of fire spread *(Tolhurst 2005)*. The PHOENIX fuel mass estimates are based on a mix of qualitative and quantitative approaches and have not been confirmed by detailed empirical measurements *(Tolhurst 2005)*.The PHOENIX fuel classes are aggregated into 27 fuel type groups and include surface fuels (litter and duff), elevated fuels (live shrubs), and bark (Table 15). The fuel load for each component is defined either as a class average, or is adjusted for time since fire by parameters of the fuel accumulation curves, which, when combined with fire history data, define the mean fine fuel load in the year of the fire.

The approach to developing new fuel mass maps recognizes that both the BIOS2 model and PHOENIX fuel table require verification and possible calibration before they can be used for smoke and emission modelling purposes.

Adjustment for fire history

Both BIOS2 and PHOENIX models estimate fuels in their steady state, and therefore all field measurements were assessed against fire history shapefile provided by DELWP plots where measurements were taken within 5 years since fire (wildfire or planned burn) and were adjusted for fire history using an approach developed in *Roxburgh et al. (2015)*.

BIOS2 dataset for the period of 1983-2013 was used to extract CWD and fine fuel loads. Maximum values of the monthly mean (hereafter BIOS2_max); the 30 year mean of the annual monthly max (hereafter BIOS2_mean) were extracted as raster layers to ArcMap 10.2.2 (Esri, Redlands, CA, USA).

PHOENIX surface fuel loads *(Tolhurst 2005)* was used to assess field measurements and BIOS2 predictions. Fuel codes of PHOENIX were used to group field data by ecological vegetation classes.

Developing fuel maps

Fuel maps were developed using the following procedure

1) Predicted fuel loads from masked BIOS2 were extracted to field observations (values to points function, Spatial Analyst Tool, ArcGIS 10.2.2).

2) Extracted data was combined with PHOENIX map using spatial joint function of ArcGIS.

3) Final datasets (fine and CWD) were exported to Excel 2010 and stratified by PHOENIX fuel codes (24 fuel codes, Table 15). Observed and predicted loads were analysed for mean, median, maximum and minimum values.

4) A scaling factor was used to adjust BIOS2 raster layer based on the analysis of the data; PHOENIX dataset provided only one value per fuel code and was used to justify scaling of BIOS2.

5) A single scaling factor was used to adjust BIOS2 predictions for fine fuel loads using Raster Calculator function (Spatial Analyst Tool, ArcGIS) to produce fuel maps.

Validation data

A total of 483 field measurements were available for map development, with 454 measurements for CWD and 317 measurements for fine fuels. Around 288 observations contained both fine and CWD measurements.

Sixty data points (or 20% of the data) were randomly selected from the dataset and excluded from the analysis for validation of the maps.

BIOS2 adjustment

Field fuel loads, matching BIOS2 predictions were grouped by corresponding PHOENIX fuel codes. Because field data was unevenly distributed among PHOENIX fuel codes, all analyses were performed on averaged data to give similar weighing to all measurements.

Observed and predicted fuel loads were assessed against a 1:1 line. Scaling factors, derived from a linear regression equation were applied to adjust model predictions. Slope and an intercept of the linear regression were estimated using a Solver function (Frontline Systems, Inc. Incline Village, NV, USA) of Excel 2010 based on the smallest difference of square standard deviations (SSD) between observed and predicted fuel load.

Table 15. **PHOENIX** fuel codes and their descriptions used in data analysis

Fuel Code	Description
F03	Riparian Forest shrub
F04	Wet Forest shrub & wiregrass
F05	Damp Forest shrub
F08	Forest with shrub
F09	Forest herb-rich
F10	Dry Forest shrubs
F11	Dry Open Forest shrub/herbs
G03	Ephemeral grass/sedge/herbs
G04	Temperate Grassland / Sedgeland
M03	Mallee shrub/heath
M04	Mallee spinifex
S01	High Elevation Shrubland/Heath
S02	Riparian shrubland
S04	Moist Shrubland
S06	Broombush / Shrubland / Tea-tree
S07	Sparse shrubland
S10	Wet Heath
S11	Dry Heath
W01	High Elevation Woodland shrub
W02	High Elevation Woodland grass
W06	Woodland Grass/Herb-rich
W07	Woodland Heath
W08	Gum Woodland heath/shrub
W09	Gum Woodland grass/herbs

Results

Adjustments of VFNP dataset to uniform CWD classes

Fine twigs (6-25 mm) accounted for 10% and $CWD_{25\text{-}100\ mm}$ for 36% of the total CWD loads. Scaling factors of 0.187 x $CWD_{100\ mm+}$ and 0.671 x $CWD_{100\ mm+}$ were applied to fine twigs and $CWD_{25\text{-}100\ mm}$ categories respectively to harmonise CWD results in Table 16.

Table 16. Conversion factors for CWD fuels used to adjust VFMP data

CWD pool	Mass, t ha^{-1}	%
Fine twigs (6-25 mm)	3.0±0.48	12.2
$CWD_{25\text{-}100\ mm}$	7.1±0.71	35.0
$CWD_{100+\ mm}$	17.6±2.41	52.8
Total	**28.0±3.02**	**100**

Developing scaling factor for fine fuel map

A total of 275 fine fuel measurements were intersected with 23 PHOENIX fuel codes, while remaining 12 fuel codes had no corresponding field measurements. Seven fuel codes had less than three replicates and three fuel codes (F08 ‘Forest with shrub’, F09 “Forest herb-rich’ and W07 “Woodland Heath”) had above 30 measurements each.

BIOS2 predictions were distributed more uniformly than field measurements. Fuel loads assigned to PHOENIX fuel codes were comparable to field average and max values (data not shown).

Averaging data by fuel code revealed that BIOS2 tended to under-predict fuel loads with the majority of the data lying above 1:1 line (Figure 65, left). Scaling BIOS2 resulted in more evenly distributed data along 1:1 line (Figure 65 closed symbols). PHOENIX fuel loads had a parallel rather than 1:1 distribution of the data (Figure 66).

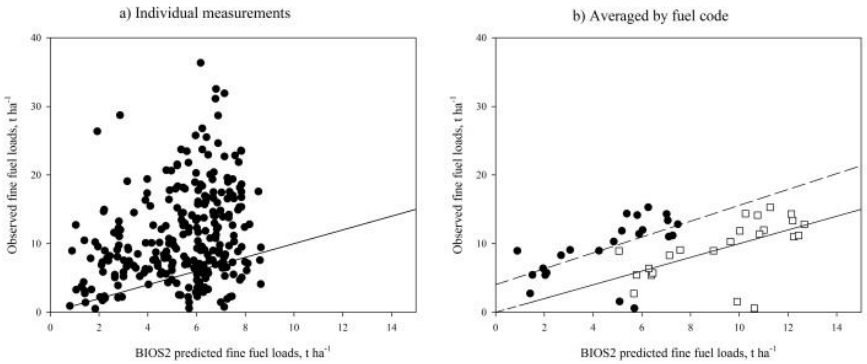

Figure 65 Observed fine fuel loads individually and grouped by fuel code. Closed symbols are before the adjustment and open symbols are after model adjustment. Solid line represents 1:1, dashed lines are linear regressions before calibrations.

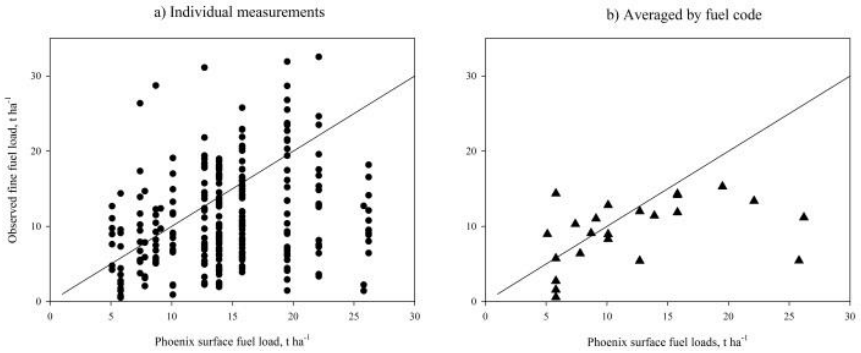

Figure 66 Individual measurements of fine fuel loads used in PHOENIX RapidFire and grouped by fuel code. Solid line represents 1:1.

Obtained scaling factors were applied to the validation data which showed a significant improvement in the slope of the data distribution (Figure 65, closed symbols). Scaling factors were used for the development of the final map of fine fuels (Figure 67).

.

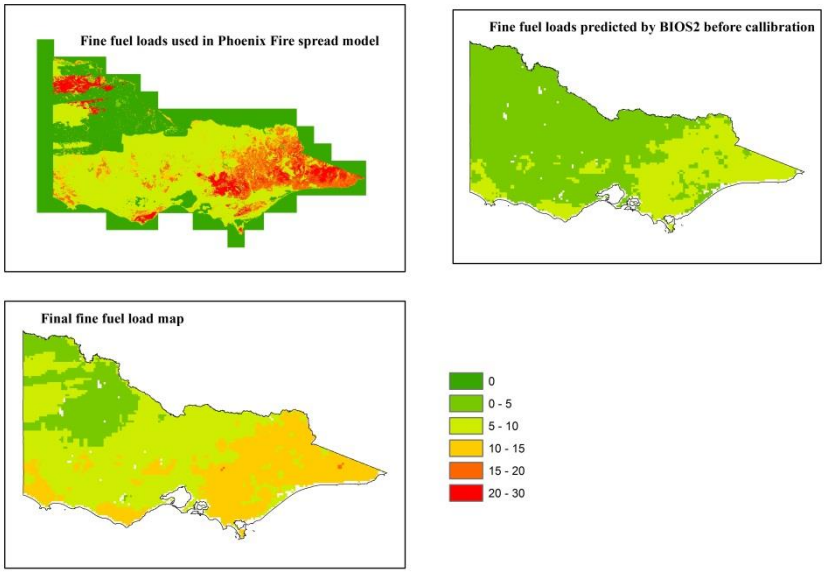

Figure 67. Map of fine fuel loads for Victoria. Fine fuels include duff, and litter and twigs with diameter ≤6 mm. Fuel loads are in t ha^{-1}

Developing scaling factors for CWD fuels

A total of 410 data points were available for the analysis of CWD. They corresponded to 27 fuel codes where four fuel codes had less than three replicates and four fuel codes had above 30 measurements (data not shown). Eight fuel codes were not represented in the analysis. BIOS2 did not reflect spatial variability of CWD loads in the field.

BIOS2 greatly over-predicted CWD loads for low productivity forests such as mallee (M01, M03, M04) and shrublands (S02 and S06). For highly productive forests such as wet forests, BIOS2 predictions were 2-4 times lower than field measurements (F04, F05 and G04).

In contrast to fine fuel, CWD loads were more broadly distributed along 1:1 line (Figure 68). Scaling BIOS2 resulted in improved predictions of CWD loads but didn't lead to more uniform distribution of the data along 1:1 line (Figure 68 open symbols). Derived scaling parameters were applied to the validation data producing a similar pattern as the main CWD data (Figure 69).

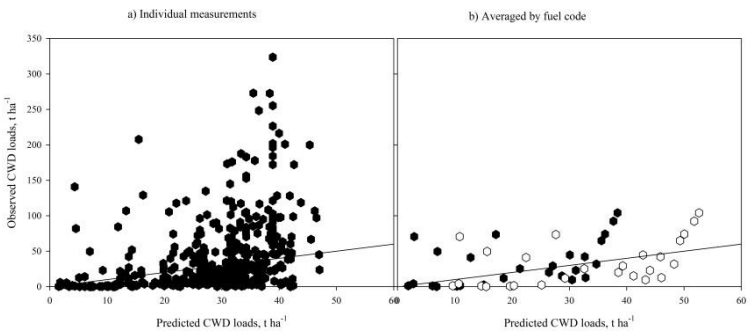

Figure 68. Predicted and observed CWD loads before (closed symbols) and after adjustment (open symbols) Values are means grouped by PHOENIX fuel codes

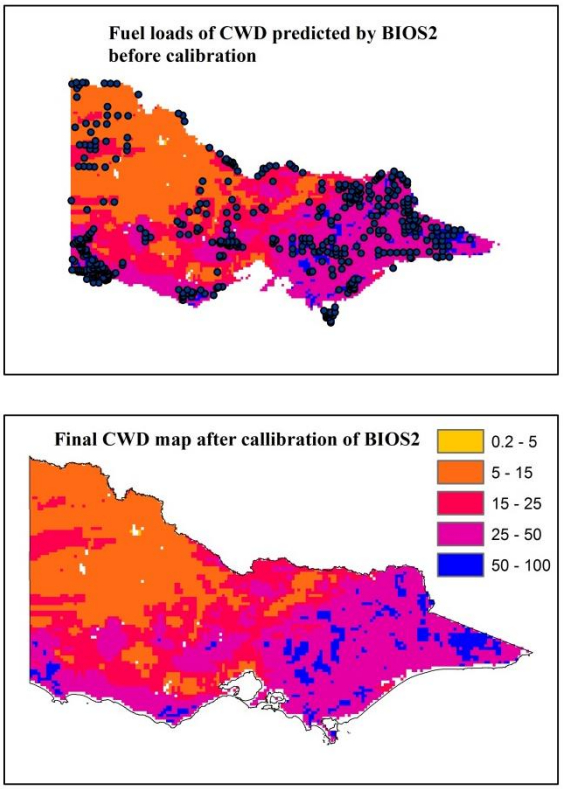

Figure 69. Map of CWD fuel loads for Victoria. CWD fuels include twigs and logs with diameter >6 mm

Appendix C: Fire behaviour

Introduction

Current Australian forest fire behaviour prediction systems such as the McArthur Forest Fire Danger Meter (FFFM) *(McArthur 1967)*, the Western Australian Forest Fire Behaviour Tables (FFBT) *(Sneeuwjagt and Peet 1998)* and the Dry Eucalypt Forest Fire Model (DEFFM) *(Gould et al. 2007a; Gould et al. 2007b; Cheney et al. 2012)* consider only the contributions to fire behaviour from the fine (<6 mm diameter) fuels.

These fuels, comprising mostly fallen leaf, bark and twig material, are considered thermally thin (i.e., they respond very quickly to changes in the thermal environment around them). Thus they rapidly absorb heat from an approaching fire, ignite and release the bulk of their potential chemical energy in the flame front. As a result the combustion of these fine fuels and their influence on the behaviour and spread of a bushfire has been the focus of much of past research into bushfire behaviour.

The physical dimensions of coarser fuel elements (i.e., >6 mm diameter), such as fallen branches, boughs and toppled stems (collectively known as CWD or downed woody fuel) mean that they are not thermally thin and thus take time to absorb heat to raise them to the temperatures required for the onset of thermal degradation *(Beall and Eickner 1970)*. Consequently, CWD generally ignites during the passage of the flame front and burns out well after the flame front has passed. Thus the combustion of coarser fuels has been found to play little direct role in contributing to heat output from the actively spreading part of a bushfire, its behaviour or speed *(Andrews 1986)*. As a result, the combustion of CWD has not received much attention in this regard.

However, the combustion of CWD fuel components does play a significant role in other aspects of bushfire behaviour, particularly behind the fire front, including the radiant heat flux and firefighter safety *(Sullivan et al. 2002)*, the fire intensity, severity and burning depth *(Cruz et al. 2012)*, and particulate and gas emissions, especially those related to the generation of smoke and greenhouse gases *(Bertschi et al. 2003)*.

Little is known about the characteristics of the particulate and gas emissions from the combustion of many types of CWD, particularly CWD found in the sclerophyll forests of south-eastern Australia. In order to attempt to fill this gap, this component of the project undertook controlled burning experiments involving fallen branch material in the range 6 – 50 mm in diameter to quantity both the emissions released by CWD and the effect CWD has on fire behaviour.

Objective

The objective of this phase of the study was to quantify the effect of CWD on the fire behaviour (in particular rate of spread) of those fires.

The working null hypothesis of these experiments was that the rate of spread of fires burning in fuels with CWD would be no different to that of fires burning without CWD.

Results

Combustion efficiency

Figure 70 shows the combustion efficiency for all fuels (fine and CWD) for the heading fires and backing fires measured as the difference between the pre-fire fuel loads and post-fire loads expressed as a fraction of the pre-fire fuel loads. In the case of CWD experiments, the overall combustion efficiency is a weighted sum of the individual fuel element combustion efficiencies.

With the larger number of replicates in the heading fire experiments, the overall mean was 0.833, meaning that on average only 16.7% of the original fuel mass in these experiments was left incompletely combusted after the experiment.

There is very little variation in combustion efficiency of the heading fires across the treatments with the means of each treatment ±0.02 of the overall mean.

The overall range of values was also relatively tight with the minimum being 0.632 in Treatment 2 (6t/ha CWD) and the maximum being 0.924 in Treatment 3 (12t/ha CWD).

The combustion efficiencies for the backing fire experiments are very similar to those of the heading fire experiments. The highest value was 0.860 in Treatment 3 (12t/ha CWD) and the lowest was 0.515 in Treatment 2 (6t/ha CWD). Excluding the latter as an outlier, the mean combustion efficiency was 0.833, almost exactly the same as for the heading fires. The low number of replicates of this fire mode, however, reduces the overall reliability of such metrics.

While there is little difference in combustion efficiencies either across treatments or fire spread mode as measured after the experiment, there were clear differences observed in the way in which fuels were consumed. Residual burning after the passage of the flame zone was highest in the heading fires and highest in the CWD, many of which continued flaming long after the fine fuels had ceased combustion. The backing fires had very little residual combustion in the fine fuels as a result of the slower rates of spread.

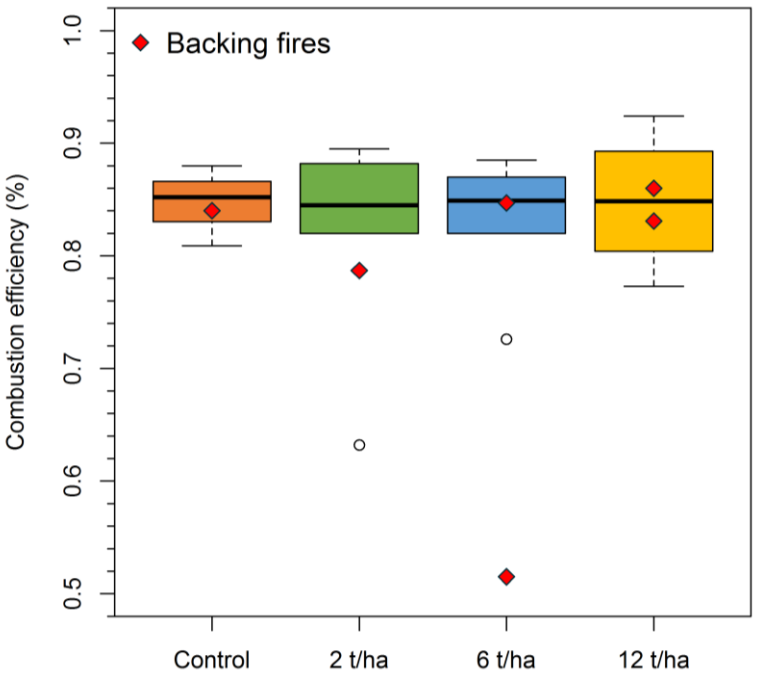

Figure 70: Boxplot of the combustion efficiencies for all fuels (fines + CWD) measured for heading fire experiments. The overall mean was 0.833. Overlayed are red diamonds showing the individual combustion efficiencies for all fuels (fines + CWD) for the backing fire experiments.

Heading fire – rate of forward spread

The results of the rate of spread analysis are given in Figure 71-81. Figure 71 shows the matrix of interval rate of spread results for the control (Figure 71a) and three treatments (Figure 71b-d). Also in each graph is displayed the mean interval rate of spread for each interval (orange lines). Interval rate of spread is the average rate of spread across each individual 0.5 m interval along the fuel bed. These are then summarised in Figure 72.

Cumulative rate of spread is the average speed over the total distance covered at each 0.5 m interval.

Figure 73 shows the matrix of cumulative rate of spread results for the control (Figure 73a) and three treatments (Figure 73b-d). The mean of all values in each interval are shown in the orange line and summarised in Figure 74.

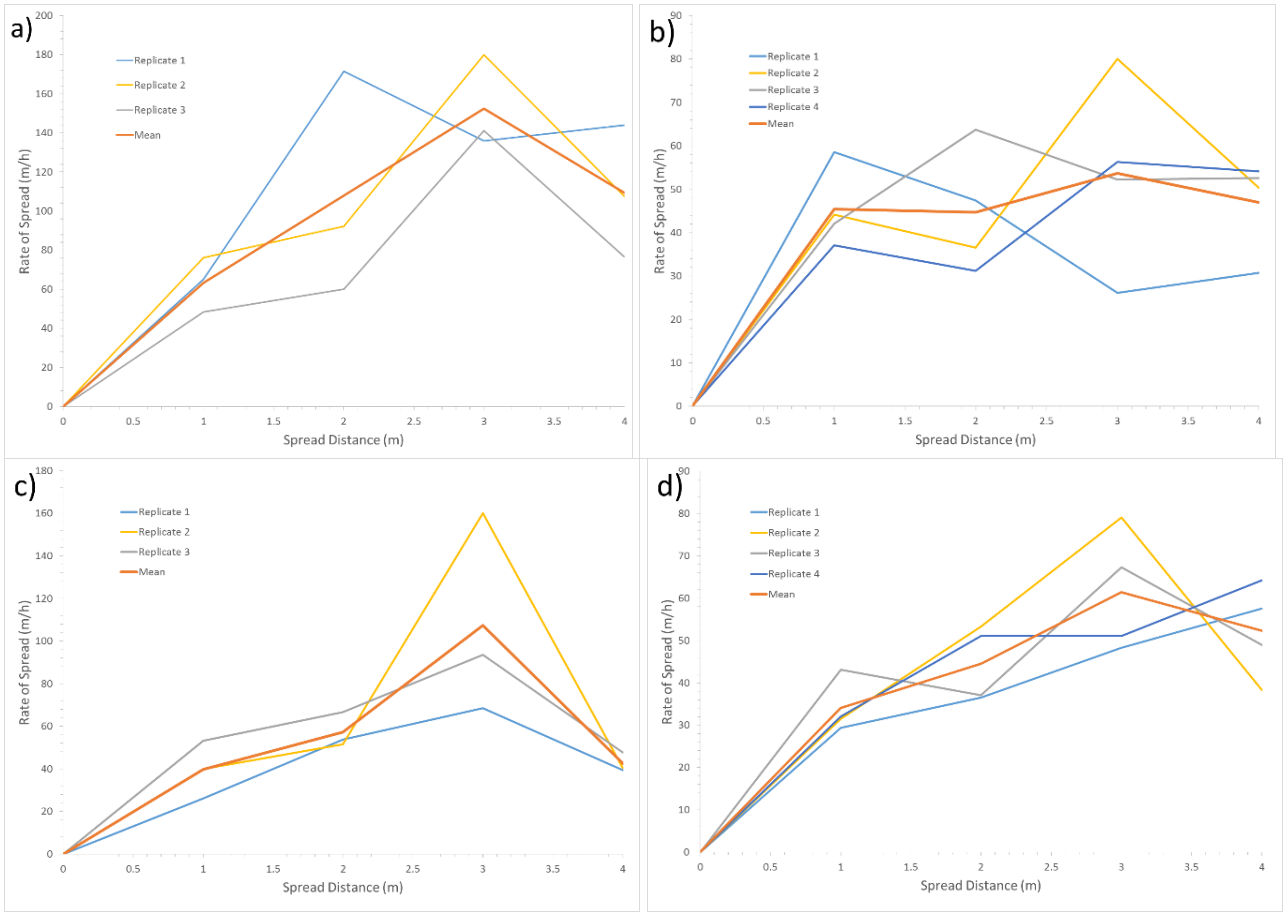

Figure 71: Interval rate of spread for the a) control (i.e., no CWD), b) 2 t/ha CWD treatment, c) 6 t/ha CWD treatment, and d) 12 t/ha CWD treatment. Interval rate of spread is the average speed for each 0.5 m interval of the fuel bed.

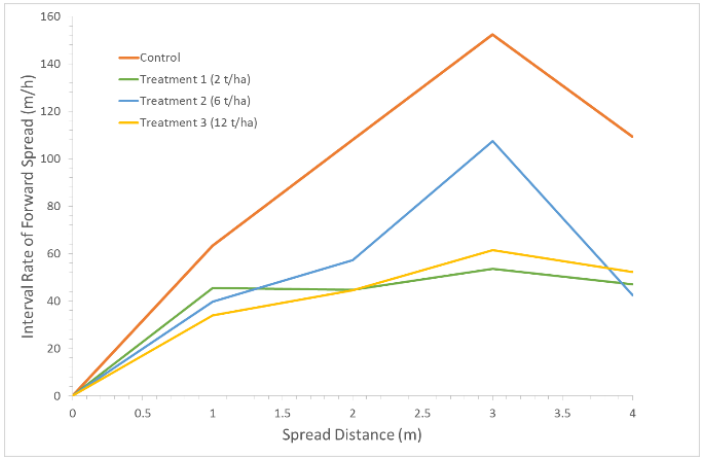

Figure 72: Summary of the mean interval rates of spread given in Figure 71 for the control and each treatment.

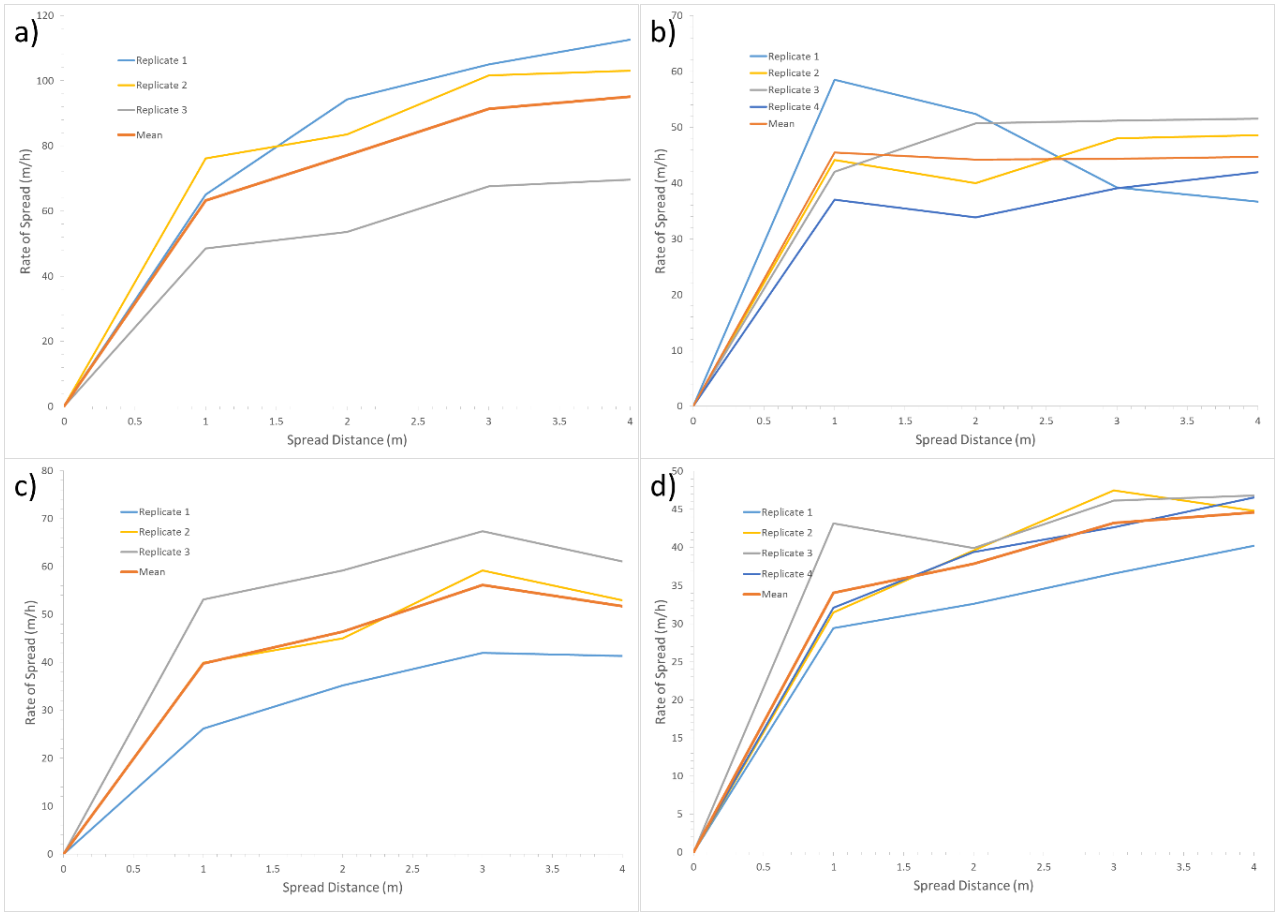

Figure 73: Cumulative rate of spread for the a) control (i.e., no CWD), b) 2 t/ha CWD treatment, c) 6 t/ha CWD treatment, and d) 12 t/ha CWD treatment. Cumulative rate of spread is the average speed over the total distance covered at each 0.5 m interval of the fuel bed.

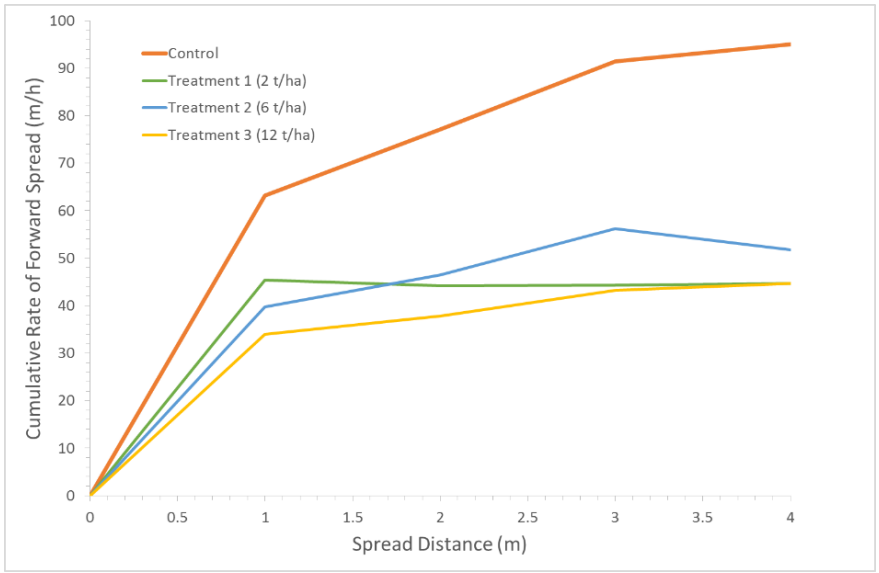

Figure 74: Summary of the mean cumulative rates of spread given in Figure 73 for the control and each treatment.

In each case, the acceleration of the fire from ignition is clearly evident. In some cases (Figure 71b), all fires in a treatment continued to accelerate but their rate of increase of acceleration decreased. In some cases, the behaviour in a treatment was highly variable. Some fires slowed after attaining a peak rate of spread in the first or second intervals. In other cases, fires slowed then accelerated again. In all cases, however, fires appeared to be heading towards a steady-state rate of spread just prior to reaching the end of the fuel bed.

Analysis of the cumulative rates of forward spread confirms that many of the fires were slowing their acceleration toward a steady-state rate of spread. The spread of the cumulative rate of spread at the end of the experiment (i.e., at 4.0 m mark) is relatively narrow across all the experiments, suggesting a conformity of results across the replicates. These are illustrated in a box plot in Figure 75.

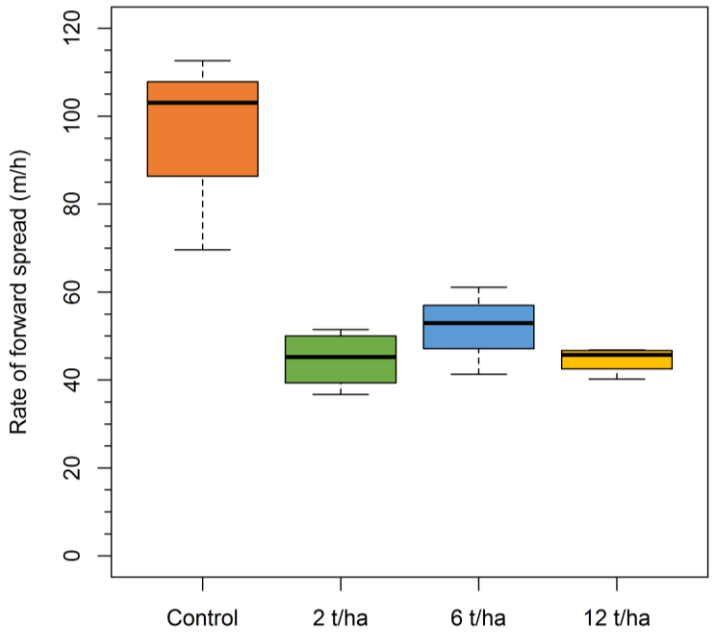

Figure 75: Box plot of the distributions of mean cumulative rates of spread for the control and three treatments. The control is clearly statistically different from all the treatments.

Figure 75 shows that the rate of forward spread in the control was clearly different to the rates of forward spread in the treatments. Table 17 provides a summary of Student's t-test for statistical significance of the difference between the control and treatments and between the treatments. From this table and Figure 75, the difference between the rate of forward spread in the control and all three treatments is statistically significant (at the $\alpha = 0.05$ level). The differences between the rate of forward spread in the treatments is not statistically significant.

Table 17: Summary of p-values quantifying statistical significance of difference between control and treatments and between treatments in heading fires. (Values marked with an * are statistically significant at the $\alpha = 0.05$ level).

	Control	Treatment 1	Treatment 2	Treatment 3
Control	-	0.032*	0.028*	0.031*
Treatment 1 (2 t/ha)	-	-	0.182	0.493
Treatment 2 (6 t/ha)	-	-	-	0.176
Treatment 3 (12 t/ha)	-	-	-	-

While air speed in the Pyrotron was strictly controlled and found to not vary more than 2 percent over the mean, the moisture content of the fine fuel was not strictly controlled but its variation was limited through oven drying. Figure 76 shows the variation in measured FMC across the treatments and the control. The maximum range of variation was exhibited in the 12 t/ha treatment (10.2% - 12.6%). This range encompassed the FMCs of the other two treatments and the control. The range of the control was the smallest (11.7% - 12.5%). Statistical analysis of the difference in FMC between the control and treatments showed that they were not significant. The FMC difference closest to approaching statistical significance (p = 0.09) was between the control and Treatment 2 (6 t/ha).

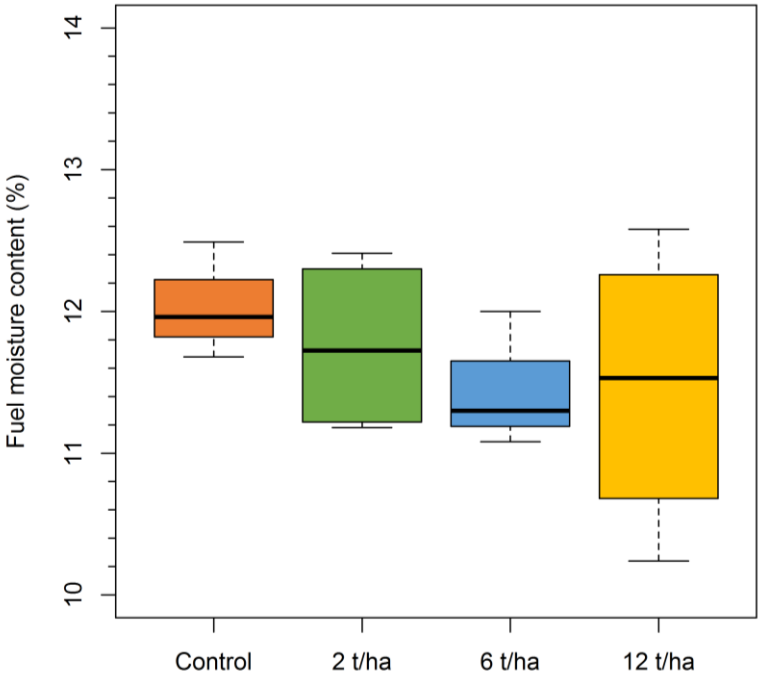

Figure 76: Boxplot showing the range in measured fine fuel moisture content across each of the fuel treatments and the control.

Figure 77 shows a graph of the range of fine fuel FMCs measured prior to each experiment against the mean cumulative rate of forward spread for each experiment and separated by treatment. The linear line of regression of all the points shows a reasonably flat (slope = 3.0375) relationship between FMC and rate of forward spread, with an R^2 correlation coefficient of 0.0078. Analysis of the differences between the individual rates of spread and their mean gives a mean bias error of zero and a mean average error of zero. These metrics confirm that there is no meaningful trend with FMC in the rate of forward spread.

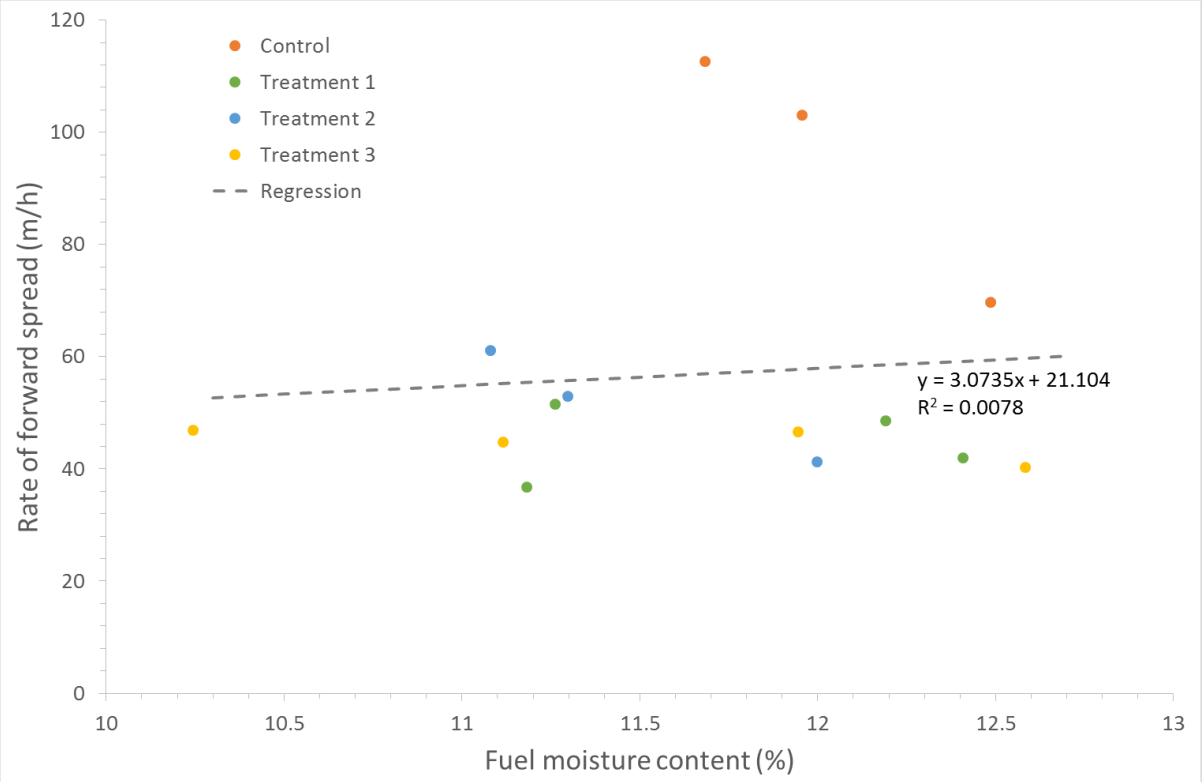

Figure 77: A graph of the range of fine fuel moisture contents measured prior to each experience plotted against the mean cumulative rate of forward spread of each experiment and coloured by treatment. A regression line through the data is also shown, along with the equation for this line.

While there are slight negative trends between each rate of forward spread and FMC within each treatment (as is expected from our understanding of the effect of fuel moisture on rate of spread *(Sullivan In press)*), this trend played no role in influencing the behaviour of the forward spread fire between treatments. Consequently, the observed differences between treatments are a result of the treatment and not of changes in FMC between experiments.

Rate of backing spread

Figure 78 shows summary graphs of the rates of spread observed in the backing fire experiments. Very little difference in rate of backing spread as a result of treatment is apparent in these graphs. As with the heading fire results, the interval rate of spread (Figure 78 left) exhibits more variation than the cumulative rate of spread (Figure 78 right).

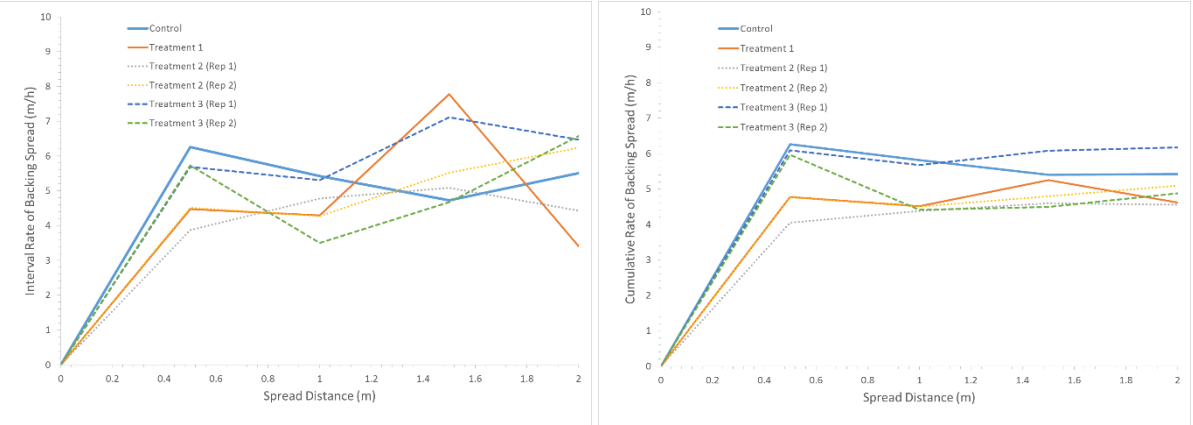

Figure 78: Summary graphs of the backing fire experiments rates of spread. Left) The interval rate of backing spread. Right) The cumulative rate of backing spread.

Unlike the heading fire cumulative rate of spread, the rate of backing spread is much more consistent across the life of the fire after ignition is completed, not exhibiting the acceleration to steady state rate of spread.

Due to the lack of replication, Student's t-test could not be applied to the backing fire rate of spread data to determine the statistical significance of any differences between treatments. Instead the simplest statistical test *(Pocock 2006)* was applied to individual cumulative rates of backing spread (Table 18).

Table 18: Summary of p-values quantifying statistical significance of difference between control and treatments and between treatments in backing fires. (Values marked with an * are statistically significant at the α = 0.05 level).

	Control	Treatment 1	Treatment 2	Treatment 3
Control	-	0.4013	0.4247	0.488
Treatment 1 (2 t/ha)	-	-	0.4761	0.3897
Treatment 2 (6 t/ha)	-	-	-	0.4129
Treatment 3 (12 t/ha)	-	-	-	-

Thus, none of the differences between the treatments or control were found to be significant. This suggests that in fires spreading against the wind, the presence of CWD makes no difference to the rate of backing spread of a fire.

Figure 79 shows that, similar to the heading fire experiments, the limited range of fine FMC values exhibited little effect on the rate of backing and thus did not influence the effect of the treatments. Only one Treatment 2 appears instead of the two replicates used for determining rate of backing spread as the FMC values for the first replicate in this treatment were corrupted.

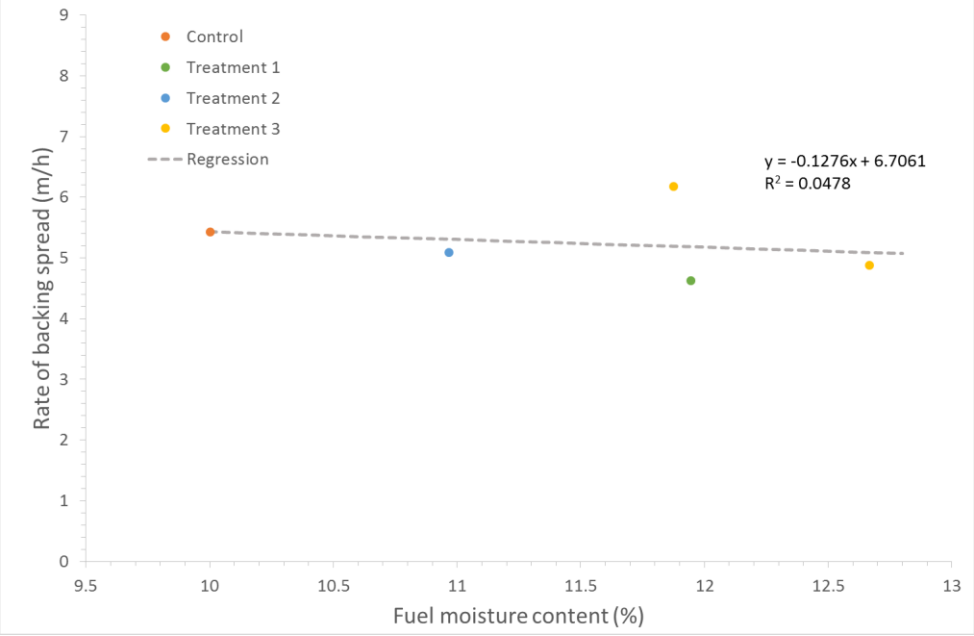

Figure 79: A graph of the range of fine fuel moisture contents measured prior to each experience plotted against the mean cumulative rate of backing spread of each experiment and coloured by treatment. A regression line through the data is also shown, along with the equation for this line.

Discussion

The presence of CWD on the forest floor can have significant impacts on a range of important factors, not the least of which are firefighter safety, smoke production and effects on human health, and greenhouse gas emissions. This component of the research project provided the repeatable burning conditions necessary to quantify the emissions profiles of key greenhouse gases and other combustion products as discussed elsewhere in this report.

These experimental fires were conducted in the CSIRO Pyrotron under strictly controlled environmental conditions to ensure that the only varying factor was the variable of interest—the amount of CWD present on the fuel bed. The Pyrotron enabled the study of the combustion of the CWD under the same circumstances that would be experienced in a free-burning prescribed or wildfire but in a manner that was both safe and repeatable. Such an approach ensured that the ignition and subsequent combustion, consumption and extinguishment of burning CWD was as close to how it happens in the field. Previous studies of burning branch and log material has generally being conducted with the material ignited artificially and allowed to burn in isolation from the combustion of surrounding material as would normally occur.

The intent of the design of the experiment was to replicate the conditions normally associated with prescribed burning—generally dry enough to burn well but not so well that the fire becomes unmanageable. Thus the range of moisture content and wind speed values used in the study were representative of such operational burning conditions. While the actual FMC could not be predetermined with a great deal of accuracy, its range and thus influence on fire behaviour was limited and within the intended prescription. Wind exhibited the least variation of all experimental components and thus was highly repeatable.

The results of the experiments disproved the working hypothesis that the presence of CWD would not affect fire behaviour in regard to fires burning with the wind (i.e. heading fires). In regard to fires burning into the wind, the hypothesis was confirmed.

For heading fires there was a clear impact of the presence on CWD on the rate of forward spread with fires burning in the absence of CWD (i.e. the controls) spreading approximately twice as fast as fire burning in the presence of CWD (the treatments). The physical explanation for this is not clear and would require additional experimentation and analysis to identify.

Possible explanations include an increase in the turbulence in the air driving the fire forward as a result of the increased roughness length of the fuel bed reducing the effectiveness of the convective heat transfer processes to unburnt fuel downwind of the flame front, the greater absorption of convective and radiative heat transfer from the flame reducing the energy received by the fine fuels and thus the rate of combustion driving the propagation of the flame front, or, probably most likely, the retardation of the progress of the flame front through the fine fuels due to blocking by the presence of the CWD.

Furthermore, the interaction of flame from burning fine fuels with the turbulence generated and blocking of heat transfer immediately in the lee of a branch was quite complex. For those situations where the size and arrangement of the branch meant that ignition was only slightly slower than surrounding fine fuels, the branch played little role in affecting rate of spread, except for the cases where the convection from the combustion of the branch reduced the effectiveness of the flame reaching the unburnt fuel beneath it. In situations where ignition of the branch was substantially slower than the surrounding fuel, if height of flames from burning fine fuels immediately up wind of the branch was sufficient to be turbulently bent over the branch, then the branch also played little role in affecting the overall rate of spread.

Observations of the fire behaviour identified that in situations where a branch at right angles to the air flow halted the forward progress of the fire, the fire front burnt around the branch, joining up some distance downwind of the branch in a ‘bear-hug’. The subsequent burning out of the unburnt fuel inside the ‘bear hug’ may have generated sufficient convective draw to slow the spread of the fire immediately downwind of it. This same affect was observed in other cases where branches were aligned at an angle to the wind.

The lack of effect of CWD on backing fire spread suggests that the dominant factor determining the spread of fire into the wind was happening on a time scale similar to the ignition of the CWD. Thus, the ignition of the fine fuel and propagation of the fire edge into the wind was not slowed by the presence of branch material.

These observations together lead to a likely explanation being related to inhibition of direct flame contact with fine fuels. This may be a result of a number of processes interacting and further research is required to unpick the root cause.

The link to direct flame contact suggests that the effect of CWD on heading fires may be much reduced when fire spread is primarily through fuel layers much taller than the height of any CWD, such as near-surface or shrub fuels. However, the impact of CWD may remain quite significant in such fuels in fires that are still developing, either due to ignition at a point or burning under marginal conditions (as would be found in many locations within a prescribed fire).

It is interesting to see that the amount of CWD had no significant effect on the overall rate of spread, either forward or backing. This suggests that the increase in the roughness length due to the presence of more CWD either had no effect or its effect had such a small threshold that further increases in roughness length failed to impact the rate of spread. It may be that the retardation of the flame front in heading fires was saturated with the first level of treatment and that further study at CWD loads less than 2 t/ha would be required to isolate the threshold value precisely and the dominating relation between CWD load and rate of forward spread.

Further research is also required to determine the influence of branch orientation, size class distribution and moisture content on rate of spread.

Models of fire behaviour that assume only the state of the fine fuel is important for determining rate of forward spread may be missing a critical component. Physically-based fire spread models (those built from the ground up on fundamental principles) that do not, either explicitly or implicitly, take into account the effect of CWD on rate of forward spread, may over-predict the speed of the fire when CWD is present.

Models developed from the empirical study of fire in natural forest will incorporate the effects of CWD implicitly, even if not quantified. Such effects may partly explain residual error found in field studies *(Mulvaney et al. 2016)*.

Conclusions

Experiments were conducted in the CSIRO Pyrotron under highly repeatable conditions to investigate the effect the presence of CWD had on the rate of spread of fires burning with and against the wind. Conditions were controlled such that no variable other than the amount of CWD was significant.

It was found that, under the same burning conditions, the presence of CWD had a direct impact on the rate of forward spread of fires but not on the rate of backing spread of fires. In heading fires the rate of spread presence of CWD was approximately half that of heading fires in the absence of CWD, regardless of the amount of CWD. In backing fires no significant effect of CWD was detectable.

This suggests that the mechanism that moderates the speed of fire burning through CWD is related to the time of ignition of the CWD and that the scale of this time is markedly different in heading fire conditions but not in backing fires.

Appendix D: Emission factors

Introduction

Atmospheric models rely on emission inventories to simulate atmospheric composition and evolution. Many inventories for fires emissions (e.g. Global Fire Emissions Database (GFED3) *(van der Werf et al. 2010)*, FINN *(Wiedinmyer et al. 2011)*) are built using the algorithm introduced by *Seiler and Crutzen (1980)*. This algorithm estimates the emissions of a trace gas from a vegetation fire by multiplying together the area of vegetation burnt, the fuel load in this area, the combustion efficiency of the fire and the emission factor of the trace gas.

The area burnt by a fire can be retrieved either by satellite or by investigation on the ground. The fuel load, which is the amount of combustible vegetation per unit of area, is usually estimated by environmental and conservation organisations. EFs are usually derived from emission ratios (ERs) of combustion products. The ERs and MCE can be calculated following *Meyer et al. (2012a)*.

MCE is defined as:

$$MCE = \frac{\Delta CO_2}{\Delta CO + \Delta CO_2}$$

Where $\Delta C_i = [C_i]_{smoke} - [C_i]_{ambient}$, i.e. the difference between the molar concentration of trace species i in the smoke sample and its concentrations in ambient air up-wind of the combustion source. It is used to characterize the relative amount of flaming and smouldering combustion. While pure flaming has an MCE near 0.99, smouldering combustion occurs at low MCE (~0.65-0.85).

The ERs are defined as:

$$ER_i = \frac{\Delta C_i}{\Delta CO_2 + \Delta CO + \Delta CH_4}$$

and the EFs relative to fuel mass *(Andreae and Merlet 2001)* are defined as:

$$EF_i = \frac{ER_i}{CC}$$

where CC is the carbon content of the burned fuel, estimated at 50%.

EFs can be determined either through controlled measurements in the laboratory, smoke plume measurements using aircrafts or ground level sampling in the field. Currently available EFs for PM and VOCs have been reviewed in *Andreae and Merlet (2001)* and *Akagi et al. (2011)*. They provide a limited set of data on EFs from fires or prescribed burns in temperate forests (either pine-oak forests or coniferous forests). In most cases the EFs were derived from aircraft measurements which capture mixed plumes of flaming and smouldering emissions lofted during the initial stages of a fire. They have very limited temporal coverage and therefore may underestimate the smouldering emissions.

Until this study no reliable EFs of $PM_{2.5}$ from fires or burns in sclerophyll forests of south-eastern Australia were available. Also little is known about the characteristics of the particulate and gas emissions from the combustion of many types of CWD, particularly CWD found in the sclerophyll forests of south-eastern Australia.

In order to attempt to fill this gap, both laboratory and field measurements were done to determine EFs for key pollutants under various burning conditions.

Objective

The study aimed at finding explanatory variables (such as combustion efficiency) that can be easily measured or estimated and can explain much of the observed variation in EF. These explanatory relationships can then be used to extrapolate measured EFs to a wider range of fuel and burning conditions. The derived particle EFs and chemical characteristics along with the explanatory relationships will help to better forecast and manage air quality impacts from prescribed burns on nearby communities

Results

Laboratory measurements

Controlled burning experiments involving fallen branch material in the range 6 – 50 mm in diameter were done to study the combustion properties of CWD and to quantity the GHG, particulate matter (PM), reactive volatile organic compounds (VOCs) and mercury emissions released by CWD under a

fixed set of wind and fuel moisture conditions using the CSIRO pyrotron (0). Sampling was conducted by either drawing air through sample tubes located at the end of the wind tunnel approximately 1m above the Pyrotron floor or by open-path FTIR with its line of sight including a cross section of the exit section of the Pyrotron (Figure 80 and 0).

Figure 80: Sampling setup for Pyrotron experiments, in-situ sampling lines (black arrow) and open-path FTIR sampling line (red arrow)

Table 19 lists the MCE and EFs of CO_2, CO, CH_4, $PM_{2.5}$ mass, a number of PM chemical components and selected VOCs for the different fuel treatments. Measurements of CO_2, CO, CH_4 were made using two different sampling and measurement techniques (see Appendix D1). Differences in the measurements can be attributed to sampling geometry.The open path Fourier transform infrared spectroscopy (OP-FTIR) instrument was located outside and installed with an angle that allows the open path to cover a section of the exit section of the tunnel (Figure 80). The cascade laser instruments were sampling from a bypass line starting by a tube centred in the cross-section of the tunnel (~1 m from all 4 walls) and approximately 1 m before the tunnel end (Figure 80). This set up means the cascade laser instruments are more sensitive to inhomogeneity in the tunnel than the open path FTIR.

Table 19: Emission factors (g kg^{-1} fuel) of CO, CO_2, CH_4, $PM_{2.5}$ and selected VOCs by fuel load.

	0 t/ha CWD Control	2 t/ha CWD	6 t/ha CWD	12 t/ha CWD	Average heading	Average backing	Method
MCE	0.94	0.94	0.93	0.94	0.94 ± 0.1	0.94	
CO_2	1714 1734	1725 1725	1707 1715	1716 1707	1716 ± 22 1719 ± 24	1714 1697	CRDS OP-FTIR
CO	72.8 65.7	65.9 64.8	76.2 65.8	70.5 63.6	71 ± 13 64.9 ± 13.0	71.9 79.0	CRDS OP-FTIR
CH_4	1.89 1.9	1.89 1.5	2.44 1.7	2.35 2.2	2.17 ± 0.55 1.8 ± 0.4	2.21	CRDS OP-FTIR
$PM_{2.5}$	6.57	6.07	5.15	5.00	5.57 ± 1.21	7.0	
Levoglucosan	0.75	0.84	0.73	0.89	0.82 ± 0.19	0.92	
nssK	0.015	0.010	0.009	0.007	0.010 ± 0.003	0.014	
Levo/nssK	54.6	82.4	85.3	127.2		81.3	

Table 19 ctd: Emission factors (g kg^{-1} fuel) of CO, CO_2, CH_4, $PM_{2.5}$ and selected VOCs by fuel load.

	0 t/ha CWD Control	2 t/ha CWD	6 t/ha CWD	12 t/ha CWD	Average heading	Average backing	Method
Na^+	0.011	0.010	0.015	0.005	0.010 ± 0.005	0.014	
Cl^-	0.068	0.075	0.051	0.030	0.054 ± 0.023	0.118	
Ca^{2+}	0.021	0.081	0.066	0.014	0.049 ± 0.070	0.013	
Mg^{2+}	0.005	0.011	0.015	0.002	0.008 ± 0.013	0.002	
NH_4^+	0.018	0.026	0.016	0.015	0.019 ± 0.008	0.039	
NO_3^-	0.008	0.010	0.008	0.007	0.009 ± 0.003	0.014	
SO_4^{2-}	0.031	0.033	0.030	0.020	0.028 ± 0.006	0.028	
OC	4.7	3.5	2.8	3.2	3.6 ± 0.8	4.1	
EC	0.88	0.64	0.56	0.62	0.67 ± 0.14	1.00	
BC	1.38	1.07	0.83	0.87	1.04 ± 0.25	1.4	
Acetaldehyde	0.30	0.32	0.30	0.31	0.31 ± 0.08	0.37	SIFT
Acetic acid	2.07	1.82	1.44	1.2	1.58 ± 0.67	1.4	OP-FTIR
Acetone	0.25	0.24	0.22	0.22	0.22 ± 0.06	0.29	SIFT
Acetonitrile	0.039	0.057	0.057	0.059	0.055 ± 0.020	0.068	SIFT
Acetylene	0.091	0.12	0.11	0.096	0.10 ± 0.03	0.20	SIFT
Ammonia	0.97	0.66	0.76	0.74	0.76 ± 0.16	0.8	OP-FTIR
Benzene	0.16	0.21	0.19	0.21	0.19 ± 0.05	0.22	SIFT
Butadiene	0.054	0.058	0.034	0.030	0.043 ± 0.023	0.030	SIFT
Butanone	0.069	0.082	0.075	0.084	0.078 ± 0.029	0.099	SIFT
Ethane	0.20	0.17	0.18	0.20	0.19 ± 0.03	0.22	FTIR
Ethene	0.73	0.76	0.78	0.74	0.76 ± 0.16	0.78	OP-FTIR
	0.60	0.57	0.59	0.63	0.60 ± 0.16	0.92	FTIR
Eucalyptol	0.026	0.032	0.017	0.017	0.023 ± 0.012	0.037	SIFT
Formaldehyde	0.83	1.00	0.96	0.86	0.92 ± 0.22	0.97	OP-FTIR
Formic acid	0.23	0.19	0.19	0.18	0.19 ± 0.05	0.23	OP-FTIR
HCN	0.035	0.11	0.084	0.070	0.080 ± 0.055	0.075	SIFT
Isoprene	0.14	0.094	0.10	0.090	0.10 ± 0.03	0.20	SIFT
Methanol	0.63	0.86	0.52	0.44	0.61 ± 0.45	0.73	OP-FTIR
	0.55	0.59	0.61	0.59	0.59 ± 0.19	0.67	SIFT
Monoterpenes	0.078	0.11	0.028	0.042	0.064 ± 0.052	0.10	SIFT
Pyrrole	0.032	0.026	0.020	0.016	0.023 ± 0.015	0.031	SIFT
Trimethylbenzene	0.062	0.067	0.059	0.057	0.061 ± 0.028	0.09	SIFT
Toluene	0.43	0.42	0.39	0.39	0.41 ± 0.13	0.49	SIFT
Xylenes	0.21	0.072	0.077	0.080	0.10 ± 0.11	0.39	SIFT

Fine fuel (6mm) vs coarse fuel (6-50mm)

As can be seen in Table 19, the coarse fuel fraction had no effect on the MCE or on the $PM_{2.5}$ and VOC EFs. In terms of chemical composition of $PM_{2.5}$, the ratio of levoglucosan to non sea-salt potassium (nssK) (both wood smoke tracers) increased with increased coarse fuel fraction, suggesting that levoglucosan is dominantly emitted from coarse fuel while nssK is emitted from fine fuel (e.g. leaves), consistent with a previous research study *(Schmidl et al. 2008)*.

Evolution of the smoke plume

For each burn, three distinct phases could be identified:

- flaming propagation which covers the period between ignition and time when fire reached the end of the fuel bed
- flaming stationary which covers the period between the end of forward spread and the extinction of fine fuels
- smouldering combustion

Table 20 shows the time periods for the three phases by fuel treatment.

Table 20 Time periods (min) of the three combustion phases by fuel treatment

CWD fuel load	Flaming propagation	Flaming stationary	Smouldering
0 t/ha	2.7	5.3	< 1
2 t/ha	5.2	4.0	7.3
6 t/ha	5.2	3.7	12.6
12t/ha	5.6	4.2	14.6

The time between ignition and end of fire spread significantly increased when CWD was added to the fuel bed, with no difference between the 3 fuel loads. This is consistent with the fire behaviour results that showed a direct impact of the presence of CWD on the rate of forward spread of fires (Figure 6). The duration of the smouldering phase increased with increasing CWD fuel load. There was no difference in the duration of the stationary flaming phase between treatments.

The time resolution of the open-path FTIR system was high enough that there was sufficient data to determine an ER for VOC species measured with the system for each phase of a burn. The results are shown in Table 21 and indicate that the EFs for PM and VOC species show a strong dependence on MCE. The highest EFs were observed for the smouldering phase, while the lowest EFs were observed for the flaming propagating phase, which consumed on average about 50% of the fuel in the Pyrotron fires.

Table 21: Emission factors (g kg^{-1} fuel) and MCE for different fire phases

	Flaming propagation	Flaming stationary	Smouldering
MCE	0.98 ± 0.01	0.93 ± 0.03	0.82 ± 0.04
CO_2	1790 ± 20	1690 ± 50	1470 ± 90
CO	20 ± 10	80 ± 30	190 ± 40
CH_4	0.5 ± 0.3	2.6 ± 0.7	7.3 ± 1.7
N_2O	0.06 ± 0.02	0.07 ± 0.03	0.06 ± 0.02
$PM_{2.5}$	3.3 ± 1.6	6.4 ± 2.6	15.0 ± 9.2
Acetic acid	0.4 ± 0.4	3.0 ± 2.0	5.0 ± 1.0
Ammonia	0.2 ± 0.1	0.8 ± 0.2	2.2 ± 0.4
Ethene	0.2 ± 0.1	1.1 ± 0.5	1.5 ± 0.4
Formaldehyde	0.3 ± 0.2	1.3 ± 0.7	2.1 ± 0.8
Formic acid	0.06 ± 0.04	0.3 ± 0.1	0.6 ± 0.2
Methanol	0.3 ± 0.4	0.8 ± 0.6	1.9 ± 0.9

The time series of CO_2, CO, CH_4, N_2O, $PM_{2.5}$ and %C emitted for the control and the three fuel treatments is shown in Figure 81. The time has been normalised to the end of forward spread (EOFS). The time series shows that CO_2 concentrations peak earlier than both CO and CH_4 concentrations with most of the C emitted during the flaming phase. During the smouldering phase, emissions of CO and CH_4 increase with increasing coarse fuel load. This trend is less pronounced for $PM_{2.5}$ emissions.

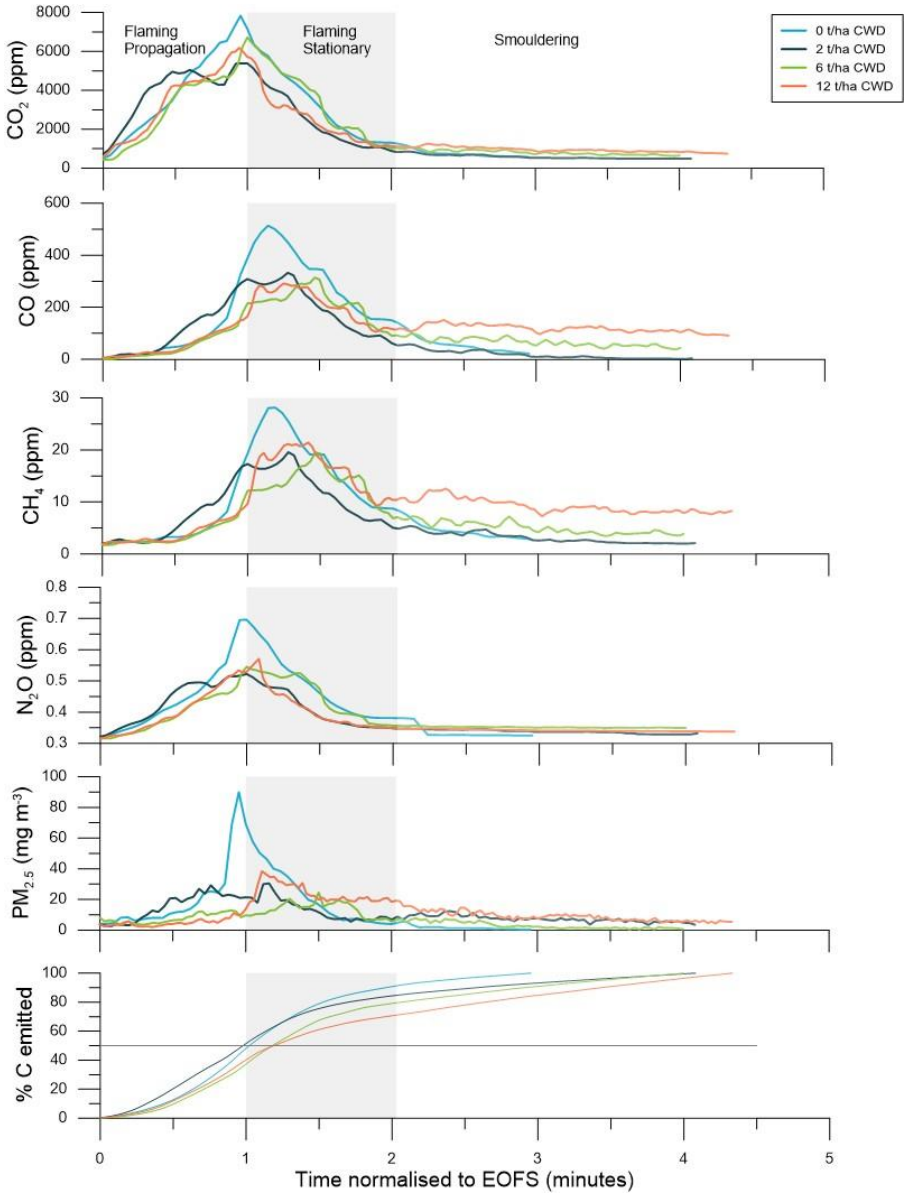

Figure 81: Time series of CO, CO_2, CH_4 and N_2O measurements during experimental burns for the different treatments

Field measurements

The team attended four prescribed burns in Victoria, two in autumn 2015 and two in spring 2015. Emissions in the field were determined by two sampling approaches: via direct sampling close to the emission source (i.e. within 1 m) and via open path infrared spectroscopy adjacent to or within the fire boundary (see 0).

Emission factors from near source sampling

Near source sampling of CO, CO_2, CH_4, N_2O and fine particles ($PM_{2.5}$) was done at four prescribed burns in Victoria in 2015. Smoke samples were collected (1) from flaming combustion by positioning the tip of the sampling probe approximately 0.5 m above the flame and (2) from smouldering-phase combustion behind the fire front and from burning of heavy fuels and logs. At each burn, 8-15 samples were collected during flaming combustion and 4-8 samples were collected during smouldering combustion.

Table 22 and Table 23 show the EFs (in g kg^{-1} fuel) for the flaming and smouldering combustion phases measured at each prescribed burn. EFs for CO, CH_4 and $PM_{2.5}$ were significantly higher during the smouldering combustion.

Table 22: Emission factors (g kg^{-1} fuel) and MCE from ground measurements of flaming combustion

	Greendale (13/04/2015) N = 9	Castlemaine (23/4/2015) N = 15	Bambra (30/09/2015) N = 8	Campbells Creek (1/10/2015) N = 15	Average all
MCE	0.94 ± 0.01	0.95 ± 0.01	0.93 ± 0.01	0.95 ± 0.01	0.94 ± 0.02
CO_2	1715 ± 21	1743 ± 19	1691 ± 27	1735 ± 27	1726 ± 29
CO	71.6 ± 12.0	54.4 ± 11.1	85.6 ± 16.2	58.8 ± 15.9	64.7 ± 17.5
CH_4	2.3 ± 0.7	1.9 ± 0.4	2.7 ± 0.7	2.2 ± 0.7	2.2 ± 0.7
$PM_{2.5}$	15.4 ± 5.2	14.6 ± 7.9	24.9 ± 8.1	18.2 ± 6.0	17.5 ± 7.5
Levoglucosan					1.54 ± 0.97
nssK					0.046 ± 0.028
Na^+					0.014 ± 0.010
Cl^-					0.169 ±0.088
Ca^{2+}					0.017 ± 0.013
Mg^{2+}					0.003 ± 0.003
NH_4^+					0.057 ± 0.018
NO_3^-					0.016 ± 0.004
SO_4^{2-}					0.082 ± 0.028

Table 23: Emission factors (g kg^{-1} fuel) and MCE from ground measurements of smouldering combustion

	Greendale (13/04/2015) N = 6	Castlemaine (23/4/2015) N = 4	Bambra (30/09/2015) N = 8	Campbells Creek (1/10/2015) N = 6	Average all
MCE	0.84 ± 0.04	0.81 ± 0.02	0.83 ± 0.04	0.85 ± 0.02	0.83 ± 0.04
CO_2	1504 ± 91	1456 ± 36	1486 ± 91	1549 ± 45	1499 ± 77
CO	192.6 ± 53.9	212.6 ± 27.3	197.2 ± 49.3	161.8 ± 24.9	190.9 ± 43.6
CH_4	9.4 ± 4.0	15.9 ± 3.9	13.2 ± 6.6	11.1 ± 3.8	12.4 ± 5.3
$PM_{2.5}$	51.5 ± 37.2	73.0 ± 40.0	55.2 ± 40.1	26.2 ± 12.0	51.0 ± 36.2
Levoglucosan					7.58 ± 3.11
nssK					0.022 ± 0.027
Na^+					0.039 ± 0.043
Cl^-					0.219 ± 0.167
Ca^{2+}					0.024 ± 0.014
Mg^{2+}					0.010 ± 0.012
NH_4^+					0.11 ± 0.06
NO_3^-					0.012 ± 0.007
SO_4^{2-}					0.066 ± 0.029

Figure 82 shows the relationship of MCE vs EF(CH_4) (left) and MCE vs EF(PM) on the right. For both compounds we can see a significant increase in the EF with decreasing MCE and also a larger scatter in EF values as MCE decreases. EFs of PM for flaming combustion range from 3 to 34 g kg^{-1}, while the range for smouldering combustion is from 10-133 g kg^{-1}. The large variability in EFs at low MCE may be due to the heterogeneity in fuel, char and combustion temperature during the smouldering combustion and the slow oxidation process leading to a low consumption of the fuel mass compared to the flaming combustion.

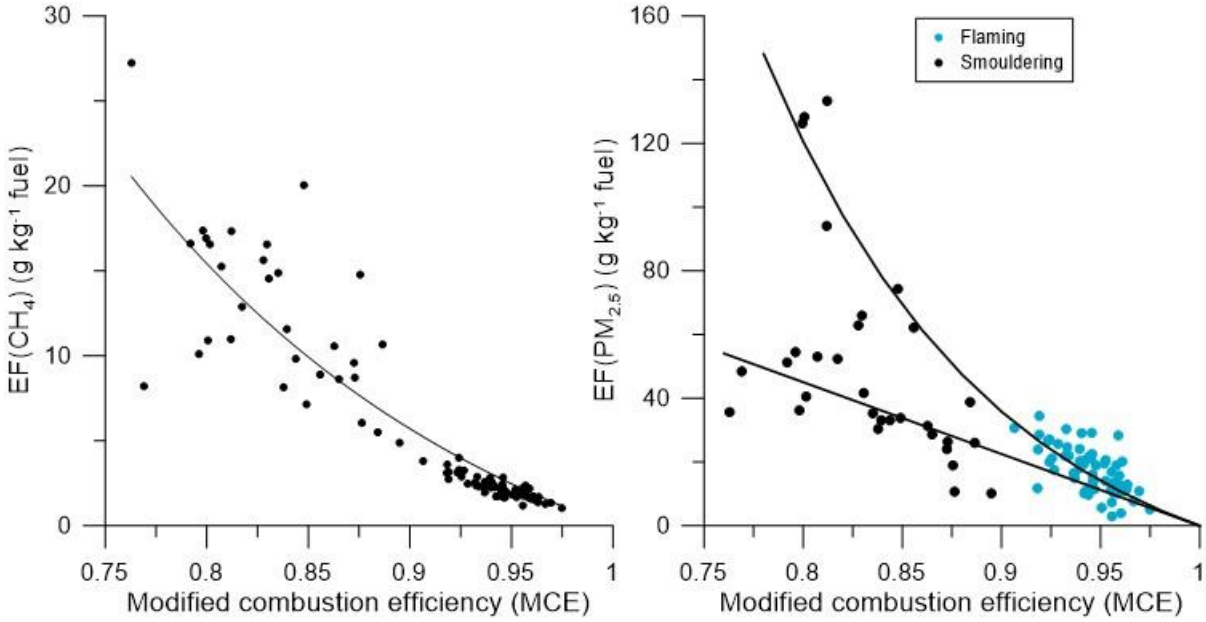

Figure 82: Emission factors (g kg^{-1}) as a function of MCE for CH_4 (left) and PM (right)

Figure 83 compares the data measured at the Victorian prescribed burns to published data from fires or prescribed burns in temperate forests.

The comparison of the dataset from this study to aircraft measurements in Figure 83a show that the flaming combustion in the Victorian study produces slightly higher EF of PM than those measured in smoke plumes measured by aircraft. This is likely due to differences in sampling methods. The airborne measurements are likely to be a mix of flaming and smouldering combustion as well as clean background air as post-flame smouldering emissions and clean background air become entrained into the smoke plume. A similar trend was observed for tower-based field measurements (Figure 83c).

Figure 83b compares the Victorian prescribed burns dataset against laboratory measurements. For flaming combustion (MCE of 0.92-0.97), there is a good agreement between the field measurements and laboratory measurements.Similarly there is good agreement between this data set and published data from ground-based field measurements (Figure 83c and d).

Figure 83 also shows that data on particle EFs at low MCE is sparse. A recent study by *Robertson et al. (2014)* showed higher particle EFs during the smouldering combustion (Figure 83d). They collected near-source smoke samples during prescribed burns in open-canopy pine-grasslands in Florida and Georgia and collected samples from both flaming combustion and smouldering combustion of fine fuels after the passage of the flaming front.

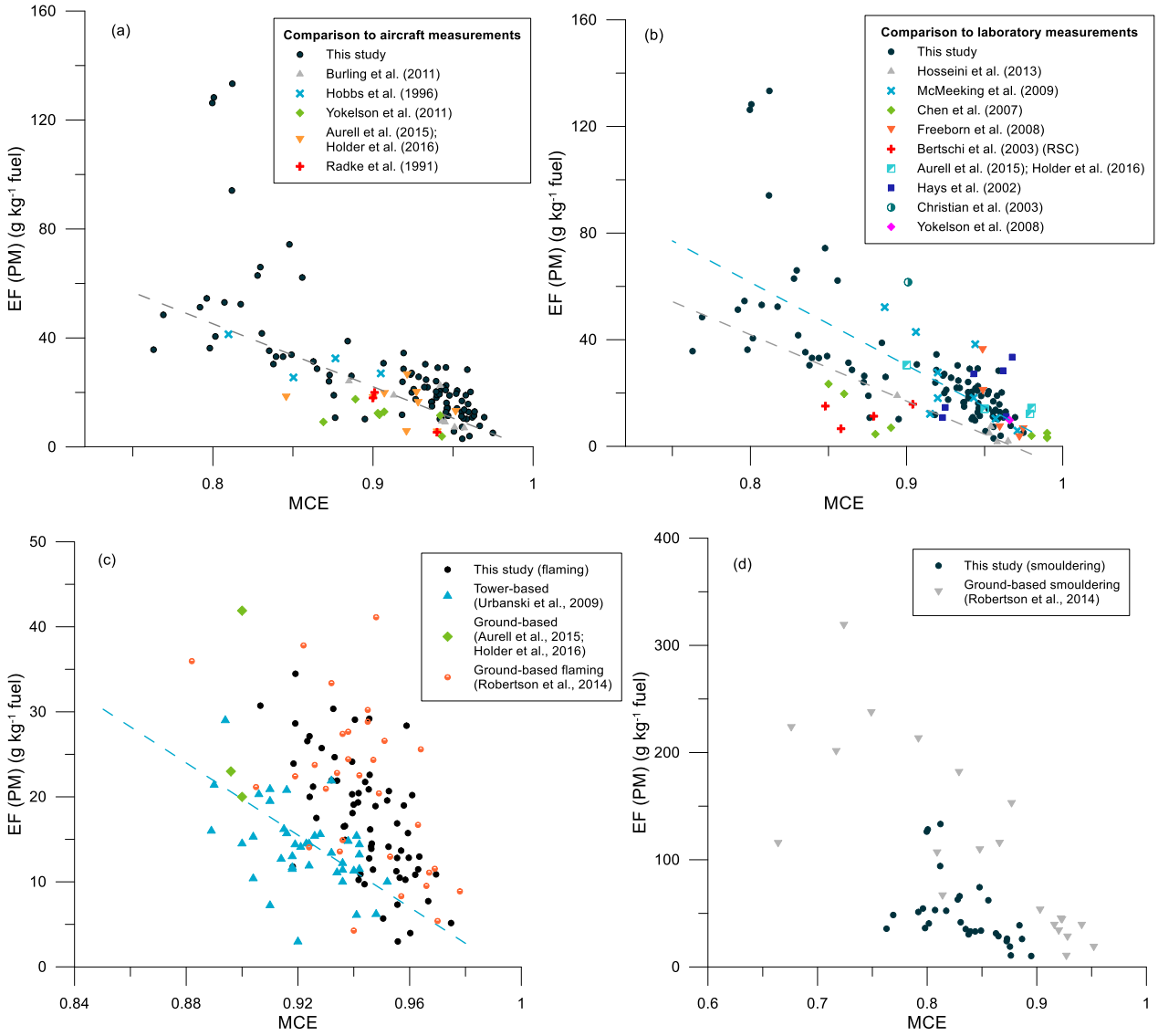

Figure 83: Comparison of emission factors of PM from this study to previous literature data

We observed two distinct trends in EF(PM) at low MCE (Figure 82). These are attributed to the combustion processes as described in *Bertschi et al. (2003)*. During pyrolysis, carbon-enriched particles are emitted, and their emissions increase as combustion efficiency decreases. Once char is formed, gasification can occur in which solid char is converted to gas-phase products such as CO_2 and CO, also referred to as glowing combustion. This is characterised by an increase in CO emissions but no concurrent increase in PM emissions. A similar trend has been observed in domestic woodheating combustion *(Meyer et al. 2008)*. While the relationship between MCE and EF(PM) for glowing combustion follows a linear trend, the relationship between MCE and EF(PM) for smouldering combustion is best fitted with an exponential curve.

Figure 84 shows the PM EFs by combustion phase with values in the boxplot representing the median EF(PM) and recommended EF(PM) for Australian temperate forest fires. The overall median EF(PM) of 38.8 g kg^{-1} fuel for smouldering combustion is in agreement with a recent estimate of 33 g kg^{-1} from the combustion of smouldering stumps and logs *(Urbanski 2014)*. As noted before, smouldering combustion releases significantly more PM than flaming combustion. As the process of smouldering combustion is highly variable, emissions of PM are more difficult to quantify. Separating the smouldering combustion into the two different processes shows that the pyrolytic process has the highest variability and also the highest EF(PM).

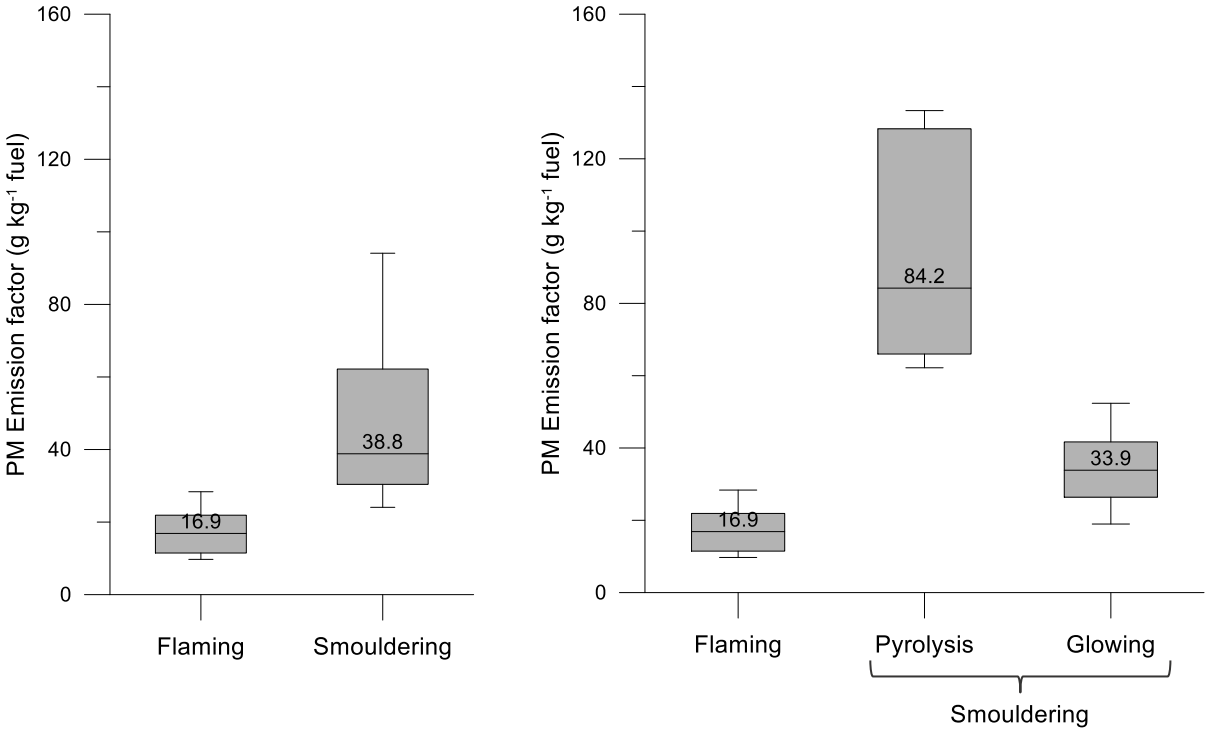

Figure 84: Distribution of PM EFs by combustion phase. Boxplots show median, 25-75%iles (box) and 10-90%iles (whiskers)

The chemical speciation of PM shows that higher emissions of potassium (K) are observed during flaming combustion (Table 22) compared to smouldering combustion (Table 23). This is consistent with findings by *Vodacek et al. (2002)* and *Amici et al. (2011)* who have shown that emissions of K appear to be a unique characteristic of flaming combustion. This could allow to separate areas of flaming combustion from areas of smouldering activity.

Emissions of levoglucosan (a biomass burning marker) dominate the smouldering combustion (Table 22). This is consistent with a previous research study that has shown higher emissions of K during burning of leaves and higher levoglucosan emissions during burning of logs *(Schmidl et al. 2008)*. The levoglucosan

fraction in PM averaged 8% during flaming combustion and 16.5% during smouldering combustion (range of 11.3-20.9%), slightly lower than the levoglucosan fraction observed in ambient samples impacted by woodheater emissions *(Meyer et al. 2011; Reisen et al. 2013)*.

Surface smoke plume

Open path FTIR measurements were conducted at two autumn burns in Victoria, Greendale and Castlemaine in 2015 and at five prescribed burns in NSW in 2012 and 2013. The results for trace gases are shown in Table 24. These EFs fall within the range of EFs measured by similar techniques at hazard reduction burns in NSW *(Paton-Walsh et al. 2014)*. Additonal data is shown in Appendix D2.

Table 24: Emission factors (g kg^{-1}) of VOCs

	Greendale (13/04/2015) N = 9	Castlemaine (23/4/2015) N = 15	Average VIC all	Average NSW all	Extratropical forest (Akagi et al., 2011)
MCE	0.93	0.91	0.92 ± 0.01	0.89 ± 0.02	0.93
CO_2	1670	1650	1660 ± 14	1620 ± 32	1509
CO	84	101	93 ± 12	118 ± 16	122
CH_4	3.1	3.3	3.2 ± 0.1	3.6 ± 1.1	5.7
Acetic acid	6	6.5	6.3 ± 0.4	3.9 ± 1.3	4.08
Ammonia	1.5	1.7	1.6 ± 01	1.6 ± 0.7	2.46
Ethene	1.1	1.2	1.2 ± 0.1	1.3 ± 0.2	
Formaldehyde	1.3	1.5	1.4 ± 0.1	1.8 ± 0.4	1.92
Formic acid	0.57	0.53	0.55 ± 0.03	0.4 ± 0.2	0.54
Methanol	1.5	1.7	1.6 ± 0.1	2.4 ± 1.1	2.70

Conclusions

The major findings from both the laboratory and field measurements showed that an increased load of CWD had no effect on EFs, but the burning conditions (e.g. flaming vs smouldering) had a significant effect on EFs. Signficantly higher EFs were observed during the smouldering combustion for PM2.5, CO, CH4 and VOCs. Furthermore, emissions during the rapid and intense flaming combustion are lofted by convection, whereas particles emitted during the slow and prolonged smouldering combustion remain closer to the ground. Due to the higher EFs and the low buoyance of the smoke from smouldering combustion, the smouldering of logs and stumps can have a much larger impact on the air quality of nearby communities than the convective plume from the flaming combustion. Appendix D1: Summary of intercomparison between emission factors measured by laser spectroscopy techniques with those measured by Fourier transform infrared spectroscopy during the 2014 Pyrotron experiment.

This report summarises the results of an intercomparison between EFs measured by laser spectroscopy techniques with those measured by FTIR during the 2014 Pyrotron experiment. When interpreting the intercomparison it is important to note the different sampling geometries of the different techniques. The laser instruments drew air through a sample tube located in the exit passage of the wind tunnel ~ 1m from the floor of the Pyrotron next to the sample tube used to fill bags (see black arrow in Figure 85). In contrast the open-path FTIR was set-up such that its line of sight included a cross-section of the exit section of the Pyrotron (see red arrow in Figure 85). Since less than half the line of sight of the FTIR typically passed through the smoke plume actual mean integrated concentrations calculated for this path are expected to be lower than concentrations measured by the laser spectroscopy in situ techniques. However, since all measurement methods depend on measuring ratios of different trace gases in order to calculate emission factors this should not invalidate the intercomparison. Furthermore, whilst the instruments are measuring approximately similar smoke samples, the ratios of different gases measured by the instruments should be in agreement.

Figure 85 Photograph illustrating the different sampling geometries for the in situ laser spectroscopy measurements and grab sample bags (black arrow) and the open-path FTIR spectroscopy measurements (red arrow).

Table 25 and Table 26 show the mean EFs and ERs measured by the different techniques for heading fires and backing fires respectively. Overall the FTIR measures lower EFs for CO and CH_4 than the laser techniques.

Table 25 Mean emission factors measured by laser spectroscopy (EFCRDS) and FTIR spectroscopy (EFFTIR) for heading fires with different fuel loads (sections 1-4) and for all burns (section 5). Standard deviations of results from different fires averaged are also given below where available.

Burn	Species	EF_{CRDS}	EF_{FTIR}	$ER_{CO\ (CRDS)}$	$ER_{CO\ (FTIR)}$	$ER_{CO\ (bags)}$	MCE_{CRDS}	MCE_{FTIR}
HL1	CO_2	1709	1701				0.935	0.933
							0.11%	-0.11%
	CO	76	78					
	CH_4	2.2	1.7	0.051	0.039	0.048		
				11.08%	-15.07%	4.00%		

Burn	Species	EF_{CRDS}	EF_{FTIR}	$ER_{CO\ (CRDS)}$	$ER_{CO\ (FTIR)}$	$ER_{CO\ (bags)}$	MCE_{CRDS}	MCE_{FTIR}
HL2	CO_2	1712	1715				0.936	0.943
		14	22				-0.37%	0.37%
	CO	74	66					
		9	12					
	CH_4	2.0	1.6	0.049	0.044	0.041		
		0.3	0.2	9.40%	-1.26%	-8.14%		

Burn	Species	EF_{CRDS}	EF_{FTIR}	$ER_{CO\ (CRDS)}$	$ER_{CO\ (FTIR)}$	$ER_{CO\ (bags)}$	MCE_{CRDS}	MCE_{FTIR}
HL3	CO_2	1705	1718				0.934	0.943
		19	5				-0.49%	0.49%
	CO	77	66					
		11	2					
	CH_4	2.3	1.8	0.053	0.048	0.047		
		0.4	0.2	8.05%	-3.14%	-4.90%		

Burn	Species	EF_{CRDS}	EF_{FTIR}	$ER_{CO\ (CRDS)}$	$ER_{CO\ (FTIR)}$	$ER_{CO\ (bags)}$	MCE_{CRDS}	MCE_{FTIR}
HL4	CO_2	1707	1721				0.935	0.945
		19	12				-0.55%	0.55%
	CO	76	64					
		11	7					
	CH_4	2.9	2.2	0.066	0.060	0.058		
		0.7	0.4	7.21%	-2.35%	-4.86%		

	Species	EF_{CRDS}	EF_{FTIR}	$ER_{CO\ (CRDS)}$	$ER_{CO\ (FTIR)}$	$ER_{CO\ (bags)}$	MCE_{CRDS}	MCE_{FTIR}
HL	CO_2	1708	1717				0.935	0.943
		16	16				-0.43%	0.43%
	CO	76	66					
		9	10					
	CH_4	2.4	1.9	0.056	0.050	0.049		
		0.6	0.3	7.87%	-3.57%	-4.30%		

Table 26 Mean emission factors measured by laser spectroscopy (EFCRDS) and FTIR spectroscopy (EFFTIR) for backing fires with different fuel loads.

Burn	Species	EF_{CRDS}	EF_{FTIR}	$ER_{CO\ (CRDS)}$	$ER_{CO\ (FTIR)}$	$ER_{CO\ (bags)}$	MCE_{CRDS}	MCE_{FTIR}
BL	CO_2	1714	1696				0.935	0.927
		7	23				0.46%	-0.46%
	CO	72	79					
		5	13					
	CH_4	2.2	2.0	0.046	0.036	0.042		
		0.2	0.4	10.50%	-11.84%	1.34%		

When we examine the time-series of measurements from the different techniques we see a common pattern emerge for most of the burns. At the start of the burn there is good agreement between the CRDS measurements and the bag sample measurements of the concentrations of CO_2, CO and CH_4 with the openpath FTS data tracking the others but lower (due to the integrated path sampling clean air also). During this initial stage all methods agree well in their determination of the CO/CO_2 ratio.

After this initial stage many burns show poorer agreement between the methods, with both concentration time-series and ratio time-series diverging. The laser measurements of CO are almost always significantly higher at the end of the burn than the open-path measurements with the bag measurements often lying between the two other measurements. This suggests that there is both a technique and a sampling bias coming into play. Near the end of the burn the comparison is really difficult to make because once the trace gases approach background values the ratios are very sensitive to small changes. It seems that the FTS data returns to near background values more often than the laser sampling techniques however I suspect that these differences at the end of the fires make little difference to the EFs and that the differences that we see are driven mainly by the divergence of the time-series in the middle of the fires.

However, it is also worth noting that the summation method that we use to calculate the EFs may be more sensitive to these divergences in CO between the two measurement techniques than other methods of calculating the EFs.

The following part shows screen shots of the comparison of the time-series using IgorPro.

Load 1burns

Solid lines = Mick's laser techniques, dotted lines =open-path FTS, diamonds = bags with bars indicating fill times.

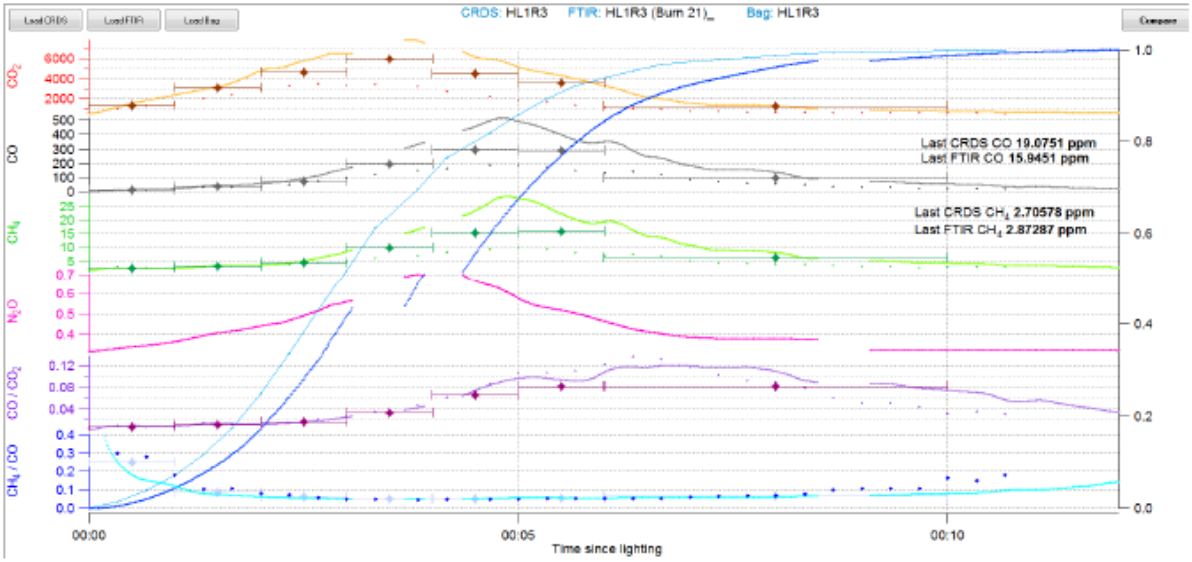

Burn	Species	EF_{CRDS}	EF_{FTIR}	$ER_{CO\ (CRDS)}$	$ER_{CO\ (FTIR)}$	$ER_{CO\ (bags)}$	MCE_{CRDS}	MCE_{FTIR}
HL1R3	CO_2	1709	1701				0.935	0.933
		0.22%	-0.22%				0.11%	-0.11%
	CO	75.8	77.8					
		-1.35%	1.35%					
	CH_4	2.22	1.74	0.051	0.039	0.048		
		12.11%	-12.11%	11.08%	-15.07%	4.00%		

Load 2 burns - Solid lines = Mick's laser techniques, dotted lines =open-path FTS, diamonds = bags with bars indicating fill times.

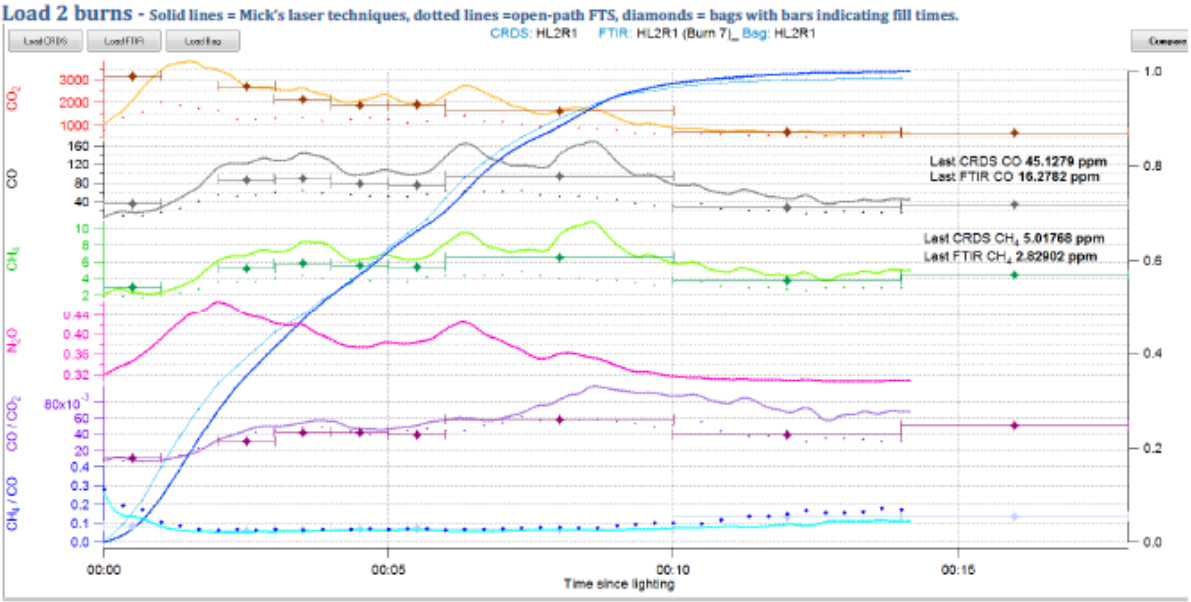

Burn	Species	EF_{CRDS}	EF_{FTIR}	$ER_{CO\ (CRDS)}$	$ER_{CO\ (FTIR)}$	$ER_{CO\ (bags)}$	MCE_{CRDS}	MCE_{FTIR}
HL2R1	CO_2	1711	1693				0.936	0.932
		0.52%	-0.52%				0.21%	-0.21%
	CO	74.3	78.4					
		-2.73%	2.73%					
	CH_4	1.93	1.9	0.046	0.042	0.031		
		0.86%	-0.86%	14.83%	6.63%	-21.46%		

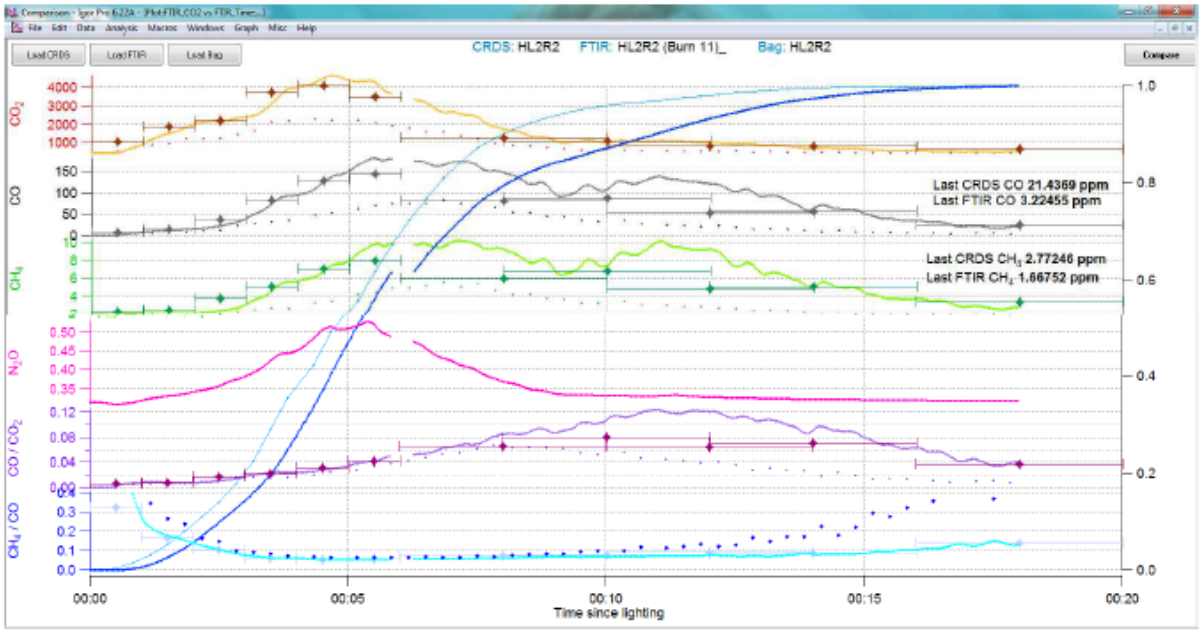

Burn	Species	EF_{CRDS}	EF_{FTIR}	$ER_{CO\ (CRDS)}$	$ER_{CO\ (FTIR)}$	$ER_{CO\ (bags)}$	MCE_{CRDS}	MCE_{FTIR}
HL2R2	CO_2	1704	1724				0.933	0.947
		-0.57%	0.57%				-0.74%	0.74%
	CO	78.2	61.5					
		11.93%	-11.93%					
	CH_4	2.23	1.61	0.050	0.046	0.040		
		16.19%	-16.19%	10.49%	1.11%	-11.60%		

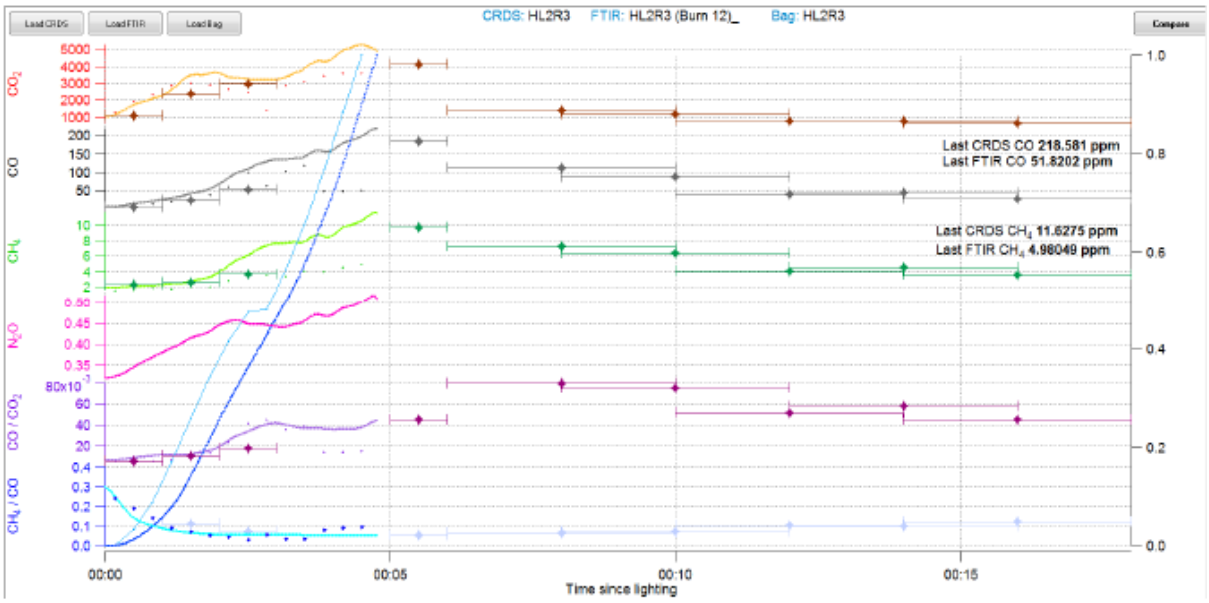

Burn	Species	EF_{CRDS}	EF_{FTIR}	$ER_{CO\ (CRDS)}$	$ER_{CO\ (FTIR)}$	$ER_{CO\ (bags)}$	MCE_{CRDS}	MCE_{FTIR}
HL2R3	CO_2	1772	1747				0.968	0.958
		0.72%	-0.72%				0.52%	-0.52%
	CO	37.5	48.6					
		-13.00%	13.00%					
	CH_4	1.02		0.047	0.031	0.043		
				17.29%	-22.66%	5.37%		

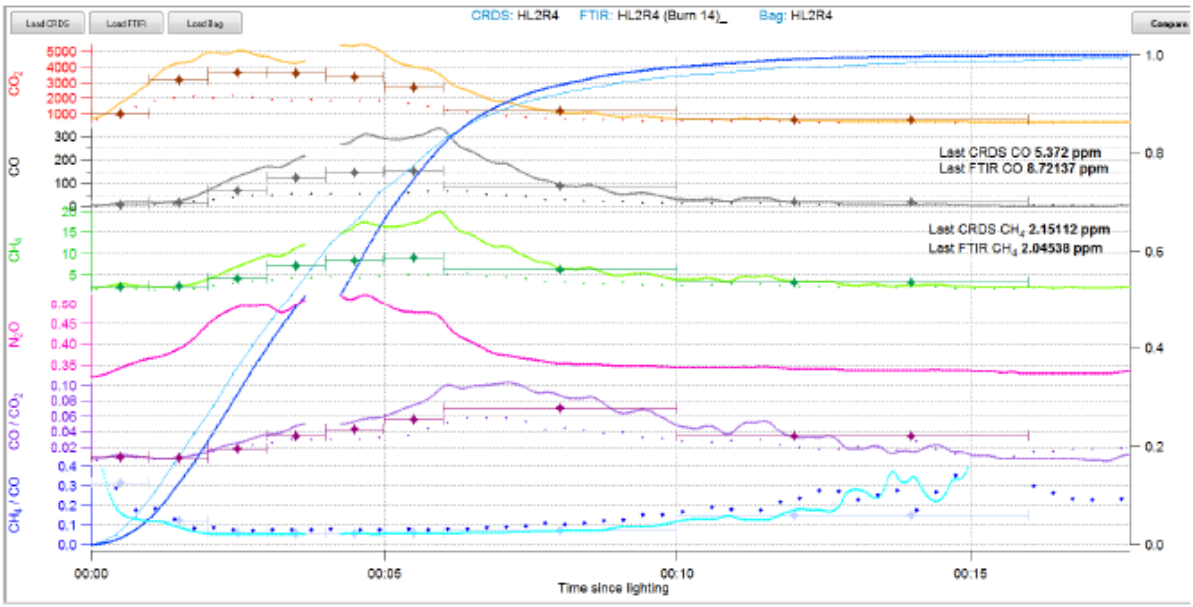

Burn	Species	EF_{CRDS}	EF_{FTIR}	$ER_{CO\ (CRDS)}$	$ER_{CO\ (FTIR)}$	$ER_{CO\ (bags)}$	MCE_{CRDS}	MCE_{FTIR}
HL2R4	CO_2	1726	1742				0.944	0.956
		-0.44%	0.44%				-0.63%	0.63%
	CO	64.7	50.9					
		11.96%	-11.96%					
	CH_4	1.85	1.5	0.050	0.052	0.045		
		10.36%	-10.36%	1.95%	5.39%	-7.34%		

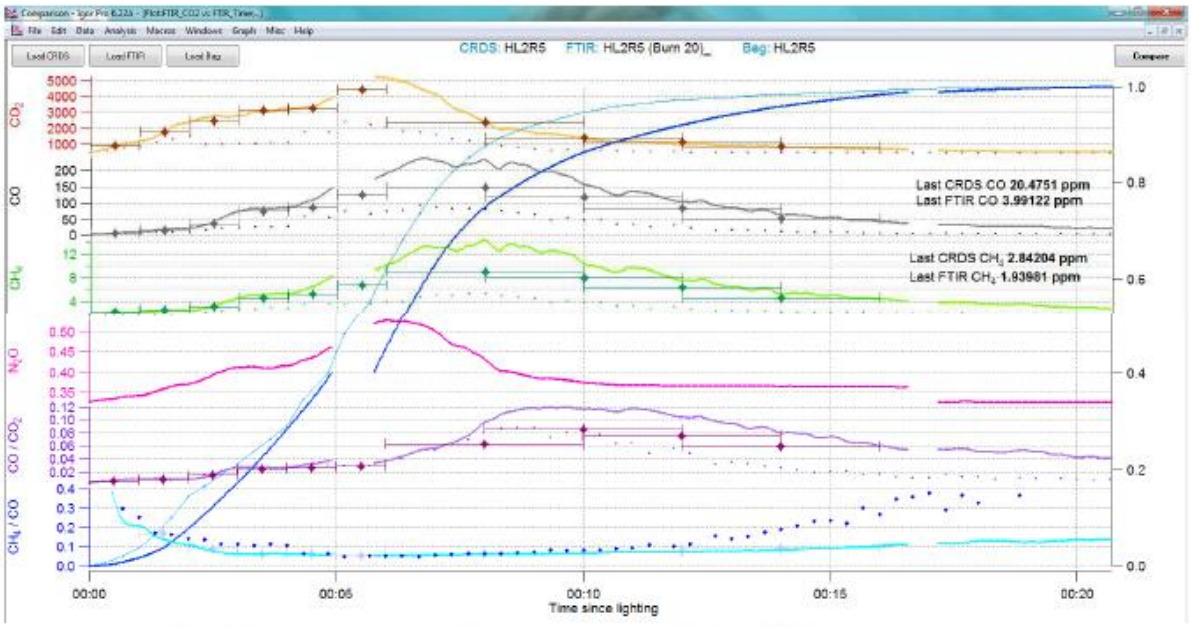

Burn	Species	EF_{CRDS}	EF_{FTIR}	$ER_{CO\ (CRDS)}$	$ER_{CO\ (FTIR)}$	$ER_{CO\ (bags)}$	MCE_{CRDS}	MCE_{FTIR}
HL2R5	CO_2	1698	1703				0.930	0.936
		-0.14%	0.14%				-0.32%	0.32%
	CO	81.8	73.6					
		5.27%	-5.27%					
	CH_4	2.36	1.57	0.050	0.037	0.047		
		20.10%	-20.10%	12.58%	-17.03%	4.45%		

Load 3 burns

Solid lines = Mick's laser techniques, dotted lines =open-path FTS, diamonds = bags with bars indicating fill times.

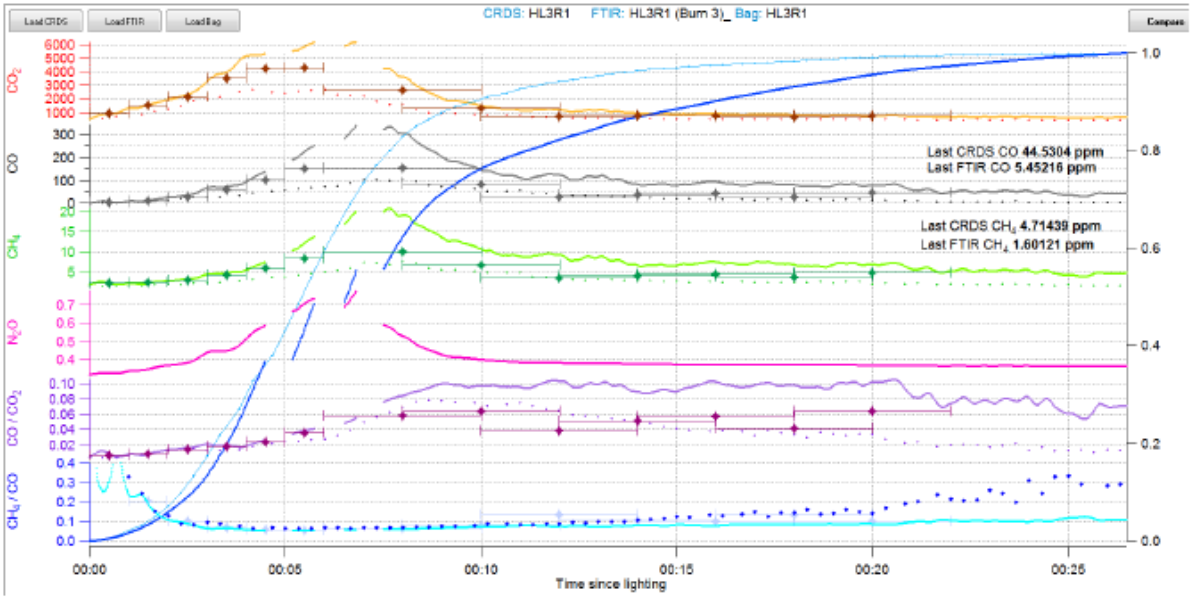

Burn	Species	EF_{CRDS}	EF_{FTIR}	$ER_{CO\ (CRDS)}$	$ER_{CO\ (FTIR)}$	$ER_{CO\ (bags)}$	MCE_{CRDS}	MCE_{FTIR}
HL3R1	CO_2	1678	1712				0.920	0.941
		-0.99%	0.99%				-1.13%	1.13%
	CO	93.2	68.2					
		15.47%	-15.47%					
	CH_4	2.89	2.13	0.054	0.055	0.046		
		15.20%	-15.20%	5.27%	5.76%	-11.03%		

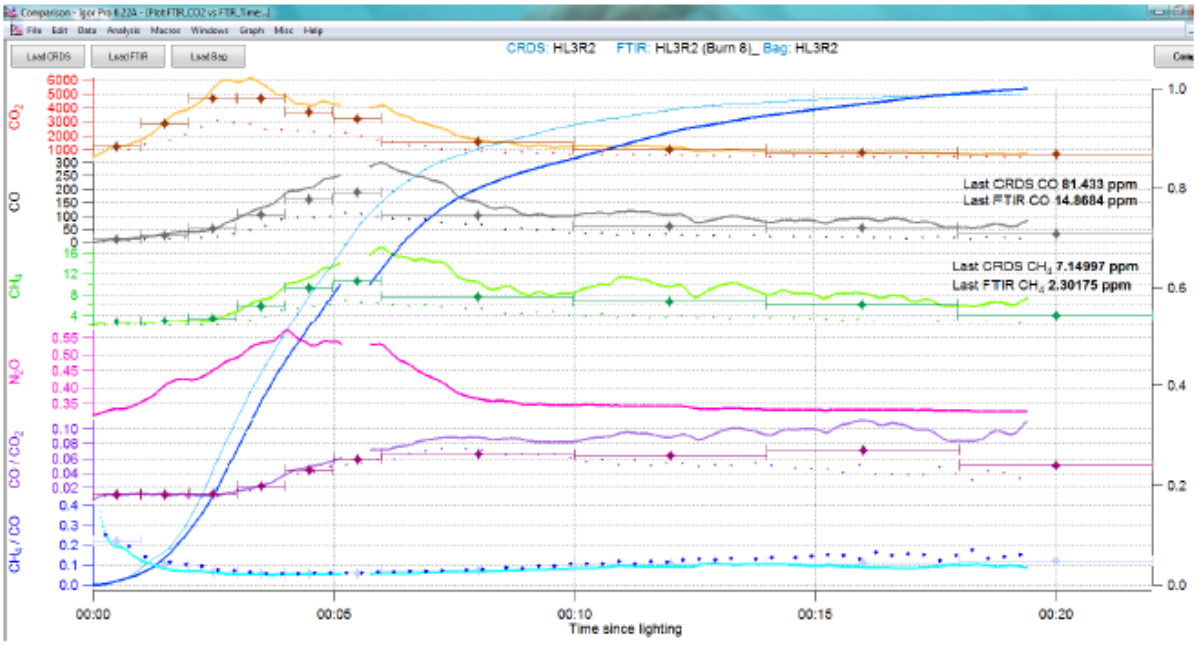

Burn	Species	EF_{CRDS}	EF_{FTIR}	$ER_{CO\ (CRDS)}$	$ER_{CO\ (FTIR)}$	$ER_{CO\ (bags)}$	MCE_{CRDS}	MCE_{FTIR}
HL3R2	CO_2	1709	1713				0.936	0.941
		-0.13%	0.13%				-0.27%	0.27%
	CO	74.9	68.1					
		4.76%	-4.76%					
	CH_4	2.01	1.7	0.047	0.044	0.042		
		8.36%	-8.36%	5.86%	-1.30%	-4.56%		

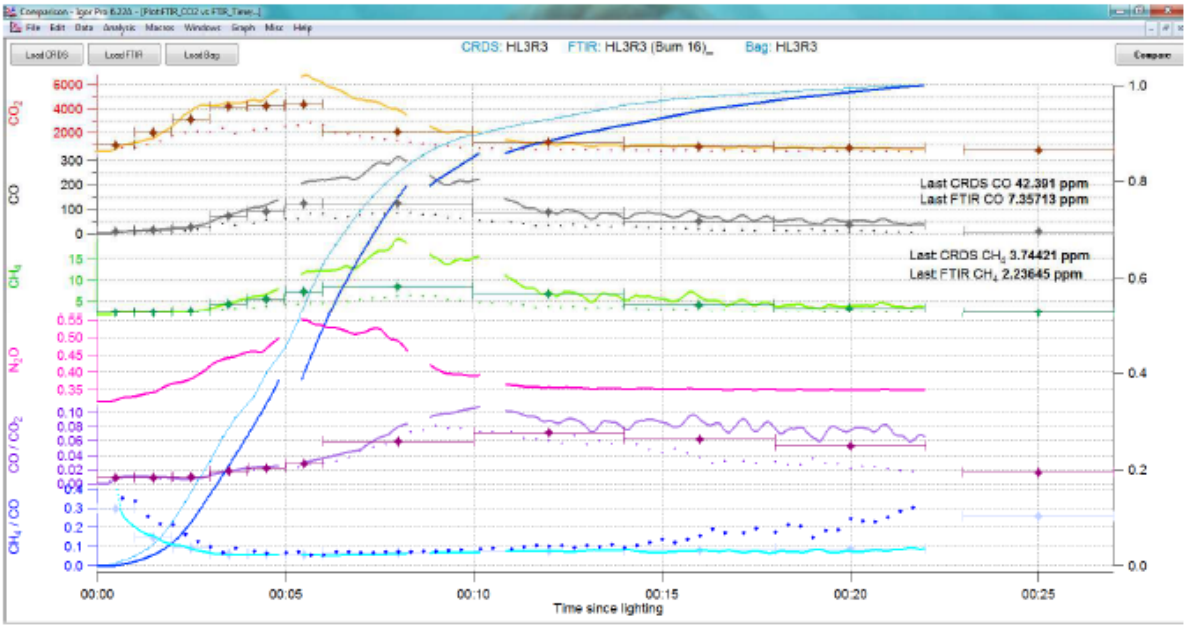

Burn	Species	EF_{CRDS}	EF_{FTIR}	$ER_{CO\ (CRDS)}$	$ER_{CO\ (FTIR)}$	$ER_{CO\ (bags)}$	MCE_{CRDS}	MCE_{FTIR}
HL3R3	CO_2	1724	1724				0.943	0.946
		-0.02%	0.02%				-0.16%	0.16%
	CO	66.3	63.0					
		2.57%	-2.57%					
	CH_4	2.11	1.65	0.056	0.046	0.052		
				9.04%	-10.51%	1.48%		

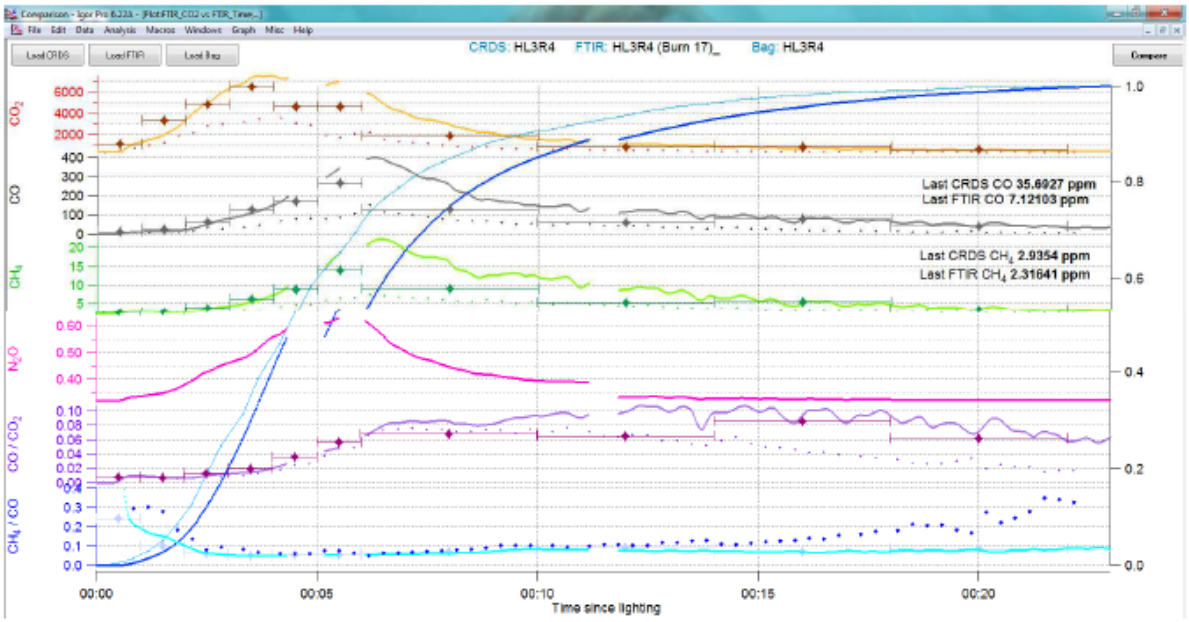

Burn	Species	EF_{CRDS}	EF_{FTIR}	$ER_{CO\ (CRDS)}$	$ER_{CO\ (FTIR)}$	$ER_{CO\ (bags)}$	MCE_{CRDS}	MCE_{FTIR}
HL3R4	CO_2	1711	1721				0.936	0.944
		-0.31%	0.31%				-0.43%	0.43%
	CO	74.3	65.2					
		6.52%	-6.52%					
	CH_4	2.34	1.72	0.055	0.046	0.047		
		15.37%	-15.37%	11.88%	-6.46%	-5.42%		

Load 4 burns

Solid lines = Mick's laser techniques, dotted lines =open-path FTS, diamonds = bags with bars indicating fill times.

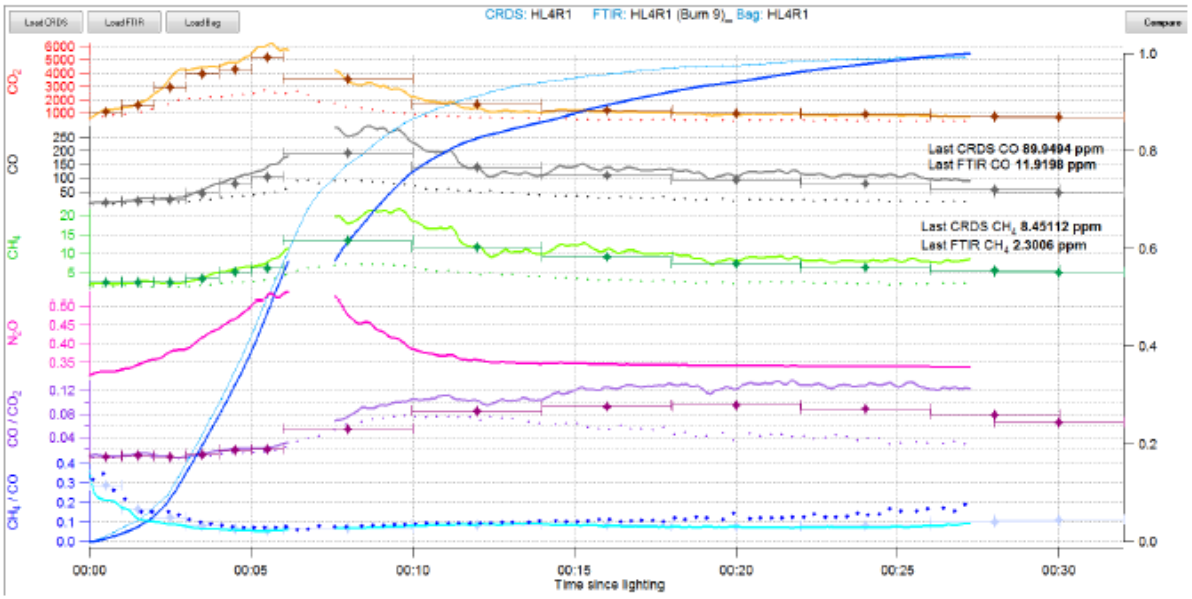

Burn	Species	EF_{CRDS}	EF_{FTIR}	$ER_{CO\ (CRDS)}$	$ER_{CO\ (FTIR)}$	$ER_{CO\ (bags)}$	MCE_{CRDS}	MCE_{FTIR}
HL4R1	CO_2	1680	1708				0.921	0.939
		-0.82%	0.82%				-0.97%	0.97%
	CO	91.6	70.1					
		13.34%	-13.34%					
	CH_4	3.78	2.63	0.072	0.066	0.064		
		17.90%	-17.90%	7.06%	-2.48%	-4.57%		

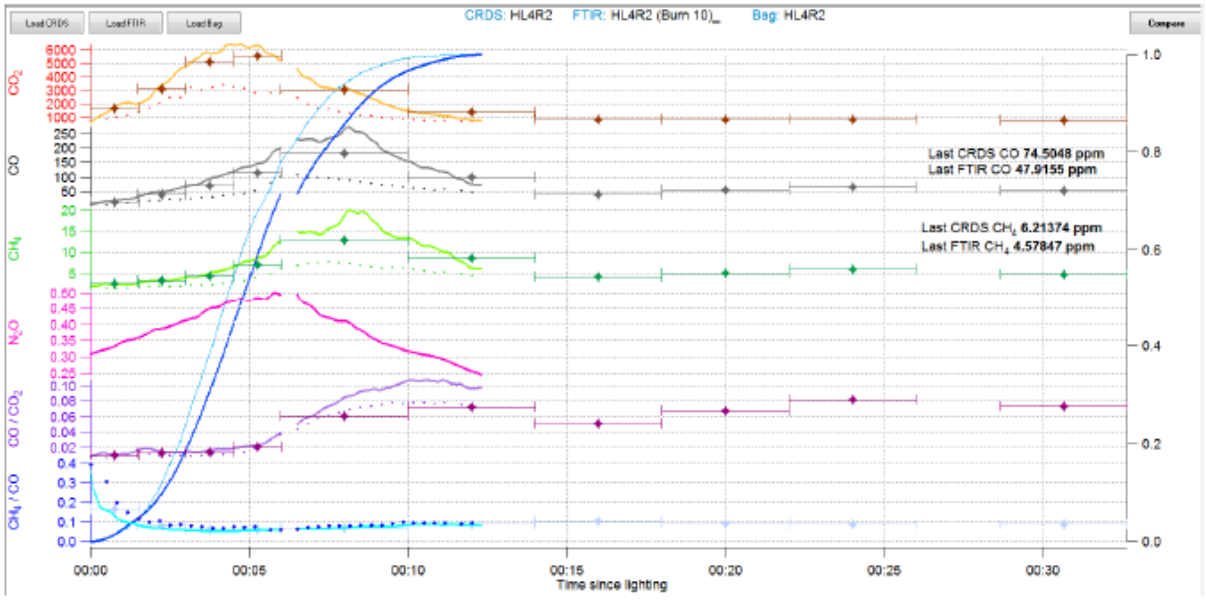

Burn	Species	EF_{CRDS}	EF_{FTIR}	$ER_{CO\ (CRDS)}$	$ER_{CO\ (FTIR)}$	$ER_{CO\ (bags)}$	MCE_{CRDS}	MCE_{FTIR}
HL4R2	CO_2	1747	1717				0.956	0.944
		0.88%	-0.88%				0.63%	-0.63%
	CO	51.7	64.8					
		-11.26%	11.26%					
	CH_4	2.02	2.28	0.068	0.062	0.062		
		-6.12%	6.12%	6.85%	-3.60%	-3.25%		

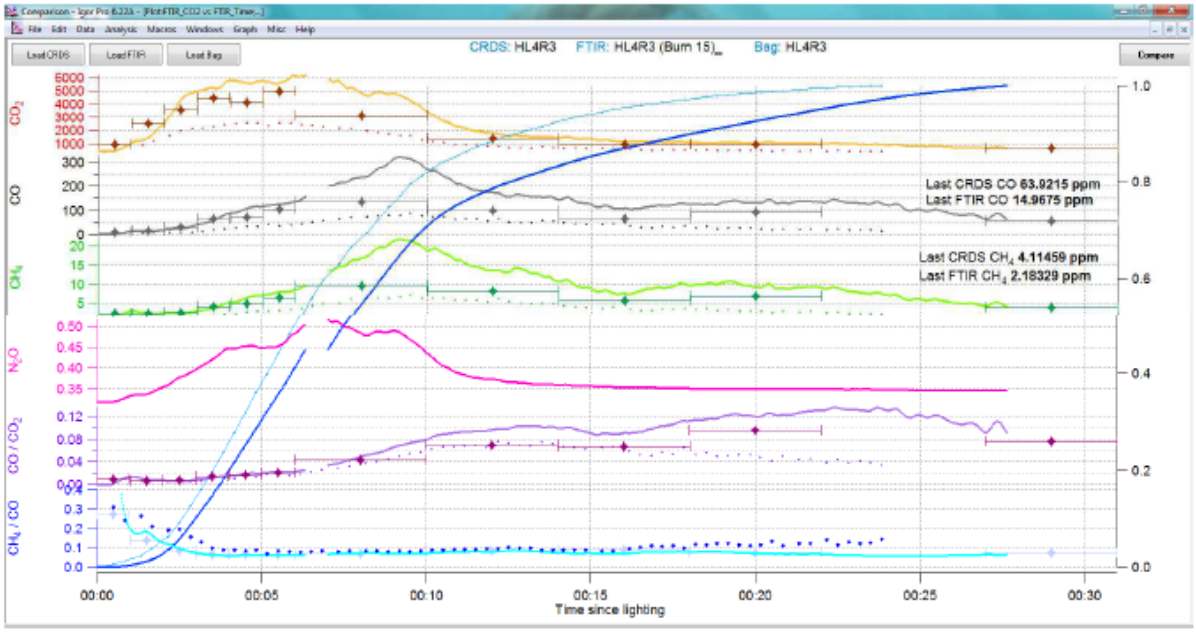

Burn	Species	EF_{CRDS}	EF_{FTIR}	$ER_{CO\ (CRDS)}$	$ER_{CO\ (FTIR)}$	$ER_{CO\ (bags)}$	MCE_{CRDS}	MCE_{FTIR}
HL4R3	CO_2	1704	1735				0.933	0.952
		-0.90%	0.90%				-1.01%	1.01%
	CO	77.8	56.1					
		16.19%	-16.19%					
	CH_4	3.09	2.29	0.069	0.072	0.063		
		14.81%	-14.81%	1.90%	5.00%	-6.90%		

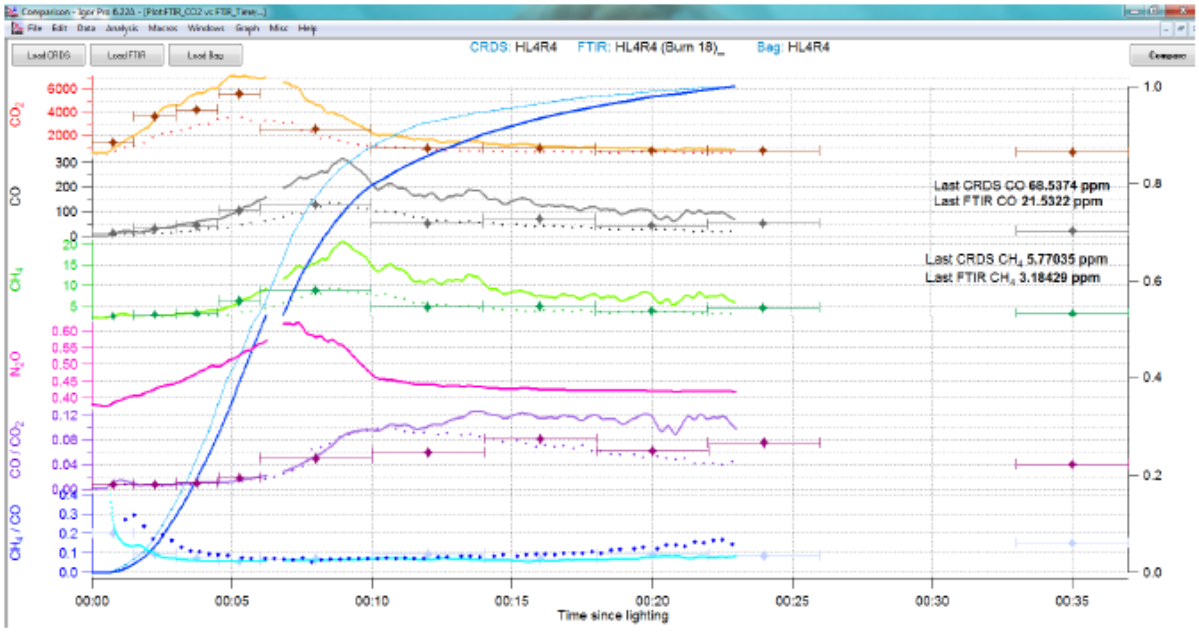

Burn	Species	EF_{CRDS}	EF_{FTIR}	$ER_{CO\ (CRDS)}$	$ER_{CO\ (FTIR)}$	$ER_{CO\ (bags)}$	MCE_{CRDS}	MCE_{FTIR}
HL4R4	CO_2	1721	1715				0.942	0.941
		0.19%	-0.19%				0.05%	-0.05%
	CO	67.6	68.8					
		-0.87%	0.87%					
	CH_4	2.35	1.91	0.061	0.049	0.053		
		10.29%	-10.29%	12.54%	-9.97%	-2.57%		

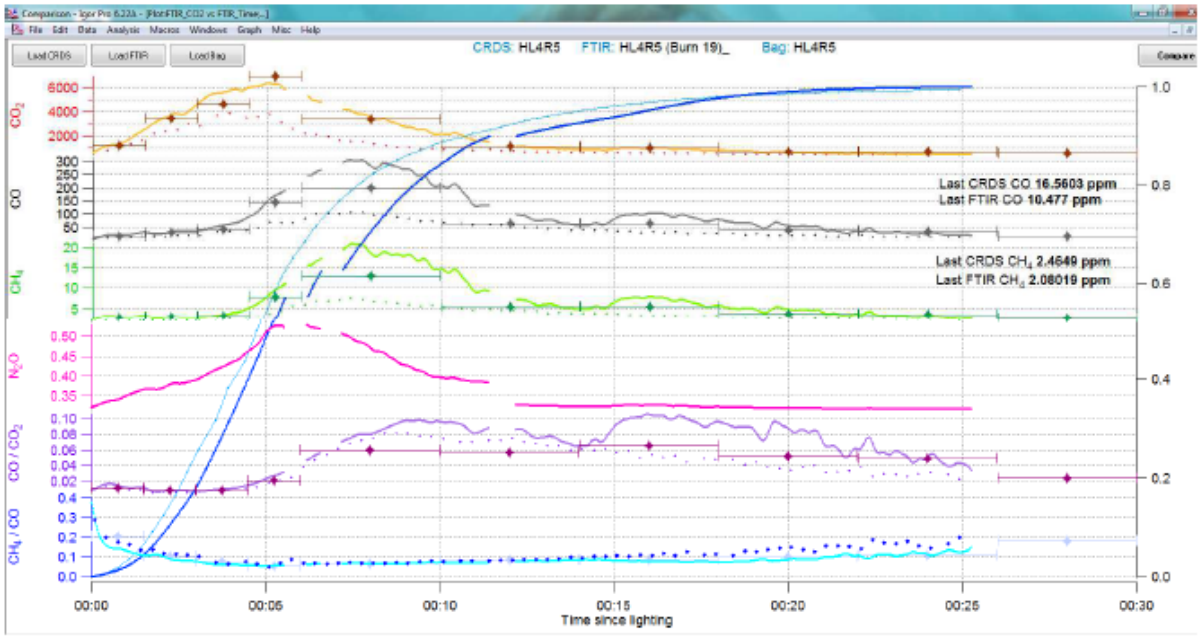

Burn	Species	EF_{CRDS}	EF_{FTIR}	$ER_{CO\ (CRDS)}$	$ER_{CO\ (FTIR)}$	$ER_{CO\ (bags)}$	MCE_{CRDS}	MCE_{FTIR}
HL4R5	CO_2	1721	1727				0.942	0.947
		-0.16%	0.16%				-0.26%	0.26%
	CO	67.8	60.9					
		5.36%	-5.36%					
	CH_4	2.37	1.89	0.061	0.054	0.054		
		11.33%	-11.33%	8.71%	-3.76%	-4.95%		

Backing Fires

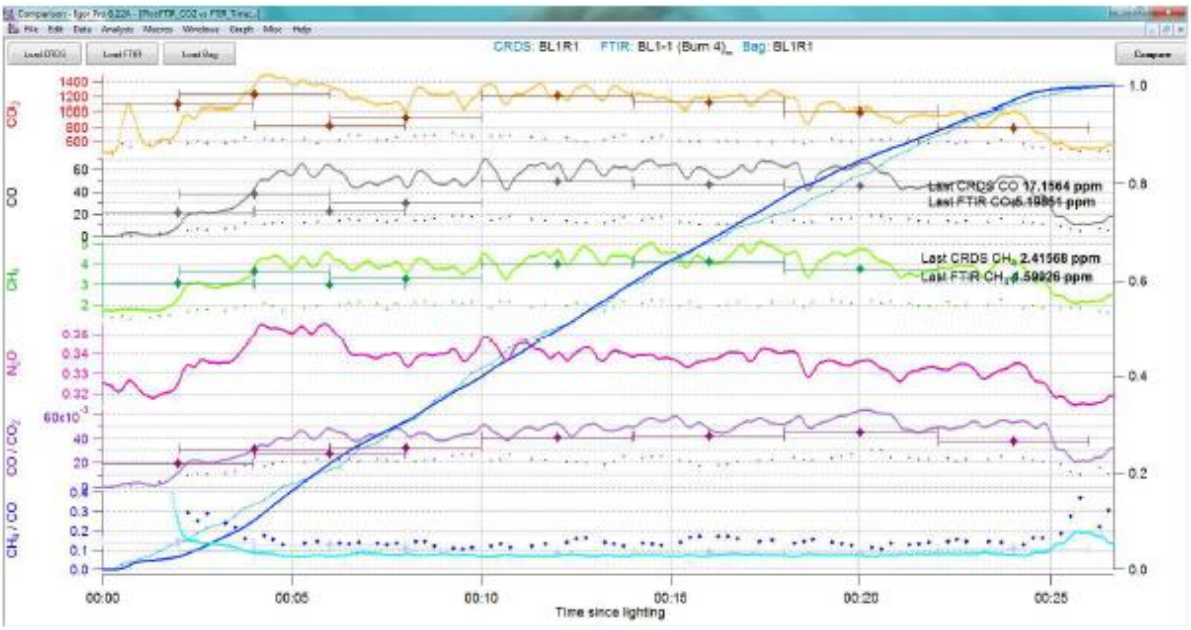

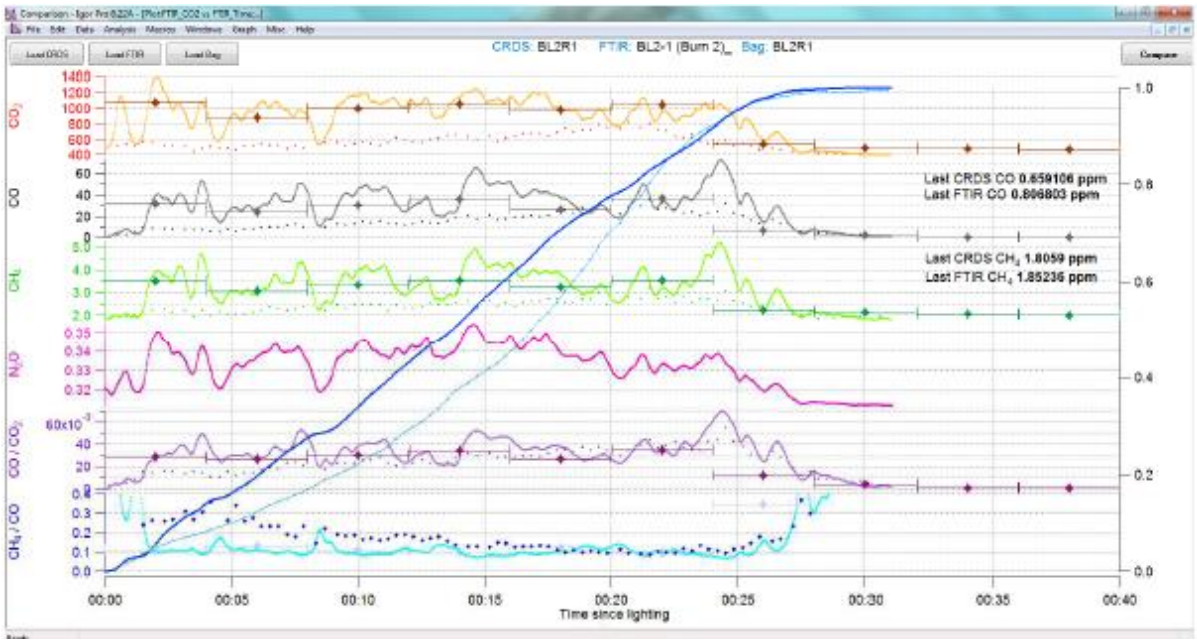

Burn	Species	EF_{CRDS}	EF_{FTIR}	$ER_{CO\ (CRDS)}$	$ER_{CO\ (FTIR)}$	$ER_{CO\ (bags)}$	MCE_{CRDS}	MCE_{FTIR}
BL1R1	CO_2	**1703**	**1709**				**0.932**	**0.938**
		-0.17%	0.17%				-0.32%	0.32%
	CO	**79.5**	**71.9**					
		5.04%	-5.04%					
	CH_4	**1.99**	**1.55**	**0.044**	**0.038**	**0.041**		
		12.42%	-12.42%	7.52%	-7.22%	-0.30%		
BL2R1	CO_2	**1715**	**1662**				**0.938**	**0.915**
		1.58%	-1.58%				1.24%	-1.24%
	CO	**71.8**	**98.0**					
		-15.45%	15.45%					
	CH_4	**1.95**	**1.96**	**0.048**	**0.035**	**0.043**		
		-0.22%	0.22%	13.39%	-16.32%	2.93%		

Appendix D2: Open-Path FTS Measurements of Emission Factors from Hazard Reduction Burns in Victoria – a report for the Smoke Transportation and Emission Modelling for Victoria Project.

Introduction

This is an interim report outlining preliminary results from an Autumn measurement campaign aimed at characterising emissions of trace gases from hazard reduction burns in Vistoria. Inclement weather and associated difficulties prevented successful measurements in 2014. In this report we describe the measurements successfully made using open-path FTIR at two hazard reduction burns at Greendale and Castlemaine (Figure 86). Preliminary findings from the Castlemaine hazard reduction burn are also presented.

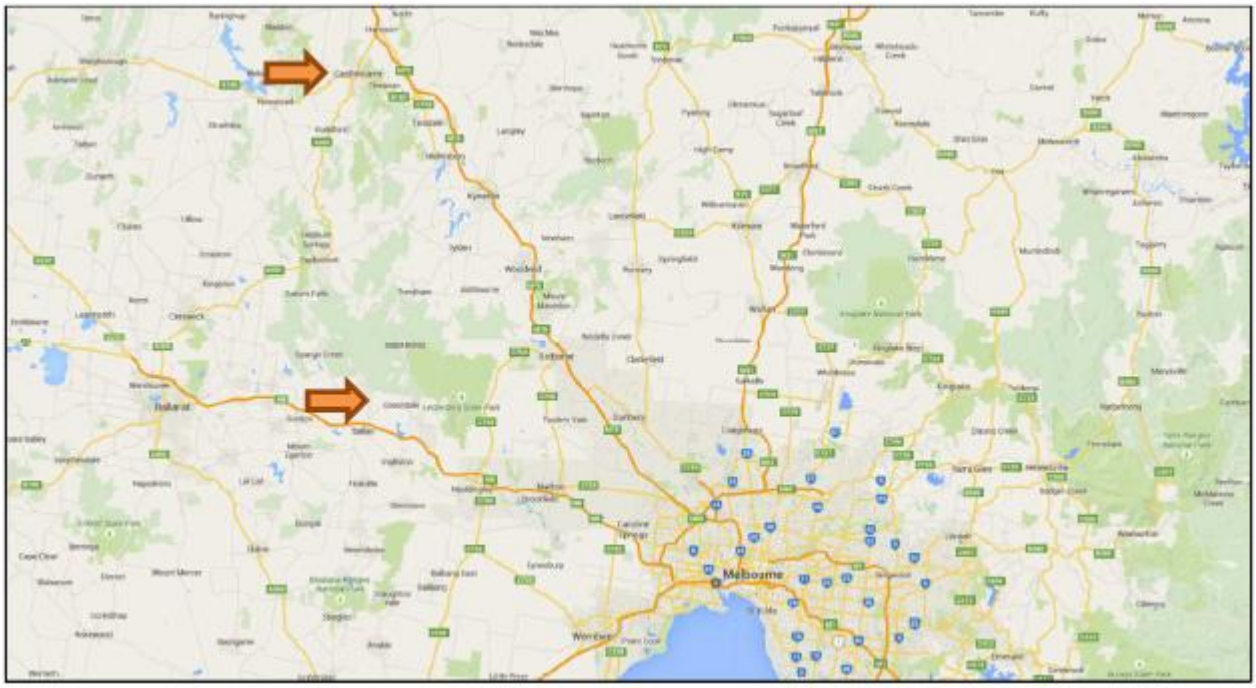

Figure 86 Arrows show the location of Greendale and Castlemaine where University of Wollongong joined CSIRO in a study of emissions from prescribed burns run by DEPI.

Greendale

On the 13th of April 2015 personnel from the Centre for Atmospheric Chemistry, University of Wollongong (Max Desservettaz and Kaitlyn Lieschke), joined staff from CSIRO (Mick Meyer and Fabienne Reisen) at a prescribed burn run by DELWP in Greendale.

The weather forecast predicted south-easterly light wind. Therefore, the open-path FTIR instrument was set up along a road on the northwest part of the burn area (Figure 87 and Figure 88). This was so that the open-path viewing geometry was such that the smoke produced in the burn should be blown into the line of sight of the instrument.

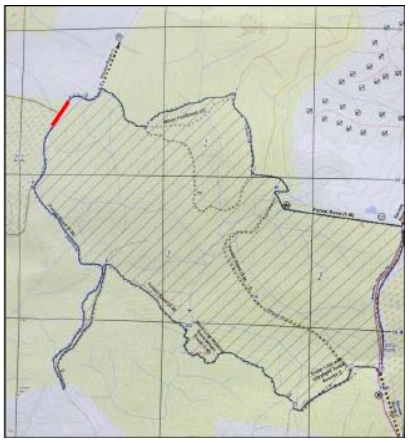

Figure 87 Map of the Greendale burn. The red line indicates the position of the open-path FTIR instrument.

Figure 88 The open-path FTIR instrument was set up along a road.

The weather prediction was accurate and thick smoke passed through the open path (Figure 89). The instrument recorded approximately 2 hours of spectra through background air and about 1.5 hours of spectra through smoke-affected air.

Due to technical issues with the temperature and pressure retrieval at the time of the burn, the analysis of the spectra has yet to pass quality assurance checks, but preliminary data shows strong correlations between methane and carbon monoxide.

Figure 89 A thick smoke surrounded the instrument a few minutes after DEPI set fire to the area.

Castlemaine:

On the 23rd of April 2015 personnel from the Centre for Atmospheric Chemistry, University of Wollongong (Max Desservettaz and Doreena Dominick), joined staff from CSIRO (Mick Meyer and Fabienne Reisen) at a prescribed burn run by DELWP in Castlemaine.

The weather forecast predicted south-easterly light wind. Therefore, the open-path FTIR instrument was set up the main touristic road going through the burn area (Figure 90 and Figure 91).

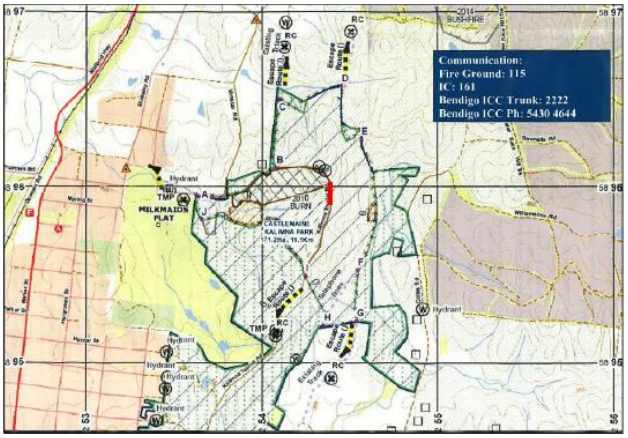

Figure 90 Map of the Castlemaine burn. The red line indicates the position of the open-path FTIR instrument.

Figure 91 The open-path FTIR instrument was set up along the road

Unlike the Greendale burn, the DELWP staff lighting the burn arrived quickly at the location chosen to set up the instrument, so the area was already covered in smoke before the instrument was running. Therefore, the instrument did not record any background air prior the burn.

The weather forecast was not fully accurate, with wind coming from south-westerly to southeasterly. During periods of south-westerly wind, the air was clear of smoke (the area to the west of the touristic road was lit up later in the day); those periods were used to deduce background concentration for the analysis. The smoke was a lot less thick than at the Greendale burn (Figure 91).

Figure 92 shows time-series of some of the trace gases measured by the open-path FTS. Periods of cleaner air can be observed through the time series of CO_2, CO and CH_4 due to the variability of the wind.

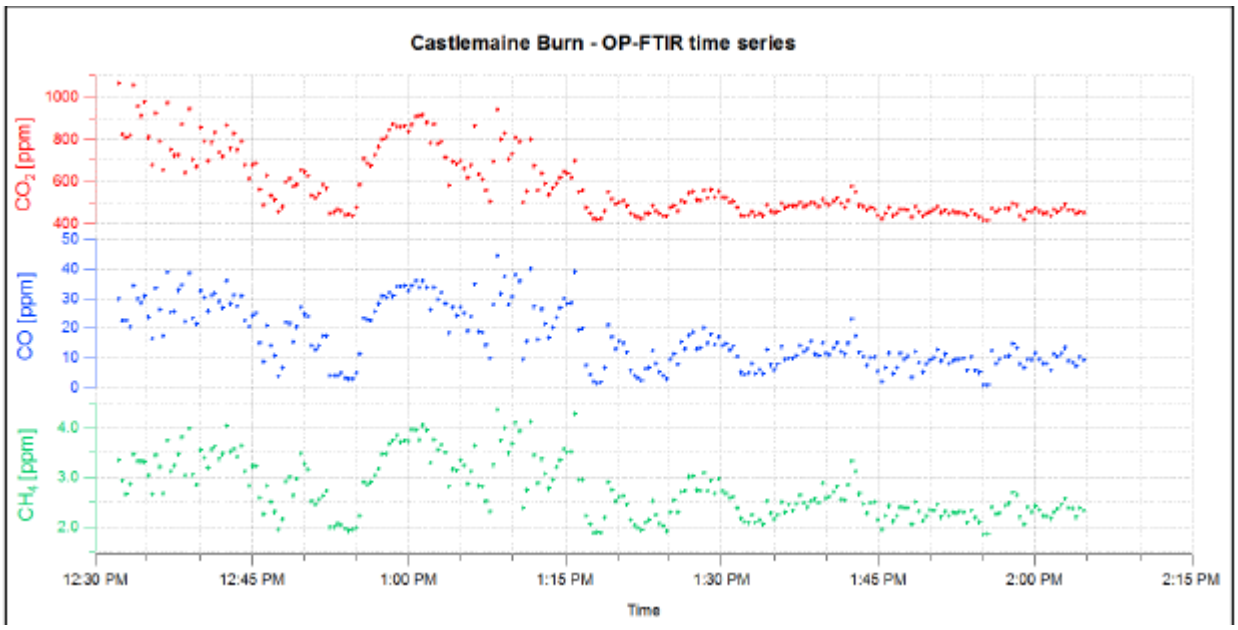

Figure 92 Time series of CO_2, CO and CH_4 at the Castlemaine prescribed burn.

In order to calculate ERs and EFs, concentrations above background (or excess concentrations) were derived using the lowest concentration of each species as background concentration. The emissions from the Castlemaine burn exhibit strong correlations; for example CH_4 CO (Figure 93).

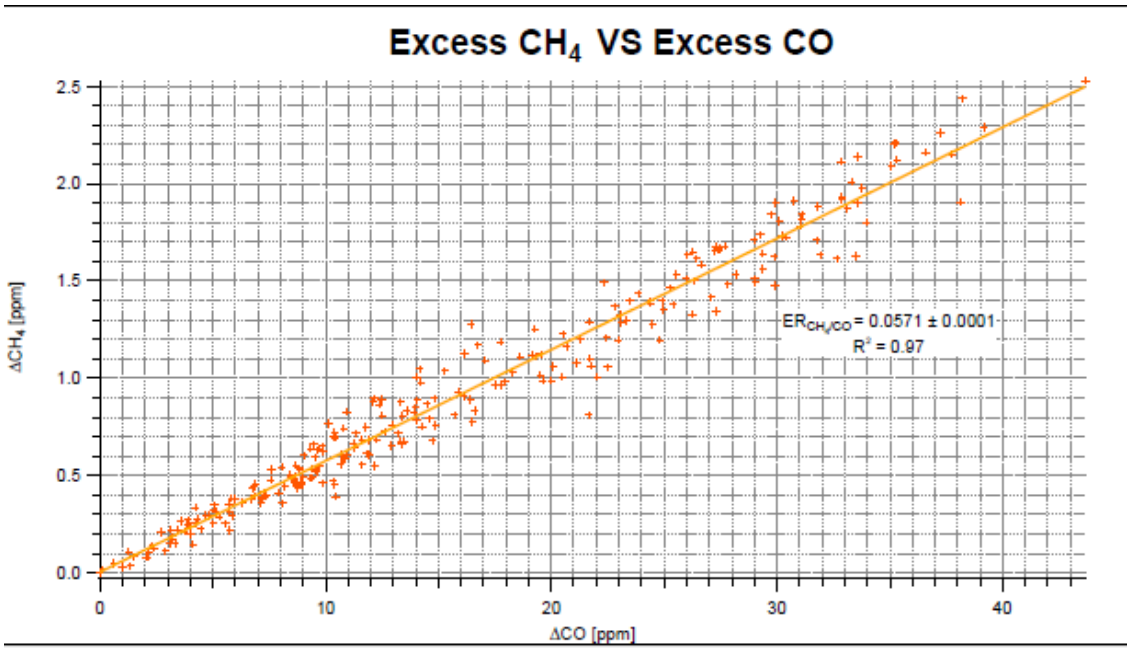

Figure 93 Methane above background versus carbon monoxide above background. The slope of the linear fitted line is the emission ratio of methane and carbon monoxide.

Emission Factor Results

Table 27 shows the EFs for trace gases measured at the Castlemaine burn in grams of trace gas emitted per kilogram of dry fuel consumed. EFs of CO_2 and CO are calculated using the summation method, whilst for all other gases EFs are calculated via the ER to CO *(Paton-Walsh et al., 2014)*. Table 27 also shows the ER of each trace gas to CO (3rd column) and the R^2 of the linear regression that yields this ER to CO (4th column).

Table 27 Castlemaine burn results.

Species	EF	ER/CO	ER/CO R^2
CO_2	1650		
CO	100.0		
CH_4	3.3	0.057	0.97
NH_3	1.7	0.028	0.98
C_2H_4	1.8	0.018	0.92
CH_3OH	1.7	0.014	0.96
H_2CO	2.1	0.020	0.89
HCOOH	0.53	0.0032	0.95
HAC	6.5	0.030	0.98

Summary and Conclusions

Due to inclement weather and logistical problems we have succeeded in making measurements at only two hazard reduction burns. In this interim report we present the data from the second of these burns at Castlemaine. EFs measured at this fire (in grams of gas emitted per kilogram of dry fuel burned) are 1650 g kg^{-1} of carbon dioxide; 100 g kg^{-1} of carbon monoxide; 3.3 g kg^{-1} of methane; 1.8 g kg^{-1} of ethylene; 2.1 g kg^{-1} of formaldehyde; 1.7 g kg^{-1} of methanol; 6.5 g kg^{-1} of acetic acid; 0.53 g kg^{-1} of formic acid and 1.7 g kg^{-1} of ammonia.

These EFs fall within the range of EFs measured by similar techniques at hazard reductions burns in New South Wales *(Paton-Walsh et al., 2014)*, leanding some confidence to their suitability for use in modelling studies. Nevertheless, the authors recommend that the data be supplemented where possible by the data from the Greendale burn and by other measurements to be made at future hazard reduction burns this Autumn.

Appendix E: Mercury

Introduction

Mercury (Hg) is a globally transported neuro toxin that poses significant health risks for human populations. Terrestrial ecosystems are globally significant natural sources and sinks of atmospheric Hg. Due to the unique volatilisation properties of Hg the occurrence of fires can substantially increase the emissions of Hg into the atmosphere, accounting for the largest natural source in the global mercury budget *(Friedli et al. 2009)*. Hg stored in vegetation, leaf litter and soil is associated with organic rich matter and is mobilised into the atmosphere during a fire, predominantly in the form of gaseous elemental mercury (Hg^0). The amount of Hg available to be released is limited to Hg accumulated in the ecosystem prior to burning *(Campos et al. 2015)*. These spikes in Hg emissions from bushfires have the potential to influence local concentrations, through wet and dry deposition, and regional to global scale Hg concentrations, through long range transport. Hg emitted from a fire also has the ability to be re-distributed into other ecosystems and waterways where it may become methylated and biomagnify up the food chain, decreasing the health of the ecosystem and posing further risk to human health. Therefore, emissions from fires has the potential to increase population exposure, as well as influencing the global Hg budget.

The frequency of both prescribed and wildfires results in Australia being one of the largest contributor to Hg emissions from biomass burning, contributing 3% of total Hg global emissions of Hg from biomass burning *(Friedli et al. 2009)*. Increasing controls on anthropogenic emissions are likely to see natural sources of atmospheric Hg, such as emissions from biomass burning, becoming more important in the global mercury budget, particularly as the instances and extent of bushfires are predicted to increase with climate change *(De Simone et al. 2015)*. Little focus has been given to understanding Hg emissions and dispersion from Australian bushfires and no published work has been undertaken to measure real time Hg concentrations from fires, prescribed or otherwise. Emissions of Hg from prescribed burns has the potential to put Australian populations at risk of Hg exposure through both direct fire fighter exposure and local to regional scale population exposure through the transport, dispersion, and deposition. Australia has recently signed onto the United Nations Environmental Program (UNEP) Minamata convention *(UNEP 2013)*. This convention includes provisions for emissions reductions, technology sharing, public awareness, and enhanced mercury monitoring in human populations, wildlife and the environment. The scope of prescribed burning may be evaluated under this legally binding treaty.

This section of the report presents the findings from laboratory experiments on mercury from fires and on the modelling of the transport and fate of mercury from prescribed burns including firefighter exposure and risk.

Methods

The overview description of the 2014 CSIRO Pyrotron experiment is outlined in appendix A. CO, CO_2 and other commonly emitted gases were simultaneously measured during the experiment concurrent with the mercury measurements to facilitate the calculation of EFs and ERs from the Australian vegetation used in the experiments. These burns were designed to be representative of vegetation common to Australian prescribed burns.

Two primary methods were employed at the Pyrotron experiment to measure Hg emitted during the burning of vegetation. The first employed grab air sampling. This approach involved collecting grab samples to analyse for gaseous elemental mercury (GEM) and is based on a pressure differential or a so-called Lung Sampler. These samplers are commonly used in air sampling methods prescribed by the USEPA *(USEPA 1987)*. Figure 94 shows these lung samplers being used at the Pyrotron experiment. In the field these samplers are slung over the shoulder of the user and a longer intake tube is used to collect the fire emission. The advantage of the lung sampler is that it avoids contamination of the sample by the pump. In this method a Tedlar bag, flushed prior to use with high purity nitrogen, is attached by a tube inside an air tight chamber (i.e., pelican case in this application). The sealed chamber is then evacuated via a pump, causing the bag to expand and draw the sample into the bag through the intake tube attached to the bag inside the case. The sample air never touches the surfaces of the pump. In this study the Tedlar bags have a volume of 10 litres and depending on the pumping speed can take from 1 to 5 minutes to fill. This method is preferable for field sampling as it is

portable and can rapidly collect many grab samples. In the field bag filling times varied depending on sampling conditions. The bags collected are analysed within 24 hrs back at the field camp using a Tekran 2537 mercury sampler. To analyse the grab samples for mercury a 2.5 minute cycle, and 1.0 L/min sampling rate was used. The principal of operation uses a gold pre-concentration and atomic fluorescence detection with a sensitivity of < 0.1 ng/m^3 (5 min samples) and sampling cycle and sampling rate operator programmable of 2.0 – 60 min and 0.5 to 2.0 L/min, respectively. At the Pyrotron bags were filled every minute during the burn duration. As seen in Figure 94 there are three lung samplers which facilitated overlapping bag filling to optimize data collection during the short burn periods. The bags were analysed for Gaseous elemental mercury using a Tekran®2537 gaseous mercury analyser at the end of each day.

Figure 94: Lung sampling set up to measure Hg emissions for the Pyrotron experiment

Figure 95 shows the sampling intakes downwind of the Pyrotron burns used jointly by CSIRO, UOW and MU. The intake with orange filter holder on the left was used by MU to continuously monitor mercury emissions during the burns. The intake was attached to a Tekran 2537 continuous mercury analyser (specifications above). The continuous monitoring was undertaken at a sample averaging rate of 2.5 minutes and sampling rate of 1 L/min. Prior to the burn a new 2 µm Teflon filter was installed. Post burn the filters were analysed in the laboratory using EPA method 1631 for the mercury content of the particulates collected thereon (PHg). The other co-located intakes sequentially to the right were used for bag sampling in collaboration with UOW and for the CSIRO sampling protocols described elsewhere in this report. As mentioned above, the bags were sampled post burn for GEM. Upwind of the burns at the Pyrotron tunnel was a second Tekran 2537 instrument used to measure continuously GEM and PHg.

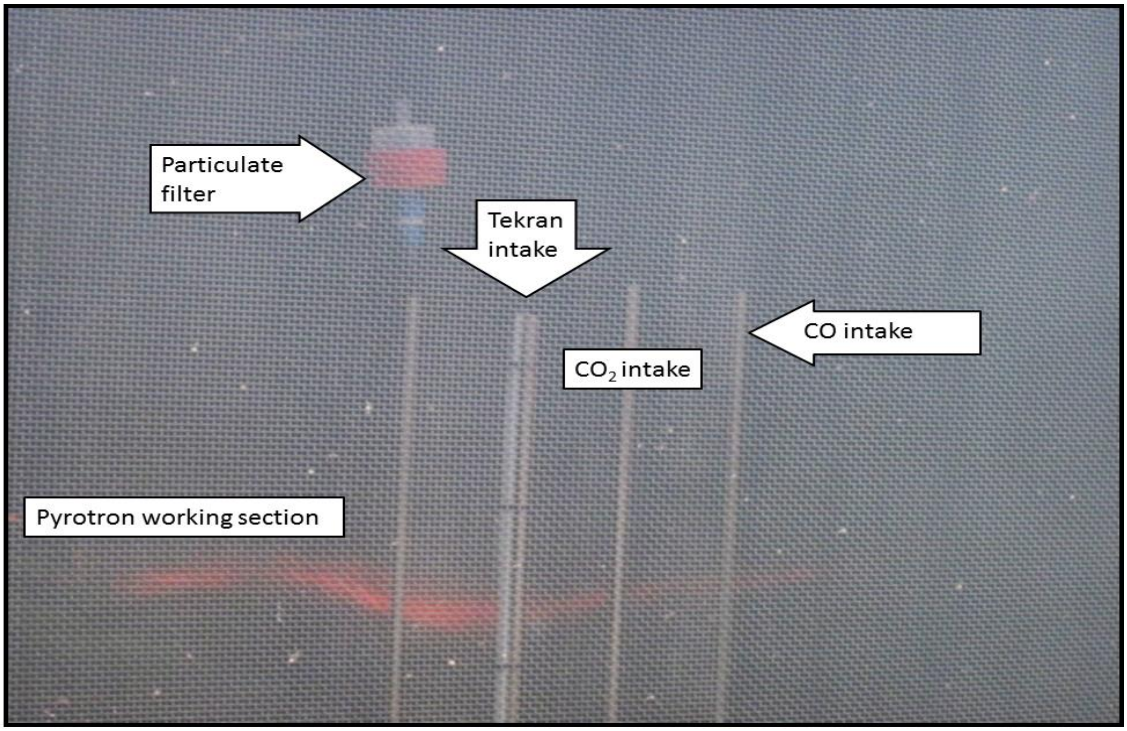

Figure 95: Sampling intakes for Hg, CO and CO_2 measurements located in the exit section of the Pyrotron wind tunnel

The MU team attended all burns set out in this program for data collection. Unfortunately, due to either weather or burn cancellation no mercury samples from actual prescribed burns scheduled were obtained. However, an extensive set of data were obtained from the Pyrotron experiments. From these data mercury EFs and ERs were determined. These were subsequently used in the modelling of population exposure described later in this report and the basis for the case studies presented here. Also, these data are the basis for the mercury aspect of the firefighter exposure estimates presented in this section of the report.

Firefighter exposure estimates were undertaken in collaboration with UOW and CSIRO, who undertook the collection of CO data using personal exposure devices. Details of the methodology are provided in Reisen and Brown, 2009. Personal exposure CO monitors were attached to 3 to 6 randomly selected firefighters attending a prescribed burn. CO was monitored continuously at 10 second intervals using an electronic data-logging dosimeter Dräger PAC III E (Dräger Safety AG & Co., Lübeck) equipped with an electrochemical sensor and measuring CO levels in air up to 2000 ppm. Full procedure is outlined in *Reisen and Brown (2009)*. The data loggers were calibrated before and after each burn using a 100 ppm CO calibration gas. These personal monitors were used as proxies for calculating the potential Hg exposure levels.

Emission ratios and emission factors from CSIRO Pyrotron experiments

Mercury emissions from each of the individual burns show a spike in emissions at the initial stages of the burn followed by a sharp decrease (Figure 96). The spike for the majority of the burns coincides with the EOFS or soon after. Emissions from the burns return to approximate background levels (<2 ng m^{-3}) soon after the fine fuels had been extinguished. The high emissions in the initial stages of the burn suggest that the majority of Hg is released during combustion of the fine fuel load where it is most likely stored in the fine fuels, with coarse fuels contributing little to the overall emissions from the burns. Bag data show slightly more varied time trends than the continuous data. This is most likely caused by differences in frequency of measurements between the two employed methods. Continuous data produced an average concentration every 2.5 minutes for all burns, creating a smoothed trend, whereas the bag collection had a higher time resolution and was therefore able to show greater variation in contrast to the smoothed average data obtained from the continuous tekran method.

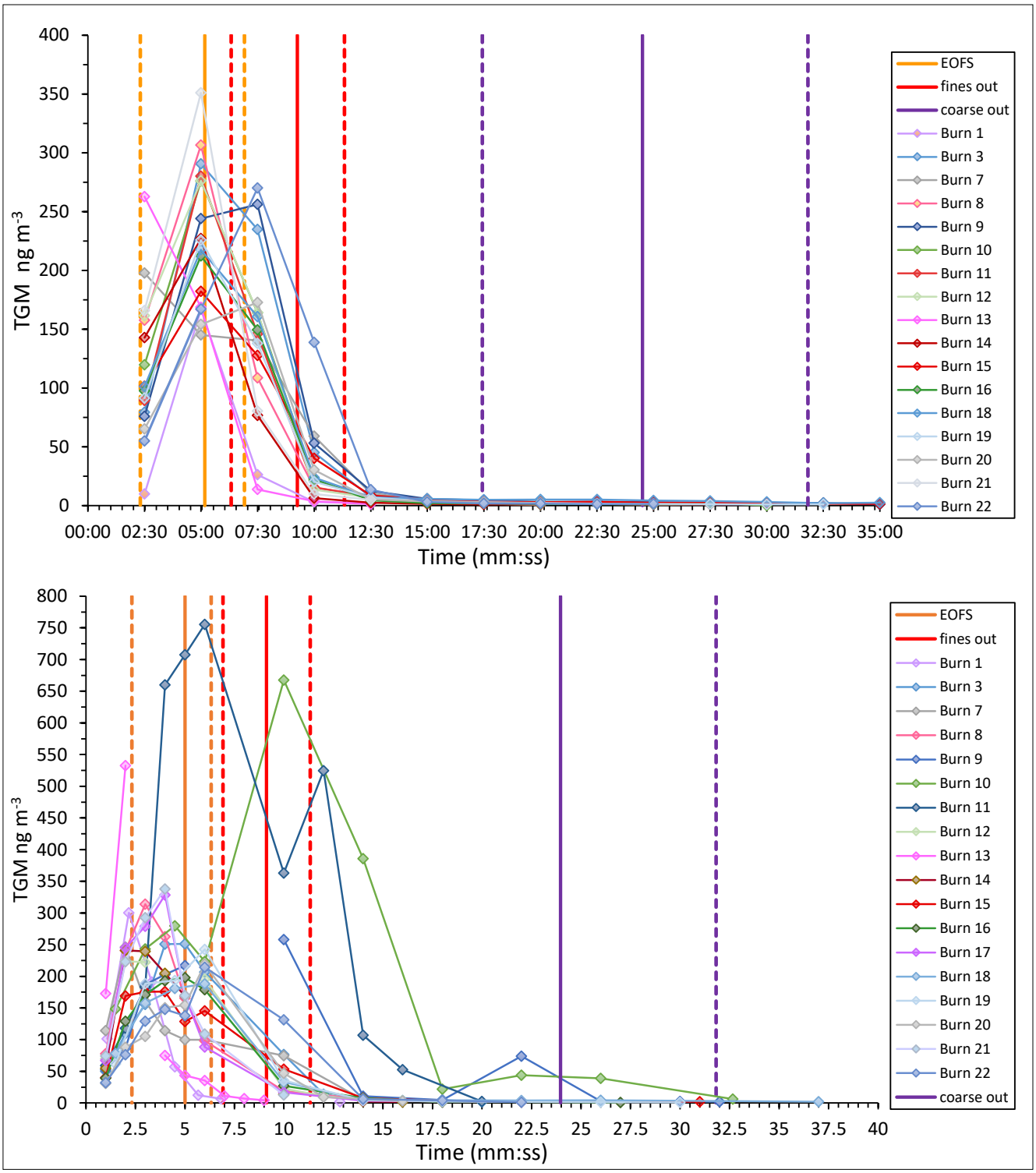

Figure 96: Continuous burn data against time (top), Hg concentrations measure using the bag method (bottom).

In order to determine both ER and EF for Hg released during a fire the relationships between carbon and Hg was looked at. Hg is strongly adsorbed to available carbon within an ecosystem and will therefore behave similarly to carbon when volatilised during a fire *(Kolka et al. 2014)*. The 26 burns were divided into the four different fuel loads for both methods and plotted with a linear regression to identify the strength of the relationships with CO and CO_2 and to calculate ERs. Correlations between Hg and CO_2 were significantly better than those observed between Hg and CO for both methods, for all fuel loads (Figure 97 and Figure 98, respectively). This is most likely a reflection of Hg release during different fire stages. Hg is primarily released from leaf litter during the flaming combustion phase, rather than smouldering phase *(Friedli et al. 2003a)*. CO is dominantly released during the smouldering phase when Hg stores appear to have been depleted, whereas CO_2, like Hg, is emitted during the flaming combustion phase *(Andreae and Merlet 2001)*.

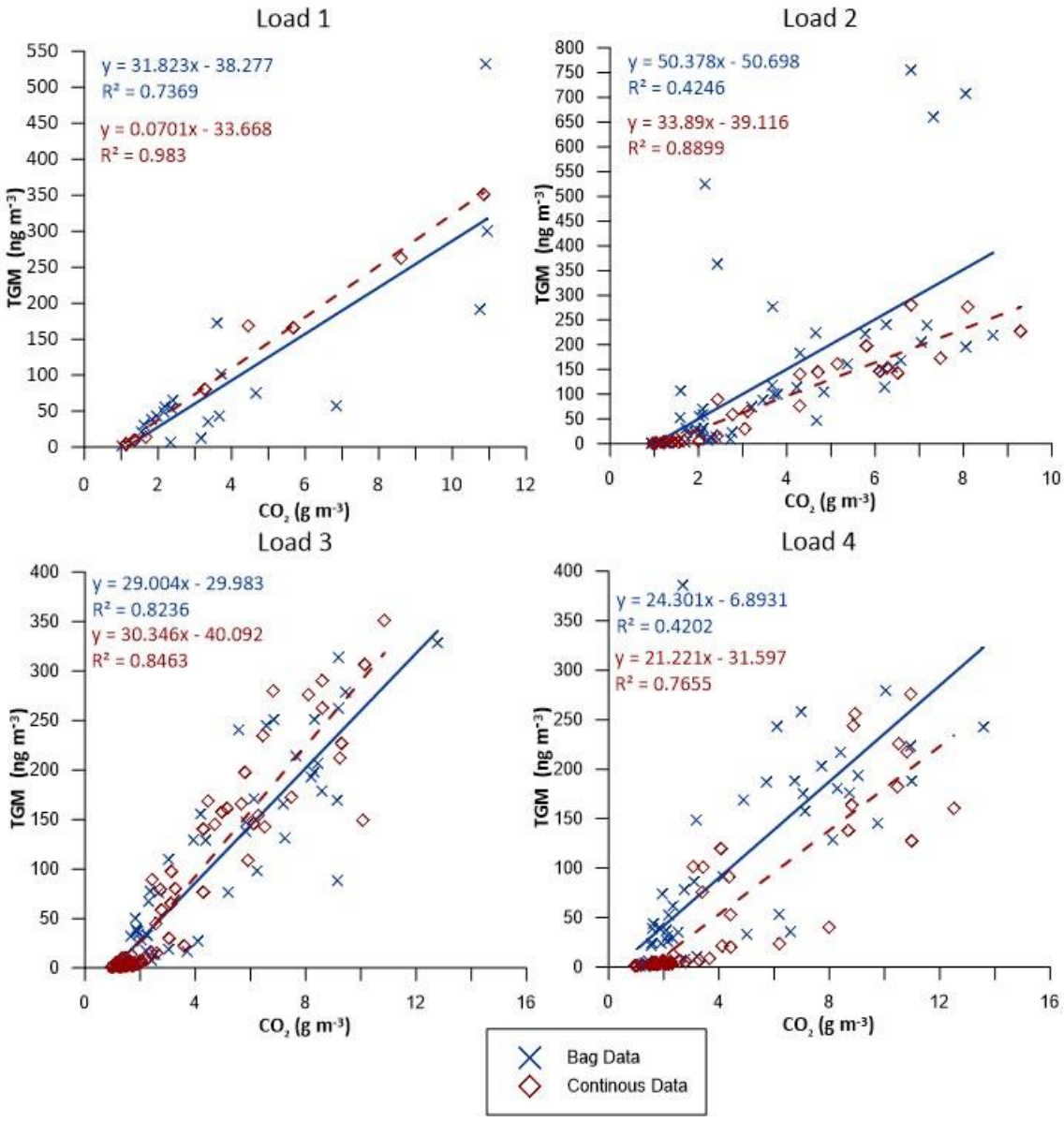

Figure 97: Relationship between Hg and CO_2 for the 4 fuel loads

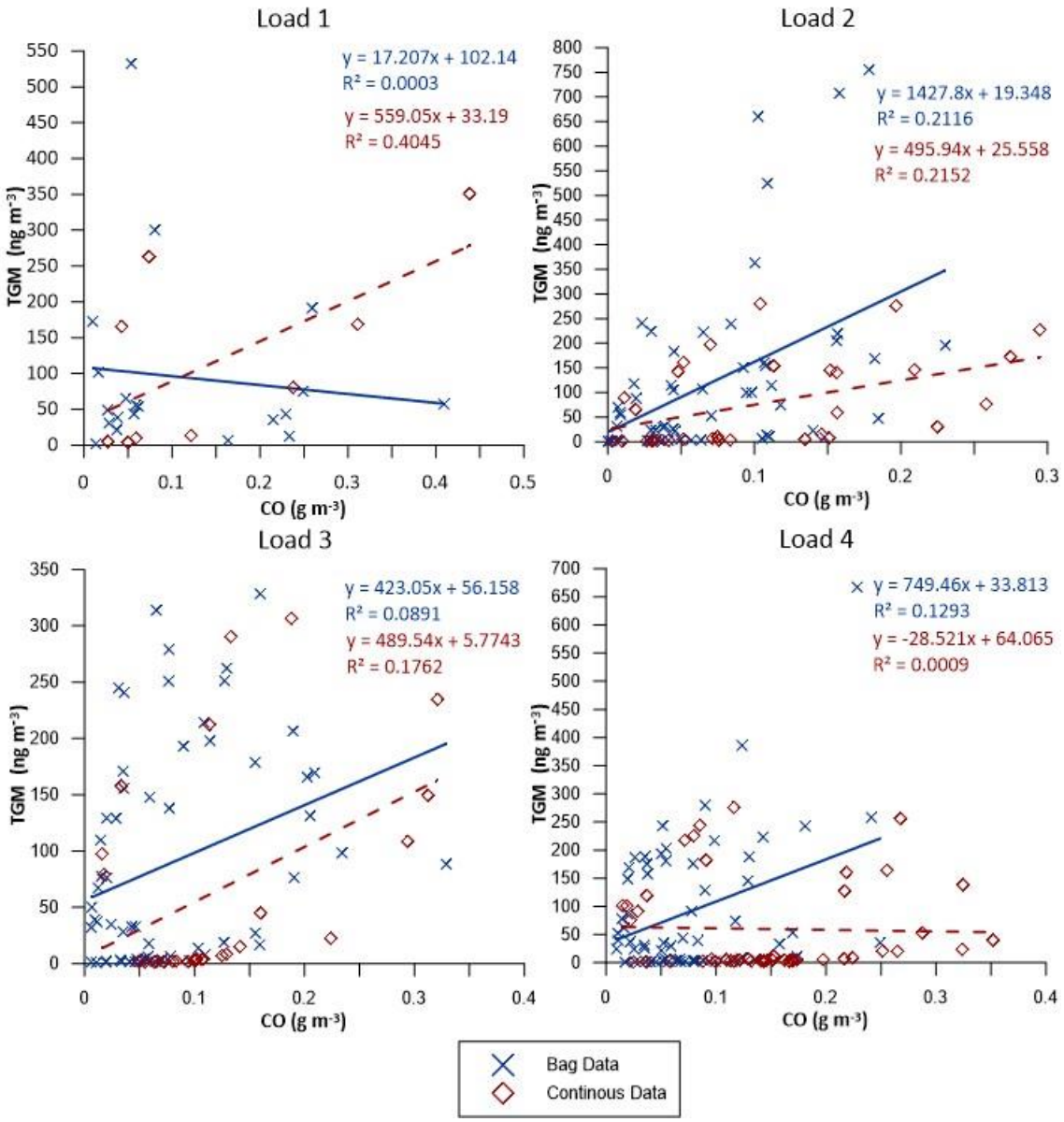

Figure 98: Relationship between Hg and CO for the 4 fuel loads

ER for Hg/CO_2 appear to have good agreement between the two methods, with only small differences in ratios. Load 4 presented with the smallest ER of 24.3 hg/CO_2 for continuous data and 21.2 Hg/CO_2, for Bag data, (Figure 99). This is likely a reflection of the ratio of fine to coarse fuels, as load 4 contained the largest quantity of coarse material and on average the lowest Hg concentrations. The other 3 fuel loads all present similar ER ranging from 29 Hg/CO_2 to 33.89 Hg/CO_{2-}. The Hg/CO data presented with too much scatter and variability between the two methods and different loads to determine any significant conclusions from this data (Figure 98). The experimental burns were designed to simulate conditions that occur during a prescribed burn. However, they generally burnt for a shorter period of time, with a maximum period of 35 minutes *(Sullivan et al. 2013)*. As prescribed burns typically burn for a longer period of time, particularly the smouldering phase when CO is dominantly emitted, it is possible that the duration of the smouldering phase was not suffient enough for the relationship between CO and Hg to be established. As CO_2 and Hg are both commonly released during the flaming combustion phase and show a stronger relationship, CO_2 was determined to be the better reference gas for the calculation of EFs.

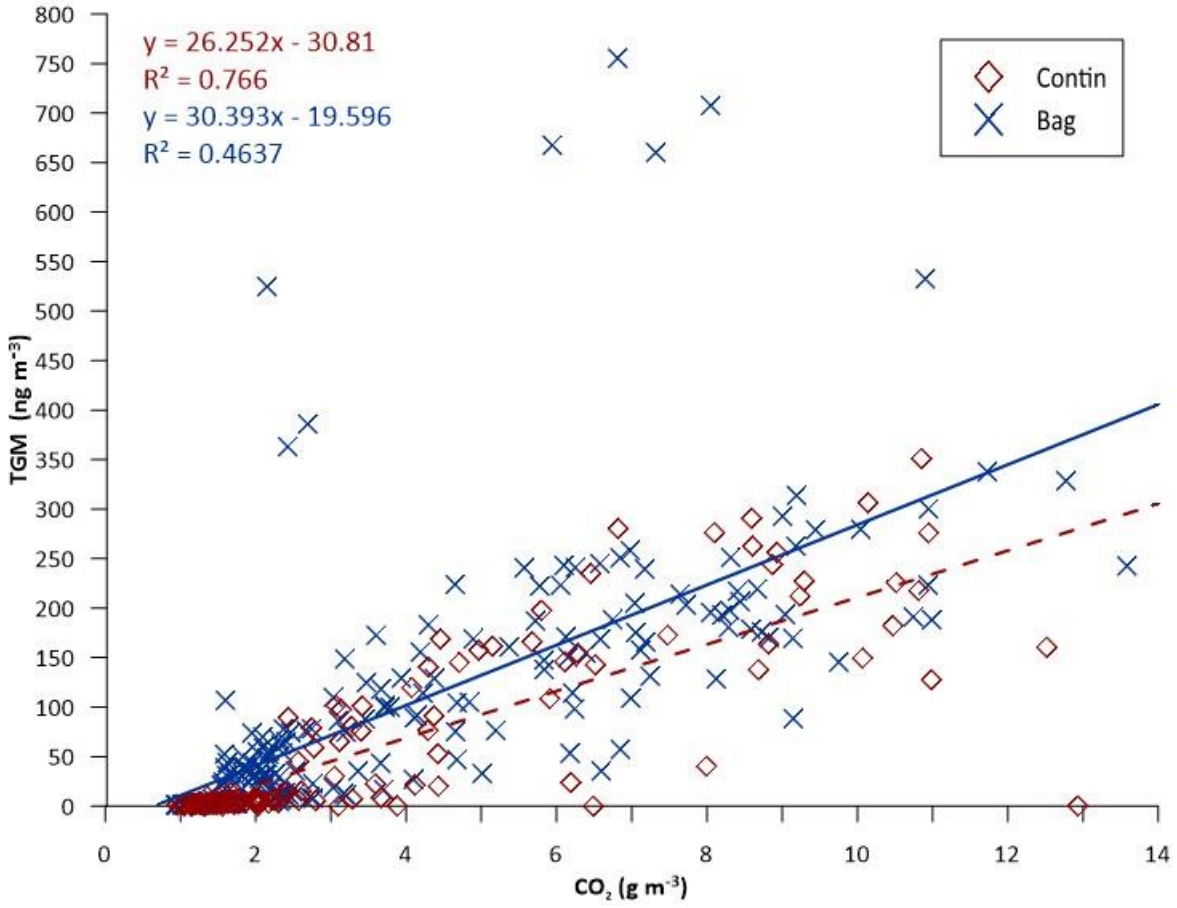

Figure 99: Emission ratio plot for TGM and CO_2 for all samples measured for continuous and bag methods

EFs were calculated for each fuel load and method using the CO_2 ERs shown in Figure 97 and equations described in appendix D (Table 28) *(Andreae and Merlet 2001)*. An EF for the backing burns was also calculated using the bag data (Table 28). An average EF for all burns was found to be 58.1 µg kg^{-1} for the continuous data and 76.7 µg kg^{-1} for bag data. These EFs are in agreement with current published emission factors for temperate forests. *Packham et al. (2009)* calculated EF for Australian vegetation to be between 59 and 290 µg kg^{-1}, while *(Friedli et al. 2003a)* estimated an EF of 112 µg kg^{-1}.

The EFs calculated here only consider Hg emitted from leaf litter and do not include emissions of Hg from soil and live vegetation. Soils have been found to contribute up to 20% Hg emitted during a fire and therefore need to be taken into consideration when calculating EF for prescribed and wild fires. Soil was not included in the fuel loads for the Pyrotron experiment and despite multiple attempts throughout the length of the study no monitoring was conducted at prescribed burns. Therefore, the influence of soil emissions on the EF for Australian forests could not be quantified.

Table 28: Hg emission factors for each fuel load undertaken during the pyrotron experiment.

	Continuous tekran data (µg kg^{-1})	Bag samples (µg kg^{-1})
0 t/ha CWD (Control)	92.7	80.0
2 t/ha CWD	72.7	86.2
6 t/ha CWD	54.1	79.7
12 t/ha CWD	43.9	64.0
Average heading	58.1	76.7
Average backing		62.7

EF for each load appears to decrease with increasing coarse material. This is further evidence that fine fuels contain the majority of Hg released during fires. Both bags and continuous method EF show the same trend. The decrease in EF with fuel load is likely caused by the increase in coarse material with each fuel load, which contains smaller concentrations of Hg than found in the fine fuels. The aim of prescribed burning is to reduce the fuel load available to burn during a fire, reducing the likelihood of a wildfire occurring or reducing the severity of the fire if one were to occur. As a result, it is dominantly the fine fuel that is burnt sufficiently to release Hg while the fire severity is insufficient to volatilise Hg from the soil (only a small portion will be emitted). Therefore, the EFs calculated here are likely to be good indicators of the Hg emissions likely to be seen during a prescribed burn.

The frequency of burns in the area will influence Hg emissions, as nearly all the Hg stored within the leaf litter is emitted when burnt. Hg takes a long time to re-accumulate back into an ecosystem. Therefore, regular prescribed burns could in the long term reduce the amount of Hg in an ecosystem. However, as Hg is unable to be destroyed it raises questions of how redistribution may impact ecosystems and human population through short term increased atmospheric concentrations and ecosystem redistribution.

Firefighter exposure to mercury during prescribed burns

Firefighters attending prescribed or wildfires are potentially at risk of exposure to the Hg released into the smoke plume. Elemental mercury vapour (Hg^0) is the dominant species emitted within the smoke plume and can pose severe health risk if inhaled in high enough levels. This is an area that has received little attention when considering Hg emitted during a fire. In an attempt to quantify the potential risk to firefighters while attending a fire personal CO monitors were attached to firefighters attending prescribed burns across Australia. These monitors were used as proxies to calculate potential Hg exposure. Hg exposure was estimated from an assumed MCE of 0.92 for front of fire and 0.85 for fire boundaries, during a prescribed burn. These values were used to calculate the potential exposure to CO (from the personal exposure monitors) plus CO_2. $CO+CO_2$ and a Hg emission factor of 31.7 µg kg^{-1} was then used to determine potential Hg firefighter exposure (Table 29). Three concentrations are given; one-hour average Hg concentration, 15-minute peak concentrations and peak concentrations over the entirety of the fire.

Current Work Safe Australia standards for occupational exposure to Hg0 vapour is 25,000 ng m^{-3} (based on a weighted average exposure over 8hours for a 5-day working week) (Safe Work Australia, 2013). This is considerably higher than the World Health Organisations (WHO) exposure threshold of 1000 ng m^{-3} for ambient annual atmospheric concentrations of Hg0. Chronic exposure to Hg0 cause kidney failure and decreased immune system, with damage to the renal system starting to occur at 15,000 ng m^{-3} over the course of a year. It also has the ability to cross the blood brain barrier where it can remain present for up to 20 years, damaging the nervous system and causing severe neurological damage *(Park and Zheng 2012)*. Visible signs of neurological damage, such as tremors, can start to occur at exposures of 30,000 ng m^{-3} within 1 year *(WHO 2000)*.

Table 29: Gaseous elemental mercury exposure standards.

	Exposure standard	
Work safe Aust.	25,000 ng/m3	8hr 5day working week
NSW health	200 ng/m3	Daily
WHO (annual ambient average)	1,000ng/m3	Annual
symptoms	10,000-30,000ng/m3	Annual
Damage Renal system	15-30,000 ng/m3	Annual
Neurological damage	30,000ng/m3	annual

Overall hourly average concentrations were consistently low, ranging from 0.8 to 116 ng m^{-3} with an overall average of 8 ng m^{-3}. These values are well below the WHO standard for the inhalation of elemental mercury of 1000 ng m^{-3}. Peak Hg concentrations were at times significantly higher than the calculated 1 hourly averages, reaching a maximum of 683.4 ng m^{-3}, with an average of 143.6 ng m^{-3}. These peak values are still below both the Work Safe Australia standards and WHO exposure standards. This indicates that while over the entirety of the fires Hg concentrations are comparatively low spikes in Hg occur that could be putting firefighters at risk. As 80% of the Hg inhaled is absorbed into

the lungs where it is then transported around the body these peak values have the potential to pose significant health risks.

The cumulative impacts of Hg exposure levels need to be taken into consideration. On average 600 wildfires occur a year and an average 150,000 ha of area burnt for prescribed burns in Victoria alone *(ABS 2004)* and firefighters are like to attend a high number of these fires over a short period of time. Hg has a biological half-life between 30 and 60 days which could mean that every time fire fighters attend a fire during this time period they could be compounding the concentrations of Hg within their bodies. Hg is one of many harmful toxins that firefighters are exposed to when attending a fire. While Hg concentrations posed here are not enough to put firefighters at immediate danger of Hg poisoning, these concentrations are still adding to the other toxins they are exposed to, reducing their overall health.

No comprehensive studies have been undertaken to date that looks at identifying exposure of firefighters to Hg while attending fires. The preliminary study undertaken as part of this report suggests that firefighters could potentially be at risk of Hg exposure both from spikes in Hg concentrations during a fire and the possible cumulative effects over the course of a fire season. More work needs to be undertaken to explore this potential health hazard through the use of personal Hg monitors in place of the CO monitors and measurements of Hg concentrations in the body over the course of a fire season.

Table 30: Fire fighter exposure to mercury during prescribed burns. Exposures calculated using the CO/Hg ERs from Pyrotron data and CO exposure measure personal monitors on firefighters in the field at prescribed burns. Hg Exposures were calculated for Peak CO values over the duration of a fire, 1-hour average CO exposure and peak CO exposure every 15 minutes.

Fire location	Monitor	Peak CO (ppm)	Peak 15-min CO (ppm)	Avg hour CO (ppm)	Hg exposure peak (ng/m3)	Hg 15 min peak (ng/m3)	Hg average (ng/m3)
Abaroo Creek - Day 1, NSW	1	310	23.33	1.75	301.3	22.7	1.7
	2	466	53.25	4.32	453.0	51.8	4.2
	3	137	9.67	2.03	133.2	9.4	2.0
	4	96	19.47	2.06	93.3	18.9	2.0
Abaroo Creek - Day 2, NSW	1	230	20.07	4.96	223.6	19.5	4.8
	2	212	15.00	3.25	206.1	14.6	3.2
	3	229	110.00	5.33	222.6	106.9	5.2
	4	125	15.90	2.96	121.5	15.5	2.9
Gulguer Plateau, NSW	1	143	11.80	2.99	139.0	11.5	2.9
	2	638	29.27	9.17	620.2	28.4	8.9
	3	127	13.47	3.09	123.5	13.1	3.0
	4	113	13.75	2.83	109.8	13.4	2.8
Lugarno South, NSW	1	703	197.27	16.64	683.4	191.8	16.2
	2	401	27.07	2.37	389.8	26.3	2.3
	3	459	42.50	5.81	446.2	41.3	5.6

	4	436	39.91	5.36	423.8	38.8	5.2
Pecky's, NSW	1	414	41.00	7.28	402.4	39.9	7.1
	2	190	19.27	5.01	184.7	18.7	4.9
	3	296	125.00	3.98	287.7	121.5	3.9
	4	238	14.07	3.71	231.3	13.7	3.6
Yeramba, NSW	1	123	17.33	5.96	119.6	16.8	5.8
	2	37	14.00	4.10	36.0	13.6	4.0
	3	42	9.53	3.50	40.8	9.3	3.4
	4	195	23.25	5.57	189.5	22.6	5.4
Wyeebo FRB VIC	1	338	45.60	14.30	328.6	44.3	13.9
	2	272	37.50	10.60	264.4	36.5	10.3
Ferny Creek FRB VIC	1	26	3.70	0.83	25.3	3.6	0.8
	2	7	1.10	0.18	6.5	1.1	0.2
	3	74	6.10	1.13	71.9	5.9	1.1
	4	71	8.80	1.77	69.0	8.6	1.7
	5	134	39.20	20.20	130.3	38.1	19.6
	6	148	25.10	14.90	143.9	24.4	14.5
Deer Park FRB VIC	1	82	13.80	4.38	79.7	13.4	4.3
	2	97	13.30	4.54	94.3	12.9	4.4
	3	87	19.70	3.23	84.6	19.1	3.1
Ngarkat FRB SA	1	316	146.00	47.70	307.2	141.9	46.4
	2	213	102.00	25.60	207.0	99.1	24.9
NT Wildlife Park	1	89	55.10	13.35	86.5	53.6	13.0
	2	122	19.60	7.39	118.6	19.1	7.2
	3	112	26.30	8.55	108.9	25.6	8.3
Mt Robertson FRB VIC	1	143	51.20	15.90	139.0	49.8	15.5
	2	210	74.00	15.80	204.1	71.9	15.4
	3	41	11.60	2.49	39.9	11.3	2.4
	4	180	51.00	8.10	175.0	49.6	7.9
Ngarkat Exp SA	1	93	39.40	7.80	90.4	38.3	7.6
	2	63	25.20	13.90	61.4	24.5	13.5
Buttongrass FRB TAS	1	7	2.00	0.30	7.0	1.9	0.3
	2	16	2.80	0.55	15.8	2.7	0.5
	3	26	4.00	0.79	25.6	3.9	0.8
	4	32	4.90	0.71	31.4	4.8	0.7

Gembrook FRB VIC	1	82	17.10	1.91	79.7	16.6	1.9
	2	211	27.10	1.74	205.1	26.3	1.7
	3	61	6.00	1.57	59.3	5.8	1.5
	4	38	7.50	1.28	37.2	7.3	1.2
Kyeema FRB VIC	1	597	295.00	68.20	580.3	286.8	66.3
	2	629	307.00	69.80	611.4	298.4	67.8
	3	554	299.00	120.00	538.5	290.6	116.6
	4	562	304.00	60.30	546.3	295.5	58.6
Langwarrin FRB VIC	1	146	54.80	13.20	141.9	53.3	12.8
	2	46	25.10	6.15	44.7	24.4	6.0
	3	217	82.00	22.20	210.9	79.7	21.6
	4	52	22.40	6.60	50.7	21.8	6.4
	5	132	39.60	5.25	128.3	38.5	5.1
Healesville FRB VIC	1	40	5.90	0.40	39.1	5.7	0.4
	2	105	49.70	4.77	102.1	48.3	4.6
	3	22	10.40	1.65	21.4	10.1	1.6
	4	331	30.00	2.89	321.7	29.2	2.8
Maroom FRB QLD	1	33	5.30	0.86	32.1	5.2	0.8
	2	46	9.40	2.39	44.7	9.1	2.3
	3	580	57.00	8.36	563.8	55.4	8.1
	4	63	5.30	0.43	61.2	5.2	0.4
Wallum FRB QLD	1	523	97.00	21.00	508.4	94.3	20.4
	2	116	26.20	3.80	112.8	25.5	3.7
	3	165	33.00	7.25	160.4	32.1	7.0
	4	102	42.00	9.36	99.1	40.8	9.1
Merribup FRB1 WA	1	64	27.60	4.96	61.7	26.8	4.8
	2	153	34.50	11.40	148.7	33.5	11.1
	3	68	30.90	4.33	66.1	30.0	4.2
	4	38	13.50	2.03	36.9	13.1	2.0
	5	204	68.30	11.80	198.3	66.4	11.5
Merribup FRB2 WA	1	90	40.60	7.89	87.7	39.5	7.7
	2	164	65.40	9.82	159.4	63.6	9.5
	3	88	33.80	5.11	85.5	32.9	5.0

Merribup FRB3 WA	1	97	14.90	1.99	94.5	14.5	1.9
	2	90	26.80	4.23	87.7	26.1	4.1
Challar FRB WA	1	118	46.80	18.00	114.7	45.5	17.5
	2	65	29.20	10.30	62.7	28.4	10.0
	3	74	21.10	4.84	71.9	20.5	4.7
	4	60	20.80	4.89	58.6	20.2	4.8
	5	97	48.20	10.20	94.6	46.9	9.9
Chrysties SB VIC	1	6	1.20	0.18	2.7	0.5	0.1
	2	9	1.58	0.21	4.0	0.7	0.1
	3	19	3.10	0.43	8.3	1.3	0.2
	4	25	2.50	0.55	10.8	1.1	0.2
Toolangi SB VIC	1	32	7.00	2.89	14.0	3.0	1.2
	2	25	6.70	3.18	10.9	2.9	1.4
TAS HB	1	23	12.50	2.82	10.0	5.4	1.2
	2	23	12.80	2.44	9.9	5.5	1.1
	3	22	11.70	2.52	9.6	5.1	1.1
	4	28	13.40	4.74	12.2	5.8	2.0
Pine SB VIC	1	54	16.20	3.36	23.2	7.0	1.5
	2	167	51.00	4.84	72.1	22.0	2.1
	3	179	80.00	5.45	77.3	34.6	2.4
	4	73	27.50	4.98	31.5	11.9	2.2
	5	299	31.00	5.39	129.2	13.4	2.3
	6	142	24.10	2.64	61.3	10.4	1.1
	7	30	5.80	1.28	13.0	2.5	0.6
	8	108	24.70	3.88	46.7	10.7	1.7
	9	26	4.90	1.17	11.4	2.1	0.5
	10	41	5.70	1.13	17.6	2.5	0.5
	11	8	3.10	0.87	3.6	1.3	0.4
	12	54	6.50	1.36	23.2	2.8	0.6
Bells Creek SB QLD	1	44	16.80	6.88	18.8	7.3	3.0
	2	31	14.70	6.03	13.4	6.4	2.6
				Average	**143.6**	**36.4**	**8.0**

Population exposure to mercury emitted during fires

Populations are at risk on a local to regional scale from wet and dry deposition, mainly through fallout during rainfall, and on a global scale from dry deposition. To investigate potential population exposure a case study of the Tasmanian January 2016 bushfires was chosen. This large-scale fire event started from 13 separate fires, all ignited from lighting strikes in unusually dry vegetation, which then quickly spread to burn 72,000 Ha over a 6-week period. These were one of the largest and most ecologically damaging fires to occur in Tasmania in recent history *(Marris 2016)*. The impacts to air quality from the smoke plume not only impact much of Tasmania but also travelled across the Tasman Sea, causing significant air quality problems in Melbourne and across Victoria.

Hg emissions were modelled for the January 2016 Tasmanian fire event using the CSIRO CTM and an Hg emission factor of 58.1 µg kg^{-1} (Table 28, all fires continuous data). Model parameters were adjusted to incorporate the mechanisms and chemistry specific to Hg in the atmosphere *(Nelson et al. 2012)*. Model simulations were run from the start of the fire event (13th January 2016) until the end of January. Average Hg emissions over the entire modelled period are displayed in Figure 100. The fire event continued into February however the model was not run for the entire length. The overall average Hg emissions for the entire modelled fire event was 0.188 ng m^{-3} with a maximum Hg concentration of 7.32 ng m^{-3} occurring at the centre of the main fire.

The Hg emitted during the fire is quickly dispersed into the atmosphere and concentrations significantly reduced with distance from the fire. The direction of the smoke plume and consequent Hg emissions followed the same direction as the prevailing winds for that day. Therefore, proximity and prevailing winds were the dominant controls of potential population exposure. The Hg emissions for this fire event were established using EF calculated form the pyrotron experiment and therefore only considered the emissions from leaf litter. The severity and duration of the Tasmanian fires would have produced higher emissions than shown here as there would also have been contributions from the soil.

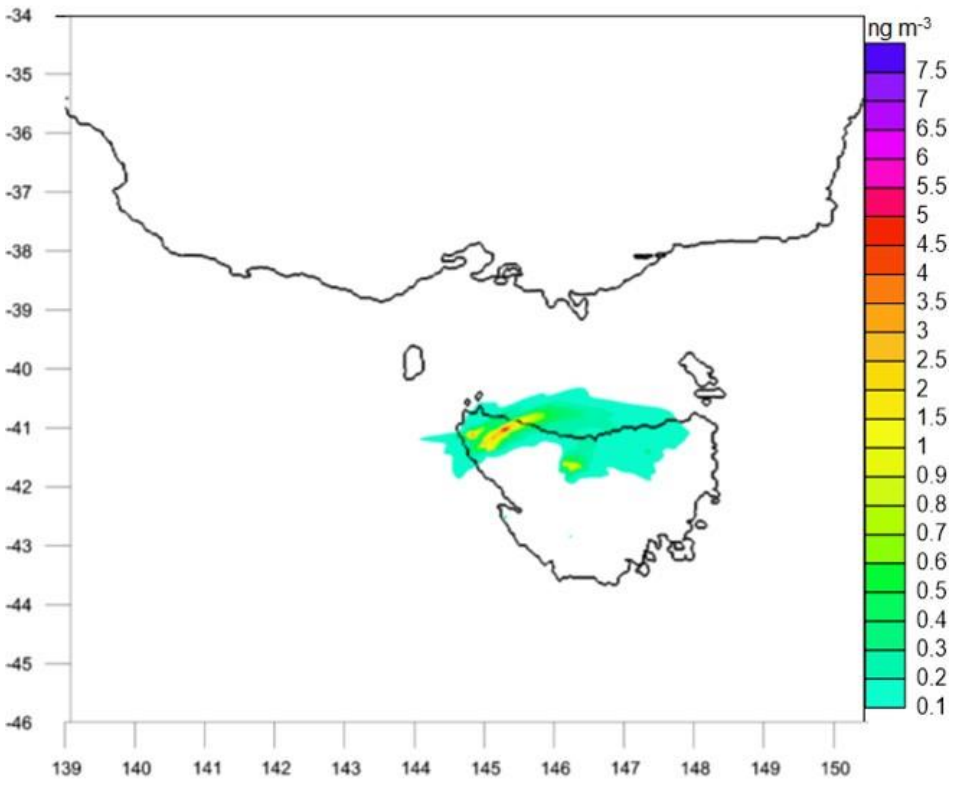

Figure 100 Average Hg concentrations from January 2016 Tasmanian fire event. Concentrations are presented for four days during the event modelled using the CTM

The concentrations observed in Figure 100 are all well below the WHO Hg atmospheric threshold of 1 µg m^{-3} and decrease rapidly with distance from the source. The low concentrations indicate that as a whole the populations close to the fires are not in immediate risk of exposure to Hg. However, these concentrations will add to those atmospheric concentrations that are already present in the region. Urban regions typically have much higher concentrations than rural regions. As the smoke plume propagates it will add to the atmospheric Hg concentrations, increasing the amount available to be inhaled by the population. This is of particular concern if the fires were to occur near an urban region or if the prevailing wind propagates the smoke plume into urban regions as seen for the Tasmanian fire event.

The Lancefield fire in Victoria was a moderate intensity fire which initially started as a prescribed burn which broke containment lines. The fire burnt for 10 days during October 2015 and burnt over 3000 hectares of bush. The Lancefield fire was located approximately 60 km north of Melbourne's CBD and as can be seen in Figure 101 the smoke plumed covered most of this heavily populated region. A maximum concentration of 0.00125 ng m^{-3} was estimated significantly lower than the Tasmanian fire concentrations and the WHO Hg thresholds. The Lancefield fire only burnt for a week over a comparatively small area compared to the Tasmanian fire. The majority of emissions were transported out to the ocean.

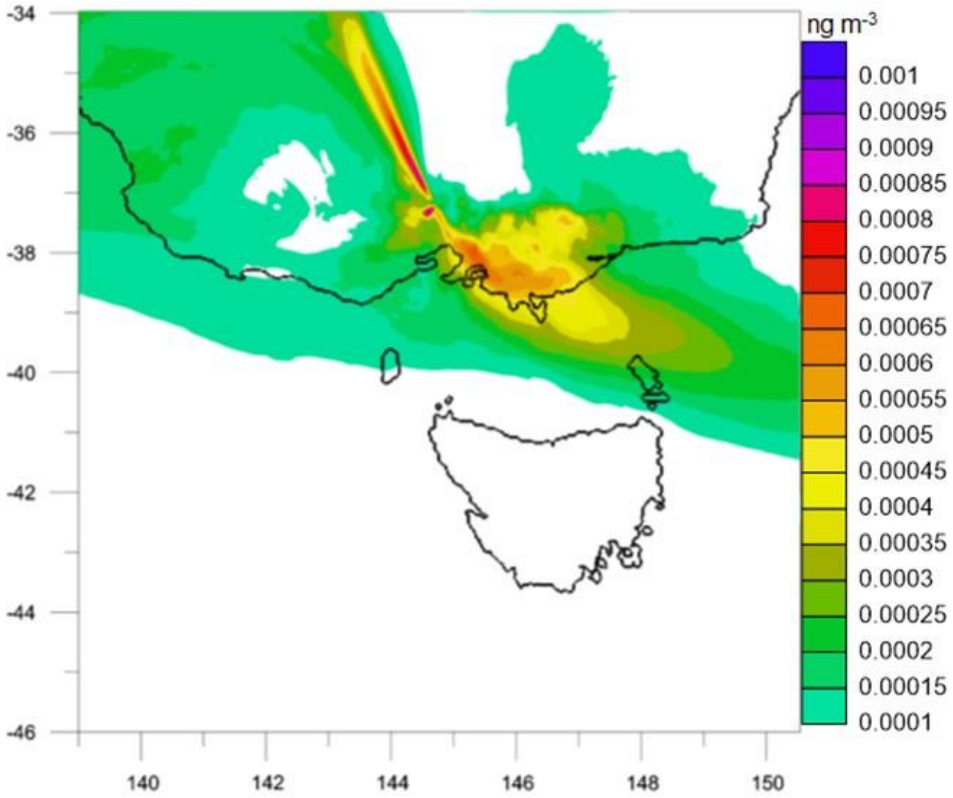

Figure 101. Lancefield October 2015 bushfire. Figure shows the average emissions across the duration of the fire.

The Tasmanian fire event was a high severity fire of long duration. It is therefore likely that the smoke plume created during the event was lofted above the planetary boundary layer and into the higher troposphere, where Hg becomes more resistant to both wet and dry deposition, travelling greater distances *(De Simone et al. 2016)*. The concentrations that reach above the boundary layer are dependent on how soon rainfall occurs after the fire and the atmospheric conditions at the time of emission. Given the long atmospheric lifetime of Hg once it reaches the upper troposphere it is most likely that deposition will occur over the oceans, to become part of the long-term Hg sinks. The rainfall that often occurs shortly after large scale fires will likely scavenge some portion of the Hg emitted in the smoke plume before it reaches the upper troposphere, leading to local deposition.

Fire intensity of the Lancefield fire likely means that the plume did not reach above the boundary layer. Therefore, emitted mercury is more likely to be trapped in the boundary layer, which is more conducive to local deposition. Emissions from low to moderate burns such as the Lancefield fire and prescribed burns are more likely to be trapped within the planetary boundary layer where they are more likely to undergo wet and dry deposition process, with deposition more likely to occur on local to regional scales *(Friedli et al. 2003b)*. However, more is needed to be known about Hg transport in the smoke plume to gain a better understanding of potential population exposure.

Release of Hg from an ecosystem during a fire can have inadvertent effects on population. Fire has the added effect of mobilising historically stored Hg. In the case of the Tasmanian fire event a large portion of the area contained large carbon sinks *(Marris 2016)*. These types of ecosystems are also commonly a store of legacy Hg. This newly mobilised Hg is then available to be redistributed to other environments through surface runoff and atmospheric deposition. This increases the likelihood of Hg being transformed by bacteria into methyl mercury (MeHg). MeHg is the most toxic form of Hg and the most common way populations are exposed. MeHg biomagnifies up the food chain, with concentrations highest in those organisms at the top of the food chain, such as fish and shellfish *(Park and Zheng 2012)*. The atmospheric concentrations from the Tasmanian fire event do not pose a direct effect to populations. However, indirect exposure caused by the redistribution and methylation of Hg could pose just as significant risk as directly inhaling high emissions from a smoke plume.

Hg species emitted during the fire event were not modelled, however, speciation will influence transportation and depositon. The majority of Hg emitted during a fire is in the form of Hg^0, however between 10% and 30% is in the form of particulate Hg (pHg) *(De Simone et al. 2016)*. PHg is readily scavenged from the atmosphere by cloud water droplets, where it is more likely to be deposited on a local to regional scale, regardless of fire severity, where it is then able to be redistributed in the ecosystem to local rivers and waterways. Once in the waterways pHg can undergo methylation to become the highly toxic methylmercury and biomagnify up the food chain. Emissions of PHg are dependent upon the fuel type, fuel moisture content, and the type of combustion. This makes modelling the rates of emissions during a fire difficult to determine *(Obrist et al. 2008)*. However, given its propensity for local deposition and quick redistribution in an ecosystem further investigation into emissions of pHg during a fire is important when considering population exposure.

Summary and Conclusions

There is a complex interplay of factors that influence Hg emissions during a fire and the subsequent human exposure. Hg emissions from Australian fires have received little attention. In order to rectify this Hg measurements were collected during the CSIRO Pyrotron experiment to gain a better understanding of Hg emitted from leaf litter under prescribed burn conditions. This data was then used to calculate ERs and EFs in the hope of better understanding Australia's contributions to the global Hg budget and identify potential Hg exposure for firefighters and populations.

An average EF of 58.1 µg kg^{-1} (continuous method) and 76.7 µg kg^{-1} (bag method) was estimated for the Pyrotron experiment with an ER of 26.25 Hg/CO_2 continuous (30.39 Hg/CO_2, Bag method).

We were unable to attend a prescribed burn to gather measurements of Hg in the field due to logistical difficulties. As such all measurements presented here are heavily reliant on the CSIRO Pyrotron burn experiment. Attending an actual fire would have allowed insight into how soils and live vegetation influence the overall EFs in Australia and determine the reliability of the EFs calculated here. More research is also needed to be undertaken to determine how different fire types influence emission rates, e.g. prescribed burns compared to wildfires.

Hg EF and personal CO monitors were used to determine potential firefighter exposure. An average hourly exposure of 8.0 ng m^{-3} with a max peak value of 683.4 ng m^{-3} was calculated. These values were considerably lower than safe work Australia exposure standards. However, consideration needs to be given to the cumulative impacts of attending multiple fires with similar or high exposures over a short period of time.

An average of 0.188 ng m^{-3} of Hg was emitted over the course of the January 2016 Tasmanian fires and 0.00125 ng m^{-3} during the October 2015 Lancefield fire. Population exposure was contained primarily to those in closest proximity to the fire source. However, even these values were considerably

lower than WHO ambient thresholds. Populations are mostly at risk from indirect exposure caused by the redistribution of mobilised Hg and methylation within the environments.

The preliminary research undertaken here indicates that more research needs to be undertaken looking into potential human health risks associated with Hg emissions. Very little work currently exists looking into firefighter exposure while attending a fire. Direct measurements of Hg exposure would allow for a clear understanding of exposure levels and help mitigate the potential health risks to fire fighters.

Appendix F: Fire Radiative Power

A review of the current techniques and applications of fire radiative power for determining fire intensity and fuel consumption rates for possible application to Australian temperate forest fuels.

Introduction

Bushfires are an important disturbance agent of the terrestrial biosphere, and represent a ubiquitous, highly variable emission source for many key greenhouse gases, air pollutants, and aerosols. By voraciously consuming biomass, releasing intense heat energy, and emitting thick plumes of smoke into the atmosphere, such large-scale fires exert several adverse effects on life, property, the environment, weather, and climate both directly and indirectly. Bushfires have a range of environmental effects at both the local and regional scale. For example, at the local scale, the reproductive biology of fire prone species is related to the level of fire activity and smoke emissions, which is a trigger for flowering or seed release *(Enright et al. 1997)*. However, it must be noted that altered fire activity (e.g. introduction of high intensity fires) is also linked to the extinction of plant populations in certain landscapes *(Keith 1996)*. Over larger temporal and spatial scales, bushfires have the potential to affect the ecological stoichiometry by altering energy and matter, thereby causing complex burn patterns and interval times *(Turner et al. 1994)*. Furthermore, regional scale burning regimes, such as that witnessed in the 1997/98 Indonesian fires, and the 2010 Russian fires exposed millions of people to hazardous air pollution. At the global scale, it is recognised that aerosols produced from bushfire emissions have significant effects on the Earth's energy budget, rainfall and atmospheric chemistry *(Rosenfeld 1999)*. Additionally, an estimation of carbon emissions from forest fire is critical, especially the need to quantify for countries that have ratified the Kyoto protocol. For these reasons, there is a pressing need to make correct assessments of fire behaviour and its impacts over a range of scientific and policy disciplines that include greenhouse gas accounting, air pollution monitoring and assessment of fire behaviour and fire warning systems.

A common measure used to assess the amount of energy released during the combustion process is fireline intensity along the fire front. Fireline intensity is defined as the product of the heat yield of the fuel (H), the weight of standing fine fuel consumed in the flaming zone (w), and the rate of forward spread of the fire line or perimeter (r) *(Byram 1959)*. It is possibly the most valuable quantitative descriptor of any fire. However, despite its importance, accurate quantification of bushfire intensity is extremely problematic. Fireline intensity uncertainties are based on the estimate of spread rate, fuel load and combustion efficiency. Defining and quantifying fireline intensity is particularly difficult for complex burn patterns that may result, for example, from multiple ignition points. These patterns can lead to stationary fires with mass fire behaviour *(McRae and Flannigan 1990)* and are characterised by significant heat release and extreme turbulence for which the concept of a moving flame front is not applicable. Additionally, bushfire events that are characterised by medium to long range ember spotting may have multiple firelines. For these reasons, assessment of the total fire energy released from bushfire by using mapped fire isochrones is somewhat unreliable over short (minutes) temporal scales.

While field studies of bushfire dynamics provide the foundation for fire sciences, remote sensing has a critical role by allowing field data to be integrated over larger spatial areas. Remote sensing provides the only practical means of measuring a large range of fire characteristics in open-air biomass burning globally and represents an indispensable tool to monitor fires safely and to provide locational and category information in near real time. Recent progress in remote sensing has allowed the development of a product that measures fire

radiative energy (FRE) and fire radiative power (FRP) (*Wooster et al. (2005)*, which have equivalent units to fireline intensity and fire power. The main difference in definition between fireline intensity as defined by *(Byram 1959)* and that defined by *Wooster et al. (2005)* is that Byram's definition only accounts for the intensity at the flame front depth whereas Wooster's definition is integrated over the different phases of combustion (i.e. flaming, smouldering and glowing).

Fire observation has rarely been a primary mission objective for the design of satellite instruments, (until recently with Landsat-8 and Sentinel-3). As a consequence, almost all sensors that can be used for fire detection and fire characterisation suffer from instrument saturation effects, relatively limited spatial and/or temporal resolution, and other limiting factors. Specifically, the temporal sampling from low earth orbit instruments is often inadequate for capturing the high temporal variability of fire occurrence and fire characteristics, and for fully resolving the fire diurnal cycle (which is known to be extreme in some areas). To date, FRE measurements have been derived from coarse-scale satellite data, and almost no fine-scale (airplane-retrieved or in-situ tower sensors) measurements have been used to augment this information on critical bushfire characteristics. Neither has there been any systematic study conducted on understanding the extent of which the environmental factors control FRE. Furthermore, FRE has rarely been validated with fuel combustion rates outside of laboratory conditions where fuel continuity or forest canopy effects are not an issue. A better representation of these factors to FRE using field experiments will allow fire managers to better quantify the intensity characteristics of both prescribed and bush fires.

If FRE is to be used globally with certainty, it is critical that a validation program be built around accurate relationships between combustion rates and FRE over a number of different vegetation and fuel types and fire intensities. Of critical importance is that such techniques be tested on moving fire fronts to investigate the different phases of combustion.

This literature review precedes an observational campaign that will examine and evaluate measurement of FRE in the southeast Australian context. Critical FRE data retrieved in this project will also contribute towards better modelling of event-driven bushfire systems. PHOENIX Rapidfire is a software-based fire simulation model that calculates the potential fire spread across the landscape under different weather conditions *(Tolhurst et al. 2008)*. The simulations are able to provide spatial information at high resolution on the fire spread rate, flame height, fire intensity and ember production. Although the model does a reasonable job at predicting fire boundaries, the model has not been adequately validated, especially in terms of how fire progression and fire intensity is affected by ember production.

This synthesis project will attempt to simultaneously address problems related to scale in both temporal and spatial resolution. We plan to make in-situ measurements and validation of fire intensity and fire power and relate that to remotely sensed FRE by plane and satellite. Further validating and developing the FRE approach has the potential to be a key data resource in accurately estimating fire severity in real time and in estimating biomass burning emissions.

In associated but separate work, we have also been evaluating relationships between climate variables (especially soil moisture), fire occurrence and FRP that has excellent potential for reformulation of forest and grassland fire danger indices. This work is described later in this report.

The ability to use remotely sensed data to measure the rate and total amount of energy emitted by bushfires offers a route into observing fire intensity variations over space and time in (near) real-time, and since the emitted energy results from oxidation of fuel carbon, such data can be used to directly estimate pyrogenic C fluxes and, via the application of the relevant emission factors, the fluxes of the other trace gas and aerosol species that result from those related processes. Such a technique for measuring the fire radiative power (FRP, Watts) was initially proposed by *Kaufmann et al. (1996)*, whilst *Roberts et al. (2005)* have successfully demonstrated the functionality of the method in African savanna ecosystems. In parallel with these developments *Wooster and Zhang (2004)* used an FRP approach to show the relative importance of fires in the boreal ecosystem. However, there are methodological challenges to using the technique in a fully quantitative manner, rather than simply for analysing relative differences, and a number of underlying science issues remain before the methodology can be routinely and confidently applied. By combining satellite and aircraft remote sensing techniques with surface-based observations

this project plans to address these issues using a relatively small-scale field experiments and will then assess if the methodology can be applied to the estimation of emissions from landscape-scale fires across relevant ecosystems of southeast Australia.

As a first step this literature review will explain the current techniques and applications of fire radiative power for determining fire intensity and fuel consumption rates for Australian temperate forest fuels. As mentioned above, it also describes other ongoing work that evaluates relationships between a range of climate variables and FRP that might see further application in fire science and management in southeast Australia.

Quantifying Emissions from Bushfires using Remotely Sensed Data (Pre FRP)

During bushfire events, the concentration of pyrogenic emissions rises directly with the amount of biomass consumed *(Delmas et al. 1995)*. There is some lesser dependence upon the degree of smouldering and flaming combustion *(Kaufman et al. 1990; Kaufmann et al. 1996)*, but nevertheless, most emissions inventories ignore this to a large extent and are most commonly simply derived simply from estimates of the amount of biomass combusted, *M*. This measure of *M* is typically driven by remotely sensed measurements of burned area (e.g. *Hao et al. (1996)* and *Scholes et al. (1996)*, derived through identifying the albedo or surface reflectance change that results from burning [reflectance]. The burned area maps are most commonly used in the equation of *Seiler and Crutzen (1980)*:

$$M = A \times B \times C \qquad (1);$$

where, *A* is the burned area (km2), B is fuel load (kg/km2), C the fraction of available fuel burned (combustion completeness), and *M* the estimated amount of dry fuel burned (kg) *Ellicott and Vermote (2012)*, which can be converted into an estimate of direct pyrogenic carbon release via multiplication by the fraction of volatile carbon contained in the fuel.

Application of the appropriate emissions factor for any particular trace gas or aerosol species allows the total mass of that particular plume constituent to be derived from the estimate of *M* provided by equation (1). The equation to then estimate emissions given the fuel consumed is:

$$E_x = EF_x \times M \qquad (2);$$

Where E_x is the emission load of species x (g); EF_x is the emission factor for species x for the specific vegetation type biome (g/kg) and *M* is the fuel burned in equation (1) *(Ellicott and Vermote 2012)*.

Unfortunately, whilst simple in form, (1) has proved problematic to parameterise in detail *(Barbosa et al. 1999; French et al. 2004)*, since knowledge of burned area is improving due to enhancements in the quality of satellite derived data sets and the burned area mapping algorithms that use them, the information on spatial and temporal observations of parameters B *and* C are not readily available, and model-based assessments have large uncertainties. The relationship between burned area and the amount of fuel combusted is strongly influenced by these uncertain fuel density combustion completeness factors, which cannot be quantified remotely. As *Barbosa et al. (1999)* illustrate, this makes current remotely-sensed emission estimates very imprecise, and results often disagree markedly with data from non-satellite earth observation sources. *Andreae and Merlet (2001)* demonstrated that for southern African savanna a comparison of estimates of total combusted biomass based on the current remotely sensed-driven approach and on historical fire-frequencies provide an order of magnitude difference. In addition *Roy et al. (2005)* found that there is a lack of agreement on the proper algorithm to characterise burned area from satellite data *(Ellicott and Vermote 2012)*. *Korontzi et al. (2004)* showed that significant differences between burned area algorithm estimates can lead to differences as large as a factor of two in estimate of biomass consumed *(Ellicott and Vermote 2012)*. *Andreae and Merlet (2001)* concluded that new tools are required to provide independent assessments of the amount of fuel combusted in vegetation fires. Improving this situation by combining observational data on spatial-temporal variations in fire extent AND fire severity was therefore considered an essential next step to improving pyrogenic emissions estimates *(GTOS 2000; Kasischke and Bruhwiler 2002; French et al. 2004)*.

Furthermore, even if under particularly stringent boundary conditions, the parameterisation of Equation (1) can be provided with sufficient accuracy, the informational outputs from such burned area mapping approaches are provided at time-scales largely inconsistent with the requirements of the atmospheric modelling community *(Moula et al. 1996; Andreae and Merlet 2001)* and are post-event. Detailed studies of the atmospheric transport and chemistry implications of

biomass burning require accurate, spatio-temporally resolved emissions data at scales appropriate to meso-meteorological models and the chemical species lifetime *(Cooke et al. 1996)*. This necessitates sub-daily sampling to capture the order of magnitude of diurnal variation characteristic of burning in savanna ecosystems *(Langaas 1993; Prins and Menzel 1994)*, particularly so when emission estimates are to be coupled with 3D atmospheric transport models to better determine their long-range consequences *(Wittenberg et al. 1998)*. Currently very little information is available on time scales more precise than weekly or monthly intervals.

Fire Radiative Power

Fire Radiative Power (FRP) is defined as a measure of the rate of radiant heat output from a fire *(Roberts and Wooster 2008)*. It has been demonstrated by *Wooster et al. (2005)* in small-scale experimental fires that the FRP is related to the rate at which fuel is being consumed. *Freeborn et al. (2008)* have shown how FRP is related to smoke emissions released. *Roberts and Wooster (2008)* explain that it is the direct result of the combustion process, whereby carbon-based fuel is oxidised to CO_2 (and other compounds) with the release of a certain heat yield. Therefore, measuring FRP and then integrating it over the whole fire provides an estimate of the total Fire Radiative Energy (FRE), which for bushfires should be approximately proportional to the total mass of fuel biomass consumed.

Vegetation fires can be thought of as the obverse of photosynthesis in which energy stored in biomass is released as heat *(Ellicott and Vermote 2012)*. Therefore, FRP is the rate of release of the radiative component of the fuel heat yield (higher FRP indicates a greater fuel consumption rate):

$$(C_6H_{10}O_5)_n + O_2 + \text{ignition temperature} \rightarrow H_2O + CO_2 + \text{heat yield} \quad (3)$$

The chain of events of reactions:

- Pre-heating of fuels ahead of the fire front and partial pyrolytic decomposition
- Ignition signifies the transfer from pre-heating to combustion in which exothermic reactions start, then a combination of flaming and smouldering combustion begins
- Flaming combustion occurs when flammable hydrocarbon gases released during pyrolysis are ignited with bushfires flaming combustion temperatures in the range of 800-1400 K *(Lobert and Warnatz 1993)*.
- Pyrolytic action involves the thermal decomposition of fuel resulting in the release of water, CO_2, and other combustible gases (e.g. CH_4) and particulate matter.
- The heat produced, often measured as heat yield (MJ/kg), is thermal energy transferred via conduction, convection, vapourisation, and radiation and provides a metric of the total potential energy released, if complete combustion of the fuel occurs *(Ellicott and Vermote 2012)*

Although other factors, including slope, fuel arrangement and wind speed influence actual heat yield in a fire event, *Stott (2000)* and *Whelan (1995)* explain that the theoretical values actually vary very little between fuel types *(Ellicott and Vermote 2012)*.

Using Stefan-Boltzmann's Law, the radiant component is emitted as electromagnetic waves travelling at the speed of light in all directions and is proportional to the absolute temperature of the fire (assumed to be a black body) raised to the fourth power *(Ellicott and Vermote 2012)*. The relationship between fire temperature and spectral radiance was shown to closely match the Stefan-Boltmann law (Radiance = σT^4) and therefore a simple equation incorporating the sample size, emissivity of the fire (with some assumptions needed), and Stefan's constant could provide the rate of fire radiative energy, or fire radiative power, emitted as shown in equation (4) *(Ellicott and Vermote 2012)*.

$$FRP = A_{sample}\ \varepsilon\sigma\Sigma A_n T_n^4 \quad (4)$$

Where A_{sample} is the total area of the satellite pixel (m^2), ε is the fire emissivity, σ is the Stefan Boltzman constant ($5.67 \times 10^{-8} J^{-1} m^{-2} K^{-4}$), A_n is the fractional area of the i^{th} thermal component, and T_n^4 is the temperature of the i^{th} thermal component (K).

Ellicott and Vermote (2012) explain that the foundation for using measurements of FRP is based on the fact that the rate of fuel consumed is proportional to the rate if FRE.

Kaufmann et al. (1996), *(1998)* suggested that estimates of fuel load combustion and emission rates could be made from satellite observations of the radiative energy liberated during fire events *(Ellicott and Vermote 2012)*. They hypothesised that the rate of emitted energy (i.e. FRP) and rate of fuel combusted are proportional to the fire size and fuel load (A and B respectively in equation 1) *(Ellicott and Vermote 2012)*. Therefore the rate of energy released is directly related to the rate of particulate matter and trace gas emissions *(Ellicott and Vermote 2012)*. Integrating FRP over the lifespan of the fire event provides the total fire radiative energy (FRE) released, which in turn is directly proportional to the total fire emissions *(Ellicott and Vermote 2012)*. It is the radiative component that is estimated from Earth observing satellite sensors, offering an alternative method to quantifying fuel consumed, and assuming an emission factor is known, it also offers the atmospheric emission load. The relative unknowns are the energy lost in convection and conduction.

The Development of FRE and FRP

The ability to use remotely sensed data to measure the rate and total amount of energy emitted by bushfires offers an opportunity to observe fire intensity variations over space and time. Moreover, the emitted energy is a function of the fuel carbon oxidation, and such data can be used to directly estimate pyrogenic C fluxes and, via the application of the relevant emission factors, the fluxes of the other trace gas and aerosol species that result from those processes. As mentioned earlier, such a technique for measuring the fire radiative power (FRP, Watts) was initially proposed by *Kaufmann et al. (1996)* and subsequently successfully demonstrated in African savanna and Siberian boreal ecosystems *(Wooster and Zhang 2004; Roberts et al. 2005)*.

A list is presented below in chronological order of the advancement in the development of FRP:

- The first study that demonstrated the potential application of FRP and FRE for estimating fuel combustion rates and aerosol loading was by *Kaufmann et al. (1996)* and *(1998)* in a study based in Brazil.

- *Wooster (2002)* used small scale experimental fires to investigate the relationship between FRP/FRE and fuel consumption

- Further work by *Wooster et al. (2003)* and *(2005)* provided additional evidence of the effectiveness of using instantaneous and total FRE measurements to estimate biomass consumed during a fire.

- *Wooster and Zhang (2004)* demonstrated the application of MODIS FRP observations by verifying the often-proposed hypothesis that North American boreal fires are generally more intense than Russian boreal fires

- *Ichoku and Kaufman (2005)* used MODIS FRP and aerosol products to derive near real-time rates of aerosol emissions at regional scales

- *Roberts et al. (2005)* showed the effectiveness of using geostationary satellite estimates of FRP from SEVIRI to quantify rates of fuel consumption and characterise the fire intensity daily cycle

- *Freeborn et al. (2008)* in a laboratory investigation of FRE and biomass fuel consumption found their results supported the *Wooster et al. (2005)* findings and strengthened the arguments for the application of satellite measurements of FRE

- *Ichoku et al. (2008)* in collaboration with *Freeborn et al. (2008)* used laboratory investigations to examine rates of and total FRE emitted and associated aerosol emissions. In both of these studies they found the relationship between energy emitted, fuels consumed, and trace gas and aerosol emissions demonstrated the efficacy of using FRE.

- Further work by *Ichoku et al. (2008)* provided MODIS-based continental scale examples of using FRP to reveal the regional distribution of fire intensity.

- *Roberts et al. (2005)* and *Roberts and Wooster (2008)* showed the application of high temporal satellite-based FRP measurements from the SEVIRI geostationary sensor to calculate FRE and estimate biomass combusted

- *Boschetti and Roy (2009)* demonstrated a novel fusion approach to derive FRE based on temporal interpolation of MODIS FRP across independently-derived burned area estimates based on northern Australia.

- *Freeborn et al. (2009)* synthesised MODIS and SEVIRI FRP as a means of cross-calibration of their respective estimates

- *Ellicott et al. (2009)* developed a technique to parameterise the temporal trajectory of FRP and calculate the integral (i.e. FRE) using MODIS. This was done to overcome the limitation of satellites in that the observations are instantaneous energy over some discrete length of time and space. The result of this project was a global FRE product from MODIS at 0.5º spatial and monthly temporal resolution, which currently spans from 2001-2010. However, this study found that more work needed to be done on fuels typical of different regions.

- *Vermote et al. (2009)* used the *Ellicott et al. (2009)* method to estimate organic and black carbon aerosol emitted from biomass burning.

- High resolution validation of the 2008 MODIS fire detection and FRP product was conducted by *Padilla et al. (2014)*. This used the Advanced Spaceborne Thermal Emission and Reflection Radiometer (ASTER; a 14-channel imaging radiometer) to validate 1-km Terra MODIS.

More recently studies have begun applying the FRP MODIS product to address fire related research questions. For example Williamson et al 2013 used FRP to compare and contrast the severity of fires and smoke plumes in two different regions of Australia. *Peterson et al. (2013)* determined the potential of FRP for application to smoke plume injection height. Another study by *Peterson and Wang (2013)* assessed the potential application of MODIS FRP for fire weather, in that the total FRP over the fire area divided by the fire area (therefore the flux of the total FRP over the fire area) is shown to have a statistically significant correlation with surface (10m) wind speed and temperature, especially for large fire pixel clusters. Other work (described below) undertaken at Monash University as part of a PhD by Mr Alex Holmes has established relationships between climate variables (soil moisture in particular), fire occurrence and FRP with the aim of improving the FFDI.

Current Remote Sensing Approaches for Calculating FRP and Their Limitations

Ellicott and Vermote (2012) explain that unfortunately sensors are unable to separate the spatially distinct components of the fire, potentially as small as millimetres, and the equations cannot distinguish between fractional areas of the entire fire that are often at different stages of the fire cycle and that often are much smaller than the pixel itself. For this reason, different methods have been tested and employed to overcome these limitations.

There are three methods commonly employed, the bi-spectral, MODIS and MIR radiance methods (as described by *Ellicott and Vermote (2012)*:

1. The bi-spectral method uses two distinct channels, usually at 4 and 11 μm, to provide the details about the fractional size and temperature of the sub-pixel fire components *(Dozier 1981; Giglio and Kendall 2001; Wooster et al. 2005)* but it was found to be plagued by potential errors due to channel mis-registration and point spread function (PSF) differences between channels *(Giglio and Kendall 2001; Ellicott and Vermote 2012)*. *Wooster et al. (2005)* suggest that the bi-spectral method is effective, but primarily for higher resolution sensors (i.e. <1 km).

2. The current method used aboard MODIS employs a single channel approach with fire and background components retrieved solely from the mid infrared (4 μm) channel (see Justice et al, 2002; *(Ellicott and Vermote 2012)*. The method was tested by *Kaufmann et al. (1996)*; *(1998)* using the MODIS Airborne Simulator (MAS) model simulations of fire mixed-temperature pixels in in-situ measurements *(Ellicott and Vermote 2012)*. Based on these simulated fires *Kaufman et al. (1998)* found that an empirical relationship exists between instantaneous FRE (i.e. FRP) and pixel brightness temperature measured in the MODIS MIR channel (4 μm). The result was a semi-empirical relationship that forms the basis for the current FRP algorithm (equation 5) used aboard MODIS *(Ellicott and Vermote 2012)*. These same authors also demonstrated the correlation between rates of smoke emission and the observed rate of energy released using airborne observations of MAS *(Kaufmann et al. 1996)*; *(1998)*.

$$FRP[MWkm^{-2}] = 4.34 \times 10^{-19}(T^{8}_{MIR} - T^{8}_{bg,MIR}) \quad (5)$$

Where FRP is the rate of radiative energy emitted per pixel (the MODIS 4μm channel has IFOV of 1km), $4.34x10^{-19}$[MW km^{-2} $Kelvin^{-8}$] is

the constant derived from the *Kaufman et al (1998)* simulations, T_{MIR}[Kelvin] is the radiative brightness temperature of the fire component, $T_{bg,MIR}$[Kelvin] is the neighbouring non-fire background component, and MIR refers to the middle infrared wavelength, typically 4µm.

3. The final method commonly employed was developed by *Wooster et al. (2003)* who showed that FRP could also be derived using satellite based middle infrared radiances and a simple power law to approximate Plank's law. The MIR radiance method is applicable for temperatures covering the range of a typical vegetation fire (600-1500K). This approach is similar to the MODIS method but uses spectral radiance difference rather than brightness temperature.

There are a number of other limitations to using remote sensing for calculation of FRP:

1. The influence of cloud and/or aerosol when present is a major problem. When these are present, much of what the satellite sees is the emissivity of the cloud/aerosol, not the surface. The question is then how to relate this to what is happening on the ground. One possible answer to this question is to use sensor platforms, such as aircraft, that are below the cloud/aerosol layer. A further issue could be an incomplete view of the fire from overhead because of tree canopy and over-storey effects.

2. Also, scale/resolution issues are a problem. While satellites such as Landsat or SPOT can provide very high-resolution data, they have temporal resolutions that are not appropriate. On the other hand, MTSAT and its geostationary equivalents have appropriate temporal resolution, but not the spatial resolution (better than 1km). We are unaware of any research that has tried to address these combined issues. Once again availability of more flexible sensor platforms such as aircraft to the relevant agencies, may be a solution.

3. Recently, *Schroeder et al. (2010)* provided a thorough analysis of FRP, temperature and fire area estimates from moderate resolution sensors. Their results showed that the location of fires within a pixel can be biased because of the sensor's spread function, leading to as much as 75% underestimation in FRP" *(Ellicott and Vermote 2012)*.

4. Furthermore, there is large difference in the fire detection sensitivity and the estimation of FRP between satellite overpasses, due to a large viewing angle dependence *(Maier et al. 2013)*. *Maier et al. (2013)* determined that there was decrease in sensitivity with increasing viewing angle. They also determined the minimum FRP needed for MODIS to accurately detect fires was 7.1 MW, 7.4 MW and 5.8 MW for day/night, day and night detections, respectively.

5. Through random sampling, generally, the MODIS-MCD45 burned area product had an estimated detection rate of only 48% of the total burned area. This was largely dependent on the biome type with the highest accuracies in Boreal forest as well as tropical and subtropical savannah *(Padilla et al. 2014)*.

6. Another limitation has been thought to be the assumption that a single combustion factor is applicable for all fuel types and conditions (i.e. moisture content). While that will incur some bias, in general heat yield does not vary much between fuels *(Stott 2000)* and therefore until more research demonstrate otherwise, the two cited FRE-based combustion factors *(Wooster et al. 2005; Freeborn et al. 2008)* seem realistic *(Ellicott and Vermote 2012)*.

7. A final concern is that only part of the total energy being emitted from a fire is being captured by the satellite/aircraft sensor that cannot measure the energy partitioned into sensible, latent or substrate heat flux. The impact of this on the apparent relationship between FRE/FRP and (for example) emissions is unclear but should be evaluated. We propose to begin this type of analysis in our field campaign.

From the above discussion we can conclude that while fire radiative energy may provide an efficient and relatively accurate tool to monitor and measure fuel consumed by, and emissions from, fire events a more comprehensive and distributed validation of the approach must occur *(Ellicott and Vermote 2012)*.

Current and Future Satellite and Airborne Sensors Available

Currently, a plethora of satellites provide regular optical and other spectral sensor information for the entire globe, as geostationary, polar-orbiting or sun-

synchronous satellites. The main satellites/instruments to be considered are the Landsat series and MODIS instruments (onboard Terra/Aqua), due to their free data access. Similarly, the meteorological satellites of the USA (GOES), Europe (Meteosat, Envisat), and China (Fengyung), are able to provide optical and spectral data at high to moderate resolution (10's of metres to 1-3km). While those missions have a continuous scan mode, commercial missions (SPOT, RapidEye et al.) may be steerable, but have a high cost, and low repeat rates.

Recent and future launches of earth observing (EO) missions include the Landsat-8 mission (launch 11 Feb 2013), providing the continuity of the Landsat series which has been operational since the early 1970s, and the Sentinel-2/3 missions, which will be providing ongoing data availability of AATSR, MERIS and SPOT. For Sentinel-2/3, due to their planned twin configurations, global coverage is foreseen in the order of 1-5 days, depending on the instrument. The first launch will be at the end of 2014 with its twin 18 months later). The advantages of the Landsat and Sentinel missions are their operational use and their planned operational life of 20+ years, providing data security until 2035.

Geostationary satellites, such as the Meteosat (MSG, MTG) and Meteorological Satellite (MTSAT) series provide data at a relatively high temporal, but only at moderate spatial resolution. While the temporal resolution is in the order of 10-60 minutes, the spatial resolution is in the order of 1-4km, depending on the individual instruments. As it was discussed before, *Ellicott and Vermote (2012)* showed that such a spatial resolution is unlikely to be adequate. Moreover, despite their high temporal resolution, access to the data may be delayed by several hours, unless acquired directly via the meteorological services, which receive the data near real-time.

Higher resolution geostationary satellites are currently being planned, for example, ISRO's (Indian Space Research Organisation) GISAT-1 program will launch in 2017 and is planned to be in operation for 10 years. This will provide a high-resolution multispectral data (HRMX-VNIR at 50 m and HRMX-LWIR at 1.5 km), however, it will be targeted over the Indian sub continent. This will produce partial scans every 5 minutes with the total coverage over a 30-minute period.

As mentioned, the Moderate Resolution Imaging Spectroradiometer (MODIS) satellite is the currently most used satellite for fire detection and FRP estimation. This is again is a moderate resolution product with a spatial resolution between 250m and 1km depending on the infrared band used (36 in total ranging from 0.4um to 14.4um) and has two sensors on board (Terra and Aqua). The temporal coverage of Northern Australia is about 31 times within a 16-day period equating to roughly twice daily per sensor.

For the purpose of this study, the MTSAT-2 satellite of the Japan Aerospace Exploration Agency (JAXA) is located over Australia and provides thermal and spectral data at those resolutions. MTSAT-2 is planned to be operational until 2015, when it will be replaced by its successors (to be launched in 2014/15). All orbiting satellites are providing data in the order of 1-5 days, which may be limiting for the progression of fires. Consequently, a methodology needs to be developed to make use of the advantages of both satellite types.

JAXA also recently launched the Himarwari-8 geostationary satellite in late 2014. Similar to the MTSAT line of sensors, the Advanced Himiwari Imager (AHI-8) will provide 16 thermal bands of spectral data with a temporal resolution of 10 minutes. The sensor has swath coverage bounded by western India, Hawaii, Eastern Antarctica and Eastern Siberia. Not only does this provide a significant increase in the spatial coverage compared to other remote sensors but also a significant increase in the temporal resolution leading to possible operational applications. Preliminary detection results suggest that Himawari performs comparable to existing remotely sensed products however, similar detection issues, such as cloud and smoke obstruction and validation issues are still prevalent. Further validation and studies on the application of all the aforementioned remotely sensed products, are needed.

Current Products

A vast number of burnt severity and other fire indices exist that are derived using remotely sensed data. The spatial resolution varies significantly as a function of the sensor that is being used.

Burn Severity

Burn severity is generally observed using optical (visible to near-infrared) data obtained from

moderate- to medium-resolution satellites, in particular the free data obtained from Landsat (20m) and MODIS (1km). One such moderate-resolution product is issued by the Monitoring Trends in Burn Severity (MTBS; http://mtbs.gov/index.html) of the US Geological Service *(Escuin et al. 2008)*. This algorithm was also applied after the 2009 bushfires in Victoria to supply high-resolution information on the overall fire extent of Black Saturday. One of the limitations of such products is the temporal coverage, which may be reduced due to cloud/smoke coverage. Higher revisit cycles are provided by medium-resolution products, such as the global maps of burn severity provided by MODIS (eg. *(Roy et al. 2008)*. While this product has a higher temporal resolution, its spatial resolution is limited to 1km. High-resolution data products have been derived from CNES SPOT (available since 1986). Consequently, this may also be achieved using RapidEye imagery.

Fire Risk

Fire risk indices are being derived from a number of sensors. Similar to the burn severity mapping, those are primarily obtained from optical sensors, with the same spatio-temporal limitations. Further, sensors that have been used to derive fire risks include high-resolution sensors such as MERIS and AATSR. However, those sensors are research instruments and therefore have not had a long lifetime. The advantage of MERIS was its programmable operations mode that could allow targeting specified areas. A new approach to fire risk mapping has been proposed using low-resolution passive microwave products, in conjunction with MODIS data. *Piles et al. (2011)* proposed a methodology to disaggregate the low-resolution data using MODIS data and use the new soil moisture product as an indicator for fire risk (http://www.smos-bec.icm.csic.es/fire_risk_maps). A similar approach was tested for Victoria, using BoM automated rainfall data as a substitute of the soil moisture information *(Mutch et al, 2013)*. Products such as grassland curing rely on the use of models and MODIS data to derive a dryness state of the grasslands (also at 1km); the use of soil moisture as a proxy provides opportunities to transfer this to forested areas as well.

Active Fires

Active fire observations are possible using both sun-synchronous and geostationary satellites *(Schroeder et al. 2008)*, with most moderate- to low-resolution missions with products. Those products are globally available for MODIS (Figure 102) and consequently, for Australia. However, as MODIS is a sun-synchronous satellite with a repeat rate of several days, the progression of fires cannot be monitored in real-time. The use of NOAA's GEOS shows that fire hot spots may be observed using geostationary satellites. JAXA operates geostationary meteorological satellites above Australia, which produce such data that may be used for the development of such near-real time fire detection *(Zhang et al. 2012)*.

While the presented high-resolution products are technically feasible, there are severe restrictions on such data. More so than for Landsat, high-resolution data are temporally sparse (for SPOT in the order of 46 days) and are not free of charge, consequently, operational products have concentrated on the use of Landsat and MODIS. The introduction of the European Space Agency's Sentinel-2 & -3 satellites will provide free data at high-resolution and due to their proposed tandem flights (two or more satellites of the same type on different orbits), will increase the temporal resolution of the data products. However, data dissemination is currently being discussed and may require a buy-in into the data repository. With the launch of the MTSAT-2 successor Himiwari, (2014; operational 2015), the spatial resolution will improve to 0.5-2km and the temporal resolution to 10min.

There are products in Europe (Fireglobe, SMOS Fire), as well as the MODIS/LANDAST based indices. SMAP will also have some sort of a fire product for example, grassland curing.

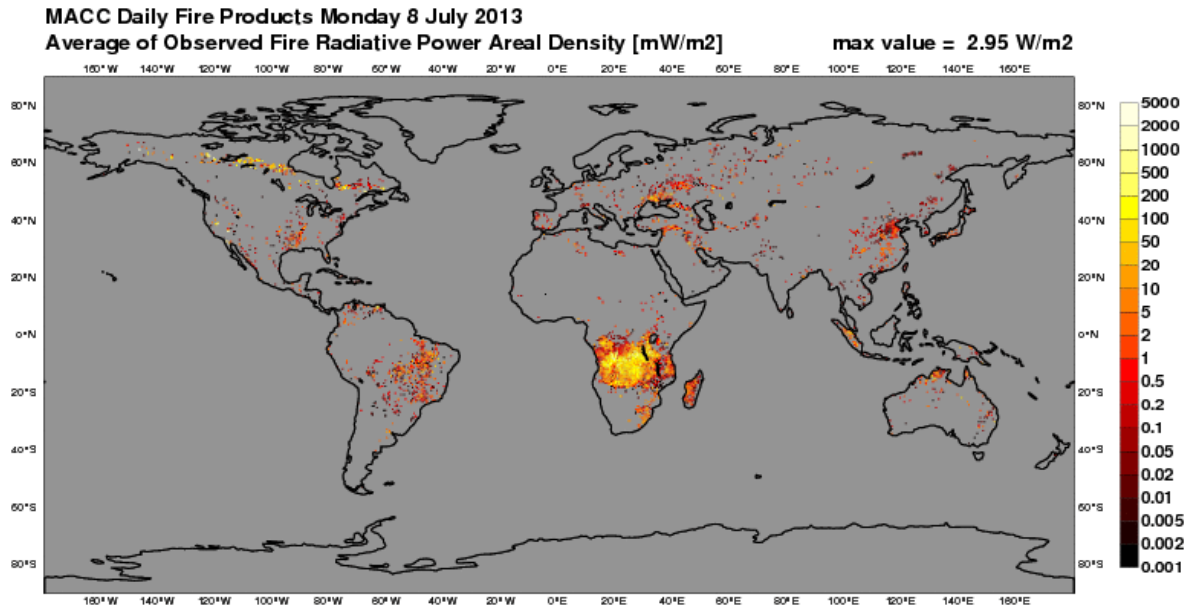

Figure 102 One of the many daily fire products created using MODIS data. Available: http://gmes-atmosphere.eu/about/project_structure/input_data/d_fire/ accessed 10th July 2013

Using FRP to Determine Fire Intensity

In Australia and across the globe, bushfires are serious environmental problems that consistently result in the loss of life and property and impact on the economic and social stability of the community. Recently, much effort has been directed at devising tools to assist in assessing the level of bushfire risk. Further effort has been directed at implementing policy and planning devices that mitigate the risks posed by bushfire. However, traditional methods and models (e.g. the McArthur FFDI and GFDI) have been found to perform poorly when used to assess the risk posed by the most extreme fires *(Harris et al. 2011)*. Currently, the national fire danger rating system specifies six broad categories that describe the potential impacts of bushfires. However, there are some key defects in the rating system that may limit its use. These include:

- The FDI describes the conditions that allow fires to start and continue burning but does not account for all fire risk factors. For example, topography, fuel availability and fire location are not taken into account in FDI calculations.
- The FDI is only valid for dry eucalypt forests and grasslands. Vegetation areas include shrubland or Mallee cannot be assessed using FDI.
- It fails the Royal Commission's recommendation for simplification of fire warnings.
- It is not a numerical scale like the cyclone warning categories (Rec 4.3) or the earthquake rating system (Richter scale).

For these reasons, the FDI cannot give a complete account of fire danger for making risk management and fire fighting decisions. To better elucidate the bushfire risk problem and to understand where improvements might be made to risk management practices, a conceptual fire severity scale was proposed by *Harris et al. (2011)*. The scale recognises that bushfire risk evolves in a manner that is dependent on the size and the rate of progression of the fire. As a consequence of the increase in the rate of area or perimeter spread of the fire, more fuel is more rapidly consumed, and hence more energy is released into the atmosphere. The rate of energy released from the fire or total fire power during combustion defines the severity of the power scale. Presumably, as more energy is released into the atmosphere, the atmosphere becomes increasingly unstable which directly influences fire behaviour through rates of spread and ember spotting. This potential fire severity scale is based upon transitions between levels of fire severity, much like the case for Cyclones (Saffir scale) and Earthquake (Richter scale). In this respect, the proposed framework directly addresses one of the issues raised by the Royal Commission into the 2009 Victorian bushfires. Although different authors have tackled this problem for other natural

hazards *(Samardjieva and Badal 2002)*; *(Pielke Jr et al. 2008)*, no such study exists for the case of bushfires. If such a scale is to be pursued and developed, correct assessment of fire impacts requires accurate documentation of where and when the fires occur, their size and/or strength, the amount of biomass burned, and the quantity of particulate and gaseous matter emitted in the smoke. Unlike most other physical objects and phenomena, because of the exothermic, aggressive, and erratic nature of large fires, their characteristics cannot be measured quantitatively in situ or even at close range.

As mentioned earlier in this report, a common measure used to assess the amount of energy being released during the combustion process is fireline intensity, a measure of the energy release along the fire front *(Byram 1959)*, while possibly the most valuable quantitative descriptor of any fire. Accurate quantification of wild-land fire intensity is extremely problematic with uncertainties around the estimates of spread rate, fuel load and combustion efficiency. Additionally, defining and quantifying fireline intensity is particularly difficult for the complex burn patterns that often occur. For these reasons, assessment of the total fire energy released from bushfire by using mapped fire isochrones is extremely unreliable. Determination of FRP/FRE via remote sensing is intrinsically a more effective approach, providing some of the limitations can be overcome.

Fuel Consumption Rates

Fuel Loads

Vegetation along the eastern coast of Australia is dominated by the genus *Eucalyptus,* with both dry and wet sclerophyll species. Eucalypts are not only fire prone but are in fact fire promotion *(Gill 1981)*. Dry sclerophyll forests (and woodlands) typically consist of multi-aged stands of a mix of eucalypts and have an understorey dominated by hard-leaved shrubs, grasses, sedges or bracken fern. The tree canopy is usually a mixture of *stringybarks, box* and *gum-barked* species. Wet sclerophyll forest typically consists of a tall eucalypt over-storey strata of multi-aged and mixed species, and a dense understorey of ferns and soft broad-leaved shrubs. Fuel arrangement in these two forest types can be divided into five layers, each based on its position in a vertical and horizontal vegetation profile *(Hines et al. 2010)*. The vegetation profile incorporates surface fine fuel, near surface fuel, elevated fuel, bark fuel and canopy fuel, for which the total ‘load’ or amount of vegetation per unit area (tonnes/hectare or kilograms/ square meter) can be assessed for each layer (Figure 103). However fuel load itself may only have a limited impact on the forward rate of fire spread; results from Project Vesta (a research project into high-intensity bushfires in dry eucalyptus forests) indicate that a stronger relationship exists between rate of spread and the attributes of the surface fuel bed and understory layer *(Gould et al. 2007a; Gould et al. 2011; Cheney et al. 2012; McCaw et al. 2012)*. The moisture content of plant material in each of the forest layers also affects the ‘availability’ of the fuel within the profile, and will therefore affect the fuel consumption rates, and hence fire intensity.

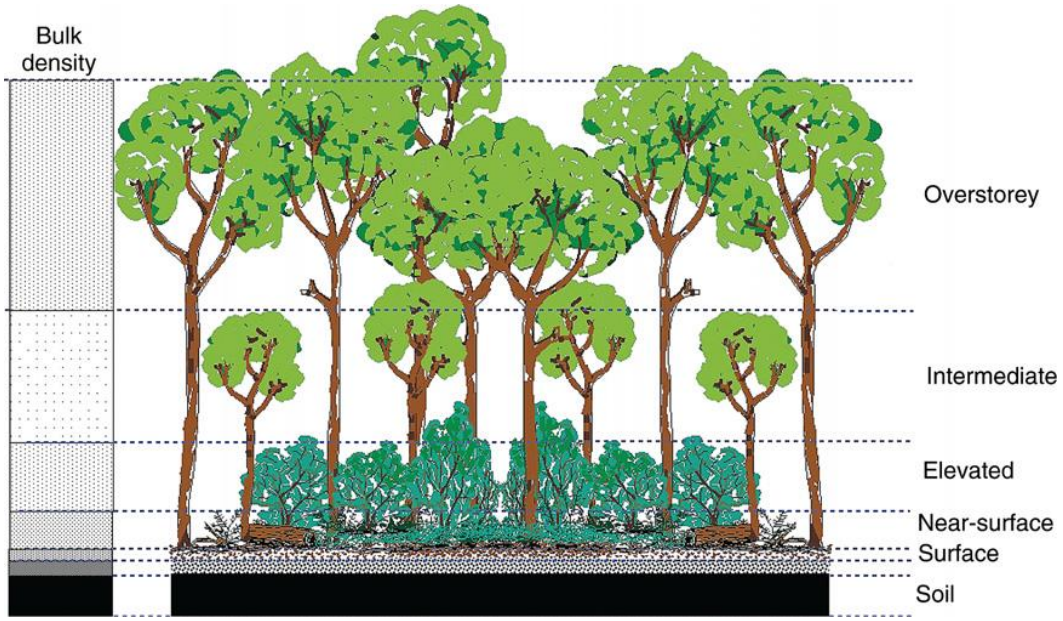

Figure 103. Fuel layers within a dry eucalypt forest that can be identified. The grey scale on the left side indicates the relative bulk density of each layer *(Gould et al. 2011)*.

Fuel Consumption

The theoretical heat yield (kJ kg^{-1}) of most fuels, which is the amount of energy released per unit mass of matter under complete combustion, is typically between 16 000 and 22 000 kJ kg^{-1} *(Luke and McArthur 1978)*, and in many studies is assumed to be 18 608 kJ kg^{-1}. The amount of energy released is very important for determining fireline intensity, and the single most important factor affecting the heat yield is fuel moisture content (FMC) *(Whelan 1995)*. Volatile oils within the vegetation also make the fuel more flammable since they burn as gases. For example, eucalyptus, which contains a high percentage of oils, has a higher heat yield than savanna grasses *(Whelan 1995)*. The amount of heat released during a bushfire also depends on the completeness of the combustion process (i.e. combustion efficiency), since 100% combustion is only achieved in the most intense fires *(Burrows et al. 1995)*. Incomplete combustion will reduce the energy output to below the potential maximum.

Consumption rates of fuels in forest fires contribute to several important features relating to fire behaviour, fire suppression and firefighter safety. The ability to accurately predict fuel consumption rates, particularly of coarser woody fuels (i.e. >6mm) is essential in planning prescribed fires *(Hollis et al. 2010)* since fire planners often need to make important trade-offs between ecological values and reduction targets. Although, fuel consumption rates of woody fuels is often a neglected part of fire science, recent research suggests that the proportion of woody fuel burnt in eucalypt forest types varies accordingly to a range of variables that include fuel age, past burn severity and climate *(Burrows et al. 1995; Hollis et al. 2010)*.

Fire behaviour prediction systems around the world incorporate fuel structure in various ways. For example, the U.S. FDRS uses specific information about the fuel properties (e.g. fuel depth, particle size and fuel bulk density), whereas Australian and Canadian fire behaviour guides use fuel hazard, quantity or height to predict fire behaviour in a particular vegetation or fuel type. However, it is widely acknowledged that both the quantity and structure of the various vertical fuel layers varies spatially and temporally *(Burrows et al. 1995)*. Although, fuel quantity is useful to characterise the combustion properties of specific fuel types (e.g. surface), the fuel structure of forest types may conceal other properties of the vegetation that actually determine how it burns. To further elaborate, fine fuels at the surface and near the surface rapidly burn away in the flaming zone of surface fires in Australian sclerophyll forests and contribute most to fire rate of spread and fireline intensity. In a laboratory experiment, *Burrows (2001)*

determined the residence times of flaming, glowing and smouldering combustion of different size fuels, and results suggest that the larger fuel sizes take typically longer to burn, and much of the fuel weight loss occurs during the glowing and smouldering phases of combustion. Similarly, *Cheney (1990)* measured the residence time of individual fuel particles in thinning debris in young stands of *E. seiberi* in N.S.W, Australia to estimate the contribution of woody fuels in the flaming zone of a fire front. Results from Cheney, confirmed *McArthur (1962)* observations that material <6 mm in diameter contributes most to the heat release of a moving fire. Although, FRE may be meaningful for heat release with uniform quantities and proportions of various fuel structural types, it does not specify the relative importance of the different fuel classes, which is an important aspect of interpreting fire impact.

The different phases of combustion are an important aspect of fire science to consider in mapping and determining FRE since it is based on average radiative properties of any given cell. This would imply that any FRE calculation on a moving fire front would inherently contain the different phases of combustion, where most of the combustion would be behind the flame front. The active flaming combustion zone is typically in the order of 5 to 100 metres, depending on the intensity of the fire. Therefore, satellite remote sensing techniques with low cell resolution would not adequately quantify fire intensity as is defined by *Byram (1959)*. For example, *Byram (1959)* suggested that fireline intensity could realistically vary between 15 and 100,000 kW m^{-1}. These huge extremes of fire behaviour have been documented many times in the literature; for example fireline intensity in the tropical savannas of northern Australia have been noted to be ~8,000 kW m^{-1}, and in wet sclerophyll forests fireline intensity is often in the range of 50,000 to 100,000 kW m^{-1} in fast moving fires *(Kilinc et al. Unpublished)*. However, fireline intensity derived from FRE measurements for the Sydney 2002 bushfires suggest values of between 15 and 75 kW m^{-1}, and are much lower compared to the reported values of 8,000 kW m^{-1} (*Wooster et al., 2003*). Clearly, there are discrepancies between Byram's approach and FRE that need to be resolved. Some of these issues as discussed relate to assumptions on combustion rates, fuel quantity and fire behaviour estimates as well as a poor understanding of the combustion processes and measurements that are captured using remote sensing, including the lack of complete view of the fire from overhead because of canopy effects.

Recommendations

This literature review has highlighted the need to evaluate techniques for the direct measurement of fire intensity and heat output for Victorian vegetation for a range of possible purposes including plume rise and emissions calculations. In order to achieve this, following objectives must be met:

a) Validation of satellite FRP measurements against surface measurements of radiative flux

b) Assessment of fire intensity estimate by the PHOENIX Rapidfire Model using flux tower measurements of heat release rates/fluxes from two field campaigns

c) The assessment of the potential of satellite or aircraft monitoring of combustion characteristics using FRP for operational applications

Other Relevant Work at Monash University

Fire "risk" can be defined as not only the probability of an event, but also includes the socio-economic risk i.e. values and expected losses *(Hardy 2005)*. However, generally, it refers only to the likelihood of ignition (both man- made and caused by lightning). Fire "severity", refers specifically to the effect a fire has on environmental system *(Hardy 2005)*. However, "severity" can also be defined by its extent and by the intensity of a fire *(Wooster et al. 2005)*. This can be heavily affected by both the climate and biological system (land-climate systems). Traditional methods of estimating fire risk such as the McArthur FFDI and the GFDI specify categories that are defined using climate parameters such as, temperature, wind speed, current and previous rainfall and relative humidity. The current national (Australia) danger rating system only describes potential impacts of fires qualitatively and a quantitative scale of severity is not included in the system. Due to this, in extreme fires cases such as the Black Saturday fires in Victoria, the FFDI has been found to perform poorly *(Harris 2011)*. This could be due to the large wet bias in the formulation of the drought/soil moisture parameter *(Dharssi et al. 2011)*. However, it could also be due to the linear approach of the current danger rating system. This can be improved through an investigation of the temperature and soil moisture parameters and their effect on fire intensity and the subsequent effect on fire risk/danger. Fire intensity can be defined as the measure of radiant heat output from a fire *(Kaufman*

et al. 1998; Wooster et al. 2005) and is a function of the rate at which fuel is being consumed. As described earlier Fire Radiative Power (FRP) is defined as the rate of energy released per metre squared and can be a useful tool for quantifying the impact and severity of individual fires as well as emissions (*Roberts et al., 2005*). As FRP is a measure of the heat output of a fire through fuel consumption it is directly affected by temperature, moisture and vegetation conditions *(Kaufman et al. 1998; Wooster et al. 2005)*. However, as mentioned, FRP has seldom been investigated in relation to fire risk and its effect on the land-atmosphere interaction, particularly, energy feedbacks.

Despite data for various climate variables being available at high spatial and temporal resolution, the McArthur FFDI is typically validated against large sets of fire observations. These datasets can contain large amounts of erroneous data and usually only provide the extent of a fire that is being monitored. With advances in remote sensing technology, both active fire hotspots and FRP can be observed using various sun-synchronous and geostationary satellites *(Schroeder et al. 2008)*. One such product, MODIS (Moderate Resolution Imaging Spectroradiometer), provides instantaneous FRP, formulated by comparing the difference in brightness temperature emitted at the infrared wavelength between the background and a fire pixel *(Wooster et al. 2005)*. The MODIS FRP product (MOD14A1/MYD14A and MCD45A1) provides daily snapshots at 500m resolution *(Justice et al. 2002)*. Through using modelled and remotely sensed data, the accuracy and effect of intensity and various climate variables have on fire risk can be assessed qualitatively.

Relationship between climate variables, fire occurrence and FRP and implications for calculation of FFDI

We have investigated the relationship between FRP and daily temperature, wind speed, relative humidity, NDVI (the Normalized Difference Vegetation Index) and various measures of soil moisture. As mentioned FRP is a measure of fire intensity given in megawatts. This has been investigated for all MODIS fires between 2000 and 2013 across Australia and for each climate regime therein with a particular focus on the Black Saturday Fires in southeastern Australia (7/2/09). There is a strong relationship between, dry, hot conditions and an increasing occurrence of fire as well as an increase in the FRP for those fires. From Figure 104 it can be seen that the maximum temperature increases with increasing FRP with the peak at around 38 - 40 degrees; likewise, as RH approaches zero, FRP increases exponentially. The relationship between wind speed and FRP appears to be less clear, with a range of wind speeds recorded. The results suggest that wind speed is more significant in determining fire extent and spread rather than determining fire intensity. Probably the most revealing of the variables most commonly related to fire, is soil moisture. In Figure 104 the soil moisture proxies API, SPI, KBDI and MSDI are the Antecedent Precipitation Index, the Standardised Precipitation Index, the Keetch-Byram Drought Index and the Multivariate Standardised Drought Index, respectively. There appears to be a distinct relationship between FRP and soil moisture, with FRP increasing exponentially with decreasing soil moisture, as it tends to zero. These relationships can be more easily identified when examining data for the Black Saturday fire. From Figure 105 we can see that regions in which the fires occur all have higher temperature, lower RH, and lower NDVI than the surrounding areas (with soil moisture being uniformly low across Victoria).

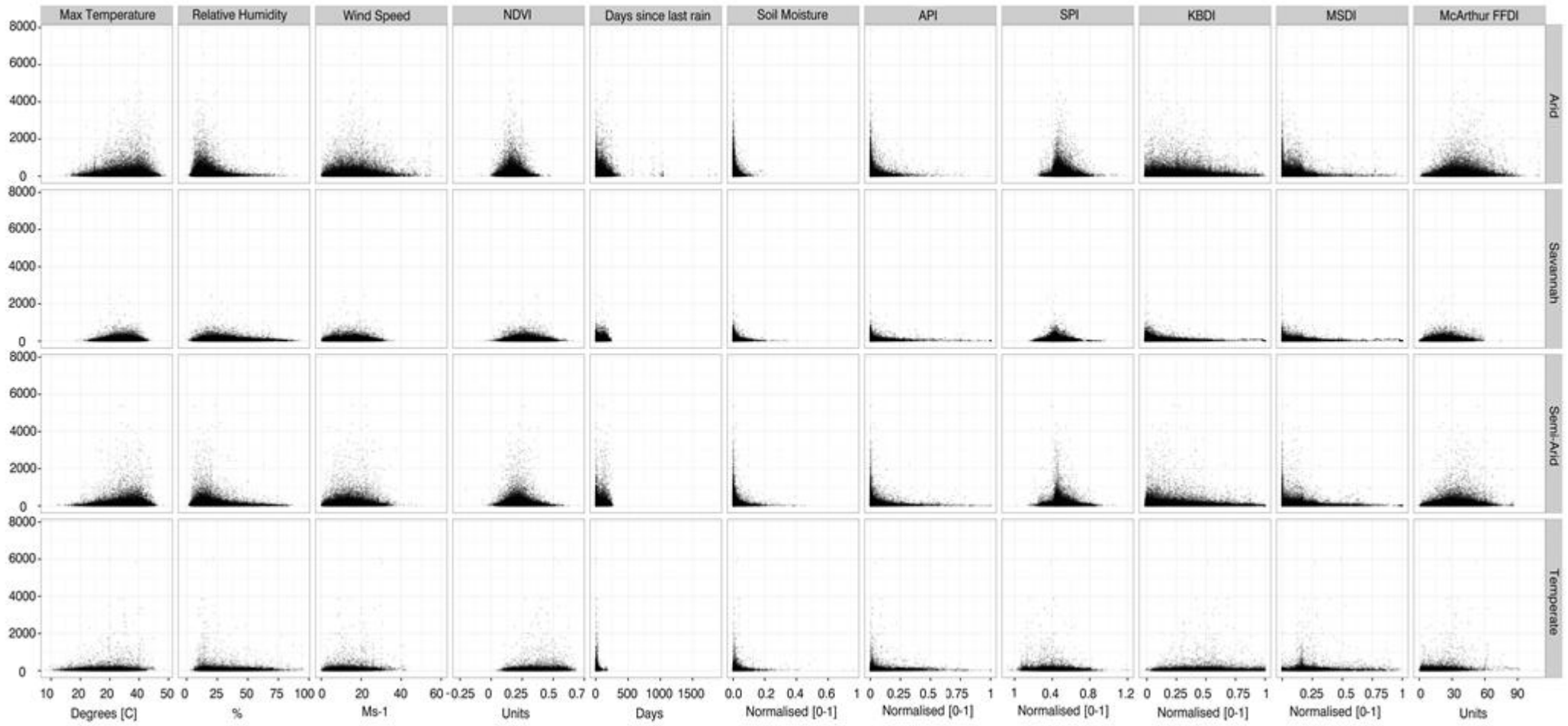

Figure 104 Scatter plot array of Tmax, RH, wind speed, NDVI, days since last rain, soil moisture, API, SPI, KBDI, MSDI and FFDI against FRP for all fires detected by the MODIS for Australia between 2000 and 2014. Fires are also split into the Koeppen climate regions most prevalent in Australia.

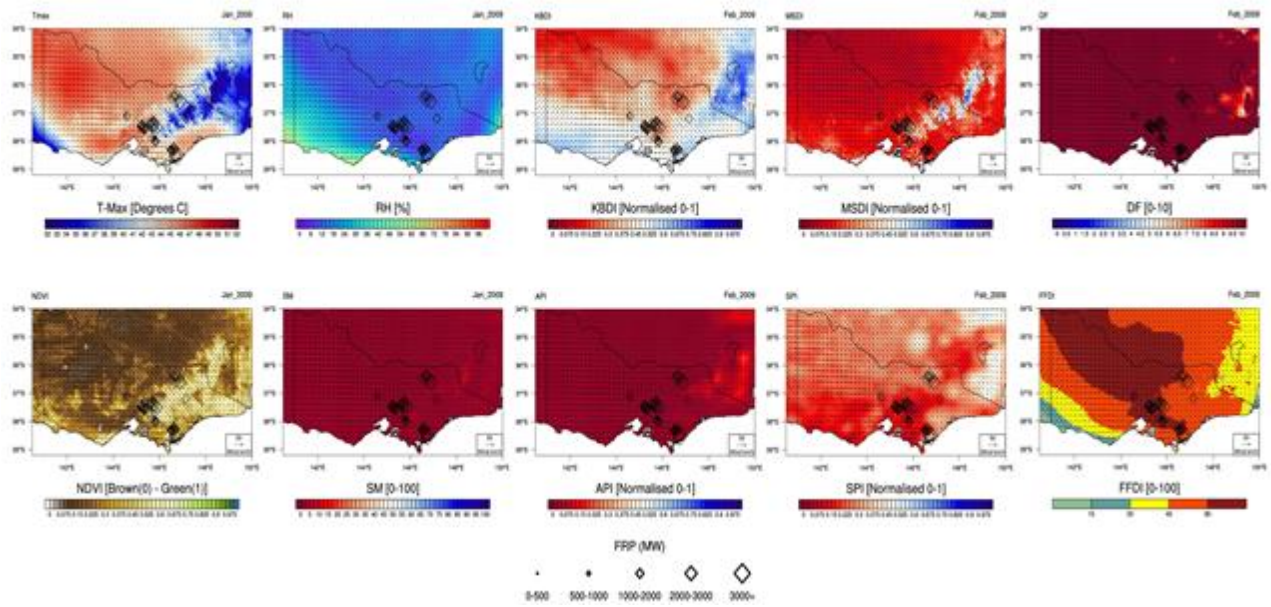

Figure 105 Maps of Tmax, NDVI, RH, SM, KBDI, API, MSDI, SPI, FFDI and DF (Drought Factor) with fire locations overlaid for Victoria during the Black Saturday Fires (7/2/2009). The relative size of diamonds indicates the relative FRP. Wind vectors are also shown as arrows relative to reference of 50 ms-1.

A range of analyses (not shown here) suggests that API shows the clearest relationship with observed soil moisture and also with FRP. Due to this more direct relationship with soil moisture, the effect of changing the moisture indices used in the current formulation of the FFDI was investigated. Simply, API, KBDI, MSDI and SPI were substituted into the drought factor component of the FFDI formula and the consequent values compared against MODIS-detected fires. Despite the stark differences in moisture between indices, in each case, the resultant FFDI is very similar, with almost no change in the drought factor (plots not shown here). The drought factor appears to be completely dominated by the ”days since last rain” and the ”last rain” component. When comparing patterns seen in Figure 105 the drought factor actually closely resembles both the API and the actual soil moisture, due to the direct relationship between rainfall, soil moisture and API. As can be seen particularly for the Black Saturday fires, the extreme drought factor across Victoria is not reflected in the FFDIs. Changes in FFDI appear to be mostly due to changes in temperature and relative humidity. As relative humidity is in part a function of temperature, this would mean that temperature contributes to a significant portion of the FFDI function. As is seen in Figure 104 there appears to be a gamma distribution of fire occurrence for temperature, relative humidity and wind speed; i.e. as these tend to more extreme conditions, the resultant increase in FRP and fire occurrence may not be reflected. However, this may just be due to the reduced sample size at such extreme conditions. Similarly, the resultant FFDI does not reflect an increase in the intensity of a fire; e.g. as FFDI increases, FRP increases along a normal curve. Not only does the current FFDI not reflect changes in FRP and soil moisture but also it does not reflect the changes in vegetation moisture nor in fuel load. This can be clearly seen both for the Black Saturday fires and for fires detected by MODIS between 2000 and 2014.

We are currently working on a formulation of the FFDI that would reflect changes in FRP and fire occurrence and will validate this against the current FFDI using MODIS-derived fire hotspots. Following this we will use CMIP5 projections of soil moisture to determine the change in fire danger due to climate change between the reference period of 2000-2010 and 2050-2060.

Appendix G: Fire activity modelling for use in smoke predictions

Document summary

This report summarises the work undertaken by the University of Melbourne in 2014/2015 to link fire activity modelling and smoke emissions modelling, as part of a project coordinated by CSIRO to develop predictions of smoke emissions and impacts from bushfires and prescribed burns in Victoria.

The report provides an overview of the research tasks and presents key findings. It also describes some of the key challenges in smoke emission prediction, documents the chosen fire modelling approach and associated software, and presents the results of some case studies of fires in Victoria.

The report includes a discussion of model limitations and uncertainties, and recommendations are made for further development. Note that this edition of the report describes software enhancements provided in 2016 at the request of CSIRO.

Acknowledgements

The authors would like to acknowledge the significant advice and assistance provided by Mr Derek Chong (University of Melbourne), Mr John Loschiavo (City of Banyule), Mr Brett Cirulis (University of Melbourne), Mr Dave Van Bockel (Parks Victoria), Dr Julian Di Stefano (University of Melbourne) and Dr Stuart Matthews (NSW Rural Fire Service).

Further information

This research was undertaken in accordance with a CSIRO Collaborator Agreement *(CSIRO and University of Melbourne 2013)*, and University of Melbourne Research Agreement LEX #22050 *(University of Melbourne 2013)*.

Technical details can be found in the project plan *(Walsh and Duff 2014)*, the progress report *(Walsh et al. 2015)*, CRC publications *(BCRC 2013; BNHCRC 2014)* and CSIRO publications *(Cope et al. 2014; Lee and Cope 2014)*.

For further information, please contact the Bushfire Behaviour and Management group at the University of Melbourne.

Kevin Tolhurst kgt@unimelb.edu.au

Sean Walsh sean.walsh@unimelb.edu.au

Thomas Duff tjduff@unimelb.edu.au

Objectives and scope

This report summarises the work undertaken by the University of Melbourne as part of the collaborative project '*Smoke Transportation Modelling and Emission Modelling for Victoria*', involving several research partners and managed by CSIRO.

The University of Melbourne was contracted to predict information about smoke and heat emissions from bushfires and planned burns. This information is intended as input data for a CSIRO-developed atmospheric modelling system designed to predict smoke transport and exposure resulting from fires in Victoria. A simplified outline of the prediction system is shown in Figure 106.

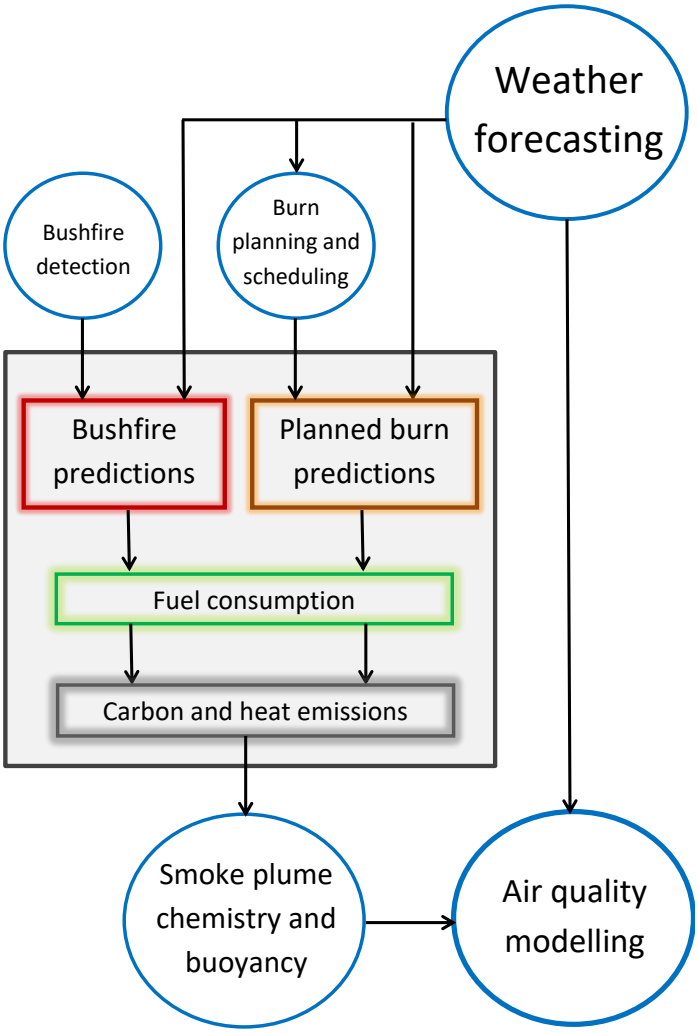

Figure 106. Simplified diagram of the smoke forecasting system. The box indicates the scope of the work described in this report.

Background

Smoke from large fires can affect human health *(Tham et al. 2009; Youssouf et al. 2014)*, visibility *(McMeeking et al. 2006)* and vineyard crops *(Kennison et al. 2009)*, as well as having negative effects on recreation, tourism and general amenity.

During major bushfires, intense smoke plumes may impact on major population centres, potentially affecting millions of people. The movement of these plumes can be complex; for example, on the 11th Feb 2014, smoke from far-east Victoria reached the surf coast and Geelong before it reached eastern Melbourne, because part of the plume was transported quickly over water, where wind speeds are higher (Figure 107).

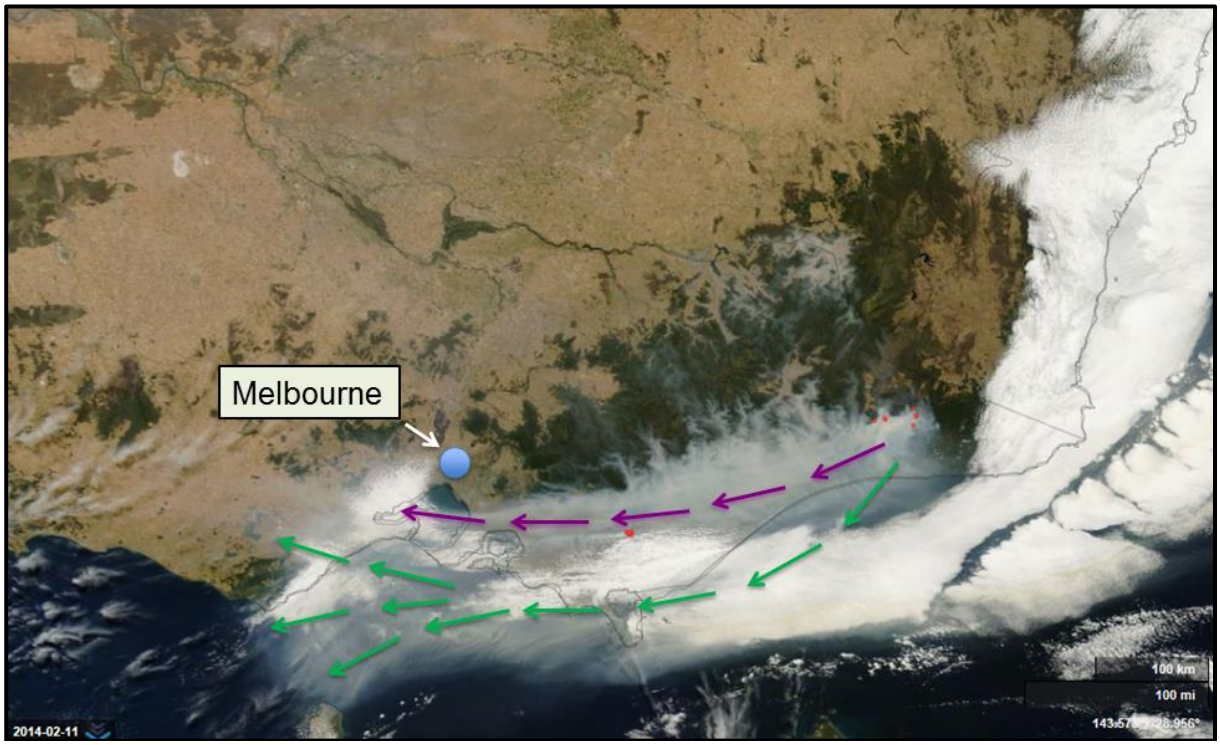

Figure 107. Bushfire smoke affecting Victoria (MODIS, 11th Feb 2014). Purple arrows show smoke transport over land; green arrows show transport over water.

The impacts of smoke on sensitive people (which includes the elderly and those with chronic respiratory disease) can be reduced if protective actions are taken, such as staying indoors and closing windows *(DoH 2013)*. However, public health authorities will only issue advice if an extended period of smoke at high concentrations is expected. For this to work effectively, an accurate forecasting system is needed, and a key input into such a system is the rate of smoke emissions.

Planned burns can also result in significant smoke emissions (Figure 108). Smoke concentrations are usually lower than those seen during major bushfires, but smoke exposure can occur over longer periods, as burning is typically done during calm weather, and often extends over several weeks, increasing the amount of time that smoke remains within the affected area.

Burns will inevitably generate some smoke impacts, but through careful management, these impacts can be minimised whilst still achieving the intended burn outcomes. A system that could accurately forecast smoke emissions and impacts could form part of this process of keeping impacts to a minimum, by providing information to assist burn planning and scheduling.

Figure 108. Planned burn at St. Andrews, Victoria, 30th March 2015.

For both bushfires and planned burns, it is important to predict the rate of heat release as well as the rate of smoke emissions. Heat release is needed because this affects the rate at which the plume rises vertically, which has a significant effect on smoke concentrations downwind of the fire *(Lee and Cope 2014)*.

Current practice for forecasting smoke in Victoria includes a combination of manual methods *(Walsh 2014)* and automated tools *(Wain and Mills 2006)*. However, these systems do not include quantitative calculations of the smoke emission rate, which depends on the rate of progress of the fire and the rate at which fuel is consumed.

This problem is addressed in the current project by using fire behaviour modelling to estimate the rate of fuel consumption, and consequently the rates of smoke and heat release. This approach can be applied to fires that have ignited but not finished burning, as well as fires that have not yet been ignited. It can also be adapted to support the prediction of different scenarios, for example by using a range of different weather forecasts to drive the fire prediction model. The following section provides further detail on the application of fire behaviour modelling to smoke emissions.

Integration of fire prediction and smoke modelling

Fire prediction and fuel consumption

A number of smoke forecasting systems have been developed in Europe, the USA and Canada *(Meyer et al. 2013a)*. Many of these systems rely on detection of active fires and simple assumptions about fire growth. These systems also rely on locally developed fuel models that cannot be directly applied to Australian forest fuels. Therefore such models are of little direct use for operational smoke predictions in Victoria, although some components are useful, for example the USA-developed *BlueSky* system *(Larkin et al. 2009)*, which has been employed by CSIRO to provide a framework for smoke modelling *(CSIRO 2014)*.

For modelling bushfires, this project has used an established Australian fire propagation system, PHOENIX RapidFire[2] *(Tolhurst et al. 2008)*. This software system predicts the future development of a bushfire given a weather forecast and ignition details, plus spatial datasets describing vegetation fuels, topography, barriers to fire propagation (such as roads) and fire history.

To track the rate at which fuel is consumed in a fire, the PHOENIX software was extended to record details of the incremental area burnt after each time step of the model (

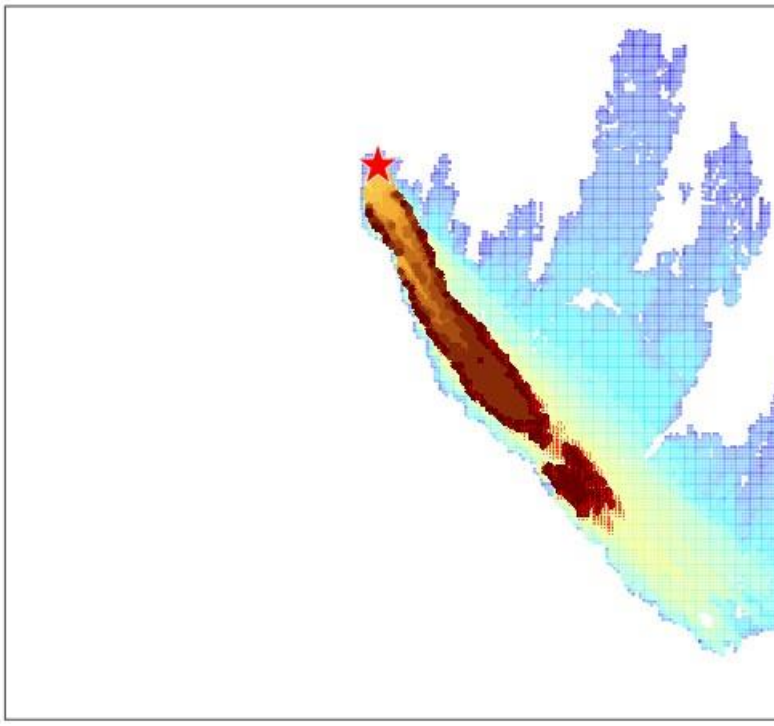

Figure 109). Within that area, the consumed fuel is counted and assigned a time and location. This generates a sequence of data on fuel consumption throughout the duration of the simulated fire.

[2] Hereafter this will be referred to simply as PHOENIX.

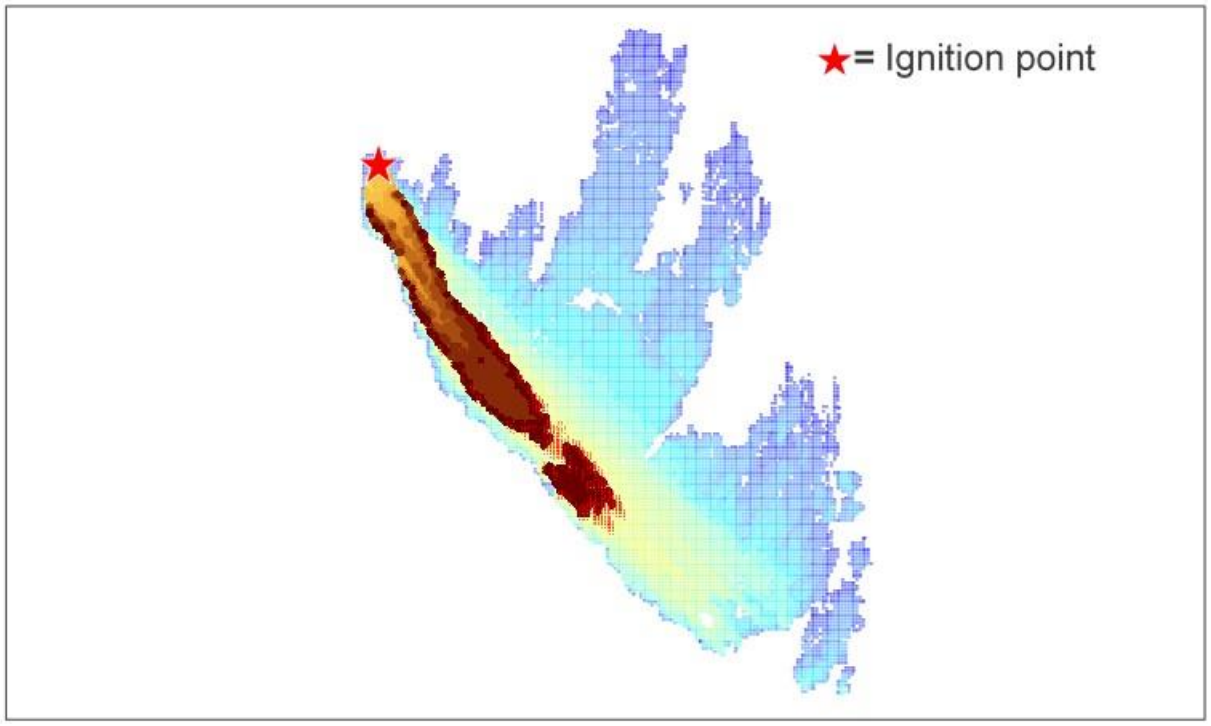

Figure 109 PHOENIX simulation of the Kilmore East Fire on 7th Feb 2009 *(Walsh et al. 2015)*. Fire activity to 4:05 pm is shown in brown, and fire activity from 4:05 to 4:14 pm (one time step) shown in red.

For planned burns, there are no established models that can perform an equivalent prediction. PHOENIX was designed and calibrated for high intensity, fast-moving bushfires, and has not been evaluated for low intensity planned fires, which typically involve a complex ignition process and a patchwork of many slow-moving fires under mild weather conditions.

More fundamentally, the ignition pattern for planned burns is usually determined by the burn controller on the day of the burn *(Tolhurst and Cheney 1999)*. Emulating the detailed judgements of an experienced burn controller would require extensive research into the decision-making process as well as accurate prediction of fine-scale weather and fuel conditions. These significant research tasks are beyond the scope of the current work.

Consequently, fire propagation modelling is not yet suitable for predicting smoke emissions from future burn. For this reason, a specialised simulator for planned burns was developed *(Walsh et al. 2015)*, described in detail in section 4.2 of this report. Fuel consumption information (including location, amount of fuel burnt and time of consumption) is recorded in the same way as described above for bushfires.

Application to smoke modelling

This project component quantifies the burning of fine fuels in flaming phase combustion. After flaming combustion has finished, there is usually an extended period of smouldering combustion with significant amounts of coarse fuel being consumed (Figure 110). It is beyond the scope of the current work to quantify emissions from coarse fuel consumption. Similarly, no attempt has been made here to quantify the smouldering combustion of fine fuels, which can occur in the lower (wetter) layers of forest litter.

The objectives set by CSIRO for this project component were to compute the carbon and heat emissions rates from fires. The next section of this report describes the development of models for estimating carbon and heat emissions from bushfires and planned burns. Fire behaviour results are also output by these models to assist with future research into the links between fire behaviour and smoke emissions.

Note that although this project component has established links between fire behaviour and smoke

emission rates, a full linkage of fire behaviour, smoke emission and atmospheric models is not attempted here. Significant work is underway in other project components to develop methods to convert carbon emissions into chemical smoke profiles *(Meyer et al. 2013b)*, and to find suitable techniques for using heat emissions to model the buoyant rise of smoke plumes *(Lee and Cope 2014)*.

Figure 110 Coarse fuel combustion at the St. Andrews burn, 30th March 2015.

Model development

Bushfire emissions model

Overview

The PHOENIX bushfire simulator, currently used by the Victorian Department of Environment, Land, Water and Planning (DELWP), was used as the basis for building a model of carbon and heat emissions from active fires. As the operational version of PHOENIX does not output the necessary information needed to compute a time sequence of fire emissions, some extensions and modifications were made to the software.

A fire simulation is initiated by specifying a number of ignition events, either as points or as established fire perimeters. Using forecast weather, and landscape information including topography, vegetation fuels and fire history, PHOENIX then simulates the likely progress of the fire. The simulation proceeds using variable-length time steps (up to a maximum of 20 minutes), and continues until user-specified end time, which is typically several hours from the first ignition.

For this project, the PHOENIX software was modified so that at the end of each model time step, all the area burnt during that time step is identified (Figure 111), and the total amount of fuel consumed in this area is calculated. The amount of fuel consumed is then converted into carbon and heat emissions data and assigned a location and time.

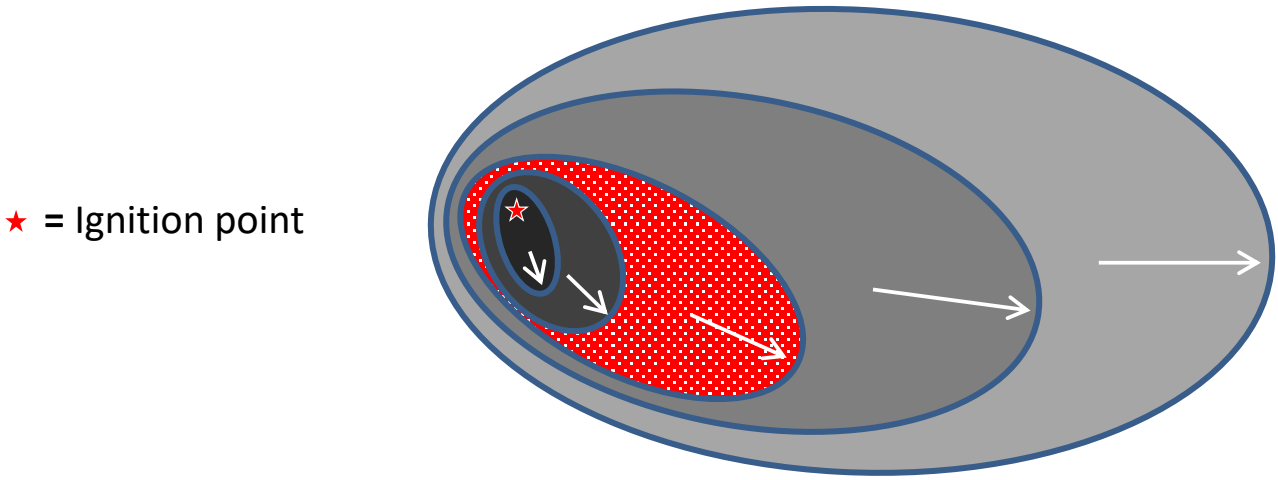

Figure 111 Time steps in a PHOENIX fire simulation. The highlighted area (in red) represents the area burnt during one time step.

Emissions for one model time step are assigned a point location by calculating a weighted centroid of all the model grid cells that were burnt during that time step. The weighting function is constructed so that areas of higher fuel load are given greater weight, as these will have the most effect on carbon and heat emissions.

All emissions data, including locations and times, are recorded throughout the fire simulation. At the end of the simulation the data are summarised and written to result files. The process is described in the flowchart in Figure 112. For details of how to operate the model, please refer to Appendix 1.

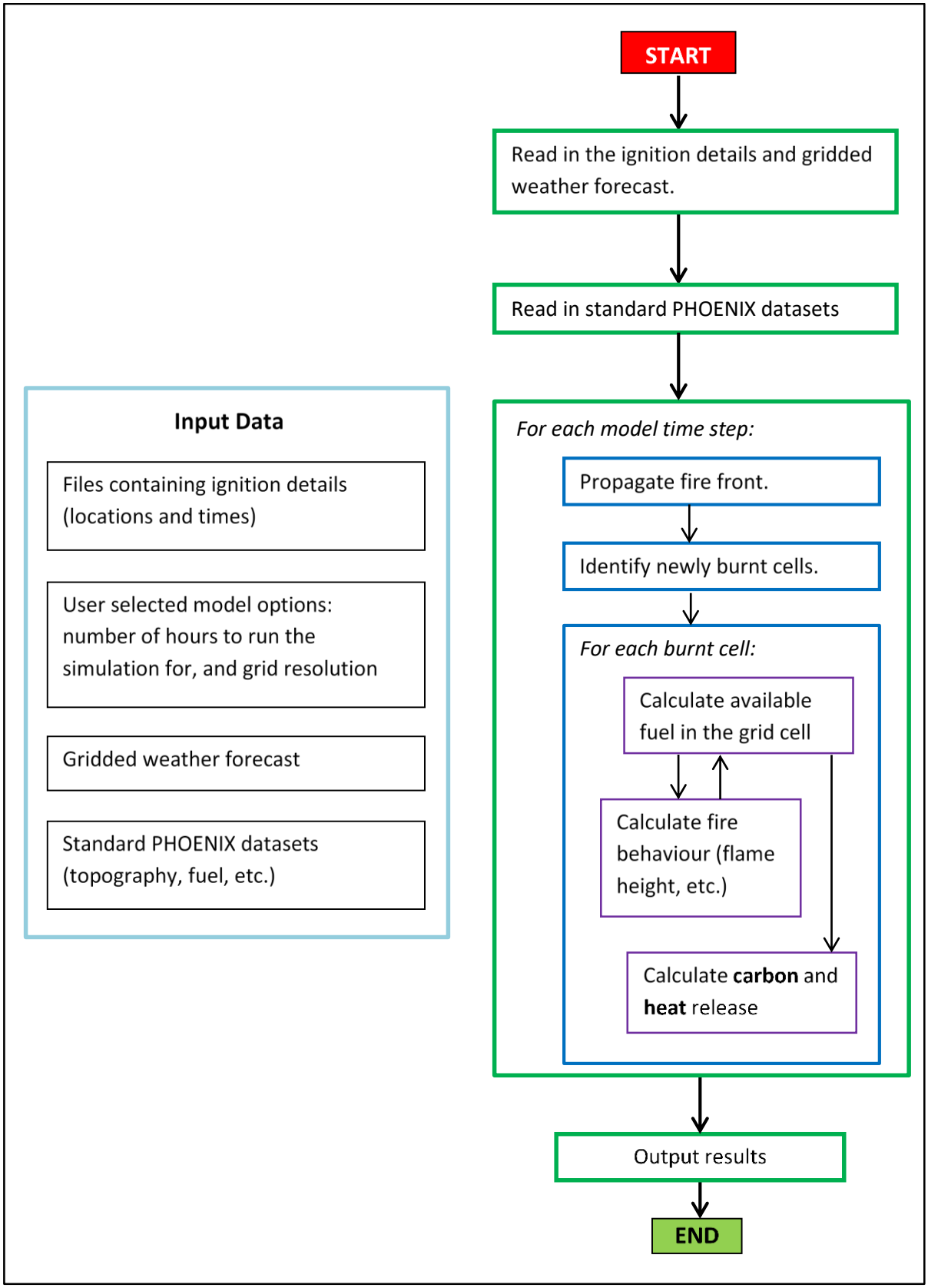

Figure 112 Overview of the system for modelling bushfire emissions.

Fuel loads and fuel consumption

The main factor affecting emissions from a bushfire is the rate at which fuel is consumed by the fire. Only 'fine' fuel is considered here, which includes dead fuels less than 6 mm thick and live fuels less than 2 mm thick *(Tolhurst and Cheney 1999)*. This section explains how vegetation fuel is handed within the fire simulation.

In the PHOENIX model, vegetation fuel is represented by two broad classes – forest and grassland. Sub-classes ("fuel types") are used to distinguish different levels of fine fuel load. Fuel types are derived by combining information on native vegetation, commercial plantations, land use patterns and urban areas *(Tolhurst et al. 2012)*. Fine fuel load refers to the mass of fine vegetation fuel per unit area, usually expressed in tonnes per hectare (t/ha).

Fine fuel is further classified into 'strata' (Figure 113). For grasslands, all fuel is assigned to a single stratum (*grass*), whilst for forests, three strata are used (*surface*, *bark* and *elevated*, with *surface* including both surface litter fuels and near-surface fuels). Note that canopy fuels are not included in the PHOENIX model.

For each of these strata, fine fuel load is mapped across Victoria at 30 m resolution, using vegetation type and the time since the last fire at each location *(Tolhurst et al. 2007)*. The PHOENIX fire history input data file is used in the calculation of time since fire at each point in the landscape, which is simply the time difference between the most recent fire at that location, and the time of the fire simulation.

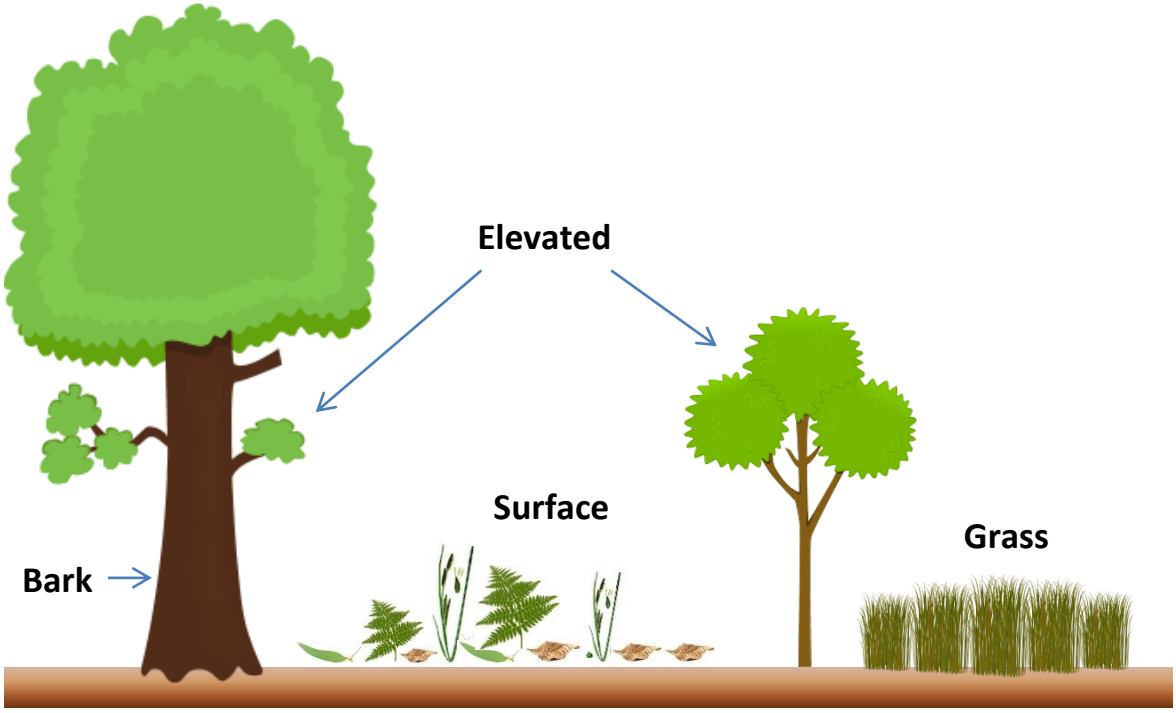

Figure 113 Fine fuel strata in the PHOENIX model. Canopy fuel loads are excluded.

A further step is needed to calculate the amount of fuel that is 'available' to be burnt by fire. In general, when fire passes over a section of the landscape, only some of the total fuel will be dry enough to burn. This is accounted for by applying a fuel availability factor; with different factors used for grass fuels and forest surface fuels.

For grass fuels, fuel availability is determined by the fraction of grass that has reached a 'cured' state, expressed as a percentage from 0-100% *(Martin et al. 2009; Anderson et al. 2011)*. For forest surface fuels, availability is determined by a 'drought factor', a value from 0-10, with 10 indicating that all fine fuel is available *(McArthur 1967; Finkele et al. 2006)*.

Both the level of curing and the drought factor are provided by the Bureau of Meteorology in daily

gridded weather forecasts. Within the PHOENIX model, the drought factor is modified to account for the effects of slope and aspect, as north to north-west facing slopes tend to be drier due to increased solar radiation.

The amounts of elevated and bark fuels consumed by fire are not adjusted by fuel availability factors but are dynamically adjusted using a function of modelled flame height. As flame heights increase, a greater proportion of the elevated (shrub) and bark fuels are included in the fire simulation.

Thus, the total amount of fuel consumed at a point in the landscape is a dynamic calculation, dependent not only on the fuel load (a function vegetation type and time since last fire), but also on weather forecasts (curing and drought factor) and fire behaviour (flame height).

Carbon and heat emissions

The amount of carbon released to the atmosphere is calculated by multiplying the fuel consumed in each stratum by a carbon mass fraction. The literature on carbon mass fractions in vegetation was reviewed, and suitable values for Australian fuels were chosen: 47.7% carbon for surface, elevated and bark fuels *(Thomas and Martin 2012)* and 31.0% carbon for grass fuels *(Eslemont et al. 2007)*. Further details can be found in *(Walsh et al. 2015)*.

The amount of heat released is determined by the amount of fuel consumed multiplied by a Heat Yield value (H). A generic value of H=18,700 kJ/kg is used here *(Alexander 1982)*, consistent with values reported elsewhere *(Sullivan et al. 2002; Morandini et al. 2013)*.

Heat yields are typically measured by calorimetry and describe the average heat release over flaming and smouldering combustion, with an adjustment to subtract the latent heat from vaporisation of water in the fuel. There is some evidence to suggest that heat release during smouldering is higher than during flaming *(Ohlemiller and Corley 1994)*, indicating that flaming-phase heat yields should be lower than the average value. However, due to a lack of studies confirming this effect in Australian fires, no correction has been made to the H value.

A further factor relates to the direction of released heat. It is expected that whilst most of the emitted heat will be released upwards and will influence plume rise, some will be lost downwards to the soil. Using an average of published data *(Burrows 1999)*, the total heat release was reduced by 6.5% to account for downward heat loss.

Model outputs

To simplify the interface between this software and atmospheric models, emission results are converted to hourly data. For carbon and heat emissions, this is a simple total over all time steps within each hour. To determine an emission location, a weighted centroid is computed over all model grid cells burnt in each time step during the hour.

If a time step is split over two hours (e.g. 2:58 pm to 3:11 pm), the results are partitioned and allocated to both hours according to the number of minutes falling within each hour. Hourly results are written to a CSV (comma separated values) file.

Version 1.0.0.2 of the software also generates two additional files, one which provides a summary of fire behaviour, emissions and cumulative burnt area for each model time step, and another which provides spatial details of all the model grid cells that were burnt during each time step.

Example results

The following figures illustrate how carbon and heat emissions are generated for the simulation of the Kilmore East fire, a severe event which occurred on Black Saturday (7th Feb 2009). The fire simulation begins at 11:45 am and runs to 10:00 pm, burning 44,049 ha. (Note that the actual Kilmore East fire was significantly larger than this, partly because of pyrocumulus cloud development and consequent lightning ignitions which are not represented in the model). More details about this case study can be found in the project progress report *(Walsh et al. 2015)* and in a study prepared for the 2009 Victorian Bushfires Royal Commission *(Tolhurst 2009)*.

Progress of the simulation up to 4:14 pm, highlighting fire activity during one time step (4:04 pm to 4:14 pm), is shown earlier in this report (Figure 109). The weighted centroid corresponding to this time step is shown in Figure 114.

Weighted centroids for the entire fire simulation are shown in Figure 115, which shows how the path of emission locations follows the progression of the fire front.

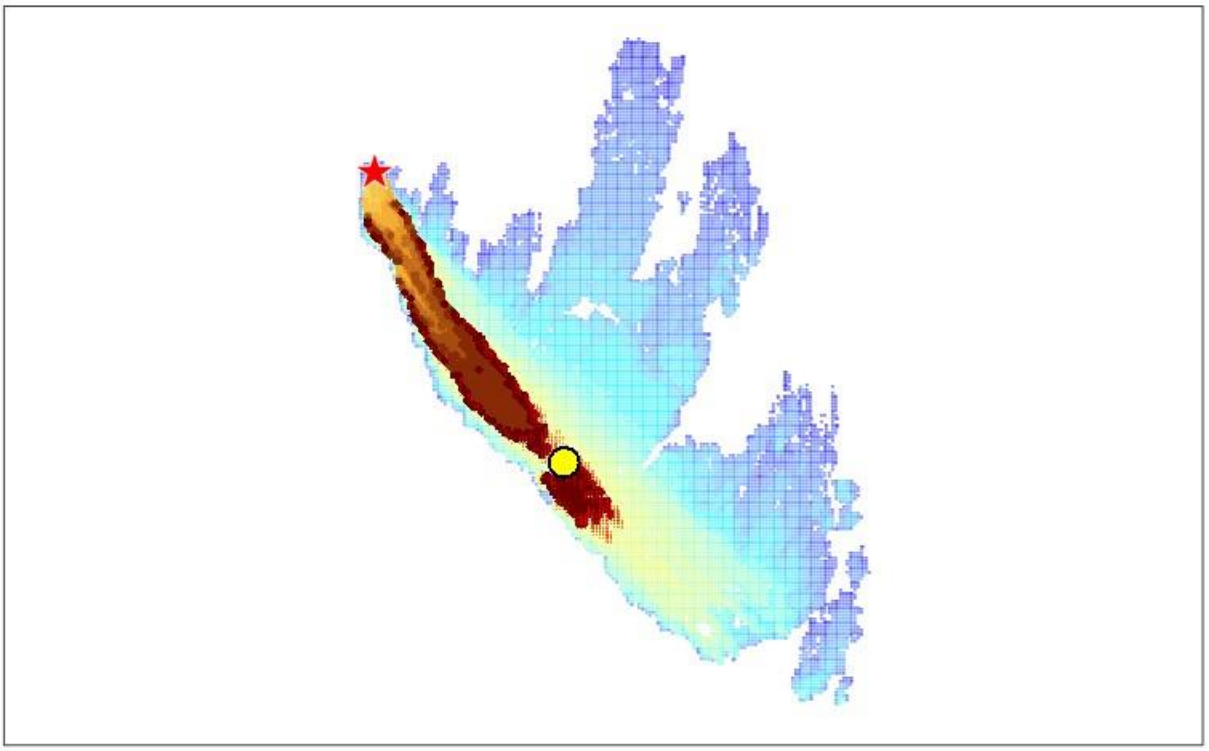

Figure 114 Example of a centroid (shown as a large yellow circle) used to represent one time step of the Kilmore East fire simulation (see Figure 109).

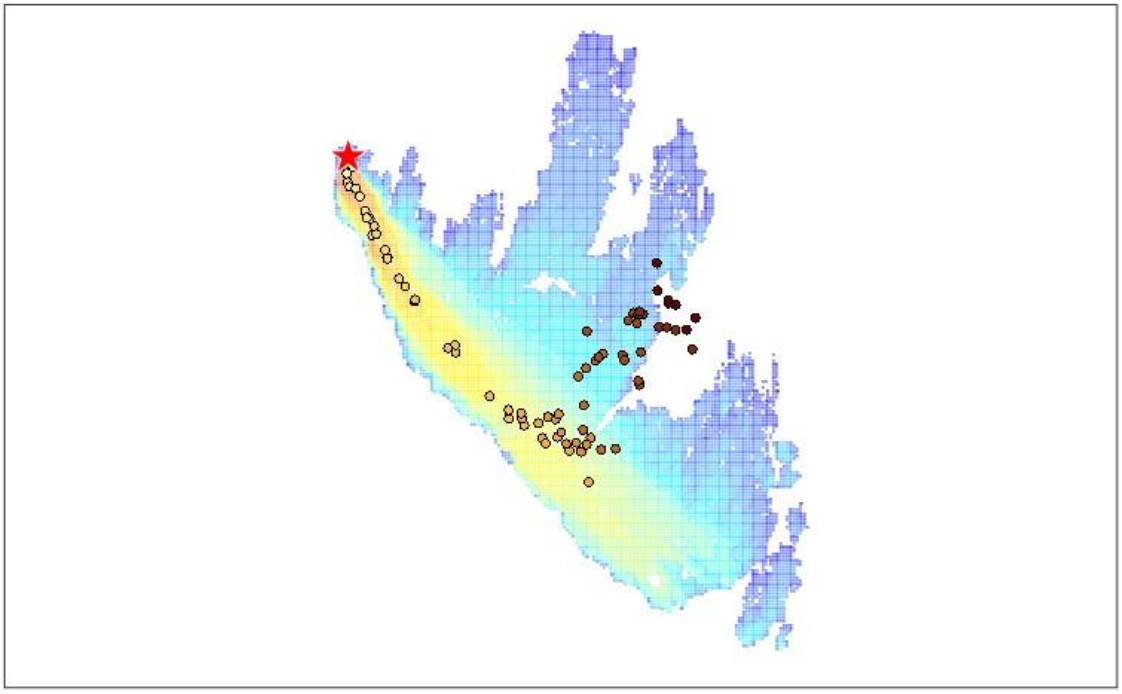

Figure 115 Path of weighted centroids over the duration of the fire simulation (the colour of circles indicates time progression).

Figure 116 shows the rate of fuel consumption during the Kilmore East fire simulation, expressed on a per-minute basis. Figure 117 shows the corresponding carbon and heat emission rates. Note that total heat release from the Kilmore East fire was extremely large (in this simulation, 20000 TJ).

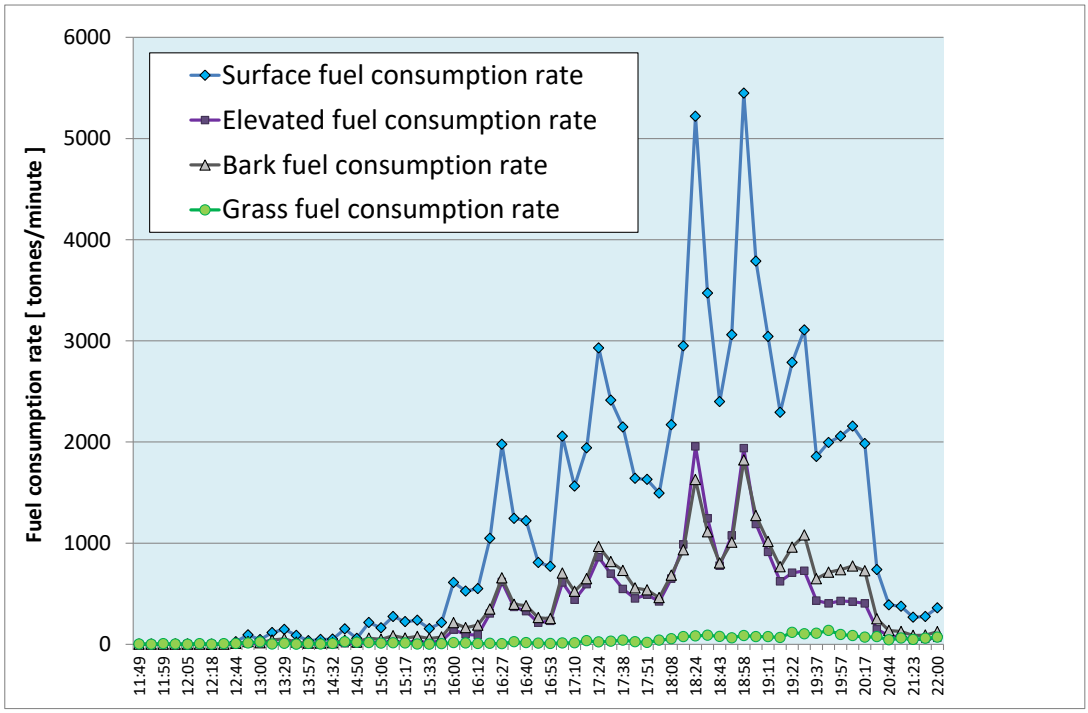

Figure 116 Predicted time series of fuel consumption (Kilmore East fire).

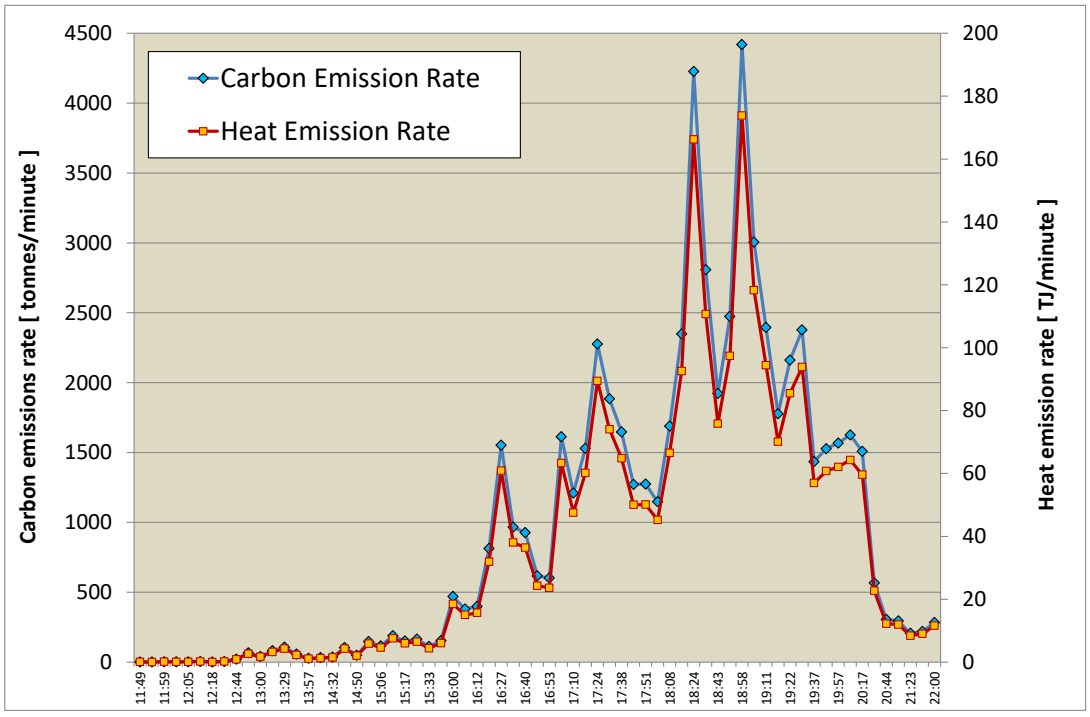

Figure 117 Predicted time series of carbon and heat emissions (Kilmore East fire).

Planned burn emissions model

Overview

The science of bushfire simulation is reasonably well established, with a number of models developed and in operation internationally. In contrast, very few models have been developed for simulating planned burns in a manner that would allow the calculation of fuel consumption and smoke emission rates during the burn.

One important study used a fire propagation model to drive an emissions model, achieving good results when compared with experimental fuel consumption rates *(Ferguson et al. 2001)*. However, as mentioned earlier, fire propagation modelling is not a suitable method due to the problems associated with determining an ignition pattern in advance of the burn.

Figure 118 Hand ignition at the McMahon's Creek burn (13-14 March 2015). The ignition pattern for a burn is typically decided on the day of the burn by the burn controller, with verbal instructions issued to ground and aerial ignition crews.

In Australia, the National Pollutant Inventory provides a simple technique which uses an average forest fuel load, the expected burn area and emission factors to estimate total emissions for specific pollutants *(EA 1999)*. This provides an estimate of the total fuel consumption and emissions, but not the rate of fuel consumption or emissions during the burn. Also, in this method, no account is taken of the effect of different weather conditions on fuel availability.

Given the lack of suitable models, a custom planned burn simulator was developed for this project. Some key components of the PHOENIX software (including fuel, topography, and weather) were used as the starting point for this development. In the process, a number of specific issues were identified and addressed, which are listed in Table 31.

Table 31 Development of the planned burn model – issues and solutions.

Model development issues	Approach / solution
The area within the burn boundary that is actually burnt is a key input for estimating emissions from fires *(Ottmar et al. 2008)*. In a typical burn, not all of the area within the boundary is treated with fire. Burn prescriptions usually include a target percentage of area to burn, the "Burn Coverage Objective", which can vary from 30-100%. Because the fuel load varies significantly within the boundary, the amount of fuel consumed depends critically on which areas actually burn. This is difficult to determine without a full fire simulation.	This problem is addressed by assuming that the Burn Coverage Objective will be achieved and using an "ignition strategy" to decide the order in which areas within the boundary are burnt. In the current version of the simulator, a map of predicted fuel moisture is prepared using a simplified physical model *(Matthews et al. 2010)*, and the software burns from 'dry' areas to 'wet' areas, until the coverage objective is reached. This ignition strategy is based on safe burning practice - dry areas need to be burnt early in the day when fire danger values are lower.
The number of days it takes to complete a burn and the timing of fire activity on each day are not known before the burn is conducted. A large burn may take several days to complete, and the timing often depends on a range of factors including local fuel and weather conditions, and external issues such as smoke complaints, which are difficult to predict in advance.	The burn model prepared for this study is designed to simulate a single day burn. This effectively assumes that a multi-day burn can be partitioned by the model operator into several blocks to be simulated separately on different days. It is also assumed that the model operator will be able to specify a start and end time for each single-day simulation.
The fuel availability at each location within the burn boundary needs to be estimated. This determines the fraction of surface fuel that is combustible, given the weather conditions at the time that fire reaches that location. Forecast weather and drought factor values from the Bureau of Meteorology are provided as hourly data, but only on a coarse grid (~2.3 km x 2.3 km, or about 530 ha per grid cell). This scale is not able to represent the variation in fuel availability in forested ridges and gullies.	This is addressed by using a recently developed feature of PHOENIX - an algorithm to downscale the forecast drought factor to account for canopy density, slope and aspect. As each part of the landscape is burnt in the simulation, the downscaled drought factor is calculated for the time of day that the location is burnt, thus making use of the hourly detail provided in the forecast, and the spatial detail provided by the downscaling algorithm.
The relative amounts of fuel consumed in each fuel stratum (Figure 113) is difficult to predict in a low intensity fire. This is likely to depend upon the burn prescription and on the ignition pattern decided by the burn controller.	The current model requires the software user to specify which fuel strata to include in the fire. It is assumed that this selection applies across the entire burn.
Forecast wind speed and direction are provided by the Bureau of Meteorology on a coarse grid, and do not account for the effects of local topography and vegetation. Wind speed is a key input into fuel moisture and fire behaviour calculations.	The existing PHOENIX approach is used, which involves two adjustments to the standard 10 m open-terrain wind forecast. The first adjustment involves the use of the *WindNinja* system, which is a mass-balance method to adjust wind vectors for the effect of hills and gullies on airflow *(Forthofer et al. 2010)*. The second adjustment (Wind Reduction Factor) is dependent on the vegetation type, and is used to estimate wind speed under the forest canopy at a height of 1.5 m. No corrections are made for local thermal effects such as anabatic or katabatic winds.

The rate of fuel consumption during the burn needs to be determined. The amount of area subject to flaming fire activity clearly begins at zero and ends at zero, but the time profile in between is unknown, and will depend heavily on the ignition process.	This is addressed by assuming a piecewise linear time profile for flaming fire activity *(Sandberg and Peterson 1984; Ng and Walsh 2002)*. The profile consists of three phases – a rapid ignition phase in which the flaming area increases linearly, a steady state phase in which flaming area remains roughly constant, and an extinction phase represented by a linear decrease in flaming area (see Figure 126 for an example profile).

With these issues addressed, the burn simulator was coded and tested. An overview of the simulator is shown in Figure 119. A burn simulation is able to generate estimates of total fuel consumption and hourly rates of carbon and heat release, as well as maps of the predicted burnt area. Carbon and heat emissions are calculated from fuel consumption in the same way as for bushfires.

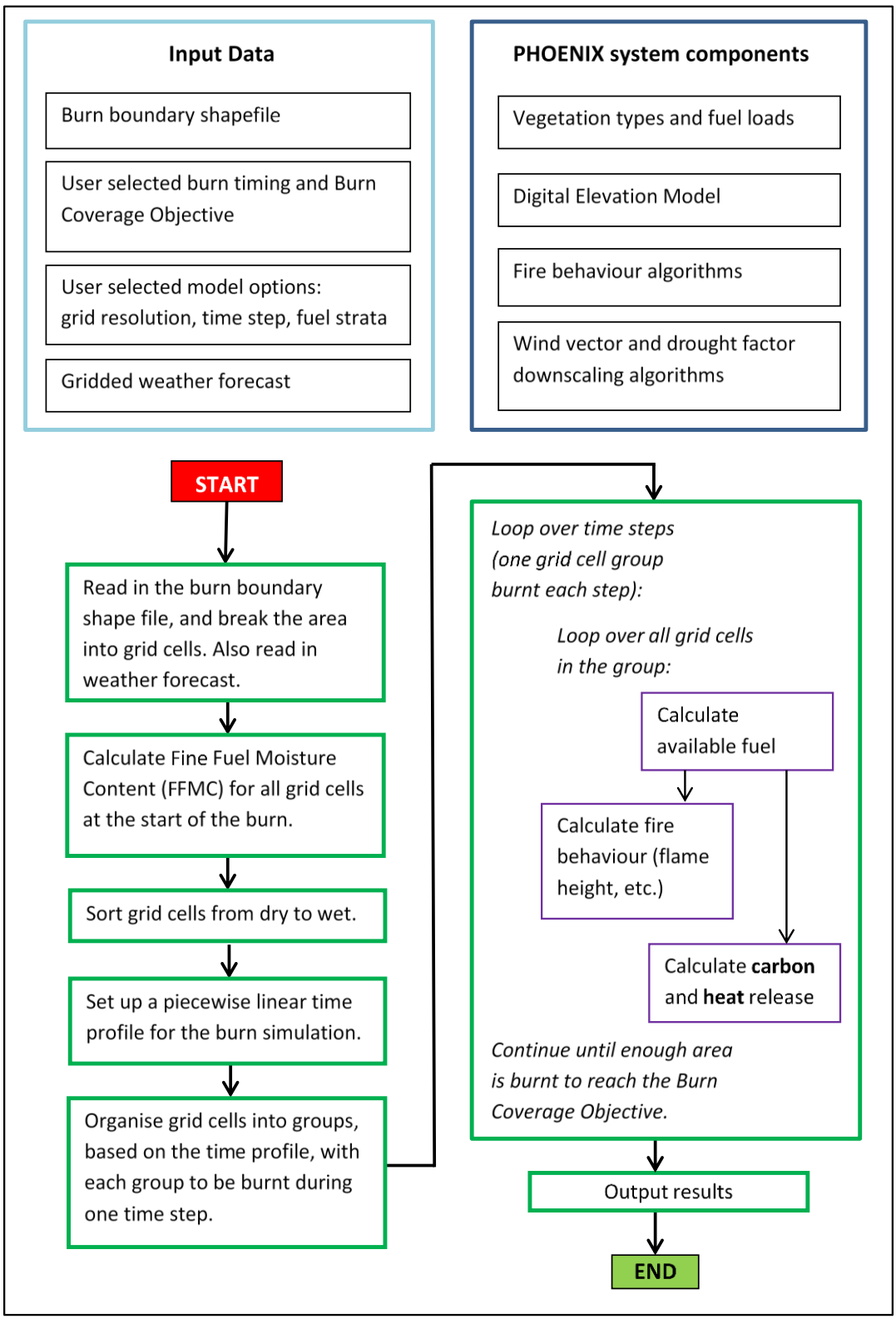

Figure 119 Overview of the system for modelling planned burn emissions.

Flame height and fireline intensity

As the burn simulator does not use fire propagation, fire behaviour calculations such as rate of spread, flame height and fireline intensity *(Byram 1959)* are not required in order to run the simulation. However, in order to provide information to assist with future research into fire behaviour and smoke emissions, estimates of flame height and fireline intensity are calculated and output along with carbon and heat emissions data.

In a PHOENIX bushfire simulation, flame height and fireline intensity are calculated using an adaptation of the McArthur Mk5 fire danger calculator *(McArthur 1967)*. The calculations account for the interaction of slope and wind, and also allow for dynamic inclusion of elevated and bark fuels according to flame height.

This approach is not suitable for planned burns, which typically involve much lower fireline intensities, outside the range of applicability of the Mk5 fire danger system. Therefore, for the burn simulator, the Mk5 calculator was replaced with McArthur Leaflet 80 controlled burning guide *(McArthur 1962)*. This guide is available in equation form *(Gould 1994)*, making it suitable for use in simulation systems. Leaflet80 equations were integrated into the burn simulator, with some minor modifications:

- The simple fuel moisture model in Leaflet 80 was retained to ensure compatibility with the fire behaviour calculations, except for the addition of a smoothing function applied between the hours of 11 am and 1 pm, to avoid unrealistic discontinuities in the transition between the desorption phase (6 am - midday) and absorption phase (after midday); and
- For determining the wind speed at 1.5 m above ground, the simple wind reduction relationship in Leaflet80 was replaced with the PHOENIX Wind Reduction Factor, allowing the under-canopy wind speed to vary with different vegetation types.

Flame height and fireline intensity results are calculated for each model grid cell as it is burnt in the simulation, with average results determined for each time step. These values are then converted into hourly averages, which are output along with carbon and heat release data.

Example results

The burn simulator was tested against a case study (Henderson Creek, Otway Ranges, Victoria) for which detailed ground-based and satellite observations have been made *(Loschiavo 2012)*. The burn boundary covered an area of 408 ha, within which a 343 ha study area was established. A ground-based GPS survey of the burnt edge was conducted, and RapidEye 5 m satellite imagery was obtained *(Tyc et al. 2005)* and processed by DEWLP staff to determine burn severity. The study area, observed burnt edge and burn severity data are shown in Figure 120.

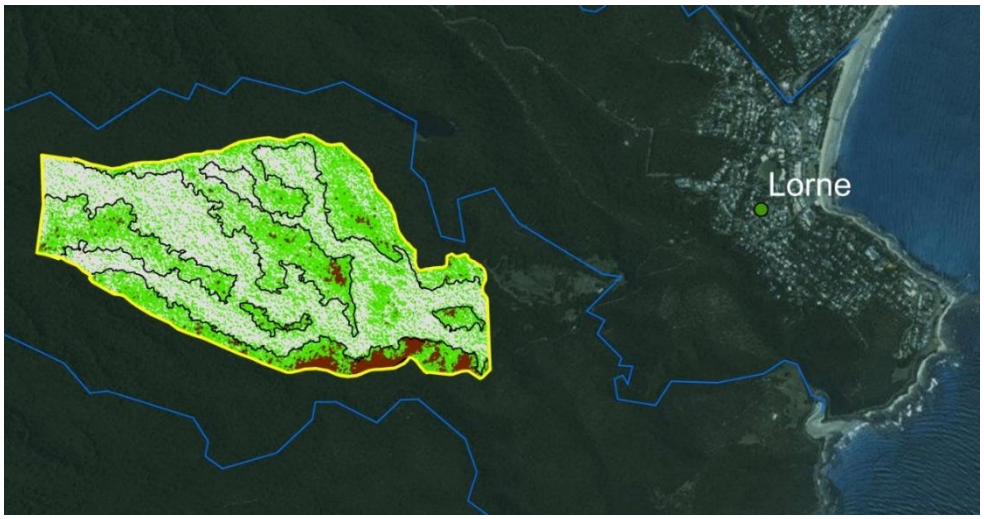

Figure 120 Henderson Creek study area (yellow b), ground-observed burnt edge (black lines), and satellite-derived burn severity (grey=unburnt, green=surface burnt with minimal or no canopy scorch, brown=extensive canopy scorch).

Except for one section towards the south-east of the study area, there is good spatial agreement between the burnt area as observed by the ground survey and the severity assessment, which were conducted independently. Based on the ground survey data, 49.5% of the study area was found to be burnt.

Figure 121 shows estimated fine fuel loads (surface + near-surface) before the burn, using the PHOENIX fuel model. The majority of the area was burnt in the 1983 Ash Wednesday fires, with no recorded fire activity in the 29 years from 1983 to 2012, resulting in significant fuel accumulation. There are two vegetation (fuel) types in the study area, "*Wet forest with shrub & wiregrass*" (wet forest) and "*Forest herb-rich*" (foothills forest), with estimated fuel loads of 24 t/ha and 14 t/ha respectively.

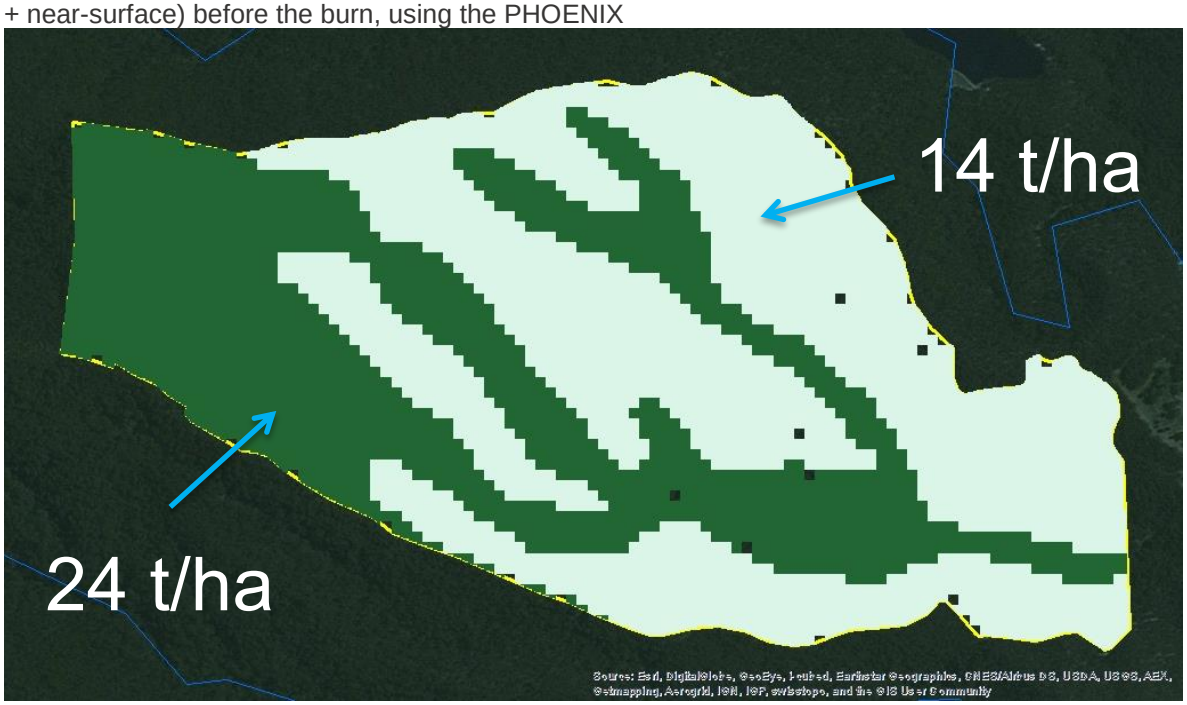

Figure 121 Model predicted surface + near-surface fine fuel loads.

The site includes a number of ridges and gullies, which can be seen in the topographic data used in PHOENIX (Figure 122). This data is used to derive slope and aspect, which are key inputs into fuel moisture and fire behaviour calculations.

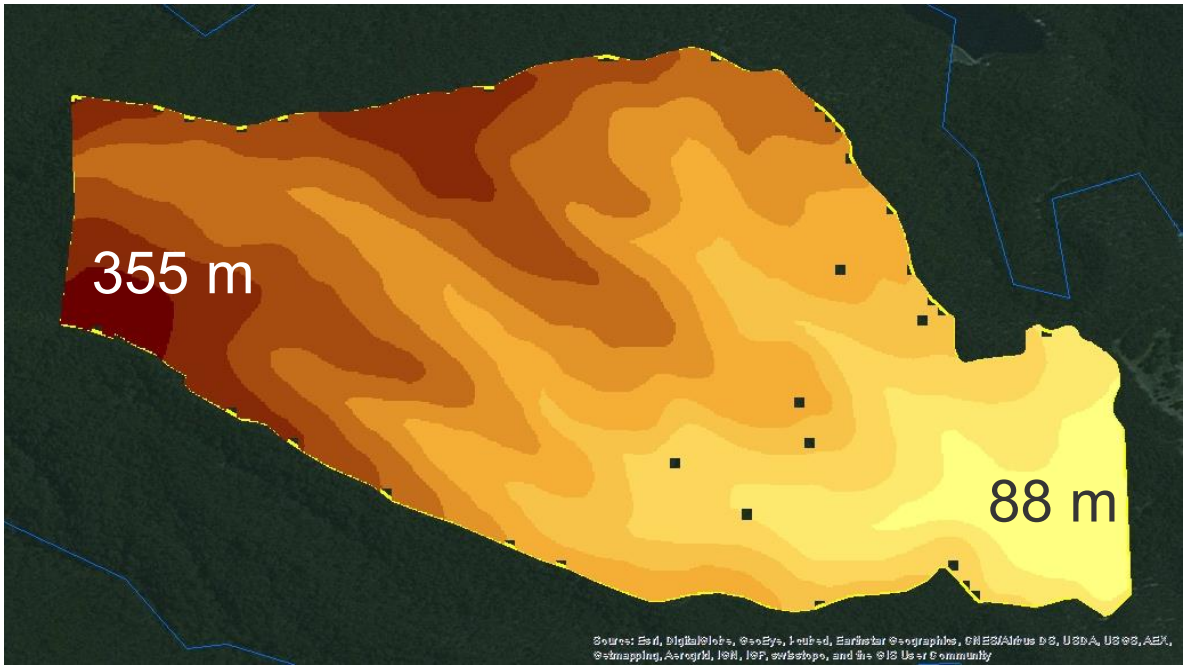

Figure 122 Digital elevation model.

Fuel availability was predicted to be highly variable across the site. Figure 123 shows the downscaled drought factor (0-10) at the start of the burn, with the highest values on north-facing slopes in the foothills forest type, and lowest values on south-facing slopes in the wet forest type.

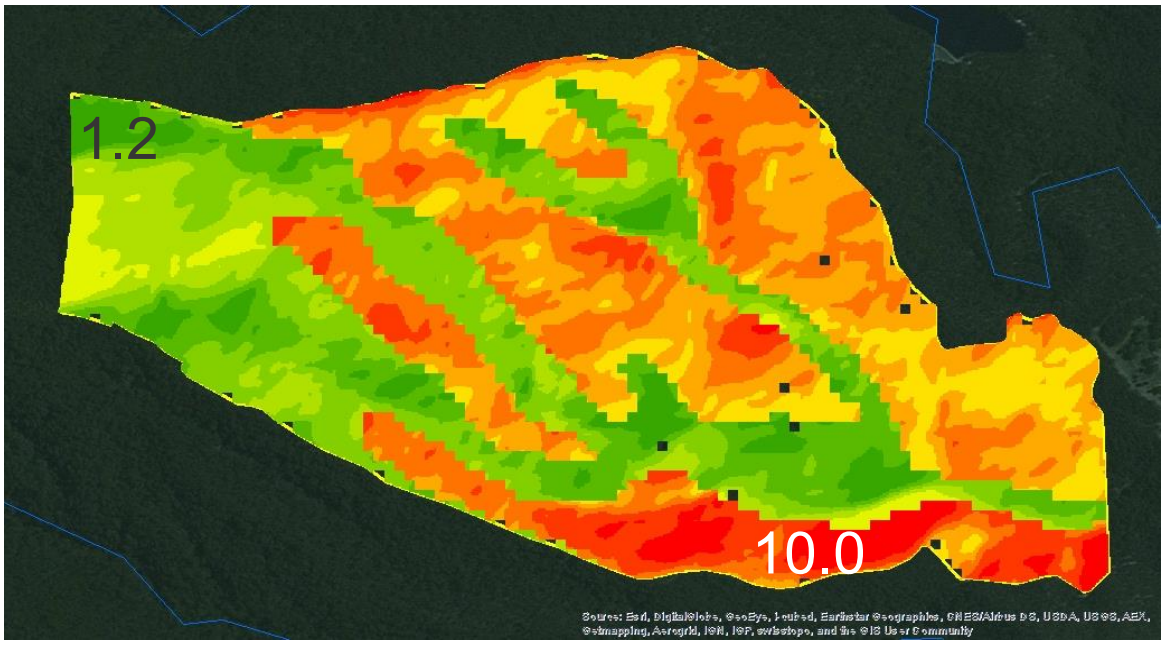

Figure 123 Predicted drought factor at the start of the burn.

Predicted fine fuel moisture content at the start of the burn is shown in Figure 124. The north-facing slopes towards the south of the site are predicted to be relatively dry, whereas the gullies within denser vegetation towards the west of the site are expected to be much wetter. The vertical artefact seen towards the middle-left of the image is actually the boundary of a grid cell from the gridded weather

forecast, which supplies wind speed, temperature and humidity. Wind speed is downscaled in the model, but temperature and humidity are not, resulting in some minor discontinuities.

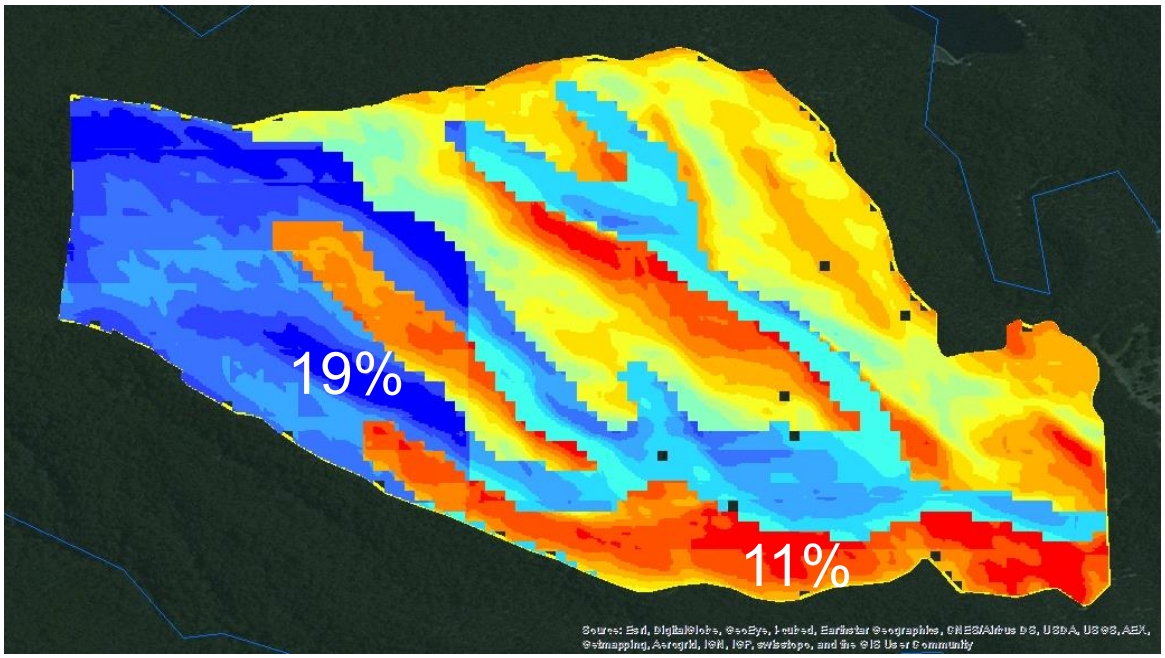

Figure 124 Predicted fine fuel moisture content (FFMC) at the start of the burn.

The first ignition for the 404 ha burn occurred at 11:55 am, but within the study area, the first ignition occurred at 1:00 pm, so the simulation was started at this time. This was actually a 2-day burn, but as the model is currently configured for single day burns only, the simulation was set up by assuming that all fuel was consumed on the first day (30th March 2012). This enables comparison of the model's spatial predictions with observed burn outcomes, although the predicted emission rates are likely to be higher than actual emission rates on the first day of the burn.

The simulation was set to run for 12 hours from 1:00 pm. BCO was set to 50% (the observed burnt fraction within the study area), with the intention of testing the model's spatial performance. The original burn coverage objective (specified in the burn prescription) was not suitable as input in this case, as it relates to the original 408 ha boundary, which is larger than the study area. A more comprehensive test of the model would involve checking predictions against burn outcomes for a range of burns under different conditions, using the original coverage objective values, but this has not been attempted here.

The default time step of 15 minutes was used, and default values were also used for the ignition time fraction (30%) and extinction time fraction (50%). The fuel strata selection was set to "S", so that only surface fuel would be burnt. The spatial resolution of the model was set to 5 m, to match the resolution of satellite imagery available for the site (Figure 125). Weather forecast files were chosen as the most recent predictions available prior to the burn, dated 29th March 2012 18:18 (UTC).

Figure 125 shows the burn boundary prediction, after running the model to completion, overlaid on the observed burnt area determined from the ground survey.

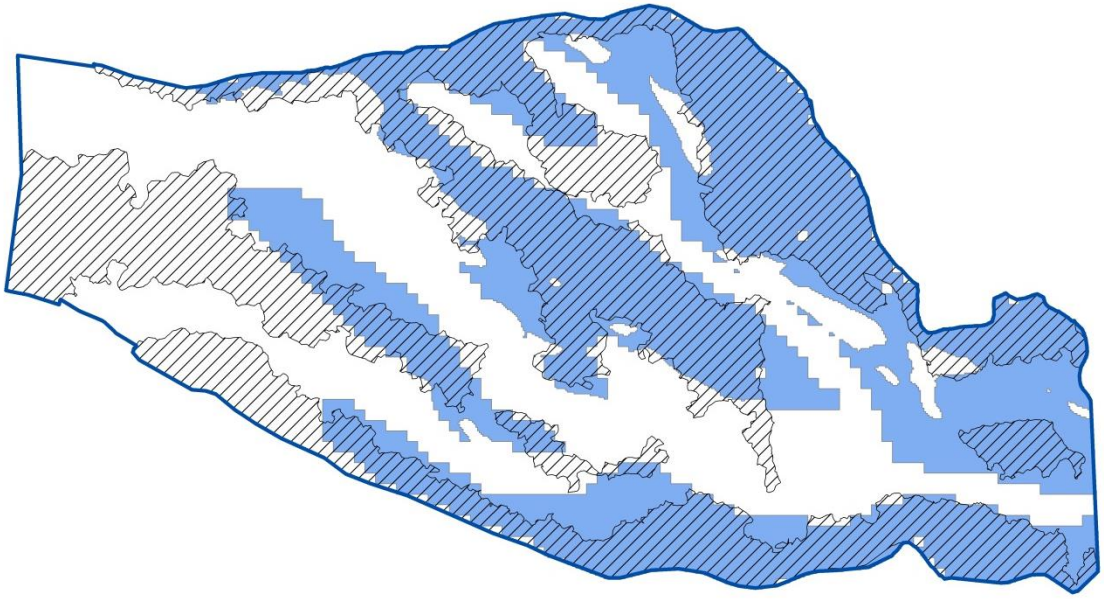

Figure 125 Predicted pattern of burnt area (blue), compared with ground-mapped burnt area (black lines).

The results show good agreement between the predicted boundary and the ground survey, except for the western area of the site, which was considered to have high fuel moistures in the model. Further investigation showed that this was because the vegetation in this area is a dense/wet forest type, and the shading factor assigned to this vegetation type is probably too high, particularly in north-facing areas[3].

Figure 126 shows the model predicted time profile of flaming area and carbon emissions for the Henderson Creek simulation. The area of flaming activity (blue curve) is assumed in the model to follow a piecewise linear profile, with the breakpoints of the profile being user adjustable (defaults are 30% of time spent in the 'Ignition Phase', and 50% of time spent in the 'Extinction Phase').

[3] Further research is currently underway to improve the canopy shading algorithm. Early results indicate a significant improvement can be achieved in the spatial prediction for this case study.

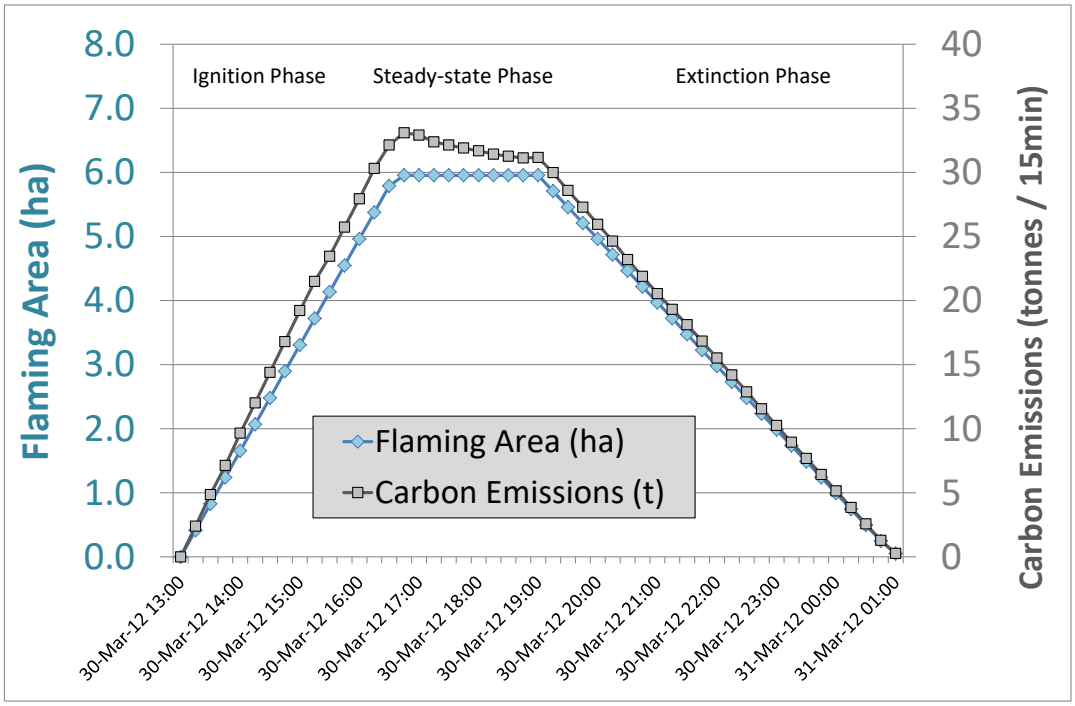

Figure 126 Henderson Creek burn - predicted time sequence of fire activity.

Because the fire simulation begins with dry areas and progresses to wet areas, the fire moves through areas of different fuel load and fuel availability. In this simulation (undertaken with a Burn Coverage Objective of 50%), the dry areas tend to have higher fuel availability (drought factor). This is why the rate of carbon emissions (grey curve) is higher during the early stages of the simulation.

Carbon and heat emissions results for each time step were then converted to hourly emission values (Figure 127).

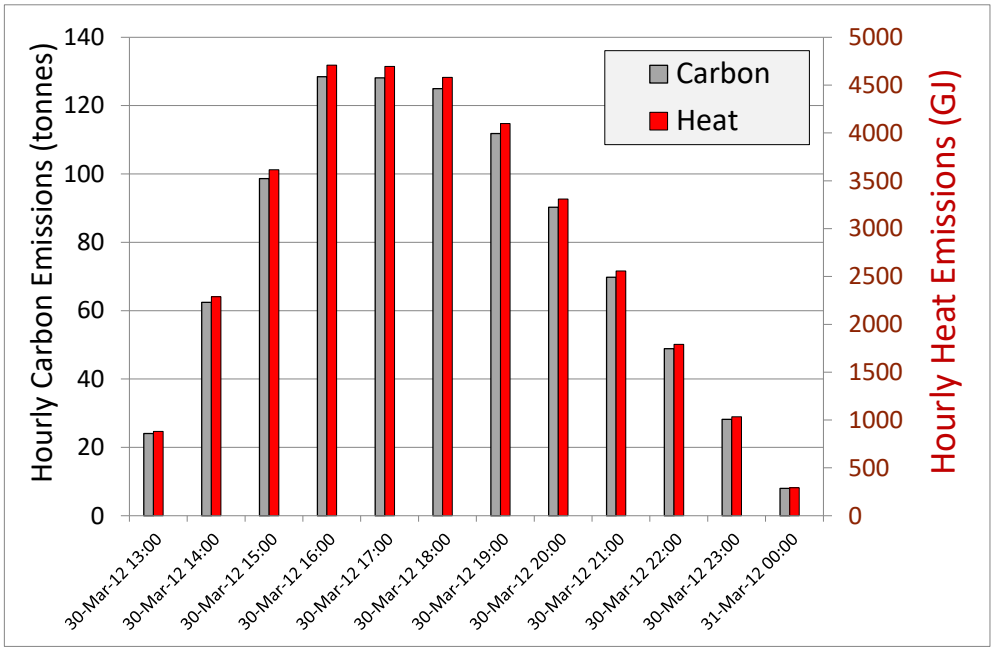

Figure 127 Henderson Creek burn - predicted hourly carbon & heat emissions.

No Australian data could be found to enable testing of the time profiles of carbon and heat emissions. In theory the total fuel consumption can be evaluated from field measurements of pre- and post-burn fuel loads, but this requires an exact consistency between the field method and the model definition of fuel, which is difficult to achieve in practice. For example, in the Henderson's Creek study, litter fuel loads were carefully measured but near-surface fuel loads were not, thus complicating the comparison of measured fuel loads with the combined surface and near-surface data within PHOENIX.

Table 32 shows the total carbon and heat emissions predicted for the Henderson Creek burn. For comparison, results are also derived using the default fuel loading for forests in Victoria (7.22 t/ha) in the National Pollutant Inventory (NPI) Emissions Estimation Manual *(EA 1999)*. For the NPI-based calculation, a 50% burn coverage was assumed, and commonly used values were chosen for carbon fraction (0.5) and heat yield (18,700 kJ/kg), with no correction for downward heat loss.

Table 32. Comparison of predictions with a simple NPI-based method

	PHOENIX FireFlux	**NPI Emissions Estimation Manual**
Total carbon emissions (tonnes)	924	618
Total heat emissions (TJ)	33.9	23.1

In this case, the prescribed burn simulator gives higher results than the NPI method because the total available surface fuel load within the simulated burnt area (after accounting for the drought factor) is estimated at 11.3 t/ha, which is higher than the NPI default fuel loading of 7.22 t/ha. Clearly, the burn simulator provides much greater flexibility in dealing with different vegetation types, although verification is needed to test predictions of total and available fuel across a range of forest types and weather conditions. Further work is currently being undertaken to identify suitable data from Victorian burns that will allow model verification.

Software implementation

Supported operating systems

The bushfire model and planned burn model have been combined together into a software package called PHOENIX FireFlux (v1.0.0.2, 4th May 2016). This software is available on Microsoft Windows 7 and LINUX, in the form of an executable file and a set of standard input data files. PHOENIX FireFlux operates via a command-line interface only and does not contain a graphical user interface.

The LINUX version is available with scripts providing a simpler command-line interface. This version makes use of template XML files, which are edited automatically by the script to insert key details such as the user's chosen spatial resolution and weather forecast file. It also generates a log file which records the progress of the simulation, including diagnostic messages where necessary.

To make the code more portable across different platforms, some code changes were made, mainly to deal with different file pathname conventions (e.g. "/" is used in LINUX whereas "\" is used in Microsoft systems). However, these changes were not sufficient to make the software accessible on other platforms, because the code is written in .NET, a Microsoft-specific framework.

The problem of converting the software to LINUX was solved by using the "Mono" open-source .NET implementation, which supports LINUX, Android and other non-Microsoft systems *(Easton and King 2004; Mamone 2005)*. Mono must be installed before the software will operate on a LINUX platform.

The model has been successfully implemented on the NCI (National Computational Infrastructure) *Raijin* supercomputer, and the University of Melbourne *Edward* supercomputer. These systems run CentOS LINUX.

Running the model – operation, inputs and outputs

Appendix 1 describes the command-line arguments used to control the two models provided in the software. The bushfire model can be operated by simply specifying a set of ignition points and a fire duration, but the planned burn model requires somewhat more detailed information, including a burn boundary and the expected timing, duration and area coverage of the burn.

As with the operational version of PHOENIX, the software also expects a number of key data files to be present to provide details of vegetation fuel, topography, barriers to fire propagation (such as roads) and fire history. The software makes use of standard gridded weather forecast files for Victoria

which are available on a daily basis from the Bureau of Meteorology *(BoM 2015)*.

The bushfire model outputs the following data:

- A CSV file containing carbon and heat emissions, fire activity centroid locations and fire behaviour parameters, aggregated over each hour (*_fire_activity_HOURLY.csv)
- A CSV file containing carbon and heat emissions, fire activity centroid locations, fire behaviour parameters and cumulative burnt area, aggregated over each model time step (*_fire_activity_TIMESTEPS.csv)
- A CSV file detailing the location of all the grid cells burnt during each model time step (*_fire_activity_BURNTCELLS.csv)
- Standard PHOENIX outputs indicating the spatial results of the prediction:
    - A Google Earth file (*.kmz)
    - A static image of the fire prediction (*_img.png, *_img.pgw, and *_img.png.aux.xml)
    - If required, spatial output files (see SHPOPT setting in *run_bushfire_model.bash*):
        - Shapefiles containing the model predictions as grid cells (*_grid.shp, *_grid.shx, etc)
        - Shapefiles containing the model predictions as points (*_pts.shp, *_pts.shx, etc)

The planned burn model outputs the following data:

- The same three “fire activity” files described above (*_fire_activity_HOURLY.csv, *_fire_activity_TIMESTEPS.csv and *_fire_activity_BURNTCELLS.csv)
- Shapefiles representing the spatial model predictions (*_burn.shp, *_burn.shx, etc). These files summarise fire behaviour and landscape parameters for the burnt area. To see spatial information over the entire burn polygon, set the burn coverage objective to 100%.

Software ownership

The PHOENIX model and its derivatives are jointly owned by the Department of Environment, Land, Water and Planning (50%), the University of Melbourne (25%) and the Bushfire & Natural Hazards CRC (25%). This software is copyright and must not be copied or distributed without permission from the owners.

Prediction uncertainty and model limitations

Underlying system components and data

The emissions models presented in this study rely on an adequate representation of vegetation fuels, and on assumptions about which vegetation elements are consumed by fire and converted to carbon and heat.

Vegetation types in PHOENIX are represented by broad fuel types *(Tolhurst et al. 2012)*, but there may be significant variation in the extent of live and dead fuels due to local micrometeorology, and extended interface zones (ecotones) between vegetation types. Apart from the downscaling of drought factor (fuel availability) using slope and aspect, very little of this fine-scale variation is represented in the model. Vegetation types are mapped at 30m resolution across Victoria, which should be adequate for most applications.

The fuel accumulation curves used in PHOENIX require accurate information on time since the last fire. This is coded in the “Fire History” input file, which needs to be kept up to date by the software operator. The time since last fire is used in separate fuel accumulation calculations for surface fuel (which includes near surface), elevated fuel and bark fuel.

The models also rely on a gridded weather forecast, in the Australian Digital Forecast Database format *(BoM 2015)*. A standard forecast includes temperature, relative humidity, wind speed and direction, cloud cover, grass curing, drought factor (fuel availability) and the Keetch-Byram Drought Index (KBDI) *(Keetch and Byram 1968)*. Due to the nature of numerical weather forecasting, uncertainty in some parameters (such as KBDI and drought factor, which are dependent on rainfall) may be higher than for other parameters.

Within PHOENIX, forecast wind vectors are downscaled to account for the effect of hills and gullies on airflow, using a mass-balance method *(Forthofer et al. 2010)*. The forecast drought factor is downscaled using a function of vegetation type, KBDI, slope and aspect, in order to represent the increased fuel availability on dry north-facing and north-west-facing slopes. No attempt is made to

downscale cloud cover, grass curing, KBDI or temperature.
More details about the input data and assumptions used in the PHOENIX model can be found in a Bushfire CRC report *(Tolhurst et al. 2007)*. These limitations must be kept in mind when using the PHOENIX FireFlux system for predictions of carbon and heat emissions from fires.

Bushfire model

Modelling the future development of a bushfire contains inherent uncertainties. This is partly due to uncertainties in the input data (such as weather forecasts and fuel loads), but also due to the highly non-linear nature of fire propagation, which can make simulations sensitive to initial conditions *(Dunn 2007)*.

In a fire model, the internal representation of key processes can also affect model uncertainty. For example, in a severe bushfire where the seeding of spot fires is a major factor, the development of the fire will be sensitive to the rate of ember production *(Rochoux et al. 2014)* and the probability of an ember igniting a spot fire, which is affected by fuel moisture and local wind speed *(Ellis 2015)*. Simulations will therefore be sensitive to the internal parameterisation of these processes.

A common source of uncertainty in bushfire simulation is the initial fire location. For example, an observer who is travelling on a road may see a smoke plume, but be unable to estimate the actual fire location. In this situation it is common for the fire location to be recorded as occurring on the road, or at a nearby intersection. If such a location is used directly as the ignition point for a simulation, then depending on the accuracy of the location record, it may result in a fire being started very close to the road but on the upwind side, causing the fire to spread a short distance before being extinguished by the road barrier. This and other problems are addressed in operational fire forecasting by employing specialist Fire Behaviour Analyst (FBAN) staff, who review inputs to simulations, and verify and approve forecast outputs before they are used in decision making.

The accuracy of weather forecasts can significantly affect fire predictions, and one approach is the use of an automatically generated weather ensemble *(Finney et al. 2011)*. However, the full range of uncertainty in a fire prediction will be larger than that associated with weather variations *(Salvador et al. 2001; Bachmann and Allgöwer 2002; Jones et al. 2004; Cruz and Alexander 2013)*. Some work has been undertaken to examine the sensitivity of PHOENIX fire predictions to factors such as ignition location, ignition time, model resolution, fuel load and weather, showing complex interactions between wind and slope in forest fire simulations *(Chong et al. 2013)*.

The bushfire model assumes that once flame heights reach 1 m, elevated and bark fuels will be accessible to the fire, and that for flame heights above 2 m, all elevated and bark fuels will be consumed. This assumption is likely to be reasonable for many forest types, except for heathlands with very low canopy heights, and wet forests with a very tall shrub layer. Also, in a bushfire that has developed into a crown fire, some or all of the canopy biomass will be consumed, but as canopy fuel loads are not represented in the model, this component will be missing from the emission estimates.

The model of emissions presented here considers only flaming phase fuel consumption, and only includes fine fuel *(Tolhurst and Cheney 1999)*. In severe bushfires, the greatest level of fire activity will occur on a small number of days during which fire weather is extreme, which is often only a single day. Therefore, in terms of the overall smoke emission rate, it is likely that emissions based on the flaming phase consumption of fine fuel should provide a good approximation to the highest smoke emission rates during a rapidly developing bushfire. Predictions are likely to be less accurate for prolonged fire events involving significant coarse fuel consumption.

Note that the perimeter-ignition feature in version 1.0.0.2 of the software is based on a rarely-used feature of PHOENIX RapidFire, and as such needs to be used with some care. So long as input perimeters are clockwise polygons, fire propagation will always be outward from the perimeter. However, there is a known limitation with PHOENIX perimeter ignitions, which can result in a small number of embers being generated from backing fire, which subsequently land within the perimeter causing a small amount of fire activity in already burnt ground. The net contribution to carbon and heat emissions is generally very small. For long running fires, ignition from an observed perimeter is likely to generate much more accurate predictions than starting from a point some days prior.

A further important consideration is that bushfires are often subject to active fire suppression. Whilst PHOENIX includes features to enable simulation of suppression, the current configuration of the model assumes that no suppression will be applied. This should be a reasonable approximation for very large and severe fires, for which suppression is often ineffective. For less intense fires where suppression is more successful, the model may generate an overestimate of flaming phase fine fuel consumption and smoke emissions.

Prescribed burn model

The burn simulator uses a simplification of the original Matthews fuel moisture model *(Matthews et al. 2010)* which does not accept rainfall as input, but instead calculates the dynamic exchange of moisture between the fuel and the atmosphere. This means the absolute values of predicted fuel moisture content may be too low (dry) in the days after recent rain. However, fuel moisture predictions are only used here in a relative spatial sense to decide on a burn sequence, so there is likely to be little impact on burn model predictions.

The simulator is best suited to medium to large sized burns, where the ignition process is likely to follow a broad strategy. For small burns which are intensively managed because they are close to residential areas or other sensitive land uses, the model is unlikely to be able to predict the pattern of burnt area (unless the Burn Coverage Objective is very high). Intensively managed burns can include special interventions including highly customised ignition patterns, and sprinklers to protect specific areas. For these burns, a conservative (upper) estimate of carbon and heat emissions can be obtained by using a Burn Coverage Objective of 100%.

As the simulator does not attempt to predict which way a fire will propagate (for example, down or up a particular slope in the landscape), flame height and fireline intensity data need to be treated with caution. These results are best used in a relative rather than absolute sense. For example, the spatial pattern of predicted fireline intensity will reflect variations in fuel load and fuel availability but will not be able to represent the effect of the burn controller's decisions about the type of fire to use (backing, flanking or head fire), or ignition point spacing. Similarly, temporal variations in weather will be represented in changes in predicted fire behaviour during the burn, but the results will not reflect variations in how fire has been applied over this time.

A further limitation is that the sequence of the burn is determined only by an initial map of fuel moisture at the start of the burn. During the progress of a burn, some areas that were initially 'wet' may become 'dry', resulting in differences between the model representation and the true pattern of fuel moisture. This can be overcome to some extent by adjusting the scan time, which is one of the command-line arguments available in the model (see Appendix A).

As the burn model uses a simple piecewise linear function to represent fire activity and assumes that the user can specify the burn start and end time, there is likely to be some uncertainty associated with the timing of the burn, and the rate of fuel consumption. This aspect of model operation will require significant expert judgement. The two breakpoints in the piecewise linear function (Figure 126) can be adjusted through command-line arguments, which may be useful in representing differences between burns in terms of the intensity of ignition effort.

Finally, a fundamental assumption of the burn simulator is that the Burn Coverage Objective (specified in advance of the burn) will accurately reflect the proportion of area burnt within the boundary. Often this objective is specified in the burn prescription as a range of values, reflecting the difficulty of achieving a precise level of coverage. The uncertainty associated with the coverage objective can be represented by running an ensemble of simulations with different BCO values specified via the command-line interface.

Model verification – issues and challenges

The bushfire and prescribed burn emission models presented here are to be considered preliminary and approximate in nature, with significant future work required to determine model accuracy against experimental data.

A number of Australian studies have measured and characterised smoke downwind from bushfires *(Walsh 2004; Meyer et al. 2012b)* and planned burns *(Ross et al. 1980; Reisen et al. 2011; Reisen et al. 2013)*. Direct plume samples can also be taken from the edge of low intensity fires *(Hansen et al. 2007)*. However, very few estimates are available for the smoke emission rates from an entire fire.

As direct measurement of the total fire emission rate is not practical, indirect estimation methods are needed. One costly but effective approach is to use aircraft-based measurements to sample a plume

cross-section, which can be combined with wind measurements to estimate a pollutant flux. Assuming no chemical loss, conservation of mass can be used to derive the rate at which the pollutant is emitted from the ground *(Ward and Radke 1993; Hurst et al. 1994)*.

Bushfire reconstructions may be useful for mapping the progress of a large fire front, enabling comparisons with model-predicted fuel consumption rates, although that has not been attempted here. Remote sensing data may also be useful for tracking bushfires, particularly a new geostationary satellite with 10-minute temporal resolution *(JMA 2015)*.

For planned burns, aerial surveys during the burn would provide key information on the progress of fire activity. Ground-based surveys of pre- and post-burn fuel load would also provide critical information about the total amount of fuel consumed (and thus the amount of smoke emitted), but these need to be conducted in a manner that is consistent with the PHOENIX fuel data. In particular, near-surface fuel loads need to be included as well as surface (litter) fuels, and for more intense burns, elevated and bark fuel loads will also need to be quantified.

Conclusions and recommendations

Key outcomes and findings

This project component has achieved a number of outcomes:

- An established bushfire simulator has been used to generate information on carbon and heat emissions during the progress of a simulated forest fire or grass fire;
- A new model has been developed which uses fuel moisture calculations, forecast weather and end-user constraints to simulate the progress of a planned burn, allowing calculation of carbon and heat emission rates; and
- The software has been successfully converted to LINUX and implemented on the target platform (Raijin).

In the process a number of knowledge gaps have been identified:

- There is a need for more comprehensive experimental data on overall smoke emission rates from Australian bushfires and prescribed burns, to support model verification.
- The net heat yield from burning forest fuels is often assumed to be a constant, however there may be variations associated with fuel moisture content, differences between flaming and smouldering phases, and the dynamic effects of downward heat loss to soil and unburnt surface materials, which need further experimental and theoretical investigation.
- A number of studies have identified that flaming and smouldering combustion result in different smoke chemical profiles, however little information is available on the effect of variations *within* flaming fire activity (e.g. low intensity *vs* high intensity prescribed burns.)
- The ignition of a planned burn is a complex process involving the use of guidelines and expert judgement, but few records have been kept of the fine details of ignition locations and times, and it is unclear if the chosen ignition patterns vary from expert to expert (given the same conditions).

Recommendations for further development

The accuracy and range of applicability of the models presented in this project may be enhanced through further development.
For the bushfire model, it is suggested:

- that fire-weather interactions are considered, to the extent that they affect smoke production, heat release and plume buoyancy *(Achtemeier et al. 2012; Kochanski et al. 2015)*;
- that research is undertaken to examine the effect of bushfire suppression on fire propagation, smoke emission rates and smoke chemistry *(Kalabokidis 2000)*; and
- that the model be enhanced to run ensemble forecasts, where ensemble members are automatically generated to vary ignition location, key model parameters (such as spatial resolution) and weather (if external ensembles are not available).

For the planned burn model, it is suggested:

- that alternative ignition strategies are explored, including burning from high fuel availability to low fuel availability, and multi-stage strategies such as burning the perimeter followed by burning from high elevation to low elevation (a method commonly used on larger burns);

- that alternative sequencing approaches are considered, such as the use of FFDI instead of time for sequencing the burn (i.e. burn areas of low fuel moisture at times of lower FFDI, and areas of high fuel moisture at times of higher FFDI);

- that burn coverage objectives are verified against burn outcomes to determine the extent of variation from the target, or as an alternative approach, that the model is configured to burn until a threshold of fuel moisture is reached, which would avoid the need for a coverage objective, but would require significantly greater accuracy in FMC predictions;

- that research is undertaken to find methods for predicting whether head fire, flank fire or backing fire will be used at each location within the burn;

- that the model is extended to simulate multi-day burns, by repeating the fuel moisture scan at appropriate intervals during the simulation, and recreating the sequence for burning the remaining grid cells; and

- that the use of fire propagation simulation be explored, by including additional physics relevant to planned burns (such as the junction zone effect) and developing methods for automatically predicting a range of plausible ignition patterns for a specific burn.

For both models, it is suggested:

- that carbon and heat release rates are experimentally verified, using a range of methods including ground and satellite observations of smoke plumes, downwind measurements of smoke concentrations, and (where possible) direct measurement of plume composition;

- that fine fuel loads for each vegetation type are experimentally verified, considering both total fuel load and fuel availability under various weather and fuel moisture conditions;

- that models of coarse fuel load accumulation and coarse fuel availability are developed and verified in a range of forest types;

- that the dynamics of smouldering phase emissions be included *(Ward and Hardy 1991; Ferguson and Hardy 1994; Urbanski 2014)*, with quantification of smouldering combustion rates for both coarse fuel and the wetter layers of fine fuel; and

- that current techniques for downscaling weather and fuel moisture be further refined, to examine fine-scale environmental and landscape factors such as:
    - Localised rainfall, runoff and throughfall, which affect the wetting of forest fuels;
    - Canopy height and density, which affect solar radiation reaching the ground, a key influence on the drying of forest fuels; and
    - Under-canopy temperature, humidity and wind speed at various heights, which affect fire behaviour and the moisture dynamics of surface, near-surface and elevated fuels

Appendix G1 – Software user interface

Bushfire Model (LINUX version)

Usage

run_bushfire_model.bash JOBNAME POINTCSV
[PERIMETERCSV [RUNHOURS [RESOLUTION [WEATHERDIR]]]]

JOBNAME = Your chosen name for this run (no spaces or non-alphanumeric characters; underscores are OK). The main purpose of this is to give sensible names to the output files.

POINTCSV = Name of the CSV file containing point ignitions.

The file must have a header, and contain one file per ignition. Each location will be considered a separate ignition. If DateTime is not supplied, then the current computer system datetime will be used for the ignition.

If you want to run with a Perimeter ignition only, with no points, set this argument to "NONE".

Format of POINTCSV file:

HeaderLine (must be present, but content does not matter)
Longitude,Latitude[,DateTime]
Longitude,Latitude[,DateTime]
Longitude,Latitude[,DateTime]
...

PERIMETERCSV = (OPTIONAL) Name of a CSV file containing PERIMETER ignitions for the simulation.

This file must have a header, then describe each perimeter ignition, starting with the keyword "PERIMETER" and ending with the keyword "END".

The points in a perimeter must form a CLOCKWISE POLYGON, ideally a closed polygon. Each perimeter ignition should have a datetime, on the same line as the PERIMETER keyword, separated by a comma, but if this is missing, the current computer system date will be used.

If this parameter is left blank then the system will use the point ignition file only. If both point and perimeter ignitions are provided, then both sets of data will be used in the simulation. If you don't want to provide a perimeter file but want to use subsequent optional command line arguments, set this parameter to "NONE".

NOTE : For the simulation to work, there must be either a POINTCSV file, a PERIMETERCSV file, or both files provided.

Format of PERIMETERCSV file (each perimeter must run clockwise):

HeaderLine (must be present, but content does not matter)

```
                PERIMETER[,DateTime]
                Longitude,Latitude
                Longitude,Latitude
                Longitude,Latitude
                Longitude,Latitude
                Longitude,Latitude
                Longitude,Latitude
                Longitude,Latitude
                Longitude,Latitude
                END
                PERIMETER[,DateTime]
                Longitude,Latitude
                Longitude,Latitude
                Longitude,Latitude
                Longitude,Latitude
                END
                ...

RUNHOURS = (OPTIONAL) Number of hours to run the simulation for.
                      This can be a fraction, e.g. 1.5 = 90 minutes. If this
                      argument is not supplied, the model will run for 12 hours.

RESOLUTION = (OPTIONAL) Phoenix model grid resolution, defaults to 180m.

WEATHERDIR = (OPTIONAL) Override the default location for weather data. By default
                        this script will set up the weather directory so that the
                        latest GFE files are used (i.e. most up to date forecast).
```

Example

```
run_bushfire_model.bash Mickleham.csv NONE 5.0 180 ~/WEATHER/2014-02-10
```

Planned Burn Model (LINUX version)

Usage

```
run_planned_burn_model.bash JOBNAME BOUNDARY STARTDATE STARTTIME DURATION COVERAGE
                            [BURNSTRATA
                            [IGNITIONFRAC
                            [EXTINCTNFRAC
                            [RESOLUTION
                            [SCANTIME
                            [TIMESTEP
                        [WEATHERDIR]]]]]]]

JOBNAME = Your chosen name for this run (no spaces or non-alphanumeric characters;
          underscores are OK.) The main purpose of this is to give sensible names
          to the model output files.

BOUNDARY = Name of the set of ESRI SHAPE files that define the boundary of the
           target area. Must include the .shp extension.

STARTDATE = Date of first ignition, in the format dd-mmm-yyyy or dd/mm/yyyy
```

NOTE: This date can be anytime in the future, so long as you have a weather forecast available in the gridded weather (GFE) file.

STARTTIME = Time of first ignition, in the format hh:mm (24 hr clock) in LOCAL TIME

DURATION = Expected burn duration, as number of hours of flaming fire activity.

COVERAGE = Intended % of the target area to be burnt (Burn Coverage Objective). If the Burn Prescription involves a range of values (e.g. 40%-59%), use an average, or run the model more than once.

BURNSTRATA = (OPTIONAL) Fuel strata to include in the fire. Each type of fuel is represented by a single character, S=Surface,E=Elevated, B=Bark,G=Grass. Default is S (Surface fuel only). Examples:

SE = Surface + Elevated
SEB = Surface + Elevated + Bark
SB = Surface + Bark
SEBG = Surface + Elevated + Bark + Grass

IGNITIONFRAC = (OPTIONAL) Fraction of flaming hours in "ignition" phase (linear ramp-up). This should be a number between 0.0 to 0.95. Default 0.3 (30%)

EXTINCTNFRAC = (OPTIONAL) Fraction of flaming hours in "extinction" phase (linear ramp-down). This should be a number between 0.05 to 1.0. Default 0.5 (50%)

RESOLUTION = (OPTIONAL) Phoenix resolution, defaults to 30m. If you make this too small, you will run out of memory. If you make this too large, the burn profile algorithm will break down and you will see warnings and errors in the log file.

NOTE: To run at resolutions finer than 25m on Raijin, you need to clip the fuel layer to the burn boundary, to reduce memory usage. Clipping the fuel layer has to be done manually and requires editing of the XML file.

SCANTIME = (OPTIONAL) When to undertake the initial fuel moisture scan, in hours from the start of the burn. Used to decide what areas to burn first. Defaults to 0.0 hours (i.e. start of burn).

TIMESTEP = (OPTIONAL) Time step for burn simulation in minutes. Defaults to 15 minutes. Do not make this too small, or the burn profile algorithm will break down and you will see warnings and errors in the log file.

WEATHERDIR = (OPTIONAL) Override the default location for weather data. By default this script will set the weather directory so that the latest GFE files are used (most up to date forecast).

Examples

```
run_planned_burn_model.bash MyBlock MyBoundary.shp 30-Mar-2015 11:55 12 59 SEB
```

```
This will run a simulation starting at 11:55am on 30th March 2015, running for 12 hours
with a burn coverage objective of 59%, and including surface, elevated & bark fuels.
```

```
run_planned_burn_model.bash SmallBlock Small.shp 15/4/2015 13:00 8 100
```

```
This will run a simulation starting at 1:00pm on 15th April 2015, running for 8 hours,
with a burn coverage objective of 100%, burning only surface fuel.
```

```
run_planned_burn_model.bash LargeBlock Big.shp 2-Apr-2014 13:30 16.5 35 SE 0.5 0.4
```

```
This will run a simulation starting at 1:30pm on 2nd April 2014, running for 16 hours,
with a burn coverage objective of 35%, burning surface & elevated fuel, and with the
first 50% of the burn in ignition phase (linear ramp up of flaming area), and the last
40% of the burn in extinction phase (linear ramp down, fires gradually going out).
```

Operating the Windows 7 version

To operate the Windows 7 version, type the name of the executable file and you will be given a list of command-line options. Using the model this way is not straightforward as an XML file must be prepared with suitable settings (including weather, grid resolution, simulation date-times etc).
Also, for bushfire modelling, the point and perimeter ignition CSV files are not specified to the executable via command line arguments; instead the model looks for specific file names. These file names must be constructed by appending the strings _POINT.csv and _PERIMETER.csv to the stem of the project XML file name, e.g. TEST.xml, TEST_POINT.csv and TEST_PERIMETER.csv.
Please contact the University of Melbourne if further assistance is required.

```
*********************************************************************
*                                                                   *
*      >>>>>>>>>>     PHOENIX FireFlux v1.0.0.2    <<<<<<<<<<      *
*                                                                   *
*      Incorporating:                                               *
*                                                                   *
*                 > PHOENIX RapidFire 4.0.0.8 bushfire simulator    *
*                 > Prescribed burn simulator - beta version        *
*                 > Carbon and Heat fluxes                          *
*                                                                   *
*      (C) University of Melbourne, 2015,2016                       *
*                                                                   *
*********************************************************************

USAGE:

PH_FireFlux.EXE /FIRE CONTROL.XML [Duration_Hrs]

or :

PH_FireFlux.EXE /BURN CONTROL.XML Boundary.SHP StartDate
                      StartTime Duration_Hrs Burn_Coverage_Objective_%

                      [Strata to Burn(S[E][B][G])
                      [Fraction of burn hours in ignition phase
                      [Fraction of burn hours in extinction phase
                      [Time of initial fuel moisture scan (hours from start)
                      [Time Step in minutes
                      [Fire Type for output files (B/F/H) ]]]]]
```

References

ABS (2004). Year Book Australia, 2004. Australian Bureau of Statistics.

Achtemeier GL, Goodrick SA and Liu Y (2012) Modeling Multiple-Core Updraft Plume Rise for an Aerial Ignition Prescribed Burn by Coupling Daysmoke with a Cellular Automata Fire Model. *Atmosphere* **3**(3), 352-376.

AFAC (2016). 'A review of the management of the Tasmanian fires of January 2016'. (Australasian Fire and Emergency Service Authorities Council Limited: Melbourne).

Akagi SK, Yokelson RJ, Wiedinmyer C, Alvarado MJ, Reid JS, Karl T, Crounse JD and Wennberg PO (2011) Emission factors for open and domestic biomass burning for use in atmospheric models. *Atmospheric Chemistry and Physics* **11**(9), 4039-4072.

Alexander ME (1982) Calculating and interpreting forest fire intensities. *Canadian Journal of Botany* **60**(4), 349-357.

Amici S, Wooster MJ and Piscini A (2011) Multi-resolution spectral analysis of wildfire potassium emission signatures using laboratory, airborne and spaceborne remote sensing. *Remote Sensing of Environment* **115**(8), 1811-1823.

Anderson GK, Sandberg DV and Norheim RA (2004). Fire Emission Production Simulator (FEPS) User's Guide, Version 1.0. http://www.fs.fed.us/pnw/fera/feps/FEPS_users_guide.pdf.

Anderson SAJ, Anderson WR, Hollis JJ and Botha EJ (2011) A simple method for field-based grassland curing assessment. *International Journal of Wildland Fire* **20**(6), 804-814.

Andreae MO and Merlet P (2001) Emission of trace gases and aerosols from biomass burning. *Global Biogeochemical Cycles* **15**(4), 955-966.

Andrews P (1986). BEHAVE: fire behaviour prediction and fuel modelling system - BURN subsystem, part 1. General Technical Report INT-194. USDA Forest Service, Intermountain Forest and Range Experiment Station, Ogden, UT**:** 130 pp.

Aponte C, Tolhurst KG and Bennett LT (2014) Repeated prescribed fires decrease stocks and change attributes of coarse woody debris in a temperate eucalypt forest. *Ecological Applications* **24**(5), 976-989.

Aurell J, Gullett BK and Tabor D (2015) Emissions from southeastern US Grasslands and pine savannas: Comparison of aerial and ground field measurements with laboratory burns. *Atmospheric Environment* 111, 170-178.

Bachmann A and Allgöwer B (2002) Uncertainty propagation in wildland fire behaviour modelling. *International Journal of Geographical Information Science* **16**(2), 115-127.

Barbosa PM, Stroppiana D, Grégoire JM and Cardoso Pereira JM (1999) An assessment of vegetation fire in Africa (1981–1991): Burned areas, burned biomass, and atmospheric emissions. *Global Biogeochemical Cycles* **13**(4), 933-950.

Barrett DJ (2002) Steady state turnover time of carbon in the Australian terrestrial biosphere. *Global Biogeochemical Cycles* **16**(4), 1108-1108.

BCRC (2013). "Smoke transportation and emissions modelling." from http://www.bushfirecrc.com/projects/rc-10/smoke-transportation-and-emissions-modelling.

Beall FC and Eickner HW (1970). Thermal degradation of wood components: A review of the literature. Research Paper FPL 130, USDA Forest Service, Madison, Wisconsin., **:** 26 pp.

Bertschi I, Yokelson RJ, Ward DE, Babbitt RE, Susott RA, Goode JG and Hao WM (2003) Trace gas and particle emissions from fires in large diameter and belowground biomass fuels. *Journal of Geophysical Research-Atmospheres* **108**(D13), 8472-8472.

BNHCRC (2014). A three-tired smoke forecasting system for managing air pollution from planned burns, Bushfire and Natural Hazards CRC.

BoM (2015). Australian Digital Forecast Database (ADFD) User Guide. Bureau of Meteorology.

Boschetti L and Roy DP (2009) Strategies for the fusion of satellite fire radiative power with burned area data for fire radiative energy derivation. *Journal of Geophysical Research: Atmospheres* **114**(D20), D20302.

Burling IR, Yokelson RJ, Akagi SK, Urbanski SP, Wold CE, Griffith DWT, Johnson TJ, Reardon J and Weise DR (2011) Airborne and ground-based measurements of the trace gases and particles emitted by prescribed fires in the United States. *Atmospheric Chemistry and Physics* 11(23), 12197-12216.

Burrows N, Ward B and Robinson A (1995) Jarrah forest fire history from stem analysis and anthropological evidence. *Australian Forestry* **58**(1), 7-16.

Burrows ND (1999) A soil heating index for interpreting ecological impacts of jarrah forest fires. *Australian Forestry* **62**(4), 320-329.

Burrows ND (2001) Flame residence times and rates of weight loss of eucalypt forest fuel particles. *International Journal of Wildland Fire* **10**(2), 137-143.

Byram G (1959). Combustion of Forest Fuels. In 'Forest Fire: Control and Use'. (Eds K. P. Davis). pp. (McGraw Hill: New York)

Campos I, Vale C, Abrantes N, Keizer JJ and Pereira P (2015) Effects of wildfire on mercury mobilisation in eucalypt and pine forests. *Catena* **131**, 149-159.

Carter M, Howard T, Haylock K, Philpotts V and Richards J (2015). Independent Investigation of the Lancefield-Cobaw Fire. The State of Victoria, Department of Environment, Land, Water and Planning, Melbourne, VIC.

Chen LW, Moosmuller H, Arnott WP, Chow JC, Watson JG, Susott RA, Babbitt RE, Wold CE, Lincoln EN and Hao WM (2007) Emissions from laboratory combustion of wildland fuels: emission factors and source profiles. *Environmental Science & Technology* 41(12), 4317-4325.

Cheney N (1990) Quantifying bushfires. *Mathematical and Computer Modelling* **13**(12), 9-15.

Cheney NP, Gould JS, McCaw WL and Anderson WR (2012) Predicting fire behaviour in dry eucalypt forest in southern Australia. *Forest Ecology and Management* **280**, 120-131.

Chong D, Tolhurst KG, Duff TJ and Cirulis B (2013). Sensitivity analysis of PHOENIX RapidFire. Bushfire CRC.

Christian TJ, Kleiss B, Yokelson RJ, Holzinger R, Crutzen PJ, Hao WM, Saharjo BH and Ward DE (2003) Comprehensive laboratory measurements of biomass-burning emissions: 1. Emissions from Indonesian, African, and other fuels. *Journal of Geophysical Research-Atmospheres* 108(D23).

Cooke WF, Koffi B and Grégoire JM (1996) Seasonality of vegetation fires in Africa from remote sensing data and application to a global chemistry model. *Journal of Geophysical Research: Atmospheres* **101**(D15), 21051-21065.

Cope M, Lee S, Meyer CP, Wain A and Ebert B (2014). Short-term forecasting of fine particle exposure from prescribed burns and wildfires. Atmospheric Composition and Chemistry Observations and Modelling Conference, Aspendale, Victoria.

Cruz MG and Alexander ME (2013) Uncertainty associated with model predictions of surface and crown fire rates of spread. *Environmental Modelling and Software* **47**, 16-28.

Cruz MG, Sullivan AL, Gould JS, Sims NC, Bannister AJ, Hollis JJ and Hurley RJ (2012) Anatomy of a catastrophic wildfire: The Black Saturday Kilmore East fire in Victoria, Australia. *Forest Ecology and Management* **284**, 269-285.

CSIRO (2014). Smoke Emission and Transport Modelling Project - Interim Report M057.

CSIRO and University of Melbourne (2013). Collaborator Agreement - Smoke Transportation Modelling and Emissions Modelling for Victoria.

De Simone F, Cinnirella S, Gencarelli CN, Carbone F, Hedgecock IM and Pirrone N (2016) Particulate-Phase Mercury Emissions during Biomass Burning and Impact on Resulting Deposition: a Modelling Assessment. *Atmospheric Chemistry and Physics Discussions*, 1-22.

De Simone F, Cinnirella S, Gencarelli CN, Yang X, Hedgecock IM and Pirrone N (2015) Model Study of Global Mercury Deposition from Biomass Burning. *Environmental Science & Technology* **49**(11), 6712-6721.

Delaney W and Marshall A (2011). Victorian Air Emissions Inventory for 2006. 20th International Clean Air & Environment Conference, Auckland, New Zealand.

Delmas R, Lacaux JP and Brocard D (1995) Determination of biomass burning emission factors: Methods and results. *Environmental Monitoring and Assessment* **38**(2-3), 181-204.

Dennis R, Fox T, Fuentes M, Gilliland A, Hanna S, Hogrefe C, Irwin J, Rao ST, Scheffe R, Schere K, Steyn D and Venkatram A (2010) A framework for evaluating regional-scale numerical photochemical modeling systems. *Environmental Fluid Mechanics* **10**(4), 471-489.

Department of the Environment (2014). 'National Inventory Report 2012 Volume 1. The Australian Government Submission to the United Nations Framework Convention on Climate Change. Australian National Greenhouse Accounts'. (Commonwealth of Australia).

Dharssi I, Bovis KJ, Macpherson B and Jones CP (2011) Operational assimilation of ASCAT surface soil wetness at the Met Office. *Hydrology and Earth System Sciences* **15**(8), 2729-2746.

DoH (2013). "Bushfire smoke and your health." from http://docs.health.vic.gov.au/docs/doc/Bushfire-smoke-and-your-health.

Dozier J (1981) A method for satellite identification of surface temperature fields of subpixel resolution. *Remote Sensing of Environment* **11**(0), 221-229.

DSE (2011). Standard Operating Procedure 17. Measuring Soil on Ground Plots. . Department of Sustainability and Environment, Melbourne.

DSE (2012). Victorian Forest Monitoring Program Guidelines For Ground Plot Measurement Standard Operating Procedure 16. Measuring Coarse Woody Debris, Stumps and Slash Piles. Department of Sustainability and Environment, Melbourne.

Dunn A (2007). A model of wildfire propagation using the interacting spatial automata formalism. University of Western Australia.**Doctoral Thesis**.

EA (1999). NPI Emissions Estimation Technique Manual for Aggregated Emissions from Prescribed Burning and Wildfires. Environment Australia, Australian Governrment, Canberra.

Easton MJ and King J (2004). 'Cross-Platform .NET Development : Using Mono, Portable.NET and Microsoft .NET'. (Apress: Berkley, California).

Ellicott E and Vermote E (2012) The Science and Application of Satellite Based Fire Radiative Energy.

Ellicott E, Vermote E, Giglio L and Roberts G (2009) Estimating biomass consumed from fire using MODIS FRE. *Geophysical Research Letters* **36**(13), L13401.

Ellis PFM (2015) The likelihood of ignition of dry-eucalypt forest litter by firebrands. *International Journal of Wildland Fire* **24**(2), 225-235.

Engling G, Carrico CM, Kreidenweis SM, Collett JL, Jr., Day DE, Malm WC, Lincoln E, Hao WM, Iinuma Y and Herrmann H (2006) Determination of levoglucosan in biomass combustion aerosol by high-performance anion-exchange chromatography with pulsed amperometric detection. *Atmospheric Environment* **40**(Suppl. 2), 299-311.

Enright N, Goldblum D, Ata P and Ashton D (1997) The independent effects of heat, smoke and ash on emergence of seedlings from the soil seed bank of a heathy Eucalyptus woodland in Grampians (Gariwerd) National Park, western Victoria. *Australian Journal of Ecology* **22**(1), 81-88.

EPA Victoria (2015a). 'Summarising the air monitoring and conditions during the Hazelwood mine fire, 9 February to 31 March 2014: Publication 1598'. (Environment Protection Authority Victoria: Carlton, VIC).

EPA Victoria (2015b). 'Estimating air quality in the early stages of the 2014 Hazelwood mine fire: Publication 1599'. (Environment Protection Authority Victoria: Carlton, VIC).

Escuin S, Navarro R and Fernandez P (2008) Fire severity assessment by using NBR (Normalized Burn Ratio) and NDVI (Normalized Difference Vegetation Index) derived from LANDSAT TM/ETM images. *International Journal of Remote Sensing* **29**(4), 1053-1073.

Eslemont G, Maher W, Ford P and Lawrence I (2007) Riparian Plant Material Inputs to the Murray River, Australia. Composition, Reactivity, and Role of Nutrients. *Journal of environmental quality* **36**(4), 963-974.

Ferguson S and Hardy C (1994) Modeling Smoldering Emissions From Prescribed Broadcast Burns in the Pacific-Northwest. *International Journal of Wildland Fire* **4**(3), 135-142.

Ferguson SA, Peterson J and Acheson A (2001). Automated, real-time predictions of cumulative smoke impacts from prescribed forest and agricultural fires. 4th Symposium on Fire and Forest Meteorology. American Meteorological Society, Reno, Nevada, USA.

Finkele K, Mills GA, Beard G and Jones DA (2006) National gridded drought factors and comparison of two soil moisture deficit formulations used in

prediction of Forest Fire Danger Index in Australia. *Australian Meteorological Magazine* **55**, 183-197.

Finney MA, Grenfell IC, McHugh CW, Seli RC, Trethewey D, Stratton RD and Brittain S (2011) A Method for Ensemble Wildland Fire Simulation. *Environmental Modeling & Assessment* **16**(2), 153-167.

Forthofer J, Shannon K and Butler B (2010) Initialization of high resolution surface wind simulations using NWS gridded data. *Proceedings of 3rd Fire Behavior and Fuels Conference*, 25-29.

Freeborn PH, Wooster MJ, Hao WM, Ryan CA, Nordgren BL, Baker SP and Ichoku C (2008) Relationships between energy release, fuel mass loss, and trace gas and aerosol emissions during laboratory biomass fires. *Journal of Geophysical Research: Atmospheres* **113**(D1), D01301.

Freeborn PH, Wooster MJ, Roberts G, Malamud BD and Xu W (2009) Development of a virtual active fire product for Africa through a synthesis of geostationary and polar orbiting satellite data. *Remote Sensing of Environment* **113**(8), 1700-1711.

French NHF, Goovaerts P and Kasischke ES (2004) Uncertainty in estimating carbon emissions from boreal forest fires. *Journal of Geophysical Research: Atmospheres* **109**(D14), D14S08.

Friedli HR, Arellano AF, Cinnirella S and Pirrone N (2009) Initial Estimates of Mercury Emissions to the Atmosphere from Global Biomass Burning. *Environmental Science & Technology* **43**(10), 3507-3513.

Friedli HR, Radke LF, Lu JY, Banic CM, Leaitch WR and MacPherson JI (2003a) Mercury emissions from burning of biomass from temperate North American forests: laboratory and airborne measurements. *Atmospheric Environment* **37**(2), 253-267.

Friedli HR, Radke LF, Prescott R, Hobbs PV and Sinha P (2003b) Mercury emissions from the August 2001 wildfires in Washington State and an agricultural waste fire in Oregon and atmospheric mercury budget estimates. *Global Biogeochemical Cycles* **17**(2), 1039-1039.

Giglio L and Kendall JD (2001) Application of the Dozier retrieval to wildfire characterization: a sensitivity analysis. *Remote Sensing of Environment* **77**(1), 34-49.

Gill A (1981) Adaptive responses of Australian vascular plant species to fires. *Fire and the Australian biota*, 243-272.

Gould JS (1994) Evaluation of McArthur's control burning guide in regrowth Eucalyptus sieberi forest. *Australian Forestry* **57**(2), 86-93.

Gould JS, McCaw WL and Cheney NP (2011) Quantifying fine fuel dynamics and structure in dry eucalypt forest (Eucalyptus marginata) in Western Australia for fire management. *Forest Ecology and Management* **262**(3), 531-546.

Gould JS, McCaw WL, Cheney NP, Ellis PF, Knight IK and Sullivan AL (2007a). Project Vesta--Fire in Dry Eucalypt Forest: fuel structure, dynamics and fire behaviour. Ensis-CSIRO, Canberra ACT, and Department of Environment and Conservation, Perth WA**:** 228 pp.

Gould JS, McCaw WL, Cheney NP, Ellis PF and Matthews S (2007b). Field Guide: Fire in Dry Eucalypt Forest. Ensis-CSIRO, Canberra ACT, and Department of Environment and Conservation, Perth WA**:** 92 pp.

Griffith DWT (1996) Synthetic Calibration and Quantitative Analysis of Gas-Phase FT-IR Spectra. *Appl. Spectrosc.* **50**(1), 59-70.

GTOS (2000). from http://www.fao.org/gtos/.

Hansen D, Reisen F, Meyer M, Porter N and Elms T (2007). "Characterisation of Particle Emissions from the Combustion of Different Australian Vegetation." Retrieved 21 July 2015, from http://www.bushfirecrc.com/sites/default/files/managed/resource/dane-hansen-fabienne-reisen-mick-meyer.pdf.

Hao WM, Ward DE, Olbu G and Baker SP (1996) Emissions of CO2, CO, and hydrocarbons from fires in diverse African savanna ecosystems. *Journal of Geophysical Research: Atmospheres* **101**(D19), 23577-23584.

Hardy CC (2005) Wildland fire hazard and risk: Problems, definitions, and context. *Forest Ecology and Management* **211**(1-2), 73-82.

Harris S, Anderson A, Kilinc M and Fogarty L (2011). 'Establishing a link between the power of fire and community loss: the first step towards developing a bushfire severity scale'. (Victorian Government Department of Sustainability and Environment).

Haverd V, Raupach MR, Briggs PR, Canadell JG, Isaac P, Pickett-Heaps C, Roxburgh SH, van Gorsel E, Rossel RAV and Wang Z (2013) Multiple observation types reduce uncertainty in Australia's terrestrial carbon and water cycles. *Biogeosciences* **10**(3), 2011-2040.

Hays MD, Geron CD, Linna KJ, Smith ND and Schauer JJ (2002) Speciation of gas-phase and fine particle emissions from burning of foliar fuels. *Environmental Science & Technology* 36(11), 2281-2295.

Hines F, Tolhurst KG, Wilson AA and McCarthy GJ (2010). 'Overall fuel hazard assessment guide'. (Fire Management Branch, Department of Natural Resources and Environment).

Hobbs PV, Reid JS, Herring JA, Nance JD, Weiss RE, Ross JL, Hegg DA, Ottmar RO and Liousse C (1996). Particle and trace-gas measurements in the smoke from prescribed burns of forest products in the Pacific Northwest. In 'Biomass Burning and Global Change'. MIT Press, Cambridge, MA, pp. 697–715.

Holder AL, Hagler GSW, Aurell J, Hays MD and Gullett BK (2016) Particulate matter and black carbon optical properties and emission factors from prescribed fires in the southeastern United States. *Journal of Geophysical Research-Atmospheres* 121(7), 3465-3483.

Hollis JJ, Matthews S, Ottmar RD, Prichard SJ, Slijepcevic A, Burrows ND, Ward B, Tolhurst KG, Anderson WR and Gould JS (2010) Testing woody fuel consumption models for application in Australian southern eucalypt forest fires. *Forest Ecology and Management* **260**(6), 948-964.

Hosseini S, Urbanski SP, Dixit P, Qi L, Burling IR, Yokelson RJ, Johnson TJ, Shrivastava M, Jung HS, Weise DR, Miller JW and Cocker DR (2013) Laboratory characterization of PM emissions from combustion of wildland biomass fuels. *Journal of Geophysical Research-Atmospheres* 118(17), 9914-9929.

Hurst DF, Griffith DWT, Carras JN, Williams DJ and Fraser PJ (1994) Measurements of trace gases emitted by Australian savanna fires during the 1990 dry season. *Journal of Atmospheric Chemistry* **18**, 35-56.

Ichoku C, Giglio L, Wooster MJ and Remer LA (2008) Global characterization of biomass-burning patterns using satellite measurements of fire radiative energy. *Remote Sensing of Environment* **112**(6), 2950-2962.

Ichoku C and Kaufman YJ (2005) A method to derive smoke emission rates from MODIS fire radiative energy measurements. *Geoscience and Remote Sensing, IEEE Transactions on* **43**(11), 2636-2649.

Innis J, Cunningham A, Cox E, Hyde B and Porter T (2016). The January 2016 Tasmanian Bushfires - The Air Quality Perspective, Biomass Smoke in the Human Environment, Deloraine Workshop July 2016.

JMA (2015). "Himawari User's Guide." Retrieved 21 July 2015, from http://www.jma-net.go.jp/msc/en/support/index.html.

Jones SD, Garvey MF and Hunter GJ (2004) Where's the fire? Quantifying uncertainty in a wildfire threat model. *International Journal of Wildland Fire* **13**(1), 17-25.

Justice CJ, Giglio L, Korontzi S, Owens J, Morisette JT, Roy D, Descloitres J, Alleaume S, Petitcolin F and Kaufman YJ (2002) The MODIS fire products. *Remote Sensing of Environment* **83**, 244-262.

Kalabokidis KD (2000) Effects of Wildfire Suppression Chemicals on People and the Environment: A Review. *Global Nest International Journal* **2**(2), 129-137.

Kasischke ES and Bruhwiler LP (2002) Emissions of carbon dioxide, carbon monoxide, and methane from boreal forest fires in 1998. *Journal of Geophysical Research: Atmospheres* **107**(D1), 8146.

Kaufman YJ, Justice CO, Flynn LP, Kendall JD, Prins EM, Giglio L, Ward DE, Menzel WP and Setzer AW (1998) Potential global fire monitoring from EOS-MODIS. *Journal of Geophysical Research: Atmospheres* **103**(D24), 32215-32238.

Kaufman YJ, Setzer A, Justice C, Tucker CJ, Pereira MC and Fung I (1990). Remote Sensing of Biomass Burning in the Tropics. In 'Fire in the Tropical Biota'. (Eds J. Goldammer). pp. 371-399. (Springer Berlin Heidelberg)

Kaufmann Y, Remer L, Ottmar R, Ward D, Li R, Kleidman R, Fraser R, Flynn L, McDougal D and Shelton G (1996) Relationship between remotely sensed fire intensity and rate of emission of smoke: SCAR-C Experiment. *Biomass burning and global change* **2**, 685-696.

Keetch JJ and Byram GM (1968). A Drought Index for Forest Fire Control. U.S. Department of Agriculture - Forest Service Research Paper SE-38.

Keith D (1996). Fire-driven extinction of plant populations: a synthesis of theory and review of evidence from Australian vegetation. PROCEEDINGS-LINNEAN SOCIETY OF NEW SOUTH WALES, LINNEAN SOCIETY OF NEW SOUTH WALES.

Kennison KR, Wilkinson KL, Pollnitz AP, Williams HG and Gibberd MR (2009) Effect of timing and duration of grapevine exposure to smoke on the composition and sensory properties of wine. *Australian Journal of Grape and Wine Research* **15**(3), 228-237.

Kilinc M, Anderson WR, Anderson D and Price B (Unpublished) On the need for a bushfire scale that represents the bushfire hazard.

Kochanski AK, Jenkins MA, Mandell J, Beezley JD, Yedinak K and Lamb BK (2015). Smoke modelling in a coupled fire-atmosphere framework. 11th Symposium on Fire and Forest Meteorology, Minneapolis, USA, American Meteorological Society.

Kolka R, Sturtevant B, Townsend P, Miesel J, Wolter P, Fraver S and DeSutter T (2014) Post-Fire Comparisons of Forest Floor and Soil Carbon, Nitrogen, and Mercury Pools with Fire Severity Indices. *Soil Science Society of America Journal* **78**(1).

Korontzi S, Roy DP, Justice CO and Ward DE (2004) Modeling and sensitivity analysis of fire emissions in southern Africa during SAFARI 2000. *Remote Sensing of Environment* **92**(2), 255-275.

Langaas S (1993) A parametrised bispectral model for savanna fire detection using AVHRR night images. *International Journal of Remote Sensing* **14**(12), 2245-2262.

Larkin NK, O'Neill SM, Solomon R, Raffuse S, Strand T, Sullivan DC, Krull C, Rorig M, Peterson J and Ferguson SA (2009) The BlueSky smoke modeling framework. *International Journal of Wildland Fire* **18**(8), 906-920.

Lee S and Cope M (2014). Sensitivity analysis of dispersion predictions to emission model parameters, Smoke Emission and Transportation Modelling for Victoria - Milestone Report 019. Centre for Australian Weather and Climate Research.

Liu YQ, Achtemeier GL, Goodrick SL and Jackson WA (2010) Important parameters for smoke plume rise simulation with Daysmoke. *Atmospheric Pollution Research* **1**, 250-259.

Lobert JM and Warnatz J (1993) Emissions from the combustion process in vegetation. *Fire in the Environment: The Ecological, Atmospheric and Climatic Importance of Vegetation Fires*, 15-39.

Loschiavo J (2012). Comparing field-based and remote-sensed methods for mapping a prescribed burn. Department of Forest and Ecosystem Science. University of Melbourne.

Luke RH and McArthur AG (1978) Bush fires in Australia. *Bush Fires in Australia.*

Maier SW, Russell-Smith J, Edwards AC and Yates C (2013) Sensitivity of the MODIS fire detection algorithm (MOD14) in the savanna region of the Northern Territory, Australia. *ISPRS Journal of Photogrammetry and Remote Sensing* **76**, 11-16.

Mamone M (2005). 'Practical Mono'. (Springer-Verlag: New York).

Marris E (2016) Tasmanian bushfires threaten iconic ancient forests. *Nature* **530**(7589), 137.

Martin D, Grant I, Jones S and Anderson S (2009). Development of Satellite Vegetation Indices to Assess Grassland Curing Across Australia and New Zealand. In 'Australasian remote sensing and photogrammetry conference'. (Eds S. Jones and K. Reinke). pp. 211-228. (Springer: Heidelberg)

Matthews S (2010) Effect of drying temperature on fuel moisture content measurements. *International Journal of Wildland Fire* **19**(6), 800-802.

Matthews S, Gould J and McCaw L (2010) Simple models for predicting dead fuel moisture in eucalyptus forests. *International Journal of Wildland Fire* **19**(4), 459-467.

McArthur AG (1962). Control Burning in Eucalypt Forests : Leaflet No. 80. Forestry and Timber Bureau, Canberra.

McArthur AG (1967). Fire behaviour in eucalypt forests. Leaflet No. 107, Forestry and Timber Bureau, Canberra.

McCaw WL, Gould JS, Cheney NP, Ellis PFM and Anderson WR (2012) Changes in behaviour of fire in dry eucalypt forest as fuel increases with age. *Forest Ecology and Management* **271**, 170-181.

McMeeking GR, Kreidenweis SM, Lunden M, Carrillo J, Carrico CM, Lee T, Herckes P, Engling G, Day DE, Hand J, Brown N, Malm WC and Collett JL (2006) Smoke-impacted regional haze in California during the summer of 2002. *Agricultural and Forest Meteorology* **137**(1-2), 25-42.

McMeeking GR, Kreidenweis SM, Baker S, Carrico CM, Chow JC, Collett JL, Hao WM, Holden AS, Kirchstetter TW, Malm WC, Moosmuller H, Sullivan AP and Wold CE (2009) Emissions of trace gases and aerosols during the open combustion of biomass in the laboratory. *Journal of Geophysical Research-Atmospheres* 114.

McRae D and Flannigan M (1990) Development of large vortices on prescribed fires. *Canadian Journal of Forest Research* **20**(12), 1878-1887.

Meyer CP, Cook GD, Reisen F, Smith TEL, Tattaris M, Russell-Smith J, Maier SW, Yates CP and Wooster MJ (2012a) Direct measurements of the seasonality of emission factors from savanna fires in northern Australia. *Journal of Geophysical Research-Atmospheres* **117**, 20305-20305.

Meyer CP, Reisen F, Keywood MD and Crumeyrolle S (2011). Impacts of smoke from regeneration burning on air quality in the Huon Valley, Tasmania. Final Report to Forestry Tasmania. . CSIRO, Melbourne.

Meyer CPM, Luhar AK, Gillett R and Keywood MD (2008). Measurement of real-world PM10 emission factors and emission profiles from woodheaters by in situ source monitoring and atmospheric verification methods. Final Report to the Department of Sustainability, Environment, Water, Population and Communities. CSIRO, Melbourne.

Meyer M, Cope M, Lee S, Emmerson K, Keywood M and Young S (2012b). There's No Fire Without Smoke: Modelling Smoke Emissions and Transport from the 2006 Victorian Alpine Fires. Poster presentation at the AFAC 2012 conference, Perth, 28-31 August 2012.

Meyer M, Lee S, Wain A and Cope M (2013a). A Review of Smoke Emissions and Transport Modelling Systems: Milestone Report 005. Centre for Australian Weather and Climate Research, Melbourne.

Meyer M, Sullivan A and Surawski N (2013b). Smoke Emission and Transportation Modelling Project - Pyrotron Work Program M014. CSIRO.

Morandini F, Perez-Ramirez Y, Tihay V, Santoni P-A and Barboni T (2013) Radiant, convective and heat release characterization of vegetation fire. *International Journal of Thermal Sciences* **70**, 83-91.

Moula M, Brustet JM and Fontan J (1996) Remote sensing-modelisation approach for diurnal estimation of burnt biomass in the Central African Republic Savanna. *Journal of Atmospheric Chemistry* **25**(1), 1-19.

Mulvaney JJ, Sullivan AL, Cary GJ and Bishop GR (2016) Repeatability of free-burning fire experiments using heterogeneous forest fuel beds in a combustion wind tunnel. *International Journal of Wildland Fire* **25**(4), 445-455.

Nelson PF, Morrison AL, Malfroy HJ, Cope M, Lee S, Hibberd ML, Meyer CP and McGregor J (2012) Atmospheric mercury emissions in Australia from anthropogenic, natural and recycled sources. *Atmospheric Environment* **62**, 291-302.

Ng YL and Walsh S (2002). A Methodology to Estimate the Time Evolution of Bushfire and Prescribed Burning Emissions. Proceedings of the 16th Clean and & Environment Conference. Clean Air Society of Australia and New Zealand, Christchurch, New Zealand.

O'Neill SM, Larkin NK, Hoadley J, Mills G, Vaughan JK, Draxler RR, Rolph G, Ruminski M and Ferguson SA (2008). Chapter 22 Regional Real-Time Smoke Prediction Systems. In 'Developments in Environmental Science'. (Eds Bytnerowicz A, Arbaugh M, Riebau A and Andersen C). pp. 499-534. (Elsevier)

Obrist D, Hallar AG, McCubbin I, Stephens BB and Rahn T (2008) Atmospheric mercury concentrations at Storm Peak Laboratory in the Rocky Mountains: Evidence for long-range transport from Asia, boundary layer contributions, and plant mercury uptake. *Atmospheric Environment* **42**(33), 7579-7589.

Ohlemiller T and Corley D (1994) Heat Release Rate and Induced Wind Field in a Large Scale Fire. *Combustion Science and Technology* **97**(4-6), 315-330.

Okeefe A, Deacon DAG. (1988) Cavity ring-down optical spectrometer for absorption-measurements using pulsed laser sources. *Review of Scientific Instruments* **59**(12): 2544-2551.

Ottmar RD, Miranda AI and Sandberg DV (2008). Characterizing Sources of Emissions from Wildland

Fires. In 'Developments in Environmental Science'. (Eds Bytnerowicz A, Arbaugh M, Riebau A and Andersen C). pp. 61-78. (Elsevier)

Packham D, Tapper N, Griepsma D, Friedli H, Hellings J and Harris S (2009) Release of Mercury from Biomatter after Burning: Release of Mercury in the Australian Environment by Burning: A Preliminary Investigation of Biomatter and Soils. *Air Quality and Climate Change* **43**(1), 24-27.

Padilla M, Stehman SV and Chuvieco E (2014) Validation of the 2008 MODIS-MCD45 global burned area product using stratified random sampling. *Remote Sensing of Environment* **144**, 187-196.

Park J-D and Zheng W (2012) Human exposure and health effects of inorganic and elemental mercury. *Journal of Preventive Medicine and Public Health* **45**(6), 344-352.

Paton-Walsh C, Smith TEL, Young EL, Griffith DWT and Guérette É-A (2014) New emission factors for Australian vegetation fires measured using open-path Fourier transform infrared spectroscopy – Part 1: methods and Australian temperate forest fires. *Atmospheric Chemistry and Physics Discuss.* **14**, 4327–4381.

Peterson D and Wang J (2013) A sub-pixel-based calculation of fire radiative power from MODIS observations: 2. Sensitivity analysis and potential fire weather application. *Remote Sensing of Environment* **129**(0), 231-249.

Peterson D, Wang J, Ichoku C, Hyer E and Ambrosia V (2013) A sub-pixel-based calculation of fire radiative power from MODIS observations: 1: Algorithm development and initial assessment. *Remote Sensing of Environment* **129**(0), 262-279.

Pielke Jr RA, Gratz J, Landsea CW, Collins D, Saunders MA and Musulin R (2008) Normalized hurricane damage in the United States: 1900–2005. *Natural Hazards Review* **9**(1), 29-42.

Piles M, Camps A, Vall-Llossera M, Corbella I, Panciera R, Rudiger C, Kerr YH and Walker J (2011) Downscaling SMOS-derived soil moisture using MODIS visible/infrared data. *Geoscience and Remote Sensing, IEEE Transactions on* **49**(9), 3156-3166.

Pocock SJ (2006) Statistics in practice - The simplest statistical test: how to check for a difference between treatments. *British Medical Journal* **332**(7552), 1256-1258.

Prins EM and Menzel WP (1994) Trends in South American biomass burning detected with the GOES visible infrared spin scan radiometer atmospheric sounder from 1983 to 1991. *Journal of Geophysical Research: Atmospheres* **99**(D8), 16719-16735.

Radke L (1991). Particulate and trace gas emissions from large biomass fires in North America. In 'Global Biomass Burning: Atmospheric, Climatic and Biospheric Implications'. MIT Press, Cambridge, MA, pp. 209-224.

Reisen F and Brown SK (2009) Australian firefighters' exposure to air toxics during bushfire burns of autumn 2005 and 2006. *Environment International* **35**(2), 342-352.

Reisen F, Meyer CP and Keywood MD (2013) Impact of biomass burning sources on seasonal aerosol air quality. *Atmospheric Environment* **67**, 437-447.

Reisen F, Meyer CP, McCaw L, Powell JC, Tolhurst K, Keywood MD and Gras JL (2011) Impact of smoke from biomass burning on air quality in rural communities in southern Australia. *Atmospheric Environment* **45**(24), 3944-3953.

Roberts G, Wooster MJ, Perry GLW, Drake N, Rebelo LM and Dipotso F (2005) Retrieval of biomass combustion rates and totals from fire radiative power observations: Application to southern Africa using geostationary SEVIRI imagery. *Journal of Geophysical Research: Atmospheres* **110**(D21), D21111.

Roberts GJ and Wooster MJ (2008) Fire Detection and Fire Characterization Over Africa Using Meteosat SEVIRI. *Geoscience and Remote Sensing, IEEE Transactions on* **46**(4), 1200-1218.

Robertson KM, Hsieh YP and Bugna GC (2014) Fire environment effects on particulate matter emission factors in southeastern US pine-grasslands. *Atmospheric Environment* **99**, 104-111.

Rochoux MC, Ricci S, Lucor D, Cuenot B and Trouvé A (2014) Towards predictive data-driven simulations of wildfire spread – Part I: Reduced-cost Ensemble Kalman Filter based on a Polynomial Chaos surrogate model for parameter estimation. *Nat. Hazards Earth Syst. Sci.* **14**(11), 2951-2973.

Rolph GD, Draxler RR, Stein AF, Taylor A, Ruminski MG, Kondragunta S, Zeng J, Huang HC, Manikin G, McQueen JT and Davidson PM (2009) Description and Verification of the NOAA Smoke Forecasting

System: The 2007 Fire Season. *Weather and Forecasting* **24**(2), 361-378.

Rosenfeld D (1999) TRMM observed first direct evidence of smoke from forest fires inhibiting rainfall. *Geophysical Research Letters* **26**(20), 3105-3108.

Ross DG, Knight I, Packham DR and Vines RG (1980). Mathematical Smoke Dispersion Model: Prescribed Burns. Centre for Applied Mathematical Modelling, Caulfield Institute of Technology, Victoria, Australia.

Rothman LS, Gordon IE, Barbe A, Benner DC, Bernath PE, Birk M, Boudon V, Brown LR, Campargue A, Champion JP, Chance K, Coudert LH, Dana V, Devi VM, Fally S, Flaud JM, Gamache RR, Goldman A, Jacquemart D, Kleiner I, Lacome N, Lafferty WJ, Mandin JY, Massie ST, Mikhailenko SN, Miller CE, Moazzen-Ahmadi N, Naumenko OV, Nikitin AV, Orphal J, Perevalov VI, Perrin A, Predoi-Cross A, Rinsland CP, Rotger M, Simeckova M, Smith MAH, Sung K, Tashkun SA, Tennyson J, Toth RA, Vandaele AC and Vander Auwera J (2009) The HITRAN 2008 molecular spectroscopic database. *Journal of Quantitative Spectroscopy & Radiative Transfer* **110**(9-10), 533-572.

Roxburgh SH, Volkova L, Surawski N, Meyer M and Weston C, J. (2015). Review of fuel loads, burn efficiencies, emissions factors and recovery functions used to estimate greenhouse gas emissions and removals associated with wildfire on temperate forested lands. Report for the Department of the Environment, CSIRO, Canberra, Australia, pp35.

Roy DP, Boschetti L, Justice CO and Ju J (2008) The collection 5 MODIS burned area product—Global evaluation by comparison with the MODIS active fire product. *Remote Sensing of Environment* **112**(9), 3690-3707.

Roy DP, Jin Y, Lewis PE and Justice CO (2005) Prototyping a global algorithm for systematic fire-affected area mapping using MODIS time series data. *Remote Sensing of Environment* **97**(2), 137-162.

Russell-Smith J, Murphy BP, Meyer CP, Cooka GD, Maier S, Edwards AC, Schatz J and Brocklehurst P (2009) Improving estimates of savanna burning emissions for greenhouse accounting in northern Australia: limitations, challenges, applications. *International Journal of Wildland Fire* **18**(1), 1-18.

Salvador R, Piñol J, Tarantola S and Pla E (2001) Global sensitivity analysis and scale effects of a fire propagation model used over Mediterranean shrublands. *Ecological Modelling* **136**(2–3), 175-189.

Samardjieva E and Badal J (2002) Estimation of the expected number of casualties caused by strong earthquakes. *Bulletin of the Seismological Society of America* **92**(6), 2310-2322.

Sandberg DV and Peterson J (1984). A source strength model for prescribed fires in confierous logging slash. 1984 Annual meeting, Air Pollution Control Association, northwest Section.

Schmidl C, Bauer H, Dattler A, Hitzenberger R, Weissenboek G, Marr IL and Puxbaum H (2008) Chemical characterisation of particle emissions from burning leaves. *Atmospheric Environment* **42**, 9070–9079.

Scholes RJ, Kendall J and Justice CO (1996) The quantity of biomass burned in southern Africa. *Journal of Geophysical Research: Atmospheres* **101**(D19), 23667-23676.

Schroeder W, Csiszar I, Giglio L and Schmidt CC (2010) On the use of fire radiative power, area, and temperature estimates to characterize biomass burning via moderate to coarse spatial resolution remote sensing data in the Brazilian Amazon. *Journal of Geophysical Research: Atmospheres* **115**(D21), D21121.

Schroeder W, Prins E, Giglio L, Csiszar I, Schmidt C, Morisette J and Morton D (2008) Validation of GOES and MODIS active fire detection products using ASTER and ETM+ data. *Remote Sensing of Environment* **112**(5), 2711-2726.

Seiler W and Crutzen P (1980) Estimates of gross and net fluxes of carbon between the biosphere and the atmosphere from biomass burning. *Climatic Change* **2**(3), 207-247.

Simon H, Baker KR and Phillips S (2012) Compilation and interpretation of photochemical model performance statistics published between 2006 and 2012. *Atmospheric Environment* **61**, 124-139.

Sneeuwjagt R and Peet G (1998). Forest Fire Behaviour Tables for Western Australia (3rd Ed.) WA Department of Conservation and Land Management, Perth WA.**:** 59 pp.

Stott P (2000) Combustion in tropical biomass fires: a critical review. *Progress in Physical Geography* **24**(3), 355-377.

Sullivan AL (In press). Inside the Inferno: Fundamental processes of wildland fire behaviour. Part 2: Heat transfer physics and interaction. Current Forestry Reports.

Sullivan AL, Knight IK and Cheney NP (2002) Predicting the radiant heat flux from burning logs in a forest following a fire. *Australian Forestry* **1**(65), 59-67.

Sullivan AL, Knight IK, Hurley RJ and Webber C (2013) A contractionless, low-turbulence wind tunnel for the study of free-burning fires. *Experimental Thermal and Fluid Science* **44**, 264-274.

Surawski NC, Sullivan AL, Meyer CP, Roxburgh SH, Polglase PJ. (2015) Greenhouse gas emissions from laboratory-scale fires in wildland fuels depend on fire spread mode and phase of combustion. *Atmos Chem Phys* **15**(9): 5259-5273.

Tham R, Erbas B, Akram M, Dennekamp M and Abramson MJ (2009) The impact of smoke on respiratory hospital outcomes during the 2002-2003 bushfire season, Victoria, Australia. *Respirology* **14**(1), 69-75.

Thomas SC and Martin AR (2012) Carbon Content of Tree Tissues: A Synthesis. *Forests* **3**(2), 332-352.

Tolhurst K (2005) Conversion of ecological vegetation classes (EVCs) to fuel types and calculation of equivalent fine fuel loads with time since fire, in Victoria, pp 1-7,. *Unpublished*.

Tolhurst K (2009). Report on the Physical Nature of the Victorian Fires occuring on 7th February 2009. Royal Commission Expert Report, prepared by University of Melbourne.

Tolhurst K, Chong D, Duff T, Ackland A and Gretton T (2012). Interface Fuels for PHOENIX. Bushfire CRC Development Note, University of Melbourne and Victorian Department of Environment and Primary Industries, 9pp.

Tolhurst K, Shields B and Chong D (2008) PHOENIX: Development and Application of a Bushfire Risk Management Tool *The Australian Journal of Emergency Management* **23**(4), 47-54.

Tolhurst KG and Cheney NP (1999). Synopsis of the Knowledge Used in Prescribed Burning in Victoria. Department of Natural Resources and Environment**:** 97 pp.

Tolhurst KG, Chong DM and Pitts A (2007). PHOENIX - a dynamic fire characterization simulation tool. Proceedings of the Bushfire CRC Fire Behaviour Workshop, Hobart, September 2007.

Turner MG, Hargrove WW, Gardner RH and Romme WH (1994) Effects of fire on landscape heterogeneity in Yellowstone National Park, Wyoming. *Journal of Vegetation Science* **5**(5), 731-742.

Tyc G, Tulip J, Schulten D, Krischke M and Oxfort M (2005) The RapidEye mission design. *Acta Astronautica* **56**, 213-219.

UNEP (2013). 'Global Mercury Assessment 2013: Sources, Emissions, Releases and Environmental Transport'. UNEP Chemicals Branch, Geneva, Switzerland).

University of Melbourne (2013). Research Agreement Execution Request Form, LEX#22050.

Urbanski SP, Hao WM and Baker S (2009). Chemical Composition of Wildland Fire Emissions. In 'Developments in Environmental Science'. (Eds A. Bytnerowicz, M. Arbaugh, A. Riebau and C. Andersen). pp. (Elsevier)

Urbanski S (2014) Wildland fire emissions, carbon, and climate: Emission factors. *Forest Ecology and Management* **317**, 51-60.

USEPA (1987). 'Method 18 measurement of gaseous organic compound emissions by gas chromatography'. (United States Environmental Protection Agency: Washington DC).

van der Werf GR, Randerson JT, Giglio L, Collatz GJ, Mu M, Kasibhatla PS, Morton DC, DeFries RS, Jin Y and van Leeuwen TT (2010) Global fire emissions and the contribution of deforestation, savanna, forest, agricultural, and peat fires (1997-2009). *Atmospheric Chemistry and Physics* **10**(23), 11707-11735.

Vermote E, Ellicott E, Dubovik O, Lapyonok T, Chin M, Giglio L and Roberts GJ (2009) An approach to estimate global biomass burning emissions of organic and black carbon from MODIS fire radiative power. *Journal of Geophysical Research: Atmospheres* **114**(D18), D18205.

Vodacek A, Kremens RL, Fordham AJ, Vangorden SC, Luisi D, Schott JR and Latham DJ (2002) Remote optical detection of biomass burning using a potassium emission signature. *International Journal of Remote Sensing* **23**(13), 2721-2726.

Volkova L and Weston C (2013) Redistribution and emission of forest carbon by planned burning in Eucalyptus obliqua (L. Herit.) forest of south-eastern Australia. *Forest Ecology and Management* **304**, 383-390.

Volkova L and Weston CJ (2015) Carbon loss from planned fires in southeastern Australian dry Eucalyptus forests. *Forest Ecology and Management* **336**, 91-98.

Wain AG and Mills GA (2006). The Australian Smoke Management Forecast System. BMRC Research Report No. 117, Bureau of Meteorology Research Centre, Melbourne.

Walsh S (2004). Air Quality during the Victorian Bushfires of 2002-03. EPA Victoria, Publication SR5, EPA Scientific Report Series.

Walsh S (2014). Smoke and mirrors: Can we predict smoke impacts from major fires in Victoria? Presentation at EPA Victoria, 18 March 2014.

Walsh S and Duff T (2014). Fire Activity Modelling for use in Smoke Predictions - Project Plan. University of Melbourne.

Walsh S, Duff T, Chong D, Tolhurst K, Loschiavo J, Matthews S, Bockel DV, Stefano JD, Cawson J, Cope M and Meyer C (2015). Predicting the fire behaviour and environmental impacts of prescribed burns in SE Australia (poster). NSW Nature Conservation Council Bushfire Conference, Sydney.

Walsh S, Duff T and Tolhurst K (2015). Fire activity modelling for use in smoke predictions - Progress Report #1.

Ward D and Radke L (1993) Emissions measurements from vegetation fires: A comparative evaluation of methods and results. *Fire in the Environment: The Ecological, Atmospheric and Climatic Importance of Vegetation Fires* **13**, 53-76.

Ward DE and Hardy CC (1991) Smoke emissions from wildland fires. *Environment International* **17**(2–3), 117-134.

Webster JP, Kane TJ, Obrist D, Ryan JN and Aiken GR (2016) Estimating mercury emissions resulting from wildfire in forests of the Western United States. *Science of the Total Environment* **568**, 578-586.

Whelan RJ (1995). 'The ecology of fire'. (Cambridge University Press).

WHO (2000). 'WHO Air quality guidelines for Europe (Second Edition)'. (World Health Organisation: Geneva, Switzerland).

Wiedinmyer C, Akagi SK, Yokelson RJ, Emmons LK, Al-Saadi JA, Orlando JJ and Soja AJ (2011) The Fire INventory from NCAR (FINN): a high resolution global model to estimate the emissions from open burning. *Geoscientific Model Development* **4**(3), 625-641.

Wittenberg U, Heimann M, Esser G, McGuire AD and Sauf W (1998) On the influence of biomass burning on the seasonal CO2 Signal as observed at monitoring stations. *Global Biogeochemical Cycles* **12**(3), 531-544.

Wooster MJ (2002) Small-scale experimental testing of fire radiative energy for quantifying mass combusted in natural vegetation fires. *Geophysical Research Letters* **29**(21), 2027.

Wooster MJ, Roberts G, Perry GLW and Kaufman YJ (2005) Retrieval of biomass combustion rates and totals from fire radiative power observations: FRP derivation and calibration relationships between biomass consumption and fire radiative energy release. *Journal of Geophysical Research: Atmospheres* **110**(D24), D24311.

Wooster MJ and Zhang YH (2004) Boreal forest fires burn less intensely in Russia than in North America. *Geophysical Research Letters* **31**(20), L20505.

Wooster MJ, Zhukov B and Oertel D (2003) Fire radiative energy for quantitative study of biomass burning: derivation from the BIRD experimental satellite and comparison to MODIS fire products. *Remote Sensing of Environment* **86**(1), 83-107.

Yao JY, Brauer M and Henderson SB (2013) Evaluation of a Wildfire Smoke Forecasting System as a Tool for Public Health Protection. *Environmental Health Perspectives* **121**(10), 1142-1147.

Yokelson RJ, Christian TJ, Karl TG and Guenther A (2008) The tropical forest and fire emissions experiment: laboratory fire measurements and synthesis of campaign data. *Atmospheric Chemistry and Physics* 8(13), 3509-3527.

Yokelson RJ, Burling IR, Urbanski SP, Atlas EL, Adachi K, Buseck PR, Wiedinmyer C, Akagi SK, Toohey DW and Wold CE (2011) Trace gas and particle emissions from open biomass burning in Mexico. *Atmospheric Chemistry and Physics* 11(14), 6787-6808.

Youssouf H, Liousse C, Roblou L, Assamoi EM, Salonen RO, Maesano C, Banerjee S and Annesi-Maesano I (2014) Non-Accidental Health Impacts of Wildfire Smoke. *International Journal of Environmental Research and Public Health* **11**(11), 11772-11804.

Yuchi W, Yao JY, McLean KE, Stull R, Paviovic R, Davignon D, Moran MD and Henderson SB (2016) Blending forest fire smoke forecasts with observed data can improve their utility for public health applications. *Atmospheric Environment* **145**, 308-317.

Zhang X, Kondragunta S, Ram J, Schmidt C and Huang HC (2012) Near-real-time global biomass burning emissions product from geostationary satellite constellation. *Journal of Geophysical Research: Atmospheres (1984–2012)* **117**(D14).

delwp.vic.gov.au